



National Library
of Canada

Acquisitions and
Bibliographic Services Branch

395 Wellington Street
Ottawa, Ontario
K1A 0N4

Bibliothèque nationale
du Canada

Direction des acquisitions et
des services bibliographiques

395, rue Wellington
Ottawa (Ontario)
K1A 0N4

Your file Votre référence

Our file Notre référence

NOTICE

The quality of this microform is heavily dependent upon the quality of the original thesis submitted for microfilming. Every effort has been made to ensure the highest quality of reproduction possible.

If pages are missing, contact the university which granted the degree.

Some pages may have indistinct print especially if the original pages were typed with a poor typewriter ribbon or if the university sent us an inferior photocopy.

Reproduction in full or in part of this microform is governed by the Canadian Copyright Act, R.S.C. 1970, c. C-30, and subsequent amendments.

AVIS

La qualité de cette microforme dépend grandement de la qualité de la thèse soumise au microfilmage. Nous avons tout fait pour assurer une qualité supérieure de reproduction.

S'il manque des pages, veuillez communiquer avec l'université qui a conféré le grade.

La qualité d'impression de certaines pages peut laisser à désirer, surtout si les pages originales ont été dactylographiées à l'aide d'un ruban usé ou si l'université nous a fait parvenir une photocopie de qualité inférieure.

La reproduction, même partielle, de cette microforme est soumise à la Loi canadienne sur le droit d'auteur, SRC 1970, c. C-30, et ses amendements subséquents.

Canada

UNIVERSITY OF ALBERTA

**THE TURBULENT DISSIPATION OF INTERNAL SOLITARY WAVES
IN A CONTINUOUSLY STRATIFIED FLUID OF FINITE DEPTH**

by

PATRICK G. TIMKO

A THESIS

SUBMITTED TO THE FACULTY OF GRADUATE STUDIES AND RESEARCH
IN PARTIAL FULFILLMENT OF THE REQUIREMENTS
FOR THE DEGREE OF
MASTER OF SCIENCE

i.

APPLIED MATHEMATICS

DEPARTMENT OF MATHEMATICAL SCIENCES

EDMONTON, ALBERTA

SPRING, 1995



National Library
of Canada

Acquisitions and
Bibliographic Services Branch

395 Wellington Street
Ottawa, Ontario
K1A 0N4

Bibliothèque nationale
du Canada

Direction des acquisitions et
des services bibliographiques

395, rue Wellington
Ottawa (Ontario)
K1A 0N4

Your file Votre référence

Our file Notre référence

THE AUTHOR HAS GRANTED AN
IRREVOCABLE NON-EXCLUSIVE
LICENCE ALLOWING THE NATIONAL
LIBRARY OF CANADA TO
REPRODUCE, LOAN, DISTRIBUTE OR
SELL COPIES OF HIS/HER THESIS BY
ANY MEANS AND IN ANY FORM OR
FORMAT, MAKING THIS THESIS
AVAILABLE TO INTERESTED
PERSONS.

L'AUTEUR A ACCORDE UNE LICENCE
IRREVOCABLE ET NON EXCLUSIVE
PERMETTANT A LA BIBLIOTHEQUE
NATIONALE DU CANADA DE
REPRODUIRE, PRETER, DISTRIBUER
OU VENDRE DES COPIES DE SA
THESE DE QUELQUE MANIERE ET
SOUS QUELQUE FORME QUE CE SOIT
POUR METTRE DES EXEMPLAIRES DE
CETTE THESE A LA DISPOSITION DES
PERSONNE INTERESSEES.

THE AUTHOR RETAINS OWNERSHIP
OF THE COPYRIGHT IN HIS/HER
THESIS. NEITHER THE THESIS NOR
SUBSTANTIAL EXTRACTS FROM IT
MAY BE PRINTED OR OTHERWISE
REPRODUCED WITHOUT HIS/HER
PERMISSION.

L'AUTEUR CONSERVE LA PROPRIETE
DU DROIT D'AUTEUR QUI PROTEGE
SA THESE. NI LA THESE NI DES
EXTRAITS SUBSTANTIELS DE CELLE-
CI NE DOIVENT ETRE IMPRIMES OU
AUTREMENT REPRODUITS SANS SON
AUTORISATION.

ISBN 0-612-01659-5

Canada

UNIVERSITY OF ALBERTA
RELEASE FORM

NAME OF AUTHOR: PATRICK G. TIMKO

TITLE OF THESIS: THE TURBULENT DISSIPATION OF INTERNAL
SOLITARY WAVES IN A CONTINUOUSLY STRATIFIED FLUID OF FINITE
DEPTH

DEGREE FOR WHICH THESIS WAS PRESENTED: MASTER OF SCIENCE

YEAR THIS DEGREE GRANTED: 1995

Permission is hereby granted to the UNIVERSITY OF ALBERTA LIBRARY
to reproduce single copies of the thesis and to lend or sell such copies for private,
scholarly or scientific research purposes only.

The author reserves other publication rights, and neither the thesis nor exten-
sive extracts from it may be printed or otherwise reproduced without the author's
written permission.

Patrick G. Timko

SIGNED

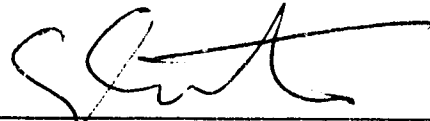
PERMANENT ADDRESS:

Box 1810
Edmonton, Alberta
T1P 1C6

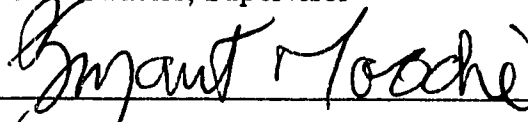
Date April 19, 1995

UNIVERSITY OF ALBERTA
THE FACULTY OF GRADUATE STUDIES AND RESEARCH

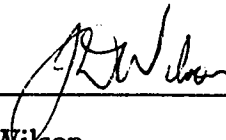
The undersigned certify that they have read, and recommend to the Faculty of Graduate Studies and Research, for acceptance, a thesis entitled THE TURBULENT DISSIPATION OF INTERNAL SOLITARY WAVES IN A CONTINUOUSLY STRATIFIED FLUID OF FINITE DEPTH submitted by PATRICK TIMKO in partial fulfillment of the degree of Master of Science in Applied Mathematics.



G.E. Swaters, Supervisor



T.B. Moodie



J.D. Wilson

Date March 13, 1995

Abstract

Enhanced mixing has been found to occur after the passage of internal solitary waves. This thesis presents a model for the turbulent dissipation of internal solitary waves in a continuously stratified fluid of finite depth. By using a simple first-order closure scheme to represent a turbulent dissipation mechanism, the governing equations lead to a Rayleigh perturbed KdV-Burgers equation which is solved asymptotically using a multiple scales perturbation technique satisfying energy balance solvability conditions. The model indicates an enhanced velocity field in the lee of the wave, which may lead to the entrainment of nutrients in the upper regions of the fluid. However, the amount of entrainment, if any, is not determined due to the simplicity of the closure scheme used.

Acknowledgements

The author wishes to acknowledge financial support for this research provided from an operating research grant awarded to Dr. Gordon E. Swaters by the Natural Science and Engineering Research Council of Canada as well as a Science Subvention also awarded to Dr. Swaters by the Department of Fisheries and Oceans. Additional financial support was provided by the Department of Mathematical Sciences in the form of a teaching assistantship.

I would also like to extend my personal thanks to Dr. Gordon Swaters who first introduced me to this subject matter. Many thanks are also due to L. Cunningham for typing and retyping this manuscript through many changes, as well as to D. Jensen for proofreading the text and D. Deveau for his ideas, suggestions and assistance regarding the production of the figures.

I wish, also, to thank my family, especially my parents, for their constant support through all my years of education and, finally, my friend, Rosanne, whose belief in me is inspirational.

TABLE OF CONTENTS

Chapter 1: Introduction	-
Chapter 2: Problem Formulation and Derivation of the Rayleigh Perturbed Korteweg-de Vries Burgers Equation	4
2.1: Problem Formulation	4
2.2: Vorticity Equation Formulation and Derivation of the Rayleigh Perturbed KdV-Burgers Equation	14
Chapter 3: Vertical Modes and the Asymptotic Solution to the Rayleigh Perturbed Korteweg-de Vries-Burgers Equation	23
3.1: The Vertical Modes	23
3.2: Time Dependent Evolution of the Streamfunction	28
3.2.1: Evolution of the main $O(1)$ pulse	32
3.2.2: The perturbation field	43
3.2.3: Emergence and Evolution of the Shelf Region	51
3.2.4: Formation and Evolution of the Dispersive Wavetail	52
3.2.5: The Solution Ahead of the Main Pulse	53
3.2.5.1: The near-field WKB power-series solution	66
3.2.5.2: The far-field WKB similarity solution	69
Chapter 4: Numerical Solution	83
4.1: The Numerical Scheme	84
4.2: Comparison of Numerical Results to Perturbation Solution	89
Chapter 5: Calculation of the Vertical Momentum Flux and Conclusion	112
5.1: Velocity Field Calculations	116
5.2: Vertical Flux Calculations	123
5.3: Conclusion	174
Bibliography	175
Appendix A	179
Appendix B	185

LIST OF FIGURES

Figure 1: The Coordinate System	5
Figure 2a-c: The Vertical Modes	29-31
Figure 3: The Solution Regions	33
Figure 4: The Unperturbed Soliton Solution	34
Figure 5a-b: Amplitude Evolution	40-43
Figure 6a-b: Phase Shift Evolution	44-45
Figure 7a-k: Evolution of Shelf and Wavetail	46-51
Figure 8a-k: Evolution of the Decaying Soliton	72-75
Figure 9a-b: Comparison of Phase Position	88-91
Figure 10a-b: Comparison of the Amplitude Evolution	92-93
Figure 11a-j: Comparison of Shelf and Wavetail Regions	94-103
Figure 12a-b: Comparison of Mass	104-106
Figure 13a-b: Comparison of Mass	107-108
Figure 14a-b: Comparison of Energy	110-111
Figure 15a-j: The Fluid Speed	124-133
Figure 16a-j: The Vertical Velocity	134-143
Figure 17a-j: The Horizontal Velocity	144-153
Figure 18a-j: Contour Plot of Streamfunction	154-163
Figure 19a-j: Contour Plot of Vertical Kinematic Momentum Flux	164-173

Chapter 1

Introduction

The Scotian shelf is characterized as a region of enhanced biological activity despite its distance from land. It has been hypothesized: "The reason for enhanced biological activity in the shelf-slope region ... may be due to higher nutrient concentrations resulting from increased vertical turbulence." (Fournier *et al.*, 1977). Sandstrom and Elliott (1984) encountered internal solitary waves (KdV solitons) during a measurement program of the Scotian shelf. They concluded that these nonlinear internal waves were "energetic enough to be probably the primary mixing mechanism in the shelf break zone." A second study (Sandstrom *et al.*, 1989) indicated that associated with these internal solitons was a turbulent layer responsible for significant dissipation.

While mathematical models for dissipating KdV solitons exist and, most recently, a model for shear-induced decay of internal solitary waves (Bogucki and Garrett, 1993), none of the existing models incorporate a turbulent dissipation mechanism for the decay of the internal solitary waves.

In order to account for turbulent effects in a fluid, the flow field is typically divided into two parts: 1) a mean flow, and 2) a perturbation representing fluctuations of the flow field about the mean flow. Substituting this two-part representation (mean flow plus fluctuation) for the flow field into the governing equations and employing the technique of Reynolds averaging introduces new unknown quantities which are nonlinear products of the fluctuation terms. Any attempt to include additional equations to define these unknown quantities introduces even more new unknowns. The production of additional unknown quantities continues, ad infinitum, for all levels of closure. The unknown quantities introduced at the first level of closure are known as Reynolds stresses and represent the transport of momentum by the fluctuating unresolved flow: the divergences of these unresolved momentum fluxes appear as forces in the evolution equations for the resolved (mean) flow. It is

possible to close the system of equations (which results from the Reynolds averaging) by equating these unknown quantities to appropriate known quantities of the flow field.

Having overcome the closure problem, the KdV equation may be derived from the governing Navier-Stokes equation via a multiple scales technique. With the incorporation of turbulence, the resulting KdV equation contains both a Rayleigh damping term and a Burgers term, and a solution may be developed via perturbation theory. However, the resulting leading order solution is not uniformly valid both ahead of and behind the wave. These nonuniformities must be accounted for and the resulting solutions for the regions ahead of and behind the wave must be asymptotically matched to obtain a uniformly valid solution.

Kaup and Newell (1978), Knickerbocker and Newell (1980), and Kodama and Ablowitz (1981) developed a solution to the Rayleigh perturbed KdV equation which indicated the development of a shelf region behind the soliton followed by an oscillatory wave tail. Kodama and Ablowitz (1981) also resolved the nonuniformity ahead of the solitary wave via a WKB-similarity theory. A first-order perturbation solution to the KdV-Burgers equation was developed by Swaters and Sawatzky (1989) as part of a study on the propagation of pressure pulses in a viscoelastic fluid filled tube.

The principal purpose of this thesis is to present a mathematical model for the turbulent dissipation of internal solitary waves in a continuously stratified fluid of finite depth as governed by a Rayleigh perturbed KdV-Burgers equation. This thesis is organized as follows: In chapter two, the governing equations for KdV solitons are derived. These equations incorporate turbulence via a first-order closure scheme and present the vertical structure as a solution to an eigenvalue problem. Chapter three presents an asymptotic solution to the Rayleigh perturbed KdV-Burgers equation developed in chapter two. As the asymptotic solution developed is singular, the solution region is divided into five subregions which may be asymptotically

matched. Chapter four presents a numerical solution to the Rayleigh perturbed KdV-Burgers equation which is compared to the solution of chapter three. Finally, chapter five presents the uniformly valid asymptotic solution from which the vertical flux (momentum) calculations are done to demonstrate the enhanced vertical mixing resulting from the passage of the solitary wave.

Chapter 2

Problem Formulation and Derivation of the Rayleigh Perturbed Korteweg-de Vries Burgers Equation

2.1 Problem Formulation

The governing equations are derived following the treatment of Leblond and Mysak (1978). We begin by establishing a Cartesian frame for a non-rotating two-dimensional ocean which is assumed to be incompressible, inviscid and stably stratified. In this frame, the fluid extends horizontally, in x , from negative to positive infinity and is bounded above and below by two rigid surfaces at $z = H$ and $z = 0$ representing the surface and the bottom of the ocean respectively (Figure 1). We are able to choose a non-rotating reference frame (thereby ignoring the Coriolis force) since the period of the internal waves of interest to us is much smaller than the inertial period.

Assuming there are no sources or sinks within the fluid, the equation describing mass conservation is

$$\frac{D\rho}{Dt} + \rho \nabla \cdot \mathbf{u} = 0, \quad (2.1.1)$$

where ρ is the density, $\mathbf{u} = (u, w)$ is the velocity field and where $\frac{D}{Dt}$ represents the total (substantial) derivative given by

$$\frac{D}{Dt} := \frac{\partial}{\partial t} + \mathbf{u} \cdot \nabla. \quad (2.1.2)$$

The horizontal and vertical momentum equations are

$$\rho \frac{Du}{Dt} = -\frac{\partial p}{\partial x}, \quad (2.1.3)$$

$$\rho \frac{Dw}{Dt} = -\frac{\partial p}{\partial z} - \rho g. \quad (2.1.4)$$

The Coordinate System

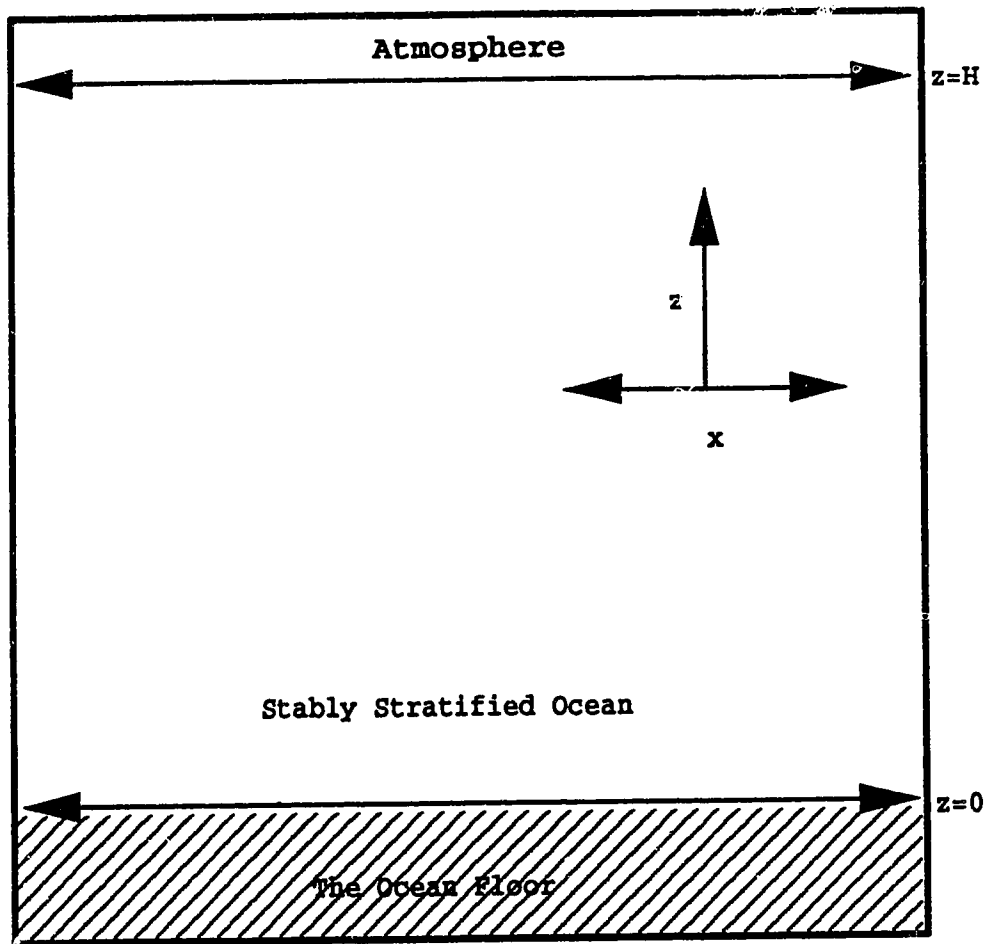


Figure 1: The Coordinate System

The coordinate system is depicted above with x extending from negative to positive infinity (increasing to the right) and z increasing positively upwards bounded below at $z = 0$ (the ocean floor) and above at $z = H$ (the ocean surface).

Here u, w represent respectively the horizontal and vertical components of the velocity field, p represents the pressure, and g the acceleration due to gravity ($g = -9.81 \text{ m/s}^2$).

Since the fluid is assumed to be incompressible, the density is constant following the motion, i.e.,

$$\frac{D\rho}{Dt} = 0. \quad (2.1.5)$$

Substituting (2.1.5) into (2.1.1) (mass conservation) yields the continuity equation

$$\frac{\partial u}{\partial x} + \frac{\partial w}{\partial z} = 0. \quad (2.1.6)$$

Equations (2.1.3)–(2.1.6) are a system of four independent equations for the four unknowns u, w, ρ, p . Hence, they represent a closed system and will completely determine the flow.

In the absence of the velocity field ($\mathbf{u} = 0$) equations (2.1.3) and (2.1.4) reduce to, respectively,

$$\frac{\partial p}{\partial x} = 0, \quad (2.1.3')$$

and

$$\frac{\partial p}{\partial z} = -\rho g. \quad (2.1.4')$$

Equation (2.1.4') is known as the hydrostatic equation. Consequently an exact nonlinear solution to equations (2.1.3)–(2.1.6) is given by

$$\mathbf{u} = 0; \quad p = p_0(z); \quad \rho = \rho_0(z), \quad (2.1.7a)$$

where p_0, ρ_0 satisfy

$$\frac{dp_0}{dz} = -g\rho_0. \quad (2.1.7b)$$

In order to discuss motions departing from this motionless hydrostatic state, we introduce time dependent pressure, p' , and density, ρ' , fields defined by

$$p = p_0(z) + p'(x, z, t); \quad \rho = \rho_0(z) + \rho'(x, z, t), \quad (2.1.8)$$

along with a spatial and time dependent velocity field $\mathbf{u} = \mathbf{u}(x, z, t)$. Substituting (2.1.8) into equations (2.1.3)–(2.1.6) we have

$$(\rho_0 + \rho') \frac{Du}{Dt} = -\frac{\partial}{\partial x}(p_0 + p'), \quad (2.1.9a)$$

$$(\rho_0 + \rho') \frac{Dw}{Dt} = -\frac{\partial}{\partial z}(p_0 + p') - (\rho_0 + \rho')g, \quad (2.1.9b)$$

$$\frac{\partial}{\partial t}(\rho_0 + \rho') + u \frac{\partial}{\partial x}(\rho_0 + \rho') + w \frac{\partial}{\partial z}(\rho_0 + \rho') = 0, \quad (2.1.9c)$$

$$\frac{\partial u}{\partial x} + \frac{\partial w}{\partial z} = 0. \quad (2.1.9d)$$

Applying the hydrostatic solution given by (2.1.7), we see that equations (2.1.9) reduce to

$$\rho \frac{Du}{Dt} = -\frac{\partial p'}{\partial x}, \quad (2.1.10a)$$

$$\rho \frac{Dw}{Dt} = -\frac{\partial p'}{\partial z} - \rho'g, \quad (2.1.10b)$$

$$\frac{D\rho'}{Dt} + w \frac{\partial \rho_0}{\partial z} = 0, \quad (2.1.10c)$$

$$\frac{\partial u}{\partial x} + \frac{\partial w}{\partial z} = 0. \quad (2.1.10d)$$

We now assume that the scale of the variations in vertical motion, w , are small when compared to the scale of the variations in density, ρ , which allows us to impose the Boussinesq approximation. Simply stated, the Boussinesq approximation replaces the density function, ρ , with a constant, ρ_* , in all terms except those which

give rise to the forces of buoyancy (Gill, 1982). Applying the Boussinesq approximation we find that equations (2.1.10a and b) become

$$\frac{Du}{Dt} = -\frac{1}{\rho_*} \frac{\partial p'}{\partial x}, \quad (2.1.11a)$$

$$\frac{Dw}{Dt} = -\frac{1}{\rho_*} \frac{\partial p'}{\partial z} - \frac{\rho' g}{\rho_*}, \quad (2.1.11b)$$

where $\rho_* \equiv \text{constant}$ is some characteristic reference density.

Equations (2.1.11) and (2.1.10c and d) are now rewritten dropping the primes from the perturbation pressure and density fields, i.e.,

$$\frac{Du}{Dt} = -\frac{1}{\rho_*} \frac{\partial p}{\partial x}, \quad (2.1.12a)$$

$$\frac{Dw}{Dt} = -\frac{1}{\rho_*} \frac{\partial p}{\partial z} - \frac{\rho g}{\rho_*}, \quad (2.1.12b)$$

$$\frac{D\rho}{Dt} + w \frac{\partial \rho_0}{\partial z} = 0, \quad (2.1.12c)$$

$$\frac{\partial u}{\partial x} + \frac{\partial w}{\partial z} = 0. \quad (2.1.12d)$$

To incorporate turbulent effects into the problem we must first make two simplifying assumptions

- 1) Any turbulence is homogeneous and the statistics are time independent.
- 2) Density, pressure and velocity fields may be divided into two parts: a mean (ensemble average) flow and fluctuations about the mean.

The first assumption allows us to impose the ergodic condition (Stull, 1988) that time, space and ensemble averages are all equal. With regards to the second assumption we define the density, pressure and velocity fields by

$$\rho = \bar{\rho} + \rho', \quad p = \bar{p} + p', \quad u = \bar{u} + u', \quad w = \bar{w} + w'. \quad (2.1.13)$$

Here, an overstruck bar represents the ensemble average and prime denotes fluctuations about this mean. The primed quantities have zero ensemble mean, i.e. they

satisfy $\overline{\rho'} = 0$, $\overline{p'} = 0$, $\overline{u'} = 0$, $\overline{w'} = 0$. Substitution of (2.1.13) into (2.1.12) leads to

$$\begin{aligned} \frac{\partial}{\partial t}(\overline{u} + u') + (\overline{u} + u') \frac{\partial}{\partial x}(\overline{u} + u') + (\overline{w} + w') \frac{\partial}{\partial z}(\overline{u} + u') \\ = -\frac{1}{\rho_*} \frac{\partial}{\partial x}(\overline{p} + p'), \end{aligned} \quad (2.1.14a)$$

$$\begin{aligned} \frac{\partial}{\partial t}(\overline{w} + w') + (\overline{u} + u') \frac{\partial}{\partial x}(\overline{w} + w') + (\overline{w} + w') \frac{\partial}{\partial z}(\overline{w} + w') \\ = -\frac{1}{\rho_*} \frac{\partial}{\partial z}(\overline{p} + p') - \frac{g}{\rho_*}(\overline{\rho} + \rho'), \end{aligned} \quad (2.1.14b)$$

$$\begin{aligned} \frac{\partial}{\partial t}(\overline{\rho} + \rho') + (\overline{u} + u') \frac{\partial}{\partial x}(\overline{\rho} + \rho') + (\overline{w} + w') \frac{\partial}{\partial z}(\overline{\rho} + \rho') \\ + (\overline{w} + w') \frac{\partial \rho_0}{\partial z} = 0, \end{aligned} \quad (2.1.14c)$$

$$\frac{\partial}{\partial x}(\overline{u} + u') + \frac{\partial}{\partial z}(\overline{w} + w') = 0. \quad (2.1.14d)$$

We now introduce the ensemble averaging operator $\langle * \rangle$

$$\langle * \rangle := \overline{*}. \quad (2.1.15)$$

Applying this averaging operator to equations (2.1.14) we have

$$\begin{aligned} \langle \frac{\partial \overline{u}}{\partial t} \rangle + \langle \frac{\partial u'}{\partial t} \rangle + \langle \overline{u} \frac{\partial \overline{u}}{\partial x} \rangle + \langle \overline{u} \frac{\partial u'}{\partial x} \rangle \\ + \langle u' \frac{\partial \overline{u}}{\partial x} \rangle + \langle u' \frac{\partial u'}{\partial x} \rangle + \langle \overline{w} \frac{\partial \overline{u}}{\partial z} \rangle \\ + \langle \overline{w} \frac{\partial u'}{\partial z} \rangle + \langle w' \frac{\partial \overline{w}}{\partial z} \rangle + \langle w' \frac{\partial u'}{\partial z} \rangle \\ = \langle -\frac{1}{\rho_*} \frac{\partial \overline{p}}{\partial x} \rangle + \langle -\frac{1}{\rho_*} \frac{\partial p'}{\partial x} \rangle, \end{aligned} \quad (2.1.16a)$$

$$\begin{aligned}
& \langle \frac{\partial \bar{w}}{\partial t} \rangle + \langle \frac{\partial w'}{\partial t} \rangle + \langle \bar{u} \frac{\partial \bar{w}}{\partial x} \rangle + \langle \bar{u} \frac{\partial w'}{\partial x} \rangle \\
& + \langle u' \frac{\partial \bar{w}}{\partial x} \rangle + \langle u' \frac{\partial w'}{\partial x} \rangle + \langle \bar{w} \frac{\partial \bar{w}}{\partial z} \rangle \\
& + \langle \bar{w} \frac{\partial w'}{\partial z} \rangle + \langle w' \frac{\partial \bar{w}}{\partial z} \rangle + \langle w' \frac{\partial w'}{\partial z} \rangle \\
& = \langle -\frac{1}{\rho_*} \frac{\partial \bar{p}}{\partial z} \rangle + \langle -\frac{1}{\rho_*} \frac{\partial p'}{\partial z} \rangle \\
& + \langle -\frac{g}{\rho_*} \bar{\rho} \rangle + \langle -\frac{g}{\rho_*} \rho' \rangle,
\end{aligned} \tag{2.1.16b}$$

$$\begin{aligned}
& \langle \frac{\partial \bar{\rho}}{\partial t} \rangle + \langle \frac{\partial \rho'}{\partial t} \rangle + \langle \bar{u} \frac{\partial \bar{\rho}}{\partial x} \rangle + \langle \bar{u} \frac{\partial \rho'}{\partial x} \rangle \\
& + \langle u' \frac{\partial \bar{\rho}}{\partial x} \rangle + \langle u' \frac{\partial \rho'}{\partial x} \rangle + \langle \bar{w} \frac{\partial \bar{\rho}}{\partial z} \rangle \\
& + \langle \bar{w} \frac{\partial \rho'}{\partial z} \rangle + \langle w' \frac{\partial \bar{\rho}}{\partial z} \rangle + \langle w' \frac{\partial \rho'}{\partial z} \rangle \\
& + \langle \bar{w} \frac{\partial \rho_0}{\partial z} \rangle + \langle w' \frac{\partial \rho_0}{\partial z} \rangle = 0,
\end{aligned} \tag{2.1.16c}$$

$$\langle \frac{\partial \bar{u}}{\partial x} \rangle + \langle \frac{\partial u'}{\partial x} \rangle + \langle \frac{\partial \bar{w}}{\partial z} \rangle + \langle \frac{\partial w'}{\partial z} \rangle = 0. \tag{2.1.16d}$$

If c represents a constant and A, B fields, we observe the following properties (Stull, 1988):

$$\begin{aligned}
\langle cA \rangle &= c\bar{A}, \\
\langle \bar{A} \rangle &= \bar{A}, \\
\langle \bar{A}B \rangle &= \bar{A}\bar{B}, \\
\langle \frac{\partial A}{\partial * } \rangle &= \frac{\partial}{\partial * } \bar{A}.
\end{aligned} \tag{2.1.17}$$

Applying (2.1.17) we find that equations (2.1.16) reduce to

$$\frac{\partial \bar{u}}{\partial t} + \bar{u} \frac{\partial \bar{u}}{\partial x} + \overline{u' \frac{\partial u'}{\partial x}} + \bar{w} \frac{\partial \bar{u}}{\partial z} + \overline{w' \frac{\partial u'}{\partial z}} = -\frac{1}{\rho_*} \frac{\partial \bar{p}}{\partial x}, \quad (2.1.18a)$$

$$\frac{\partial \bar{w}}{\partial t} + \bar{u} \frac{\partial \bar{w}}{\partial x} + \overline{u' \frac{\partial w'}{\partial x}} + \bar{w} \frac{\partial \bar{w}}{\partial z} + \overline{w' \frac{\partial w'}{\partial z}} = -\frac{1}{\rho_*} \frac{\partial \bar{p}}{\partial z} - \frac{g}{\rho_*} \bar{\rho}, \quad (2.1.18b)$$

$$\frac{\partial \bar{\rho}}{\partial t} + \bar{u} \frac{\partial \bar{\rho}}{\partial x} + \overline{u' \frac{\partial \rho'}{\partial x}} + \bar{w} \frac{\partial \bar{\rho}}{\partial z} + \overline{w' \frac{\partial \rho'}{\partial z}} + \bar{w} \frac{\partial \rho_0}{\partial z} = 0, \quad (2.1.18c)$$

$$\frac{\partial \bar{u}}{\partial x} + \frac{\partial \bar{w}}{\partial z} = 0, \quad (2.1.18d)$$

where we have also employed the identity

$$\overline{u'} = 0. \quad (2.1.19)$$

Subtracting equation (2.1.18d) from (2.1.14d) we find that

$$\frac{\partial u'}{\partial x} + \frac{\partial w'}{\partial z} = 0. \quad (2.1.20)$$

Multiplying this last equation by u' and then applying the averaging operator (2.1.15) yields

$$\overline{u' \frac{\partial u'}{\partial x}} + \overline{u' \frac{\partial w'}{\partial z}} = 0. \quad (2.1.21a)$$

Similarly, multiplying by w' and ρ' then averaging yields, respectively,

$$\overline{w' \frac{\partial u'}{\partial x}} + \overline{w' \frac{\partial w'}{\partial z}} = 0, \quad (2.1.21b)$$

$$\overline{\rho' \frac{\partial u'}{\partial x}} + \overline{\rho' \frac{\partial w'}{\partial z}} = 0. \quad (2.1.21c)$$

Finally, adding equations (2.1.21a,b,c) to equations (2.1.18a,b,c) respectively, leads to (upon application of identities (2.1.17))

$$\frac{\partial \bar{u}}{\partial t} + \bar{u} \frac{\partial \bar{u}}{\partial x} + \bar{w} \frac{\partial \bar{u}}{\partial z} + \frac{1}{\rho_*} \frac{\partial \bar{p}}{\partial x} = -\frac{\partial}{\partial x} \overline{u' u'} - \frac{\partial}{\partial z} \overline{u' w'}, \quad (2.1.22a)$$

$$\frac{\partial \bar{w}}{\partial t} + \bar{u} \frac{\partial \bar{w}}{\partial x} + \bar{w} \frac{\partial \bar{w}}{\partial z} + \frac{1}{\rho_*} \frac{\partial \bar{p}}{\partial z} + \frac{g}{\rho_*} \bar{\rho} = -\frac{\partial}{\partial x} \overline{w'u'} - \frac{\partial}{\partial z} \overline{w'w'}, \quad (2.1.22b)$$

$$\frac{\partial \bar{\rho}}{\partial t} + \bar{u} \frac{\partial \bar{\rho}}{\partial x} + \bar{w} \frac{\partial \bar{\rho}}{\partial z} + \bar{w} \frac{\partial \rho_0}{\partial z} = -\frac{\partial}{\partial x} \overline{u'\rho'} - \frac{\partial}{\partial z} \overline{w'\rho'}. \quad (2.1.22c)$$

The terms $\overline{u'u'}$, $\overline{u'w'}$, $\overline{w'u'}$, $\overline{w'w'}$, $\overline{u'\rho'}$, $\overline{w'\rho'}$ in equations (2.1.22) are unknown yielding a system of ten unknown quantities for the system of four equations ((2.1.22) and (2.1.18d)).

The first four of these terms are Reynolds stresses and the latter two terms represent the horizontal and vertical buoyancy flux. The Reynolds stresses are defined as:

$$\begin{aligned} \tau_{xx} &= -\rho \overline{u'u'}; \quad \tau_{zz} = -\rho \overline{w'w'}, \\ \tau_{xz} &= \tau_{zx} = -\rho \overline{u'w'} = -\rho \overline{w'u'}. \end{aligned} \quad (2.1.23)$$

The symmetry of the Reynolds stresses reduces the number of unknowns to nine. In order to close this system of equations we now model the Reynolds stresses (representing the momentum flux) as follows (Pedlosky, 1987):

$$\begin{aligned} \frac{\tau_{xx}}{\rho} &= 2K_H \frac{\partial \bar{u}}{\partial x}; \quad \frac{\tau_{zz}}{\rho} = 2K_V \frac{\partial \bar{w}}{\partial z}, \\ \frac{\tau_{xz}}{\rho} &= \frac{\tau_{zx}}{\rho} = K_V \frac{\partial \bar{u}}{\partial z} + K_H \frac{\partial \bar{w}}{\partial x}. \end{aligned} \quad (2.1.24)$$

The coefficients K_H and K_V in equations (2.1.24) are called, respectively, the horizontal and vertical turbulent viscosity coefficients and are assumed constant but not necessarily equal. Substitution of (2.1.24) into equations (2.1.22a,b) yields

$$\frac{\partial \bar{u}}{\partial t} + \bar{u} \frac{\partial \bar{u}}{\partial x} + \bar{w} \frac{\partial \bar{u}}{\partial z} + \frac{1}{\rho_*} \frac{\partial \bar{p}}{\partial x} = K_H \frac{\partial^2 \bar{u}}{\partial x^2} + K_V \frac{\partial^2 \bar{u}}{\partial z^2}, \quad (2.1.25a)$$

$$\frac{\partial \bar{w}}{\partial t} + \bar{u} \frac{\partial \bar{w}}{\partial x} + \bar{w} \frac{\partial \bar{w}}{\partial z} + \frac{1}{\rho_*} \frac{\partial \bar{p}}{\partial z} + \frac{g}{\rho_*} \bar{\rho} = K_H \frac{\partial^2 \bar{w}}{\partial x^2} + K_V \frac{\partial^2 \bar{w}}{\partial z^2}. \quad (2.1.25b)$$

In forming equations (2.1.25) we have employed the continuity equation (2.1.18d).

Similarly we define the horizontal and vertical eddy buoyancy coefficients B_H and B_V (Leblond and Mysak, 1978) by:

$$\overline{u'\rho'} = -B_H \frac{\partial \bar{\rho}}{\partial x}; \quad \overline{w'\rho'} = -B_V \frac{\partial \bar{\rho}}{\partial z}. \quad (2.1.26)$$

Substituting (2.1.26) into (2.1.22c) we have

$$\frac{\partial \bar{\rho}}{\partial t} + \bar{u} \frac{\partial \bar{\rho}}{\partial x} + \bar{w} \frac{\partial \bar{\rho}}{\partial z} + \bar{v} \frac{\partial \rho_0}{\partial z} = B_H \frac{\partial^2 \bar{\rho}}{\partial x^2} + B_V \frac{\partial^2 \bar{\rho}}{\partial z^2}. \quad (2.1.27)$$

Equations (2.1.18d), (2.1.25) and (2.1.27) now represent a closed system of four equations for the four unknowns \bar{u} , \bar{w} , $\bar{\rho}$, \bar{p} . One further simplification is made by assuming that the eddy buoyancy coefficients and the turbulent viscosity coefficients may be equaled in the horizontal and vertical values (i.e. $\nu = K_H = B_H$, $\mu = K_V = B_V$). Typically, for oceanic flow the horizontal flux coefficients are larger than the vertical flux coefficients. While no assumption is made as to the relative scale of the horizontal and vertical flux coefficients to each other it is assumed that both parameters are small when compared to the forces which dominate and determine the flow (i.e. the horizontal and vertical fluxes are considered “weak” forces).

By dropping the overstruck bar to simplify notation, the dimensional governing equations may be rewritten

$$\frac{\partial u}{\partial t} + u \frac{\partial u}{\partial x} + w \frac{\partial u}{\partial z} + \frac{1}{\rho_*} \frac{\partial p}{\partial x} = \nu \frac{\partial^2 u}{\partial x^2} + \mu \frac{\partial^2 u}{\partial z^2}, \quad (2.1.28a)$$

$$\frac{\partial w}{\partial t} + u \frac{\partial w}{\partial x} + w \frac{\partial w}{\partial z} + \frac{1}{\rho_*} \frac{\partial p}{\partial z} + \frac{g}{\rho_*} \rho = \nu \frac{\partial^2 w}{\partial x^2} + \mu \frac{\partial^2 w}{\partial z^2}, \quad (2.1.28b)$$

$$\frac{\partial \rho}{\partial t} + u \frac{\partial \rho}{\partial x} + w \frac{\partial \rho}{\partial z} + w \frac{\partial \rho_0}{\partial z} = \nu \frac{\partial^2 \rho}{\partial x^2} + \mu \frac{\partial^2 \rho}{\partial z^2}, \quad (2.1.28c)$$

$$\frac{\partial u}{\partial x} + \frac{\partial w}{\partial z} = 0. \quad (2.1.28d)$$

Boundary Conditions

The boundary conditions are formulated by assuming that the surface of the ocean ($z = H$) behaves as a rigid lid. It follows that there can be no net transport of fluid across this boundary, thus the vertical velocity, w must vanish at $z = H$, i.e. the fluid velocity normal to the surface $z = H$ must equal zero. The ocean floor, assumed flat, also behaves as a rigid surface. Therefore w also must vanish at $z = 0$.

In the far fields ahead and behind the perturbation flow, we assume the flow to remain in the hydrostatic state. Thus, both u and w must vanish for large positive and negative values of x .

In summary, the boundary conditions may be stated as

$$w = 0, \quad \text{at } z = 0, H; \quad (2.1.29a)$$

$$\lim_{x \rightarrow \pm\infty} u = 0; \quad (2.1.29b)$$

$$\lim_{x \rightarrow \pm\infty} w = 0. \quad (2.1.29c)$$

2.2 Vorticity Equation Formulation and Derivation of the Rayleigh Perturbed KdV-Burgers Equation

The equations governing the motion are given by (2.1.28). It follows from the continuity equation (2.1.28d) that there exists a streamfunction, $\psi = \psi(x, z, t)$, such that the velocity field is given by

$$u = -\psi_z; \quad w = \psi_x. \quad (2.2.1)$$

The vorticity equation is obtained by subtracting the z -derivative of the horizontal momentum equation (2.1.28a) from the x -derivative of the vertical momentum

equation (2.1.28b), yielding

$$\Delta\psi_t + u_x\Delta\psi + u\Delta\psi_x + w_z\Delta\psi + w\Delta\psi_z = -\frac{\rho_x}{\rho_*}g + \mu\Delta\psi_{xx} + \nu\Delta\psi_{zz}, \quad (2.2.2)$$

where

$$\Delta\psi := \psi_{xx} + \psi_{zz}, \quad (2.2.3)$$

and ψ is defined by (2.2.1). From the continuity equation (2.1.28d) we see that (2.2.2) may be rewritten as

$$\frac{D}{Dt}\Delta\psi = -\frac{\rho_x}{\rho_*}g + \mu\Delta\psi_{xx} + \nu\Delta\psi_{zz}, \quad (2.2.4)$$

where $\frac{D}{Dt}$ is the total derivative defined by (2.1.2). Substituting (2.2.1) into equations (2.1.28c) and (2.2.4) we arrive at the governing equations in vorticity form

$$\rho_t + \psi_x\rho_z - \psi_z\rho_x + \psi_x\frac{d\rho_0}{dz} = \mu\rho_{xx} + \nu\rho_{zz}, \quad (2.2.5a)$$

$$\Delta\psi_t + \psi_x\Delta\psi_z - \psi_z\Delta\psi_x = -\frac{\rho_x}{\rho_*}g + \mu\Delta\psi_{xx} + \nu\Delta\psi_{zz}. \quad (2.2.5b)$$

In order for KdV solitons to exist, there must be a balance of weak nonlinearity with weak dispersion. Typically, the dissipative forces of turbulence are also weak when compared to the forces responsible for the storage and advection of mass and vorticity. Thus, to determine the turbulent dissipation of KdV solitons, it is necessary that the governing equations represent a balance between weak nonlinearity, weak dispersion and weak dissipation.

Shallow water waves of small amplitude and low wavenumber, such as the solitons detected by Sandstrom and Elliot (1984) in the region of the Scotian shelf, may be characterized by introducing horizontal, L , and vertical, H , length scales such that $(\frac{H}{L})^2 \ll 1$. Therefore, in view of these scaling considerations, we now introduce the

following nondimensional (primed) coordinates

$$\begin{aligned} x &= Lx', & t &= \frac{L}{\sqrt{gH}}t', \\ z &= Hz', & \rho &= \epsilon\rho_*\rho', \\ \frac{d\rho_0}{dz} &= \frac{-\rho_*}{H}S(z'), & \psi &= \epsilon H\sqrt{gH}\psi', \end{aligned} \quad (2.2.6a)$$

where L and H are, respectively, typical horizontal and vertical length scales and $\epsilon = \left(\frac{H}{L}\right)^2 \ll 1$.

During a measurement program on the Scotian Shelf, Sandstrom and Elliot (1984) detected shoreward propagating solitons. The study area had a characteristic depth of approximately 160 meters and was stably stratified with potential density, σ_t , ranging from 23.0 to 27.0 with the pycnocline at a depth of about 40 meters. The solitons which were detected were observed to pass by in about 200 seconds.

Based on the above observations, we choose the vertical length scale $H = 160\text{m}$ (the depth of the fluid) and set $\rho_* = 1025 \text{ kg/m}^3$ (the average density). Since we wish to model changes in the structure of a solitary wave which passes by in a time of 200 seconds, we establish a slow time frame $T = \epsilon t$ and choose $\epsilon = \frac{1}{200}$. Given then $\epsilon = \left(\frac{H}{L}\right)^2$ we may now calculate the horizontal length scale, $L = 2000$ meters.

The density structure of the ocean may be represented by an exponential function (eg. Swaters and Mysak (1985)); it follows that $S(z)$ (as defined in (2.2.6)) may be represented as

$$S(z) = S_0^2 \exp[\gamma(z - 1)], \quad (2.2.6b)$$

where $S_0 = \left[-\frac{H}{\rho_*} \frac{d\rho_0}{dz} \Big|_{z=1} \right]^{\frac{1}{2}}$ and γ represents the nondimensional scale height $\gamma = \gamma^* H$ (γ^* is the scale height of the Brunt-Väisälä frequency which is assumed to occur in the area of the pycnocline $\frac{1}{\gamma^*} = 40$ meters). Assuming an average density change of 2 kg/m^3 over a depth of 30 meters, we find typical values for $S_0 = 0.1$

and $\gamma = 4.0$.

Substitution of (2.2.6a) into (2.2.5) yields

$$\rho'_{t'} + \varepsilon \psi'_{x'} \rho'_{x'} - \varepsilon \psi'_{x'} \rho'_{x'} - \psi'_{x'} S(z') = \varepsilon \mu' \rho'_{x'x'} + \varepsilon \nu' \rho'_{x'x'}, \quad (2.2.7a)$$

$$\Delta \psi'_{t'} + \varepsilon \psi'_{x'} \Delta \psi'_{x'} - \varepsilon \psi'_{x'} \Delta \psi'_{x'} = -\frac{\rho'_{x'}}{H^2} + \varepsilon \mu' \Delta \psi'_{x'x'} + \varepsilon \nu' \Delta \psi'_{x'x'}, \quad (2.2.7b)$$

where μ' and ν' are defined by

$$\varepsilon \mu' = \frac{\mu L}{\sqrt{gH}H^2}, \quad \varepsilon \nu' = \frac{\nu}{\sqrt{gH}L}.$$

Noting that $\Delta := \frac{\partial^2}{\partial x'^2} + \frac{\partial^2}{\partial z'^2} = \frac{1}{L^2} \frac{\partial^2}{\partial x'^2} + \frac{1}{H^2} \frac{\partial^2}{\partial z'^2} \Rightarrow H^2 \Delta = \frac{\partial^2}{\partial x'^2} + \varepsilon \frac{\partial^2}{\partial z'^2}$ we see that equation (2.2.7b) becomes

$$\begin{aligned} & (\psi'_{x'x'} + \varepsilon \psi'_{x'x'})_{t'} + \varepsilon \psi'_{x'} (\psi'_{x'x'} + \varepsilon \psi'_{x'x'})_{x'} - \varepsilon \psi'_{x'} (\psi'_{x'x'} + \varepsilon \psi'_{x'x'})_{x'} \\ & = -\rho'_{x'} + \varepsilon \mu' (\psi'_{x'x'} + \varepsilon \psi'_{x'x'})_{x'x'} + \varepsilon \nu' (\psi'_{x'x'} + \varepsilon \psi'_{x'x'})_{x'x'}. \end{aligned} \quad (2.2.7b')$$

By defining the Jacobian of two functions A, B

$$J(A, B) = A_x B_z - A_z B_x,$$

we see that the non-dimensional equations, (2.2.7a) and (2.2.7b'), may be written as

$$\rho_t + \varepsilon J(\psi, \rho) - \psi_x S(z) = \varepsilon \mu \rho_{xx} + \varepsilon \nu \rho_{xx}, \quad (2.2.8a)$$

$$\begin{aligned} & (\psi_{xx} + \varepsilon \psi_{xx})_t + \varepsilon J(\psi, (\psi_{xx} + \varepsilon \psi_{xx})) \\ & = -\rho_x + \varepsilon \mu (\psi_{xx} + \varepsilon \psi_{xx})_{xx} + \varepsilon \nu (\psi_{xx} + \varepsilon \psi_{xx})_{xx}. \end{aligned} \quad (2.2.8b)$$

In equations (2.2.8) the primes denoting the non-dimensional quantities have been dropped for notational simplicity.

From equations (2.2.8) we see that the contributions of nonlinearity, dispersion and dissipation occur over a time scale of $O(\varepsilon^{-1})$. To determine the effects of these contributions on a rightward travelling ($x > 0$) soliton, we now introduce the fast phase variable, ξ , and slow time variable, T , defined by:

$$\xi = x - ct, \quad T = \varepsilon t,$$

where c is the translation velocity in the x -direction. The fast phase variable establishes a characteristic reference frame which moves rightward with the travelling soliton while the slow time variable establishes a time frame by which it is possible to determine the effects of nonlinearity, dispersion and dissipation.

In terms of these new variables, the partial derivatives are mapped as:

$$\partial_t \rightarrow \varepsilon \partial_T - c \partial_\xi, \quad \partial_x \rightarrow \partial_\xi,$$

so that equations (2.2.8) become

$$\varepsilon \rho_T - c \rho_\xi + \varepsilon J(\psi, \rho) - \psi_\xi S(z) = \varepsilon \mu \rho_{zz} + \varepsilon \nu \rho_{\xi\xi}, \quad (2.2.9a)$$

$$\begin{aligned} \varepsilon (\psi_{zz} + \varepsilon \psi_{\xi\xi})_T - c (\psi_{zz} + \varepsilon \psi_{\xi\xi})_\xi + \varepsilon J(\psi, (\psi_{zz} + \varepsilon \psi_{\xi\xi})) \\ = -\rho_\xi + \varepsilon \mu (\psi_{zz} + \varepsilon \psi_{\xi\xi})_{zz} \\ + \varepsilon \nu (\psi_{zz} + \varepsilon \psi_{\xi\xi})_{\xi\xi}, \end{aligned} \quad (2.2.9b)$$

where $J(A, B) = A_\xi B_z - A_z B_\xi$.

Expanding the unknown function for density, $\rho = \rho(z, \xi; T)$, and the streamfunction $\psi = \psi(z, \xi; T)$ in terms of the small parameter ε we have

$$\rho(z, \xi; T) = \sum_{n=0}^{\infty} \varepsilon^n \rho^{(n)}(z, \xi; T), \quad (2.2.10a)$$

$$\psi(z, \xi; T) = \sum_{n=0}^{\infty} \varepsilon^n \psi^{(n)}(z, \xi; T). \quad (2.2.10b)$$

Substitution of (2.2.10) into (2.2.9) leads to the $O(1)$ problem

$$\rho_{\xi}^{(0)} = -\frac{S(z)}{c}\psi_{\xi}^{(0)}, \quad (2.2.11a)$$

$$\psi_{zz\xi}^{(0)} = \frac{\rho_{\xi}^{(0)}}{c}. \quad (2.2.11b)$$

From equations (2.2.11) we see that the streamfunction, ψ , satisfies

$$\frac{\partial}{\partial \xi} \left(\psi_{zz}^{(0)} + \frac{S(z)}{c^2} \psi^{(0)} \right) = 0. \quad (2.2.12)$$

Integrating (2.2.12) with respect to ξ , we have

$$\psi_{zz}^{(0)} + \frac{S(z)}{c^2} \psi^{(0)} = D(z; T),$$

where $D(z; T)$ is a constant of integration. Applying the boundary conditions (2.1.9b,c) (the flow field vanishes as $\xi \rightarrow \pm\infty$ (i.e. $x \rightarrow \pm\infty$)) it is readily seen that $D(z; T) = 0$. Thus the above equation reduces to

$$\psi_{zz}^{(0)} + \frac{S(z)}{c^2} \psi^{(0)} = 0.$$

Assuming a separable solution for $\psi^{(0)}(z, \xi; T)$ of the form

$$\psi^{(0)}(z, \xi; T) = A(\xi; T)\phi(z), \quad (2.2.13)$$

we find that $\phi(z)$ is governed by

$$\phi_{zz} + \frac{S(z)}{c^2} \phi = 0, \quad (2.2.14a)$$

subject to the boundary conditions

$$\phi(0) = \phi(1) = 0. \quad (2.2.14b)$$

Equations (2.2.14) establish the vertical modes of the flow field. There exist an infinite number of solutions to problem (2.2.14), each corresponding to one of the infinite denumerable eigenvalues, c_n . The eigenvalues and corresponding eigenfunctions will be calculated in chapter 3.

Solvability Conditions

Having determined the equation governing the vertical structure, $\phi(z)$, of the flow field, we now derive the equation governing the horizontal structure and its time evolution as given by $A(\xi, T)$. The evolution equation for $A(\xi; T)$ is now shown to arise as a solvability condition on the $O(\varepsilon)$ problem. The $O(\varepsilon)$ problem associated with (2.2.9) and (2.2.10) is

$$\rho_\xi^{(1)} + \frac{S(z)}{c} \psi_\xi^{(1)} = \frac{1}{c} J(\psi^{(0)}, \rho^{(0)}) + \frac{1}{c} \rho_T^{(0)} - \frac{\mu}{c} \rho_{zz}^{(0)} - \frac{\nu}{c} \rho_{\xi\xi}^{(0)}, \quad (2.2.15a)$$

$$\psi_{zz\xi}^{(1)} - \frac{1}{c} \rho_\xi^{(1)} = \frac{1}{c} J(\psi^{(0)}, \psi_{zz}^{(0)}) + \frac{1}{c} \psi_{zzT}^{(0)} - \psi_{\xi\xi\xi}^{(0)} - \frac{\mu}{c} \psi_{zzzz}^{(0)} - \frac{\nu}{c} \psi_{zz\xi\xi}^{(0)}. \quad (2.2.15b)$$

Solving for $\rho_\xi^{(1)}$ in equation (2.2.15a) and substituting into equation (2.2.15b) we find that the $O(\varepsilon)$ problem may be rewritten as

$$\begin{aligned} \psi_{zz\xi}^{(1)} + \frac{S(z)}{c^2} \psi_\xi^{(1)} = & -\psi_{\xi\xi\xi}^{(0)} + \frac{1}{c} \psi_{zzT}^{(0)} + \frac{1}{c} \psi_\xi^{(0)} \psi_{zzz}^{(0)} \\ & - \frac{1}{c} \psi_z^{(0)} \psi_{zz\xi}^{(0)} - \frac{\mu}{c} \psi_{zzzz}^{(0)} - \frac{\nu}{c} \psi_{zz\xi\xi}^{(0)} \\ & + \frac{1}{c^2} \psi_\xi^{(0)} \rho_z^{(0)} - \frac{1}{c^2} \psi_z^{(0)} \rho_\xi^{(0)} + \frac{1}{c^2} \rho_T^{(0)} \\ & - \frac{\mu}{c^2} \rho_{zz}^{(0)} - \frac{\nu}{c^2} \rho_{\xi\xi}^{(0)}. \end{aligned} \quad (2.2.16)$$

Recalling (2.2.11a), (2.2.13), and (2.2.14a), we see that this last equation becomes

$$\begin{aligned} \frac{\partial}{\partial \xi} \left(\psi_{zz}^{(1)} + \frac{S(z)}{c^2} \psi^{(1)} \right) = & -A_{\xi\xi\xi} \phi - \frac{2S}{c^3} A_T \phi \\ & - \frac{2}{c^3} S_z A A_\xi \phi^2 + \frac{2u}{c^3} A (S\phi)_{zz} + \frac{2\nu}{c^3} A_{\xi\xi} S \phi. \end{aligned} \quad (2.2.17)$$

Multiplying through equation (2.2.17) by $\phi(z)$ and integrating from $z = 0$ to $z = 1$ the left-hand side of equation (2.2.17) becomes

$$\frac{\partial}{\partial \xi} \int_{z=0}^{z=1} \phi(z) \left(\psi_{zz}^{(1)} + \frac{S(z)}{c^2} \psi^{(1)} \right) dz.$$

Integrating this expression by parts (twice) we have

$$\frac{\partial}{\partial \xi} \left[\left(\phi \psi_z^{(1)} - \phi_z \psi^{(1)} \right)_{z=0}^{z=1} + \int_{z=0}^{z=1} \psi^{(1)} \left(\phi_{zz} + \frac{S(z)}{c^2} \phi \right) dz \right]. \quad (2.2.18)$$

Applying boundary conditions (2.1.29) and equations (2.2.14) we find that (2.2.18) evaluates to zero. This imposes the compatibility condition that upon multiplying through by $\phi(z)$ and integrating from $z = 0$ to $z = 1$ the right-hand side of equation (2.2.17) must also equal to zero. Hence,

$$\int_0^1 \phi \left[-A_{\xi\xi\xi} \phi - \frac{2S}{c^3} A_T \phi - \frac{2}{c^3} S_z A A_{\xi} \phi^2 + \frac{2\mu}{c^3} A (S\phi)_{zz} + \frac{2\nu}{c^3} A_{\xi\xi} S \phi \right] dz = 0. \quad (2.2.19)$$

Equation (2.2.19) may be rewritten as the Rayleigh perturbed KdV-Burgers equation

$$A_T + \alpha A A_{\xi} + \beta A_{\xi\xi\xi} = -\gamma A + \nu A_{\xi\xi}, \quad (2.2.20)$$

where α, β, γ are defined by

$$\alpha = \frac{\int_0^1 S_z \phi^3 dz}{\int_0^1 S \phi^2 dz}, \quad (2.2.21a)$$

$$\beta = \frac{c^3}{2} \frac{\int_0^1 \phi^2 dz}{\int_0^1 S \phi^2 dz}, \quad (2.2.21b)$$

$$-\gamma = \frac{\int_0^1 \mu \phi (S\phi)_{zz} dz}{\int_0^1 S \phi^2 dz} = -\frac{\mu}{c^2} \frac{\int_0^1 (\phi_z)^2 S^2 dz}{\int_0^1 S \phi^2 dz}. \quad (2.2.21c)$$

The last equality in (2.2.21c) is obtained through integration by parts (twice) and application of equations (2.2.14).

Equation (2.2.20) describes the amplitude evolution of a perturbed solitary wave travelling in the positive x -direction. In chapter 3 an asymptotic solution to this Rayleigh perturbed KdV-Burgers equation will be developed subject to suitable initial and boundary conditions.

Chapter 3

Vertical Modes and the Asymptotic Solution to the Rayleigh Perturbed Korteweg-de Vries-Burgers Equation

3.1 The Vertical Modes

Before developing the asymptotic solution for the evolution of $A(\xi; T)$, we first determine the vertical structure, $\phi(z)$ of the streamfunction, $\psi^{(0)}(z, \xi; T)$. As shown in section 2.2, the vertical structure, $\phi(z)$, must be a solution to the eigenvalue problem

$$\phi_{zz} + \frac{S(z)}{c^2} \phi = 0, \quad (3.1.1a)$$

$$\phi(0) = \phi(1) = 0. \quad (3.1.1b)$$

The problem posed by (3.1.1) is a regular Sturm-Liouville eigenvalue problem. Hence there exists a countable infinite of real eigenvalues, $\{c_n\}_{n=0}^{n=\infty}$, such that

$$0 < c_0 < c_1 < \dots < c_n < c_{n+1} < \dots$$

Corresponding to each eigenvalue exists a unique eigenfunction, $\phi_n(z)$, which has n zeros for $0 < z < 1$. The set of eigenfunctions, $\{\phi_n\}_{n=0}^{n=\infty}$ form an orthonormal set which must satisfy the equations

$$\frac{d^2}{dz^2} \phi_n + \frac{S(z)}{c_n^2} \phi_n = 0, \quad (3.1.2a)$$

$$\int_0^1 S(z) \phi_n(z) \phi_m(z) dz = \delta_{nm}, \quad (3.1.2b)$$

where δ_{nm} represents the Kronecker delta.

With $S(z)$ defined by (2.2.6b), we introduce the new independent variable

$$t = \frac{2}{\gamma} \left[\frac{S(z)}{c^2} \right]^{1/2}, \quad (3.1.3)$$

such that

$$\phi_n(t) = \phi_n(z(t)).$$

Under the transformation (3.1.3), the eigenvalue problem (3.1.2) becomes

$$t^2 \phi_n'' + t \phi_n' + t^2 \phi_n = 0, \quad (3.1.4a)$$

(where $\phi_n' = \frac{d}{dt} \phi_n$ and $\phi_n'' = \frac{d^2}{dt^2} \phi_n$) with boundary conditions

$$\phi_n(\Lambda) = \phi_n(\Lambda e^{\gamma/2}) = 0, \quad (3.1.4b)$$

and orthonormal condition

$$\frac{c^2 \gamma}{2} \int_{\Lambda}^{\Lambda e^{\gamma/2}} t \phi_n(t) \phi_m(t) dt = \delta_{nm}, \quad (3.1.4c)$$

in which

$$\Lambda = t|_{z=0} = \frac{2S_0 e^{-\gamma/2}}{\gamma c}. \quad (3.1.5)$$

Equation (3.1.4a) is Bessel's equation of order zero. Hence, the solution may be written in terms of Bessel functions of the first and second kind, i.e.,

$$\phi_n(t) = A_n J_0(t) + B_n Y_0(t). \quad (3.1.6a)$$

Applying the boundary conditions (3.1.4b), we have

$$\begin{aligned} A_n J_0(\Lambda) + B_n Y_0(\Lambda) &= 0, \\ A_n J_0(\Lambda e^{\gamma/2}) + B_n Y_0(\Lambda e^{\gamma/2}) &= 0, \end{aligned} \quad (3.1.6b)$$

from which we find that a nontrivial solution will exist if and only if Λ satisfies

$$J_0(\Lambda) Y_0(\Lambda e^{\gamma/2}) - J_0(\Lambda e^{\gamma/2}) Y_0(\Lambda) = 0. \quad (3.1.7)$$

Having determined the values of Λ for which nontrivial solutions exist, we may find the eigenvalues c_n of (3.1.1) by inverting (3.1.5) so that

$$c_n = \frac{2S_0 e^{-\gamma/2}}{\gamma \Lambda_n}, \quad (3.1.8)$$

where Λ_n is the n^{th} denumerable numeric solution of (3.1.7).

The first five roots, $\Lambda_0, \Lambda_1, \Lambda_2, \Lambda_3, \Lambda_4$ of equation (3.1.7) were found numerically and are given below along with the corresponding eigenvalues, c_0, c_1, c_2, c_3, c_4 , with values $S_0 = 0.1$, $\gamma = 4.0$.

n	Λ_n	c_n
0	0.4717	0.0717
1	0.9702	0.0349
2	1.4653	0.0231
3	1.9591	0.0173
4	2.4522	0.0138

Having determined the eigenvalues, it remains to determine the constants A_n and B_n of the solution (3.1.6). It is known (Abramowitz and Stegun, 1967, equation (11.3.31)) that

$$\int^z t^{\mu+\nu+1} C_\mu(t) \mathcal{D}_\nu(t) dt = \frac{z^{\mu+\nu+2}}{2(\mu+\nu+1)} \{C_\mu(z) \mathcal{D}_\nu(z) + C_{\mu+1}(z) \mathcal{D}_{\nu+1}(z)\}, \quad (3.1.9)$$

where $C_\mu(z)$ and $\mathcal{D}_\nu(z)$ represent any two cylinder functions of order μ and ν respectively. Upon substitution of (3.1.6a) into (3.1.4c), the orthonormal condition becomes

$$\frac{c_n^2 \gamma}{2} \int_{\Lambda_n}^{\Lambda_n e^{\gamma/2}} t [A_n J_0(t) + B_n Y_0(t)]^2 dt = 1,$$

or, equivalently,

$$\begin{aligned} \frac{c_n^2 \gamma}{2} \int_{\Lambda_n}^{\Lambda_n e^{\gamma/2}} t A_n^2 J_0^2(t) dt + \frac{c_n^2 \gamma}{2} \int_{\Lambda_n}^{\Lambda_n e^{\gamma/2}} 2t A_n B_n J_0(t) Y_0(t) dt \\ + \frac{c_n^2 \gamma}{2} \int_{\Lambda_n}^{\Lambda_n e^{\gamma/2}} t B_n^2 Y_0^2(t) dt = 1. \end{aligned}$$

Since the Bessel functions $J_0(t)$ and $Y_0(t)$ are both cylinder functions, we have upon applying the identity (3.1.9)

$$\begin{aligned} & \frac{c_n^2 \gamma}{2} A_n^2 \frac{t^2}{2} \left[J_0^2(t) + J_1^2(t) \right] \Big|_{\Lambda_n}^{\Lambda_n e^{\gamma/2}} \\ & + \frac{c_n^2 \gamma}{2} 2A_n B_n \frac{t^2}{2} \left[J_0(t)Y_0(t) + J_1(t)Y_1(t) \right] \Big|_{\Lambda_n}^{\Lambda_n e^{\gamma/2}} \\ & + \frac{c_n^2 \gamma}{2} B_n^2 \frac{t^2}{2} \left[Y_0^2(t) + Y_1^2(t) \right] \Big|_{\Lambda_n}^{\Lambda_n e^{\gamma/2}} = 1. \end{aligned} \quad (3.1.10)$$

From the boundary conditions (3.1.6b) we have

$$A_n = \frac{-[Y_0(\Lambda_n) + Y_0(\Lambda_n e^{\gamma/2})]}{[J_0(\Lambda_n) + J_0(\Lambda_n e^{\gamma/2})]} B_n, \quad (3.1.11)$$

so that upon substitution of (3.1.11) into (3.1.10) we have

$$\begin{aligned} & \frac{c_n^2 \gamma}{2} \left\{ K_n^2 B_n^2 \frac{t^2}{2} [J_0^2(t) + J_1^2(t)] \right. \\ & \quad + 2K_n B_n^2 \frac{t^2}{2} [J_0(t)Y_0(t) + J_1(t)Y_1(t)] \\ & \quad \left. + B_n^2 \frac{t^2}{2} [Y_0^2(t) + Y_1^2(t)] \right\} \Big|_{\Lambda_n}^{\Lambda_n e^{\gamma/2}} = 1. \end{aligned} \quad (3.1.12)$$

Solving (3.1.12) for B_n yields

$$\begin{aligned} B_n = \frac{2}{c_n \gamma^{1/2}} & \left[\left\{ K_n^2 t^2 [J_0^2(t) + J_1^2(t)] \right. \right. \\ & \quad + 2K_n t^2 [J_0(t)Y_0(t) + J_1(t)Y_1(t)] \\ & \quad \left. \left. + t^2 [Y_0^2(t) + Y_1^2(t)] \right\} \Big|_{\Lambda_n}^{\Lambda_n e^{\gamma/2}} \right]^{-1/2}, \end{aligned} \quad (3.1.13a)$$

where K_n is defined by

$$K_n = \frac{-[Y_0(\Lambda_n) + Y_0(\Lambda_n e^{\gamma/2})]}{[J_0(\Lambda_n) + J_0(\Lambda_n e^{\gamma/2})]}. \quad (3.1.13b)$$

In summary, the eigenfunctions are given by

$$\phi_n(t) = A_n J_0(t) + B_n Y_0(t), \quad (3.1.14a)$$

where

$$A_n = K_n B_n, \quad (3.1.14b)$$

$$B_n = \frac{2}{c_n \gamma^{1/2}} \left[\left\{ K_n^2 t^2 [J_0^2(t) + J_1^2(t)] \right. \right. \\ \left. \left. + 2K_n t^2 [J_0(t)Y_0(t) + J_1(t)Y_1(t)] \right. \right. \\ \left. \left. + t^2 [Y_0^2(t) + Y_1^2(t)] \right\} \left| \frac{\Lambda_n e^{\gamma/2}}{\Lambda_n} \right|^{-1/2} \right], \quad (3.1.14c)$$

in which

$$K_n = \frac{-[Y_0(\Lambda_n) + Y_0(\Lambda_n e^{\gamma/2})]}{[J_0(\Lambda_n) + J_0(\Lambda_n e^{\gamma/2})]},$$

and

$$c_n = \frac{2S_0 e^{-\gamma/2}}{\gamma \Lambda_n}, \quad (3.1.14d)$$

where Λ_n satisfies

$$J_0(\Lambda_n)Y_0(\Lambda_n e^{\gamma/2}) - J_0(\Lambda_n e^{\gamma/2})Y_0(\Lambda_n) = 0. \quad (3.1.14e)$$

The first three vertical modes are shown in Figure 2. Since the original governing equations are nonlinear, the principle of superposition does not apply and all subsequent calculations involving the vertical structure of the streamfunction are done using the gravest mode (ϕ_0 solution).

3.2 Time Dependent Evolution of the Streamfunction

Having determined the structure of the vertical modes, $\phi(z)$, we must now determine the evolution of $A(\xi; T)$ to determine fully the streamfunction $\psi(z, \xi; T)$ (recall that $\psi(z, \xi; T)$ was chosen in chapter 2 to have the separable form $\psi(z, \xi; T) = \phi(z)A(\xi; T)$). The function $A(\xi; T)$ evolves according to the Rayleigh perturbed KdV-Burgers equation

$$A_T + \alpha A A_\xi + \beta A_{\xi\xi\xi} = -\gamma A + \nu A_{\xi\xi}, \quad (3.2.1)$$

which is a solvability condition on the $O(\varepsilon)$ problem as shown in section 2.2. Under the transformation

$$\begin{aligned} A &= \beta^{\frac{1}{3}} \left(\frac{-6}{\alpha} \right)^{\frac{2}{3}} q, \quad T' = \beta^{\frac{1}{3}} \left(\frac{-6}{\alpha} \right)^{\frac{2}{3}} T, \\ \xi' &= \left(\frac{-6\beta^2}{\alpha} \right)^{\frac{1}{3}} \xi, \end{aligned}$$

equation (3.2.1) becomes

$$q_{T'} - 6qq_{\xi'} + q_{\xi'\xi'\xi'} = -\gamma' q + \nu' q_{\xi\xi}, \quad (3.2.1')$$

where $\gamma' = \gamma \beta^{\frac{1}{3}} \left(\frac{-6}{\alpha} \right)^{\frac{2}{3}}$ and $\nu' = \nu \left(\frac{6}{\alpha\beta} \right)^{\frac{2}{3}}$.

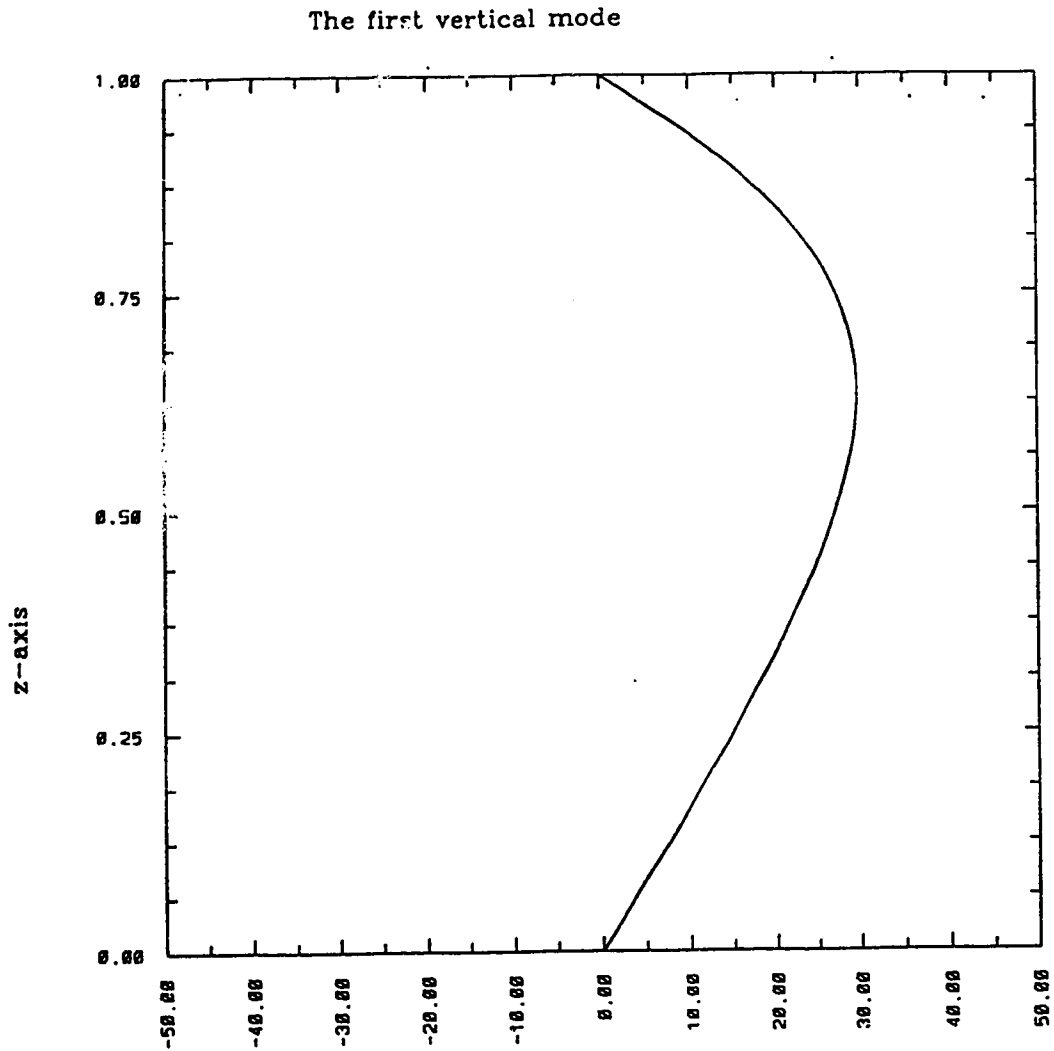


Figure 2: The Vertical Modes

Figures 2a, 2b, and 2c show the first three vertical modes ϕ_0 , ϕ_1 , and ϕ_2 , respectively. The vertical modes ϕ_0 , ϕ_1 , and ϕ_2 correspond, respectively, to the eigenvalues $c_0 = 0.0717$, $c_1 = 0.0349$, $c_2 = 0.0231$ with $S_0 = 0.1$ and $\gamma = 4.0$.

The second vertical mode

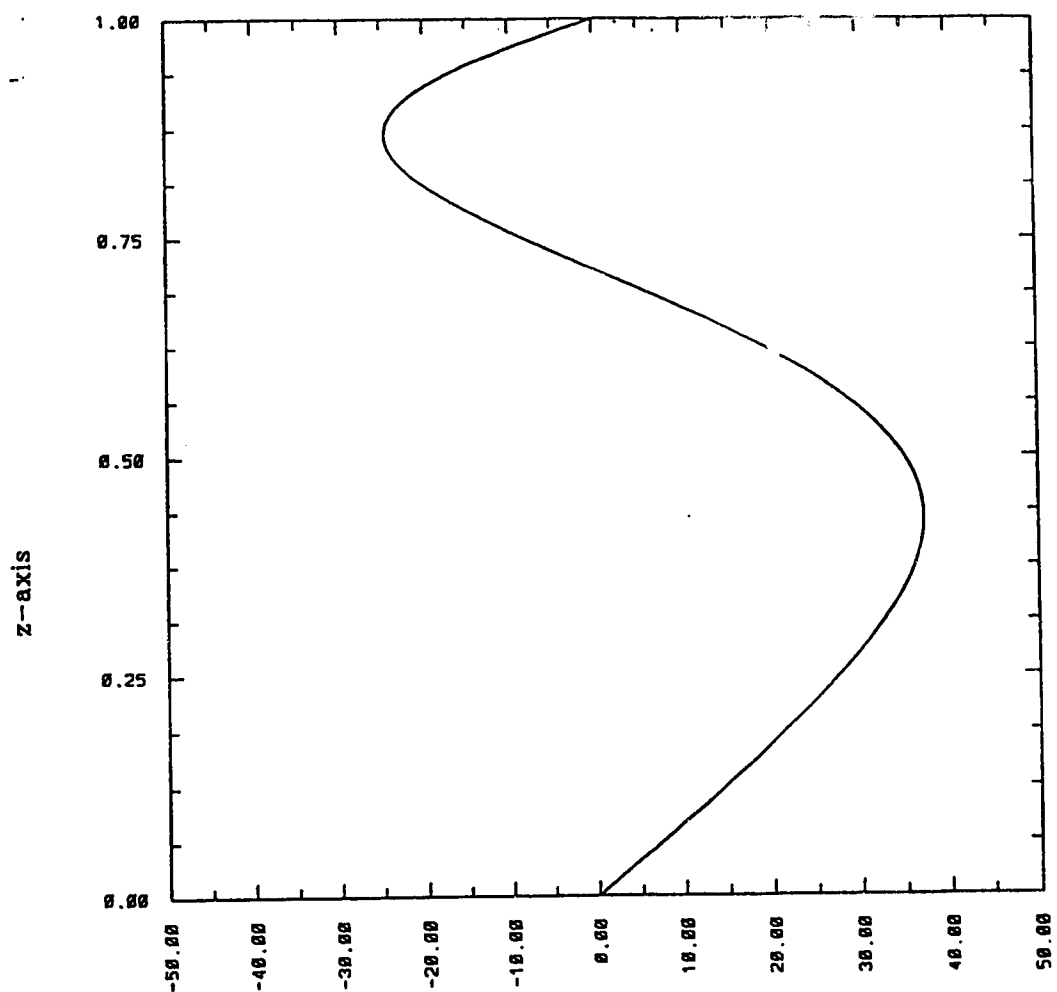


Figure 2b

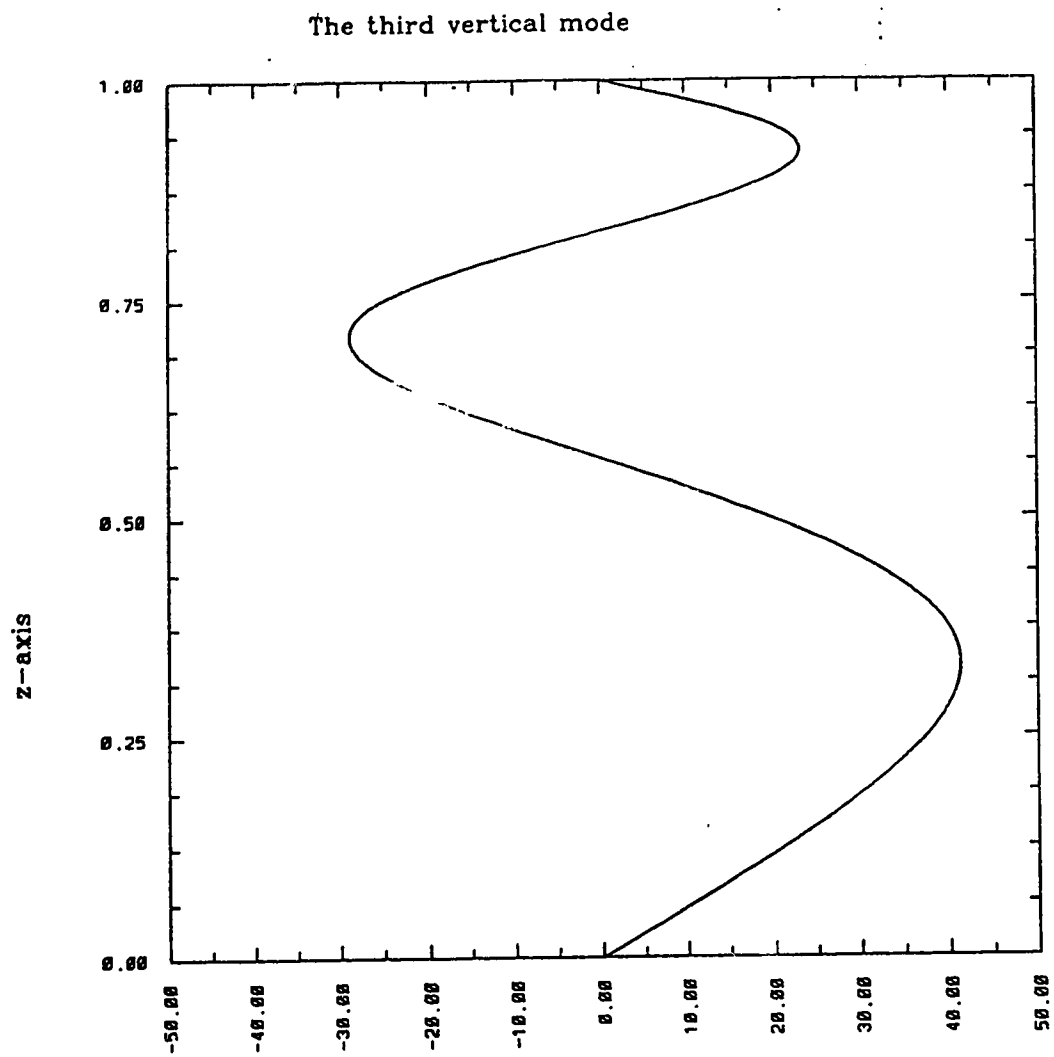


Figure 2c

In developing a solution to equation (3.2.1') we follow the procedure of Swaters and Sawatzky (1989) and break the solution region into five subregions. Equation (3.2.1') is then solved asymptotically in each of these regions; the final solution is then given by the sum of each individual region minus the contributions in the overlap zones between each region (Bender and Orszag, 1978). The various solutions regions are: 1) the $O(1)$ -amplitude main pulse; 2) the shelf region which emerges behind the main pulse; 3) the dispersive wave-tail describing the transition from the shelf to the zero-state; 4) the near field ahead of the main pulse; and 5) the far field ahead of the main pulse (Figure 3).

For notational simplicity we again drop the primes from equation (3.2.1') and rewrite it as

$$q_T - 6qq_\xi + q\xi\xi\xi = \nu(-\mu q + q\xi\xi), \quad (3.2.2)$$

where $\mu = \frac{\gamma'}{\nu} \simeq O(1)$ and we assume $\nu \ll 1$.

3.2.1 Evolution of the main $O(1)$ pulse

In the absence of forcing ($\nu \equiv 0$) the single soliton solution to (3.2.2) is given by (Kodama and Ablowitz, 1981)

$$q = -2\eta^2 \text{sech}^2 [\eta(\xi - 4\eta^2 T - \theta_0)]. \quad (3.2.3)$$

This represents a soliton with maximum amplitude $2\eta^2$ propagating at speed $4\eta^2$. The parameters η and θ_0 are taken to be real with θ_0 representing a possible phase shift. The unperturbed soliton is shown in Figure 4. The solution to (3.2.2) in region 1 (the solution region about the propagating main pulse) is constructed as follows.

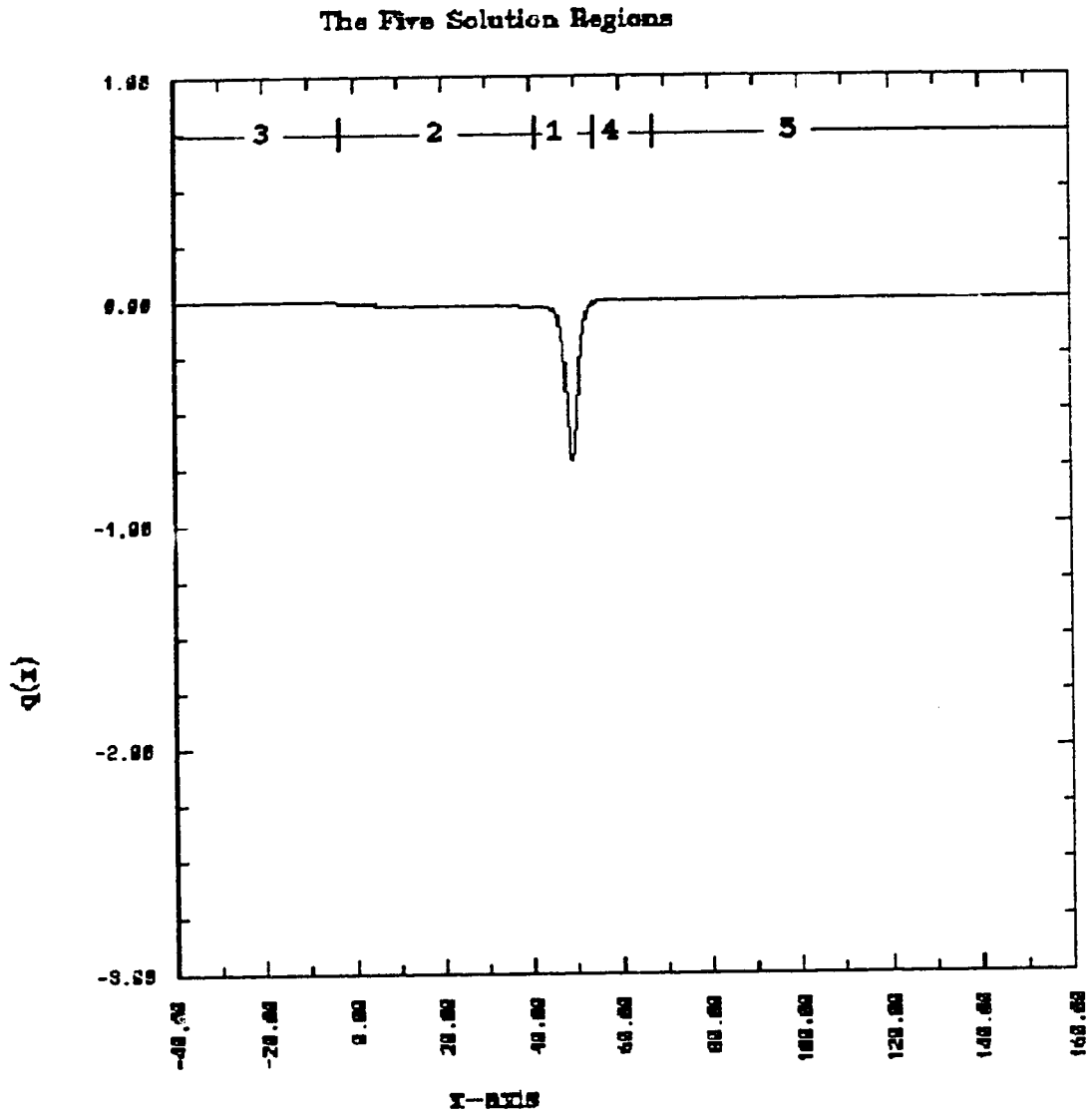


Figure 3: The Solution Regions

The five solution regions are shown graphically above. The solution regions are: 1) the $O(1)$ -amplitude main pulse; 2) the shelf region; 3) the dispersive wavetail; 4) the near field ahead of the main pulse; and 5) the far field ahead of the main pulse.

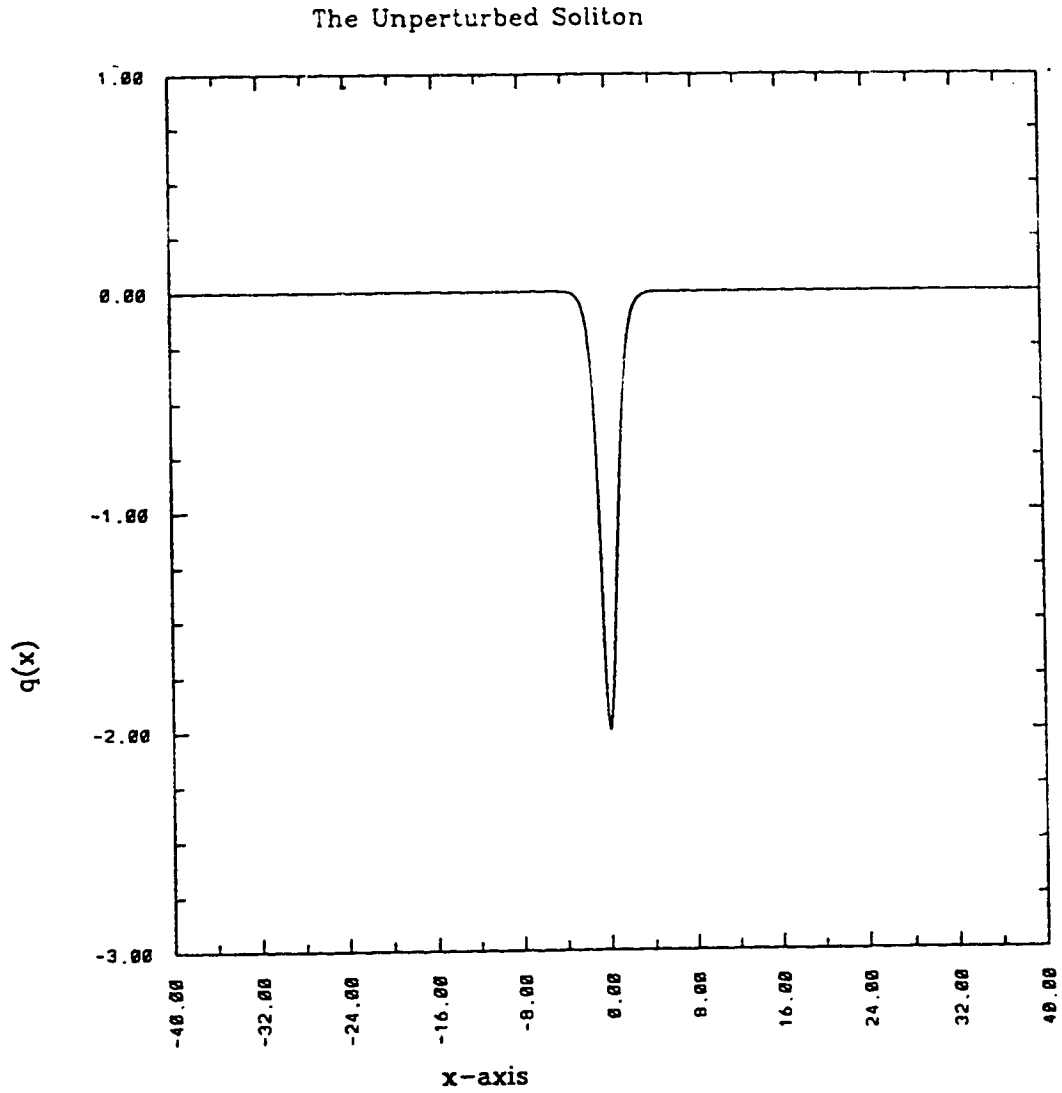


Figure 4: The Unperturbed Soliton Solution

The main pulse is assumed to dissipate adiabatically. Hence, to determine the evolution of the pulse over time scales $O\left(\frac{1}{\nu}\right)$, we now introduce the slow time variable

$$\chi = \nu T, \quad (3.2.4a)$$

where we take $\nu \ll 1$.

It is also convenient to introduce the comoving fast phase variable

$$\theta = \xi - \frac{4}{\nu} \int_0^{\nu T} \eta^2(\tau) d\tau, \quad (3.2.4b)$$

with derivatives

$$\theta_\xi = 1, \quad \theta_T = -4\eta^2(\chi), \quad \chi_T = \nu. \quad (3.2.4c)$$

In terms of this adiabatic comoving coordinate system, a multiple scales perturbation solution to (3.2.2) in the form

$$q \sim q^{(0)}(\theta; \chi) + \nu q^{(1)}(\theta; \chi) + \dots, \quad (3.2.5)$$

may be constructed. The assumption that the parameter η (the propagation velocity) is a function of slow time only, i.e. $\eta = \eta(\chi)$, is consistent with the work of Kodama and Ablowitz (1981) where this dependence was shown as a solvability condition for the perturbation expansion (3.2.5). Solvability conditions also show that the phase shift, θ_0 , is also a function of slow time only so that

$$\theta_0 \equiv \theta_0(\chi). \quad (3.2.6a)$$

Without loss of generality we take

$$\theta_0(0) = 0; \quad (3.2.6b)$$

that is, we assume that at $t = 0$ the main pulse is centered at $x = 0$.

Substituting (3.2.4) into (3.2.2) we have

$$-4\eta^2 q_\theta - 6qq_\theta + q_{\theta\theta\theta} = \nu[-\mu q + q_{\theta\theta} - q_\chi]. \quad (3.2.7)$$

With the expansion (3.2.5) the $O(1)$ problem for (3.2.7) becomes

$$-4\eta^2 q_\theta^{(0)} - 6q^{(0)} q_\theta^{(0)} + q_{\theta\theta\theta}^{(0)} = 0, \quad (3.2.8)$$

which has the soliton solution

$$q^{(0)} = -2\eta^2 \text{sech}^2[\eta(\theta - \theta_0)]. \quad (3.2.9)$$

The $O(\nu)$ problem for (3.2.7) is given by:

$$-4\eta^2 q_\theta^{(1)} - 6[q^{(0)} q^{(1)}]_\theta + q_{\theta\theta\theta}^{(1)} = -\mu q^{(0)} + q_{\theta\theta}^{(0)} - q_\chi^{(0)}, \quad (3.2.10a)$$

where

$$q_\chi^{(0)} = \frac{1}{\eta} \eta_\chi [2q^{(0)} + (\theta - \theta_0) q_\theta^{(0)}] - \theta_{0\chi} q_\theta^{(0)}. \quad (3.2.10b)$$

Before deriving an exact solution to (3.2.10a) we determine the evolution of $\eta(\chi)$ and $\theta_0(\chi)$.

Following Kodama and Ablowitz (1981) and Swaters and Sawatzky (1989), we determined the governing equation for $\eta(\chi)$ as follows. We rewrite equation (3.2.10a) in the operator form

$$\mathcal{L}(q^{(1)}) = F(q^{(0)}), \quad (3.2.11a)$$

where

$$\mathcal{L}(q^{(1)}) := -4\eta^2 q_\theta^{(1)} - 6[q^{(0)} q^{(1)}]_\theta + q_{\theta\theta\theta}^{(1)}, \quad (3.2.11b)$$

and

$$F(q^{(0)}) := -\mu q^{(0)} + q_{\theta\theta}^{(0)} - q_x^{(0)}. \quad (3.2.11c)$$

The adjoint operator associated with \mathcal{L} , denoted \mathcal{L}^A , is defined by

$$(v, \mathcal{L}(u)) = (\mathcal{L}^A(v), u), \quad (3.2.12a)$$

where (u, v) represents the inner product defined by

$$(u, v) = \int_{-\infty}^{\infty} u v d\theta, \quad (3.2.12b)$$

and u, v are test functions satisfying the boundary conditions

$$\lim_{\theta \rightarrow \pm\infty} u, v = 0, \quad \text{and} \quad \lim_{\theta \rightarrow \pm\infty} u_\theta, v_\theta = 0. \quad (3.2.12c)$$

It follows from (3.2.12) that the adjoint operator, \mathcal{L}^A , must satisfy

$$\int_{-\infty}^{\infty} (u \mathcal{L}^A(v) - v \mathcal{L}(u)) d\theta = 0,$$

or, equivalently,

$$\int_{-\infty}^{\infty} u \mathcal{L}^A(v) d\theta = \int_{-\infty}^{\infty} v \mathcal{L}(u) d\theta. \quad (3.2.13)$$

From (3.2.11b) we see that the right-hand side of (3.2.13) becomes

$$\int_{-\infty}^{\infty} v [-4\eta^2 u_\theta - 6(q^{(0)} u)_\theta + u_{\theta\theta\theta}] d\theta. \quad (3.2.14)$$

Integrating by parts and applying boundary conditions (3.2.12c), we find that the integral (3.2.14) is equal to

$$\int_{-\infty}^{\infty} u [4\eta^2 v_\theta + 6q^{(0)} v_\theta - v_{\theta\theta\theta}] d\theta. \quad (3.2.15)$$

Hence, given definition (3.2.12), it follows from (3.2.15) that the adjoint operator, \mathcal{L}^A , is given by

$$\mathcal{L}^A w = 4\eta^2 w_\theta + 6q^{(0)} w_\theta - w_{\theta\theta\theta}. \quad (3.2.16)$$

We observe that the adjoint operator is the negative of the KdV operator corresponding to equation (3.2.8) which has solution, $q^{(0)}$, given by (3.2.9). Since the solution (3.2.9) is an element of the kernel of the homogeneous adjoint operator (3.2.16), i.e. $\mathcal{L}^A(q^{(0)}) = 0$, for there to exist a nontrivial solution, the forcing function $F(q^{(0)})$ (as defined by (3.2.11c)) must be orthogonal to $q^{(0)}$ (the Fredholm Alternative). Thus $F(q^{(0)})$ must satisfy

$$\int_{-\infty}^{\infty} q^{(0)} F(q^{(0)}) d\theta = 0,$$

i.e.,

$$\int_{-\infty}^{\infty} \left\{ -\mu q^{(0)2} + q^{(0)} q_{\theta\theta}^{(0)} - q^{(0)} q_\chi^{(0)} \right\} d\theta = 0. \quad (3.2.17)$$

Substituting (3.2.9) into (3.2.17) and integrating we have

$$-\frac{16}{3}\mu\eta^3 - \frac{64}{15}\eta^5 - 8\eta^2\eta_\chi,$$

or equivalently,

$$\eta_\chi = -\frac{2}{3}\mu\eta - \frac{8}{15}\eta^3. \quad (3.2.18)$$

Equation (3.2.18) may be integrated immediately to give

$$\begin{aligned} -\chi &= \int_{\eta=\eta(0)}^{\eta=\eta(x)} \frac{d\eta}{\frac{2}{3}\mu\eta + \frac{8}{15}\eta^3} \\ &= \int_{\eta=\eta(0)}^{\eta=\eta(x)} \frac{-\frac{4}{5}\eta d\eta}{\frac{2}{3}\mu + \frac{8}{15}\eta^2} + \int_{\eta=\eta(0)}^{\eta=\eta(x)} \frac{\frac{3}{2}\mu d\eta}{\eta} \end{aligned}$$

$$= -\frac{4}{5\mu} \frac{15}{16} \ln \left| \frac{2\mu}{3} \right| + \frac{8}{15} \eta^3 \left| \frac{\eta=\eta(\chi)}{\eta=\eta(0)} \right| + \frac{3}{2\mu} \ln |\eta| \left| \frac{\eta=\eta(\chi)}{\eta=\eta(0)} \right|. \quad (3.2.19)$$

Solving (3.2.19) for $\eta(\chi)$ we have

$$\eta(\chi) = \left[\frac{10\mu\eta^2(0)e^{-4\mu\chi/3}}{10\mu - 8\eta^2(0)(e^{-4\mu\chi/3} - 1)} \right]^{\frac{1}{2}}, \quad (3.2.20)$$

where $\eta(0)$ is defined by $\eta(\chi = 0)$, (the initial condition on $\eta(\chi)$). The amplitude evolution is shown in Figure 5.

The evolution equation for the phase shift, $\theta_0(\chi)$, may be determined following Karpman and Maslov (1978). From the IST (inverse scattering transform) formalism developed by Karpman and Maslov, the evolution of the phase shift is given by

$$\theta_{0\chi} = \frac{-1}{4\eta^3} \int_{-\infty}^{\infty} (-\mu q^{(0)}(z) + q_{\theta\theta}^{(0)}(z))(z \operatorname{sech}^2 z + \tanh z + \tanh^2 z) dz, \quad (3.2.21)$$

where $z = \eta(\theta - \theta_0)$, with $q^{(0)}(z)$ given by (3.2.9) as

$$q^{(0)} = -2\eta^2 \operatorname{sech}^2 z.$$

Therefore

$$\begin{aligned} \theta_{0\chi} &= \frac{\mu}{2\eta} \int_{-\infty}^{\infty} \operatorname{sech}^2 z (z \operatorname{sech}^2 z + \tanh z + \tanh^2 z) dz \\ &\quad - \eta \int_{-\infty}^{\infty} \operatorname{sech}^4 z (z \operatorname{sech}^2 z + \tanh z + \tanh^2 z) dz \\ &\quad + 2\eta \int_{-\infty}^{\infty} \operatorname{sech}^2 z \tanh^2 z (z \operatorname{sech}^2 z + \tanh z + \tanh^2 z) dz. \end{aligned} \quad (3.2.22a)$$

Evaluation of the integrals in (3.2.22a) yields

$$\theta_{0\chi} = \frac{-\mu}{3\eta} + \frac{8\eta}{15}. \quad (3.2.22b)$$

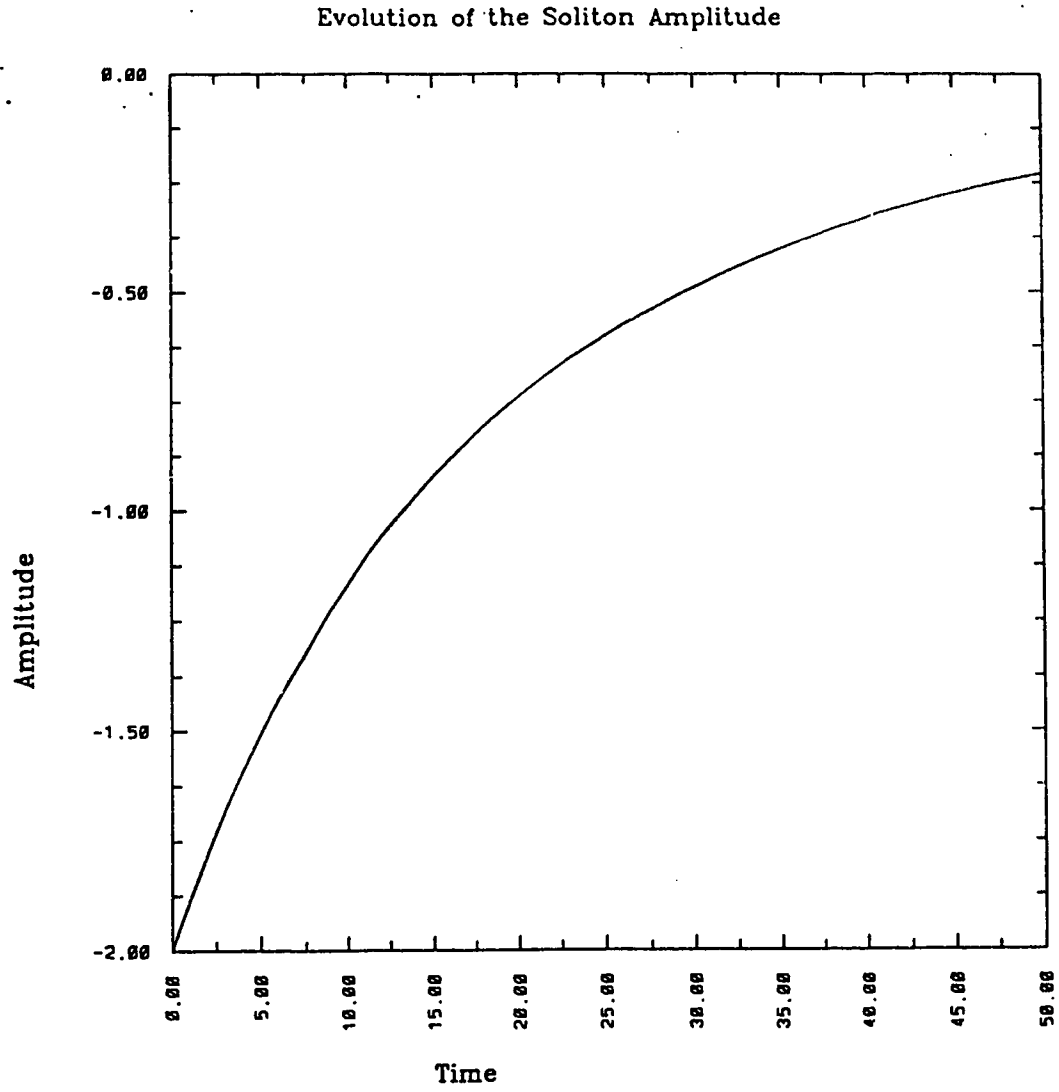


Figure 5: Amplitude Evolution

The amplitude evolution of the decaying soliton with parameters $\mu = 1.0$, $\nu = \frac{1}{40}$ (Figure 5a) and $\mu = 1.0$, $\nu = \frac{1}{100}$ (Figure 5b).

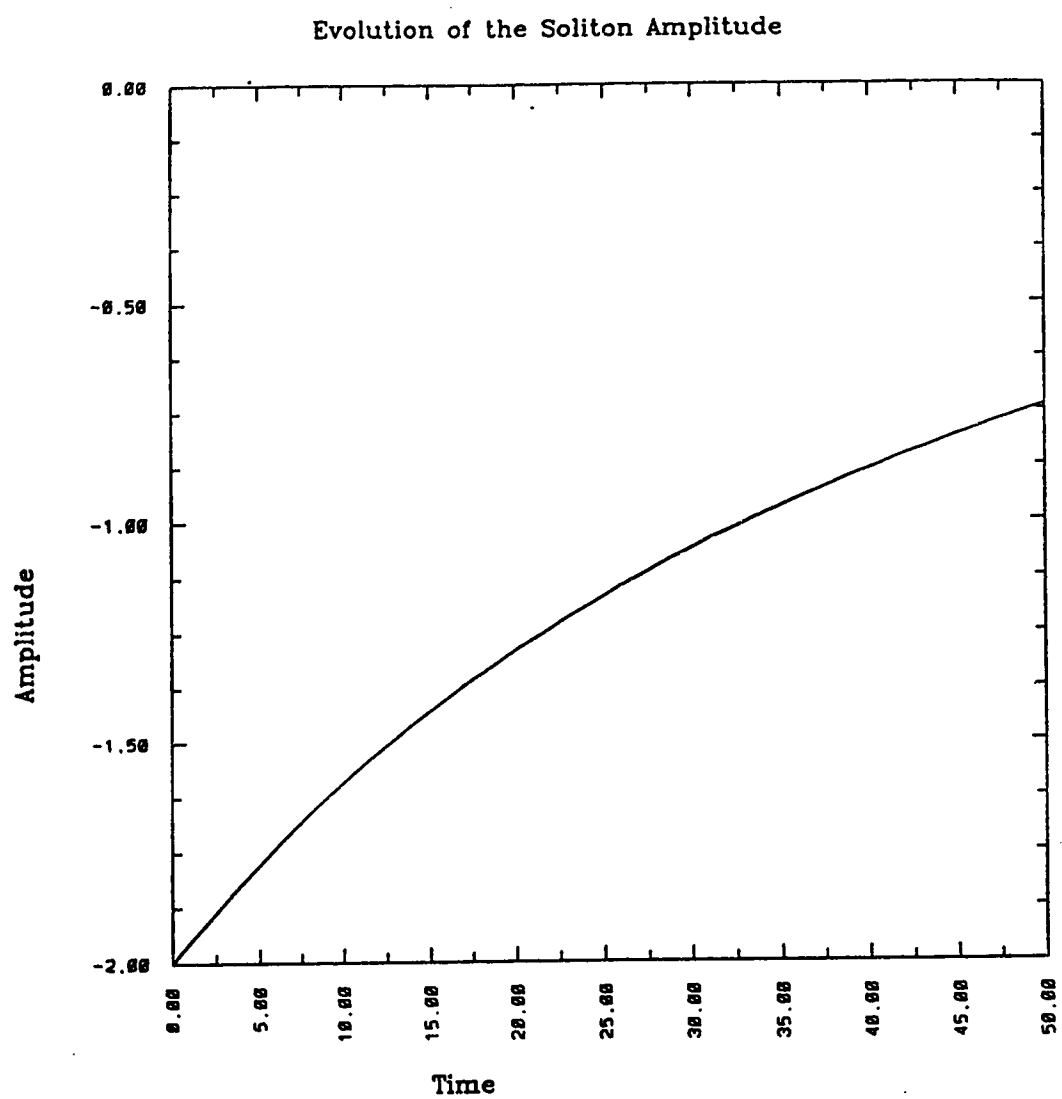


Figure 5b

Hence, given (3.2.20) we have

$$\begin{aligned}\theta_0 = & \int_0^x \frac{-\mu}{3} \left[\frac{10\mu - 8\eta^2(0)(e^{-4\mu x'/3} - 1)}{10\mu\eta^2(0)e^{-4\mu x'/3}} \right]^{\frac{1}{2}} d\chi' \\ & + \int_0^x \frac{8}{15} \left[\frac{10\mu\eta^2(0)e^{-4\mu x'/3}}{10\mu - 8\eta^2(0)(e^{-4\mu x'/3} - 1)} \right]^{\frac{1}{2}} d\chi'.\end{aligned}\quad (3.2.23)$$

From (3.2.23) it follows that

$$\begin{aligned}\theta_0(\chi) = & \frac{1}{2} \left(\frac{4}{5\mu} \right)^{\frac{1}{2}} \left\{ -3 \arcsin \left[\left(\frac{8\eta^2(0)e^{-4\mu\chi/3}}{10\mu + 8\eta^2(0)} \right)^{\frac{1}{2}} \right] \right. \\ & + 3 \arcsin \left[\left(\frac{8\eta^2(0)}{10\mu + 8\eta^2(0)} \right)^{\frac{1}{2}} \right] \\ & \left. - \left[\frac{10\mu - 8\eta^2(0)(e^{-4\mu\chi/3} - 1)}{8\eta^2(0)e^{-4\mu\chi/3}} \right]^{\frac{1}{2}} + \left[\frac{5\mu}{4\eta^2(0)} \right]^{\frac{1}{2}} \right\}.\end{aligned}\quad (3.2.24)$$

The evolution of the phase shift is depicted in Figure 6.

The leading order behaviour of the dissipating solitary wave is completely described by (3.2.9), (3.2.20) and (3.2.24), restated below for summary:

$$\begin{aligned}q^{(0)} = & -2\eta^2 \text{sech}^2[\eta(\theta - \theta_0)], \\ \eta(\chi) = & \left[\frac{10\mu\eta^2(0)e^{-4\mu\chi/3}}{10\mu - 8\eta^2(0)(e^{-4\mu\chi/3} - 1)} \right]^{\frac{1}{2}}, \\ \theta_0(\chi) = & \frac{1}{2} \left(\frac{4}{5\mu} \right)^{\frac{1}{2}} \left\{ -3 \arcsin \left[\left(\frac{8\eta^2(0)e^{-4\mu\chi/3}}{10\mu + 8\eta^2(0)} \right)^{\frac{1}{2}} \right] \right. \\ & + 3 \arcsin \left[\left(\frac{8\eta^2(0)}{10\mu + 8\eta^2(0)} \right)^{\frac{1}{2}} \right] \\ & \left. - \left[\frac{10\mu - 8\eta^2(0)(e^{-4\mu\chi/3} - 1)}{8\eta^2(0)e^{-4\mu\chi/3}} \right]^{\frac{1}{2}} + \left[\frac{5\mu}{4\eta^2(0)} \right]^{\frac{1}{2}} \right\}.\end{aligned}$$

3.2.2 The perturbation field

Having fully determined the leading order behaviour, we now construct a closed form solution for the perturbation field given by equation (3.2.10a). Integrating (3.2.10a) with respect to θ we have (upon substitution of (3.2.9))

$$\begin{aligned}
& \{-4\eta^2 + 12\eta^2 \text{sech}^2[\eta(\theta - \theta_0)] + \partial_{\theta\theta}\} q^{(1)} \\
&= \frac{-2\mu}{3} \eta \tanh[\eta(\theta - \theta_0)] + \frac{44}{15} \eta^3 \tanh[\eta(\theta - \theta_0)] \\
&\quad + \frac{4\mu}{3} (\theta - \theta_0) \eta^2 \text{sech}^2[\eta(\theta - \theta_0)] - 2\theta_0 \chi \eta^2 \text{sech}^2[\eta(\theta - \theta_0)] \\
&\quad - \frac{16}{15} (\theta - \theta_0) \eta^4 \text{sech}^2[\eta(\theta - \theta_0)] - 4\eta^3 \tanh^3[\eta(\theta - \theta_0)] \\
&\quad + \Gamma(\chi),
\end{aligned} \tag{3.2.25}$$

where $\Gamma(\chi)$ is a constant (dependent on χ) of integration.

Demanding that the perturbation field vanish as $\theta \rightarrow \infty$ so that ahead of the main pulse there is no disturbance (i.e. $q^{(1)} \rightarrow 0$ as $\theta \rightarrow \infty$) we find that

$$\Gamma(\chi) = \frac{16\eta^3}{15}. \tag{3.2.26}$$

With $\Gamma(\chi)$ given by (3.2.26) and taking the limit as $\theta \rightarrow -\infty$ of (3.2.25) we see that

$$\lim_{\theta \rightarrow -\infty} q^{(1)}(\theta, \chi) \rightarrow \frac{-\mu}{3\eta} - \frac{8\eta}{15}. \tag{3.2.27}$$

Equation (3.2.27) indicates the emergence of a shelf region behind the solitary wave. Physically this shelf is formed since the perturbed soliton cannot simultaneously satisfy both mass and energy balance laws.

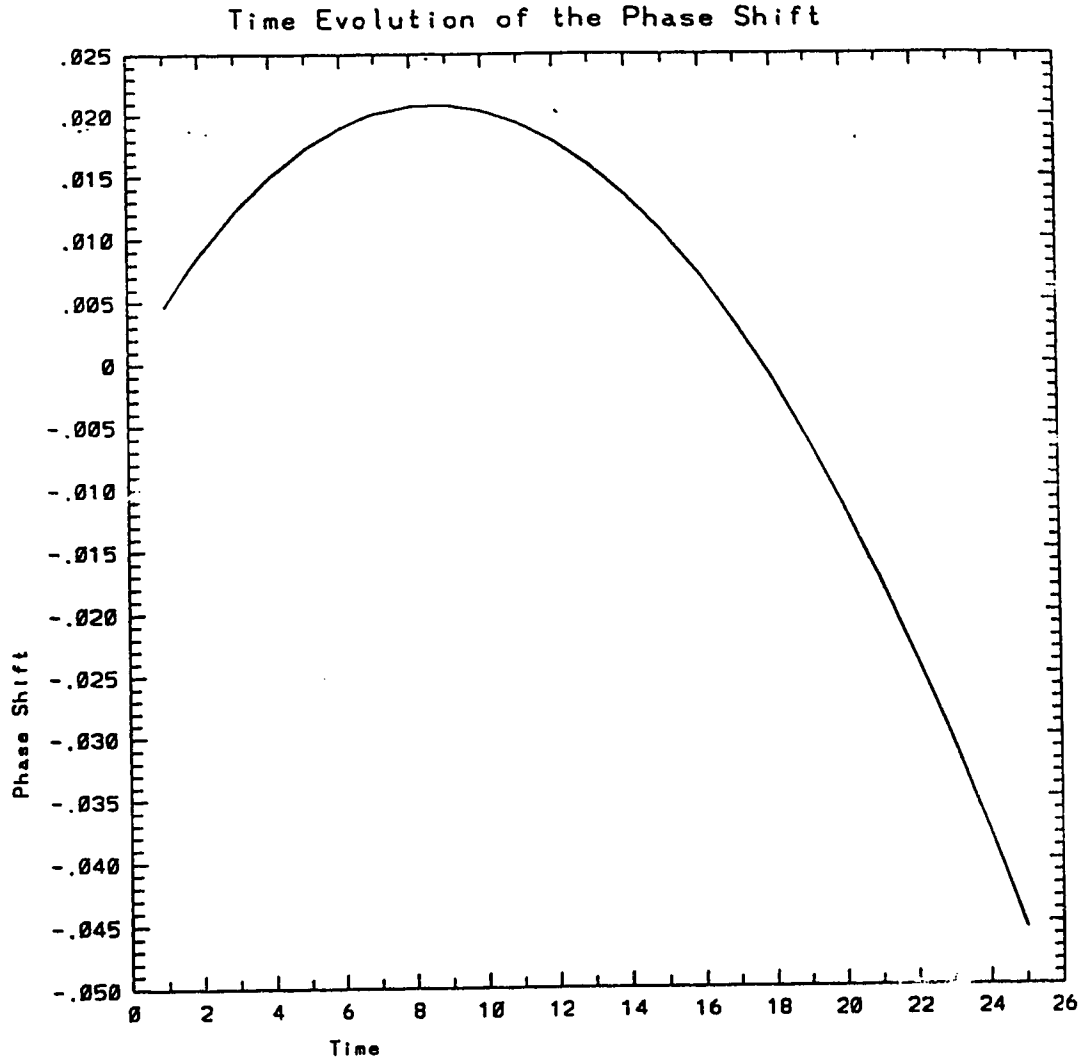


Figure 6: Phase Shift Evolution

The phase shift evolution of the decaying soliton with parameters $\mu = 1.0$ and $\nu = \frac{1}{40}$ (Figure 6a) and $\mu = 1.0$, $\nu = \frac{1}{100}$ (Figure 6b).

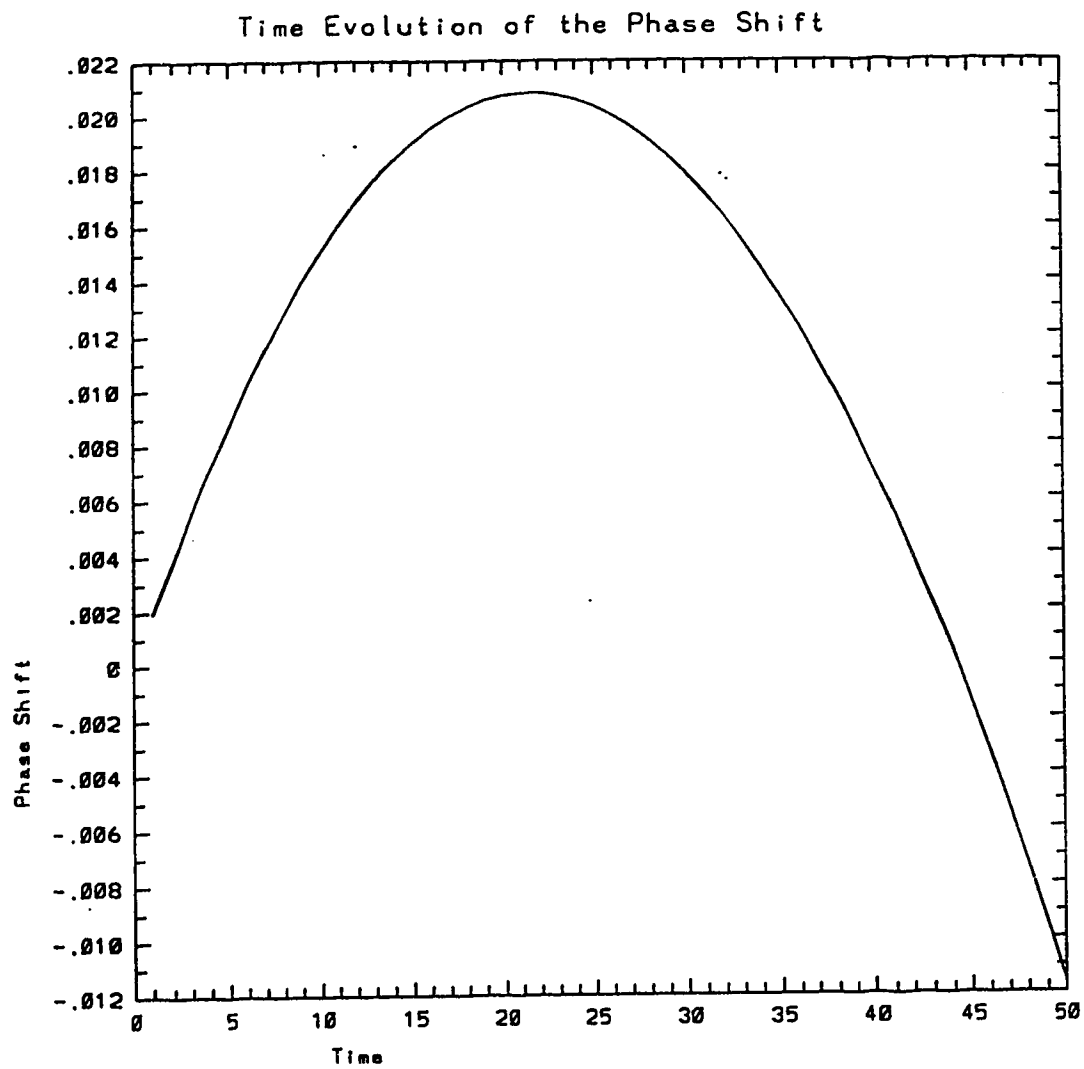


Figure 6b

Equation (3.2.25) may now be solved for $q^{(1)}(\theta, \chi)$ given $\Gamma(\chi) = \frac{2\mu\eta}{3} + \frac{16\eta^3}{15}$. Following Kodama and Ablowitz (1981) and Swaters and Sawatzky (1989), we substitute

$$\xi = \tanh[\eta(\theta - \theta_0)] \quad (3.2.28)$$

into (3.2.25) to get

$$\begin{aligned} [12 - 4(1 - \xi^2)^{-1}]q^{(1)} + [q_\xi^{(1)}(1 - \xi^2)]_\xi \\ = \frac{2\mu}{3\eta}(1 + \xi)^{-1} + \frac{2\mu}{3\eta} \ln\left(\frac{1 + \xi}{1 - \xi}\right) - \frac{8}{15}\eta \ln\left(\frac{1 + \xi}{1 - \xi}\right) \\ + \left(4\xi^2 + 4\xi + \frac{16}{15}\right)(1 + \xi)^{-1}\eta - 2\theta_{0\chi}. \end{aligned} \quad (3.2.29)$$

The homogeneous problem corresponding to (3.2.29), i.e.

$$[12 - 4(1 - \xi^2)^{-1}]q_H^{(1)} + [q_{H\xi}^{(1)}(1 - \xi^2)]_\xi = 0,$$

is an associated Legendre equation which has a regular solution given by

$$q_H^{(1)} = P_3^2(\xi) = 15\xi(1 - \xi^2). \quad (3.2.30)$$

In order to construct the particular solution to (3.2.29) we use the method of variation of parameters. Defining

$$q^{(1)} = \Phi(\xi)P_3^2(\xi) \quad (3.2.31)$$

and substituting (3.2.31) into (3.2.29), we have

$$\begin{aligned} [\xi^2(1 - \xi^2)^3\Phi_\xi]_\xi &= \frac{2\mu}{45\eta}\xi(1 - \xi) + \frac{2\mu}{45\eta}\xi(1 - \xi)\ln\left(\frac{1 + \xi}{1 - \xi}\right) \\ &\quad - \frac{8\eta}{225}\xi(1 - \xi^2)\ln\left(\frac{1 + \xi}{1 - \xi}\right) \end{aligned}$$

$$\begin{aligned}
& + \frac{\eta}{225}(16\xi + 44\xi^2 - 60\xi^4) \\
& - \frac{2\xi(1 - \xi^2)}{15}\theta_{0x}.
\end{aligned} \tag{3.2.32}$$

Integrating with respect to ξ we have

$$\begin{aligned}
\xi^2(1 - \xi^2)^3\Phi_\xi = & \frac{2\mu}{45\eta} \left[\frac{\xi^2}{2} - \frac{\xi^3}{3} \right] \\
& + \frac{2\mu}{45\eta} \left[\frac{\xi^2}{2} \ln \left(\frac{1+\xi}{1-\xi} \right) - \frac{1}{2} \ln \left(\frac{1+\xi}{1-\xi} \right) + \xi \right. \\
& \quad \left. - \frac{\xi^3}{3} \ln \left(\frac{1+\xi}{1-\xi} \right) - \frac{\xi^2}{3} - \frac{1}{3} \ln |(1 - \xi^2)| \right] \\
& - \frac{8\eta}{225} \left[\frac{\xi^2}{2} \ln \left(\frac{1+\xi}{1-\xi} \right) - \frac{1}{2} \ln \left(\frac{1+\xi}{1-\xi} \right) + \xi \right. \\
& \quad \left. - \frac{\xi^4}{4} \ln \left(\frac{1+\xi}{1-\xi} \right) - \frac{1}{6} \xi^3 - \frac{1}{2} \xi + \frac{1}{4} \ln \left(\frac{1+\xi}{1-\xi} \right) \right] \\
& + \frac{\eta}{225} \left[8\xi^2 + \frac{44\xi^3}{3} - 12\xi^5 \right] \\
& - \frac{2}{15}\theta_{0x} \left[\frac{\xi^2}{2} - \frac{\xi^4}{4} \right] + c_1,
\end{aligned} \tag{3.2.33}$$

from which it follows that

$$\begin{aligned}
\Phi_\xi = & \frac{2\mu}{45\eta} \left[\frac{1}{(1 - \xi^2)^3} - \frac{\xi}{3(1 - \xi^2)^3} \right] \\
& + \frac{2\mu}{45\eta} \left[\frac{1}{2(1 - \xi^2)^3} \ln \left(\frac{1+\xi}{1-\xi} \right) - \frac{1}{2\xi^2(1 - \xi^2)^3} \ln \left(\frac{1+\xi}{1-\xi} \right) \right. \\
& \quad + \frac{1}{\xi(1 - \xi^2)^3} + \frac{\xi}{3(1 - \xi^2)^3} \ln \left(\frac{1+\xi}{1-\xi} \right) \\
& \quad \left. + \frac{1}{3(1 - \xi^2)^3} + \frac{1}{3\xi^2(1 - \xi^2)^3} \ln |(1 - \xi^2)| \right] \\
& - \frac{8\eta}{225} \left[\frac{1}{2(1 - \xi^2)^3} \ln \left(\frac{1+\xi}{1-\xi} \right) - \frac{1}{2} \ln \left(\frac{1+\xi}{1-\xi} \right) + \frac{1}{\xi(1 - \xi^2)^3} \right. \\
& \quad + \frac{\xi^2}{4(1 - \xi^2)^3} \ln \left(\frac{1+\xi}{1-\xi} \right) + \frac{\xi}{6(1 - \xi^2)^3} + \frac{1}{2\xi(1 - \xi^2)^3} \\
& \quad \left. - \frac{1}{4\xi^2(1 - \xi^2)^3} \ln \left(\frac{1+\xi}{1-\xi} \right) \right]
\end{aligned}$$

$$\begin{aligned}
& + \frac{\eta}{225} \left[\frac{8}{(1-\xi^2)^3} + \frac{44\xi}{3(1-\xi^2)^3} - \frac{12\xi^3}{(1-\xi^2)^3} \right] \\
& - \frac{2}{15} \theta_{0x} \left[\frac{1}{2(1-\xi^2)^3} - \frac{\xi^2}{4(1-\xi^2)^3} \right] + \frac{c_1}{\xi^2(1-\xi^2)^3}. \tag{3.2.34}
\end{aligned}$$

Integrating with respect to ξ a second time yields

$$\begin{aligned}
\Phi(\xi) = & \frac{\mu}{45\eta} \left[\frac{3}{16} \ln \left(\frac{1+\xi}{1-\xi} \right) + \frac{3}{8} \frac{\xi}{(1-\xi^2)} + \frac{1}{4} \frac{\xi}{(1-\xi^2)^2} \right] \\
& - \frac{2\mu}{45\eta} \frac{1}{12(1-\xi^2)^2} \\
& + \frac{\mu}{45\eta} \left[\frac{1}{2\xi} \ln \left(\frac{1+\xi}{1-\xi} \right) - \frac{1}{8} \ln^2 \left(\frac{1+\xi}{1-\xi} \right) + \frac{1}{6} \frac{1}{(1-\xi^2)^2} + \frac{1}{2} \frac{1}{(1-\xi^2)} \right] \\
& - \frac{4\eta}{225} \left[\frac{1}{2\xi} \ln \left(\frac{1+\xi}{1-\xi} \right) - \frac{1}{8} \ln^2 \left(\frac{1+\xi}{1-\xi} \right) + \frac{1}{6} \frac{1}{(1-\xi^2)^2} + \frac{1}{2} \frac{1}{(1-\xi^2)} \right] \\
& + \frac{\eta}{225} \left[\frac{3}{2} \ln \left(\frac{1+\xi}{1-\xi} \right) + \frac{3\xi}{(1-\xi^2)} + \frac{2\xi}{(1-\xi^2)^2} \right] \\
& + \frac{\eta}{225} \left[\frac{11}{3} \frac{1}{(1-\xi^2)^2} - \frac{6\xi^2}{(1-\xi^2)^2} + \frac{3}{(1-\xi^2)^2} \right] \\
& + \frac{1}{30} \theta_{0x} \left[-\frac{1}{\xi} + \frac{1}{2} \ln \left(\frac{1+\xi}{1-\xi} \right) \right] \\
& + c_1 \left[\frac{-1}{\xi(1-\xi^2)^2} + \frac{5\xi}{4(1-\xi^2)^2} + \frac{15\xi}{(1-\xi^2)} + \frac{15}{16} \ln \left(\frac{1+\xi}{1-\xi} \right) \right] \\
& + c_2, \tag{3.2.35}
\end{aligned}$$

so that in view of (3.2.31) we have

$$\begin{aligned}
q^{(1)}(\xi) = & \frac{\mu}{3\eta} \left[\frac{3}{16} \xi(1-\xi^2) \ln \left(\frac{1+\xi}{1-\xi} \right) + \frac{3}{8} \xi^2 + \frac{1}{4} \frac{\xi^2}{(1-\xi^2)} \right. \\
& \left. + \frac{1}{2} (1-\xi^2) \ln \left(\frac{1+\xi}{1-\xi} \right) - \frac{1}{8} \xi(1-\xi^2) \ln^2 \left(\frac{1+\xi}{1-\xi} \right) + \frac{\xi}{2} \right] \\
& + \frac{\eta}{15} \left[-2(1-\xi^2) \ln \left(\frac{1+\xi}{1-\xi} \right) + \frac{1}{2} \xi(1-\xi^2) \ln^2 \left(\frac{1+\xi}{1-\xi} \right) \right. \\
& \left. + \frac{3}{2} \xi(1-\xi^2) \ln \left(\frac{1+\xi}{1-\xi} \right) + \frac{2\xi^2}{(1-\xi^2)} \right. \\
& \left. + 4\xi + 3\xi^2 \right]
\end{aligned}$$

$$\begin{aligned}
& + \frac{1}{2}\theta_{0x} \left[-(1-\xi^2) + \frac{1}{2}\xi(1-\xi^2) \ln \left(\frac{1+\xi}{1-\xi} \right) \right] \\
& + c_1 \left[\frac{-1}{(1-\xi^2)} + \frac{5\xi^2}{4(1-\xi^2)} + \frac{15}{8}\xi^2 + \frac{15}{16}\xi(1-\xi^2) \ln \left(\frac{1+\xi}{1-\xi} \right) \right] \\
& + c_2\xi(1-\xi^2). \tag{3.2.36}
\end{aligned}$$

Applying the boundary condition $q^{(1)}(\xi) \rightarrow 0$ as $\xi \rightarrow 1$ (i.e. $\theta \rightarrow \infty$) to (3.2.36), we find that the terms containing $\frac{1}{(1-\xi^2)}$ are unbounded and therefore must cancel each other for the boundary condition to be satisfied. Thus we must have

$$\frac{\mu}{3\eta} \frac{\xi^2}{4(1-\xi^2)} + \frac{\eta}{15} \frac{2\xi^2}{(1-\xi^2)} + c_1 \left[\frac{-1}{(1-\xi^2)} + \frac{5\xi^2}{4(1-\xi^2)} \right] = 0, \tag{3.2.37}$$

from which it follows upon applying the boundary condition $q^{(1)}(\xi) \rightarrow 0$ as $\xi \rightarrow 1$ (i.e. $\theta \rightarrow \infty$), that

$$c_1 = \frac{-\mu}{3\eta} - \frac{8\eta}{15},$$

hence

$$\begin{aligned}
q^{(1)}(\xi) = & \frac{\mu}{6\eta} \left[2 - 3\xi^2 + \xi - \frac{3}{2}\xi(1-\xi^2) \ln \left(\frac{1+\xi}{1-\xi} \right) \right. \\
& \left. + (1-\xi^2) \ln \left(\frac{1+\xi}{1-\xi} \right) - \frac{1}{4}\xi(1-\xi^2) \ln^2 \left(\frac{1+\xi}{1-\xi} \right) \right] \\
& + \frac{\eta}{15} \left[8 - 12\xi^2 + 4\xi - 6\xi(1-\xi^2) \ln \left(\frac{1+\xi}{1-\xi} \right) \right. \\
& \left. - 2(1-\xi^2) \ln \left(\frac{1+\xi}{1-\xi} \right) + \frac{1}{2}\xi(1-\xi^2) \ln^2 \left(\frac{1+\xi}{1-\xi} \right) \right] \\
& + \frac{1}{2}\theta_{0x} \left[-(1-\xi^2) + \frac{1}{2}\xi(1-\xi^2) \ln \left(\frac{1+\xi}{1-\xi} \right) \right]. \tag{3.2.38}
\end{aligned}$$

Since we are interested only in the particular solution, the constant c_2 is arbitrary and has been set equal to zero as it is a multiple of the homogeneous solution.

Defining

$$\phi = \eta(\theta - \theta_0),$$

and recalling (3.2.28), yields

$$\begin{aligned}
q^{(1)}(\theta; \chi) = & \frac{\mu}{6\eta} [3\text{sech}^2 \phi (1 - \phi \tanh \phi) + \tanh \phi - 1 - \phi \text{sech}^2 \phi (\phi \tanh \phi - 2)] \\
& + \frac{\eta}{15} [12\text{sech}^2 \phi (1 - \phi \tanh \phi) + 4(\tanh \phi - 1) + 2\phi \text{sech}^2 \phi (\phi \tanh \phi - 2)] \\
& + \frac{1}{2} \theta_{0\chi} [\text{sech}^2 \phi (\phi \tanh \phi - 1)].
\end{aligned} \tag{3.2.39}$$

As $\theta \rightarrow +\infty$, (i.e. ahead of the solitary wave) we note that, asymptotically,

$$q^{(1)} \sim \left(-\frac{2\mu}{3\eta} + \frac{8\eta}{15} \right) \phi^2 \exp(-2\phi), \tag{3.2.40a}$$

and as $\theta \rightarrow -\infty$ (i.e. behind the solitary wave)

$$q^{(1)} \sim \frac{-\mu}{3\eta} - \frac{8\eta}{15} + \left(\frac{2\mu}{3\eta} - \frac{8\eta}{15} \right) \phi^2 \exp(2\phi). \tag{3.2.40b}$$

From (3.2.40a) we see that ahead of the solitary wave the perturbation expansion (3.2.5) decays at a rate of $O(\phi^2 e^{-2\phi})$ while the solution (3.2.3) of the unperturbed equation decays at a rate of $O(e^{-2\phi})$. It follows that ahead of the propagating main pulse the perturbation expansion (3.2.5) is algebraically nonuniform. This nonuniformity will be removed, following the method of Swaters and Sawatzky (1989), by introducing a WKB power series and similarity solution procedure for the near and far fields ahead of the main pulse.

Behind the solitary wave we see, upon inspection of (3.2.40b), an additional exponential term which indicates that the perturbation solution (3.2.39) is exponentially nonuniform behind the main pulse (recall that (3.2.27) predicts the emergence of a shelf region, with amplitude $-\frac{\mu}{3\eta} - \frac{8\eta}{15}$, behind the main pulse).

3.2.3 Emergence and Evolution of the Shelf Region

The solution of the perturbation field (3.2.39) indicates the formation of a shelf region behind the main pulse with an amplitude given by (3.2.27). While this describes the formation of the shelf behind the main pulse, it does not describe the subsequent evolution of this shelf region. The evolution of the shelf is determined as follows.

Having assumed that at $t = 0$ the soliton is centered around $x = 0$, the leading order phase position relative to $\xi = 0$ is given by

$$\xi_c(\chi) = \frac{4}{\nu} \int_0^\chi \eta^2(\chi') d\chi'. \quad (3.2.41)$$

With $\eta(\chi)$ given by (3.2.20) we have

$$\xi_c(\chi) = \frac{30}{8\nu} \ln \left[\frac{10\mu - 8\eta^2(0)(e^{-4\mu\chi/3} - 1)}{10\mu} \right]. \quad (3.2.42)$$

The amplitude of the shelf is small ($O(\nu)$) and varies slowly with respect to T and ξ in the region $0 < \xi < \xi_c(\chi)$ (Knickerbocker and Newell (1980), Kodama and Ablowitz (1981), Swaters and Sawatzky (1989)). Thus, following Swaters and Sawatzky (1989), we introduce the stretched phase variable $\Theta = \nu\xi$ and describe the evolution of the shelf tail by an asymptotic expansion of the form

$$q \sim \nu \hat{q}^{(0)}(\chi, \Theta) + \nu^2 \hat{q}^{(1)}(\chi, \Theta) + \dots \quad (3.2.43)$$

Substituting (3.2.43) into (3.2.2) we see that the leading-order dynamics of this region are given by

$$\hat{q}_\chi^{(0)} = -\mu \hat{q}^{(0)}, \quad (3.2.44a)$$

subject to the moving boundary condition

$$\hat{q}^{(0)}(\chi, \Theta = \nu\xi_c(\chi)) = \frac{-\mu}{3\eta(\chi)} - \frac{8\eta(\chi)}{15}. \quad (3.2.44b)$$

The boundary condition (3.2.44b) satisfies the requirement that, following the dissipating soliton, the magnitude of the shelf is determined by the asymptotic behaviour of $q^{(1)}(\theta, \chi)$ as $\theta \rightarrow -\infty$ which is given by (3.2.27).

The solution to (3.2.44) is straightforward and is given by

$$q(\chi, \Theta) \sim \nu \left(\frac{-\mu}{3\eta(\hat{\chi}(\Theta))} - \frac{8\eta(\hat{\chi}(\Theta))}{15} \right) \exp(-\mu(\chi - \hat{\chi}(\Theta))), \quad (3.2.45)$$

where $\hat{\chi}(\Theta)$ (the arrival time of the main pulse) is given by

$$\hat{\chi}(\Theta) = -\frac{3}{4\mu} \ln \left[\frac{10\mu(e^{8\Theta/30} - 1)}{-8\eta^2(0)} + 1 \right]. \quad (3.2.46)$$

3.2.4 Formation and Evolution of the Dispersive Wavetail

The transition back to zero in the region $\xi < 0$ begins in the neighbourhood of $\xi = 0$ and is dominated by $O(\nu)$ -amplitude, high-wavenumber, spatially-decaying oscillations (a dispersive wavetail) (Knickerbocker and Newell (1980), Swaters and Sawatzky (1989)). Assuming that the dispersive wavetail is described by an asymptotic expansion of the form

$$q \sim \nu \tilde{q}^{(0)}(T, \xi; \chi) + \nu^2 \tilde{q}^{(1)}(T, \xi; \chi) + \dots, \quad (3.2.47)$$

we have, upon substitution of (3.2.47) into (3.2.2), the leading order behaviour of the dispersive wavetail described by

$$\tilde{q}_T^{(0)} + \tilde{q}_{\xi\xi\xi}^{(0)} = 0, \quad (3.2.48a)$$

subject to the boundary conditions

$$\tilde{q}^{(0)}(T, \xi) \rightarrow 0 \quad \text{as} \quad \xi \rightarrow -\infty, \quad (3.2.48b)$$

$$\tilde{q}^{(0)}(T, \xi) \rightarrow \left(\frac{-\mu}{3\eta(0)} - \frac{8\eta(0)}{15} \right) \exp(-\mu(\chi - \hat{\chi}(\nu\xi))) \quad \text{as } \xi \rightarrow \infty, \quad (3.2.48c)$$

where $\hat{\chi}$ is given by (3.2.46).

Introducing the similarity variable

$$X = \frac{\xi}{(3T)^{\frac{1}{3}}}, \quad (3.2.49)$$

we find that (3.2.48a) becomes

$$\tilde{q}_{XXX}^{(0)} = X \tilde{q}_X^{(0)}, \quad (3.2.50)$$

which has a bounded solution given by

$$\tilde{q}_X^{(0)} = Ai(X), \quad (3.2.51)$$

where $Ai(X)$ is the bounded Airy function. Hence, with regards to (3.2.51), we find that the solution to (3.2.48) is

$$\tilde{q}^{(0)}(T, \xi; \chi) \sim \left(\frac{-\mu}{3\eta(0)} - \frac{8\eta(0)}{15} \right) \exp(-\mu(\chi - \hat{\chi}(\nu\xi))) \int_{-\infty}^{\frac{\xi}{(3T)^{\frac{1}{3}}}} Ai(s) ds. \quad (3.2.52)$$

Equation (3.2.52) describes the formation and evolution of the dispersive wavetail. The development of the shelf and wavetail for various times is shown in Figure 7.

3.2.5 The Solution Ahead of the Main Pulse

The solution (3.2.39) is nonuniform, as indicated by (3.2.40a), with respect to the soliton phase variable θ as $\theta \rightarrow +\infty$. In order to remove this nonuniformity, we follow the procedure of Swaters and Sawatzky (1989) and develop a combination WKB-power-series similarity solution.

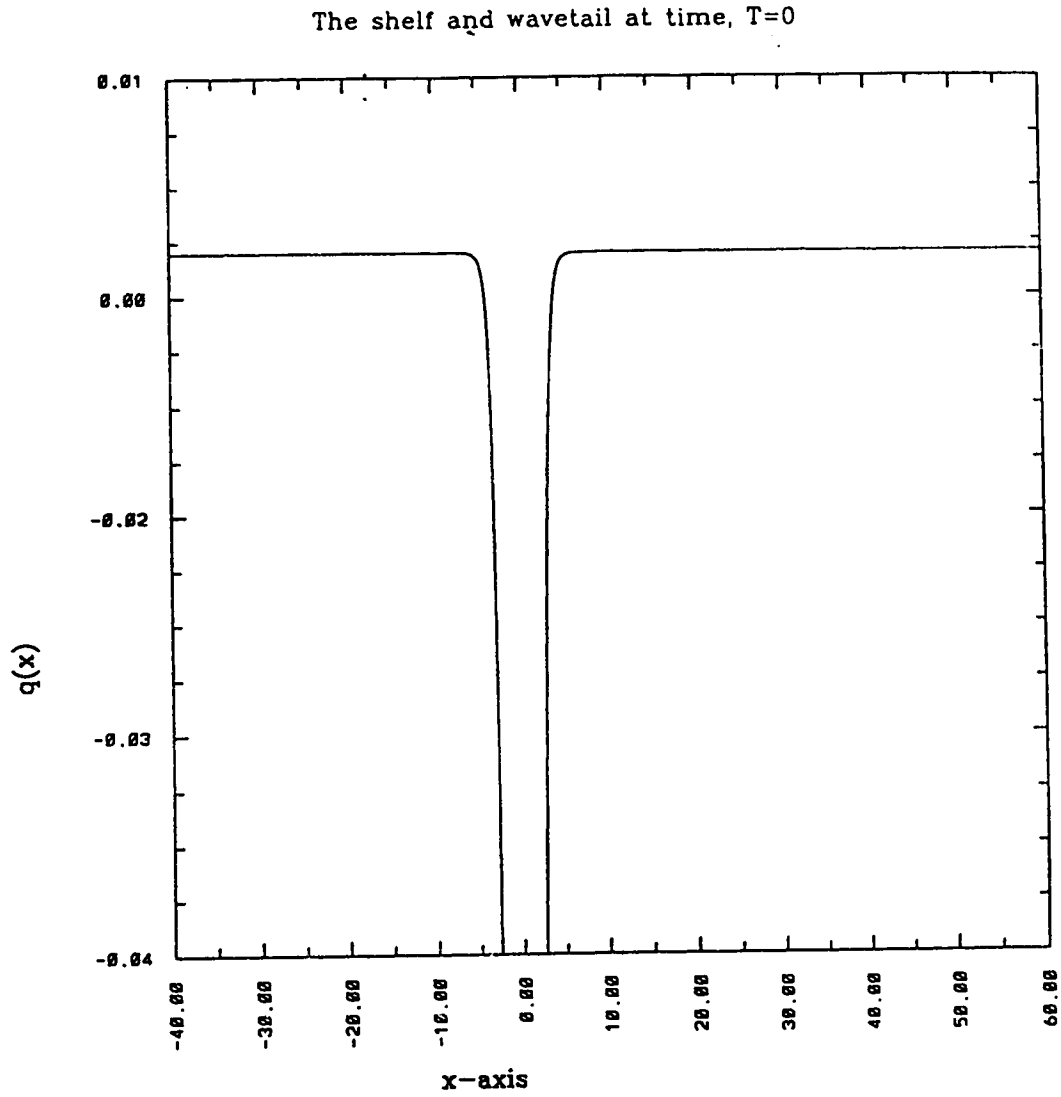


Figure 7: Evolution of Shelf and Wavetail

Figures 7a-k depict the evolution of the shelf and wavetail at times $T = 0, 1, 2, 3, 4, 5, 10, 15, 20, 25$ and 50 , respectively, for parameter value $\nu = \frac{1}{100}$.

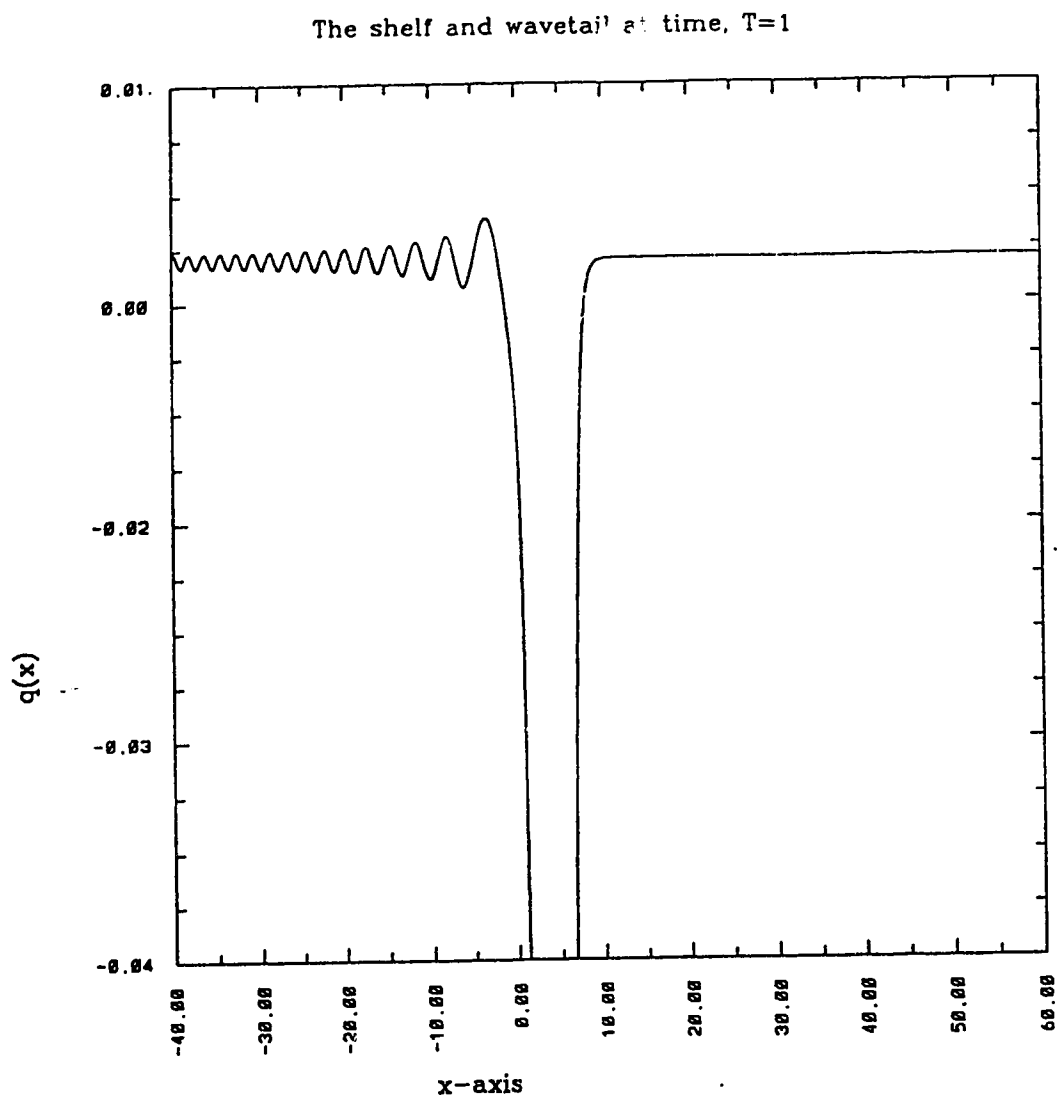


Figure 7b

The shelf and wavetail at time, $T=2$

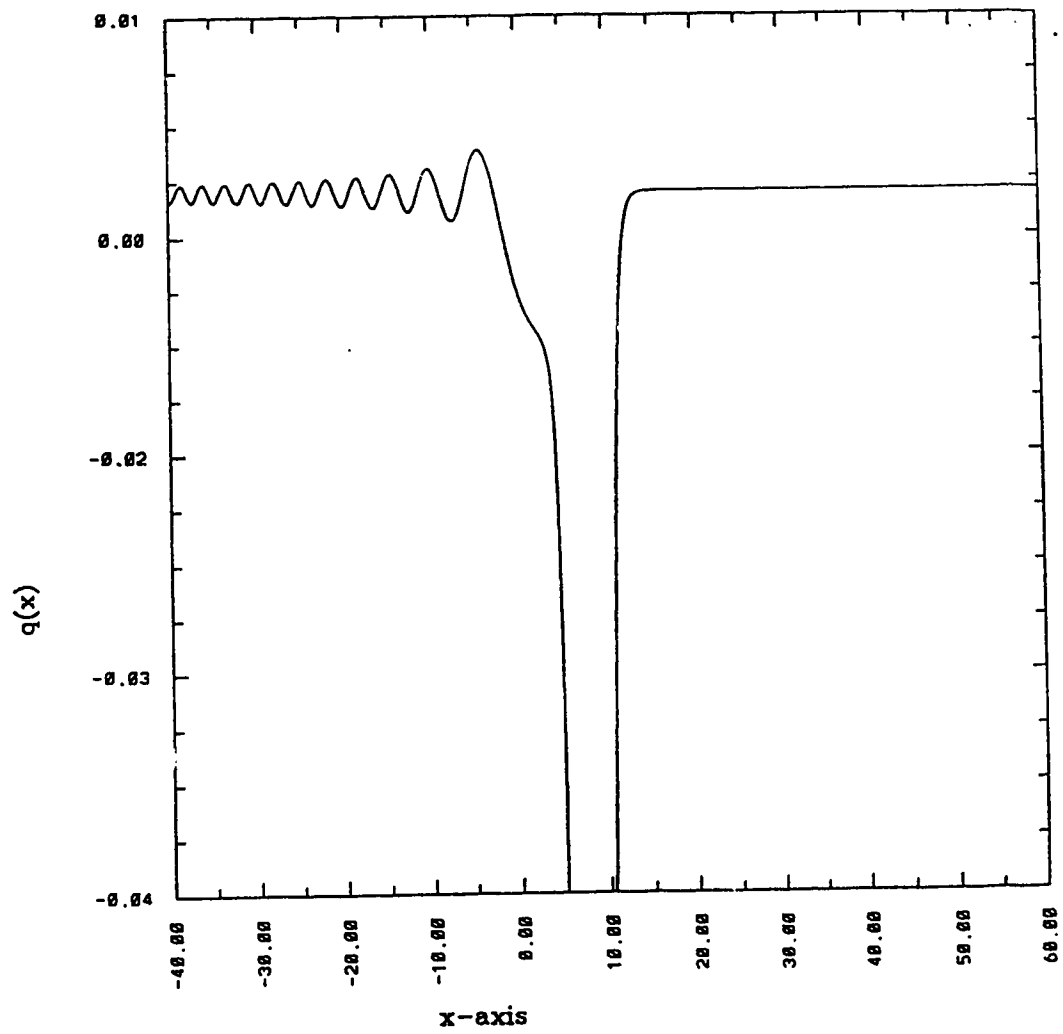


Figure 7c

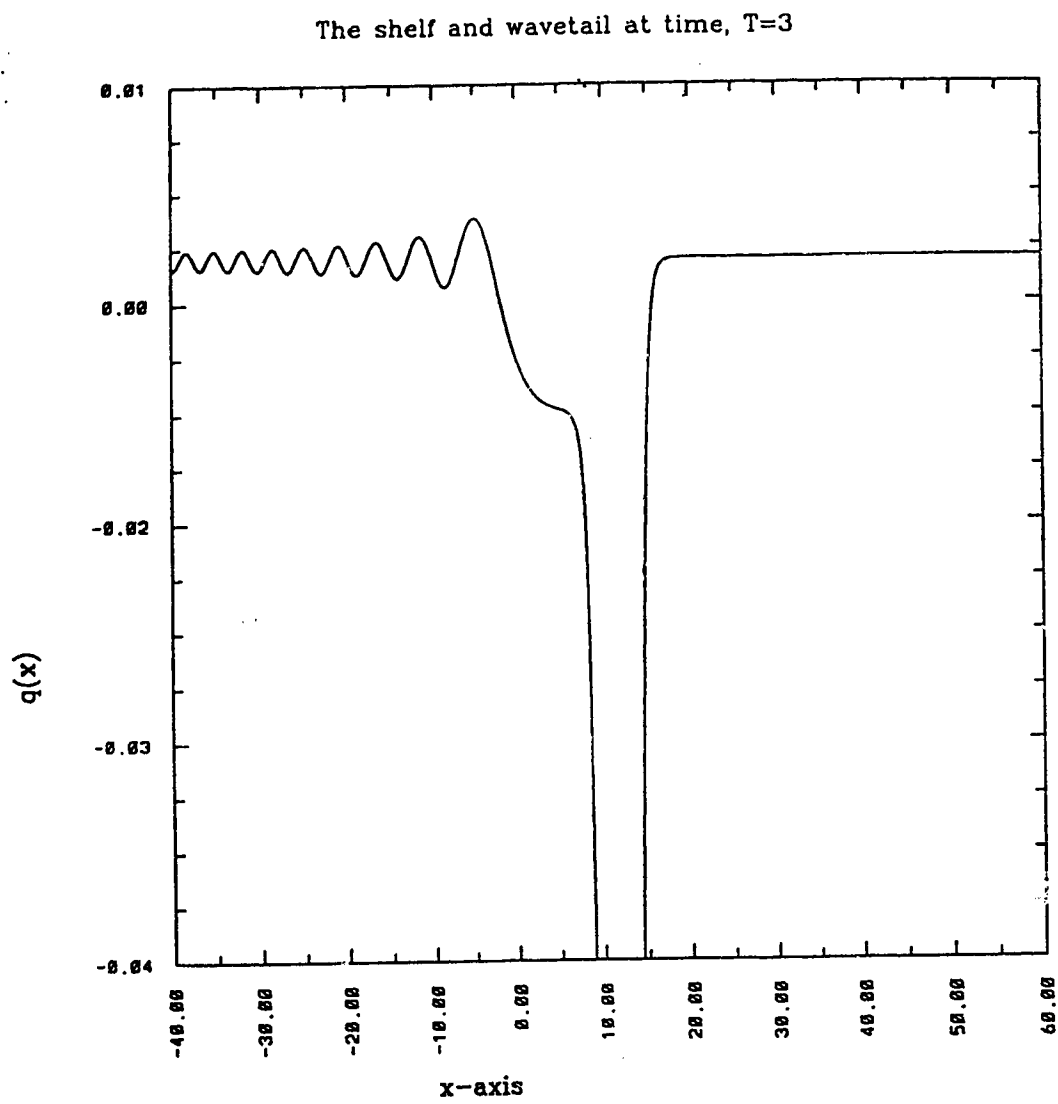


Figure 7d

The shelf and wavetail at time, $T=4$

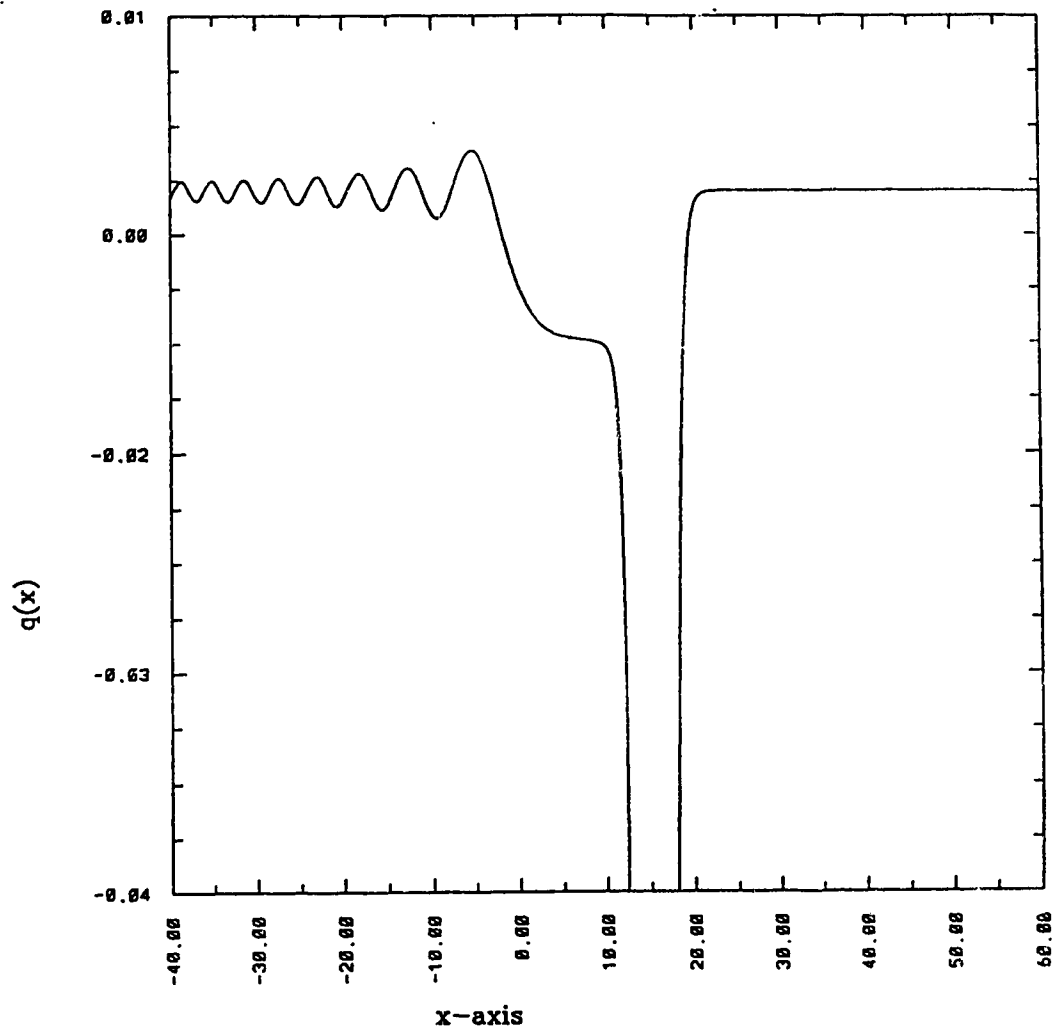


Figure 7e

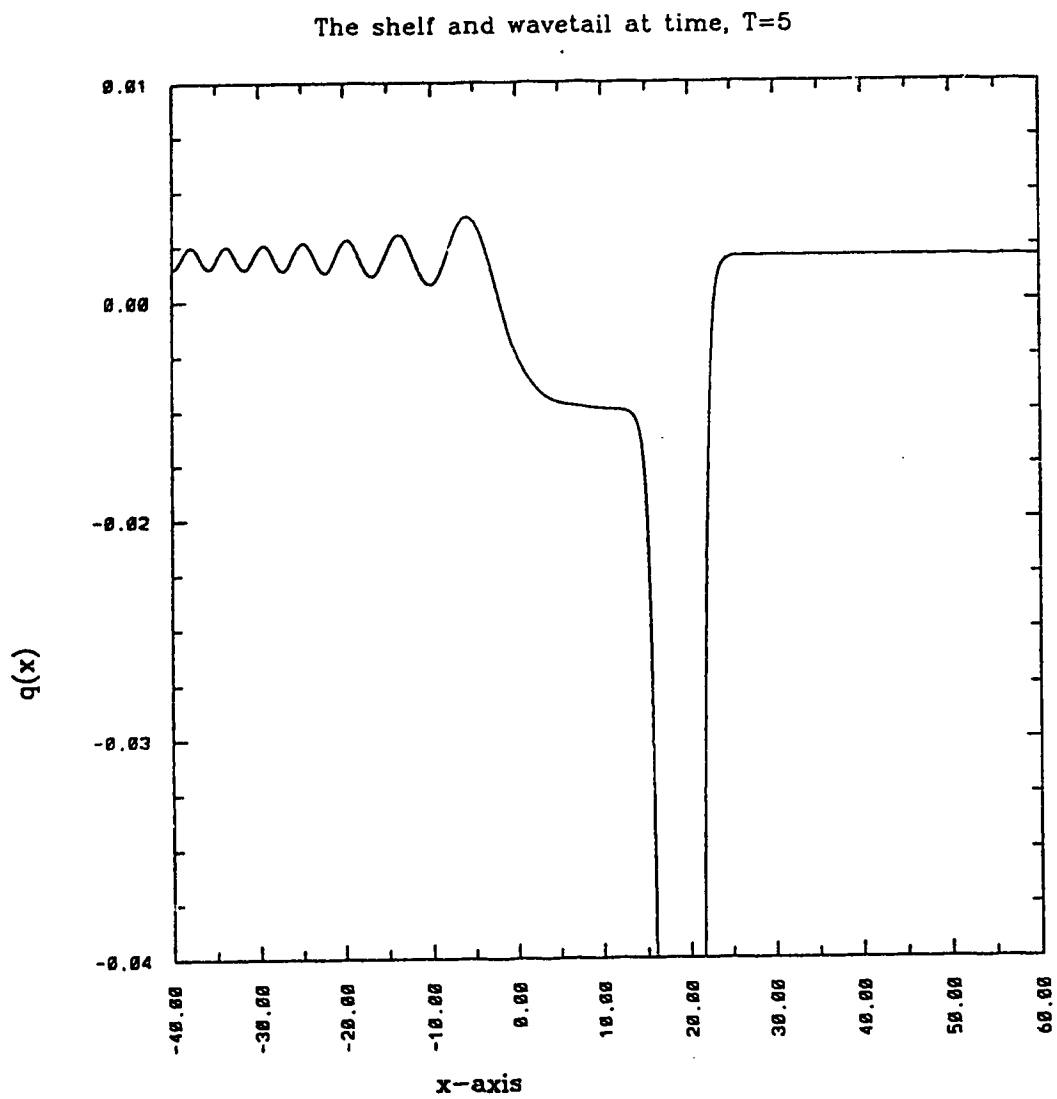


Figure 7f

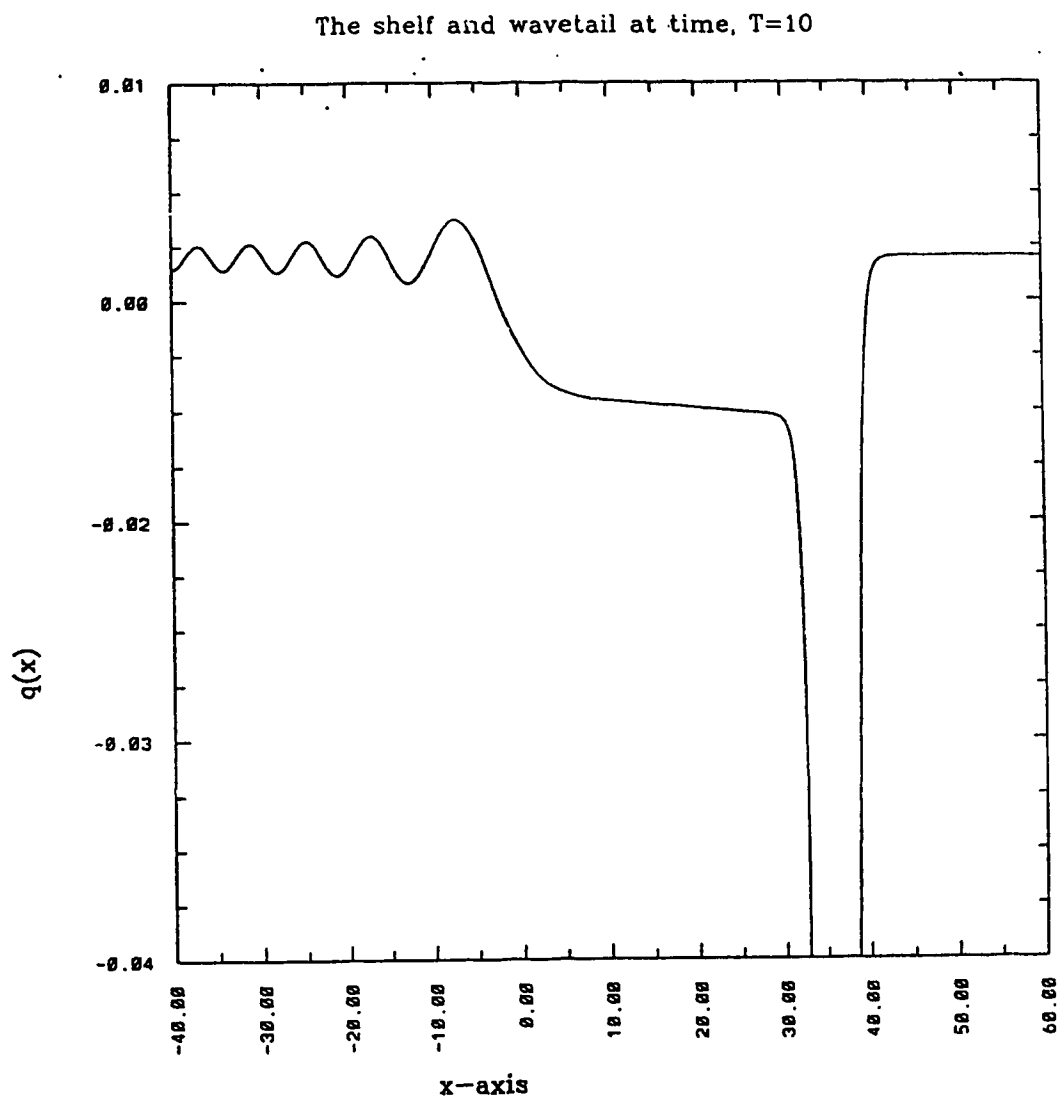


Figure 7g

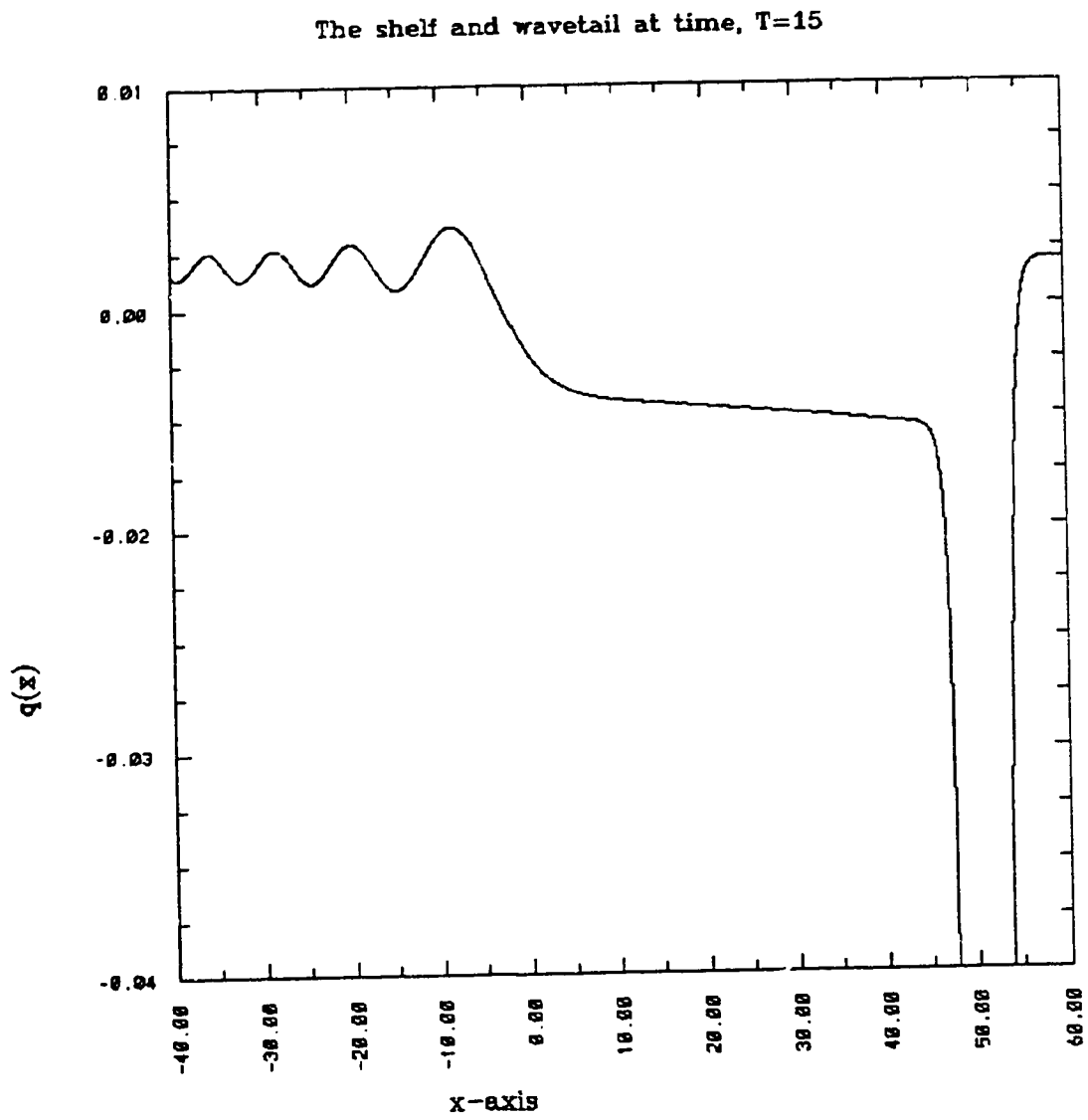


Figure 7h

The shelf and wavetail at time, $T=20$

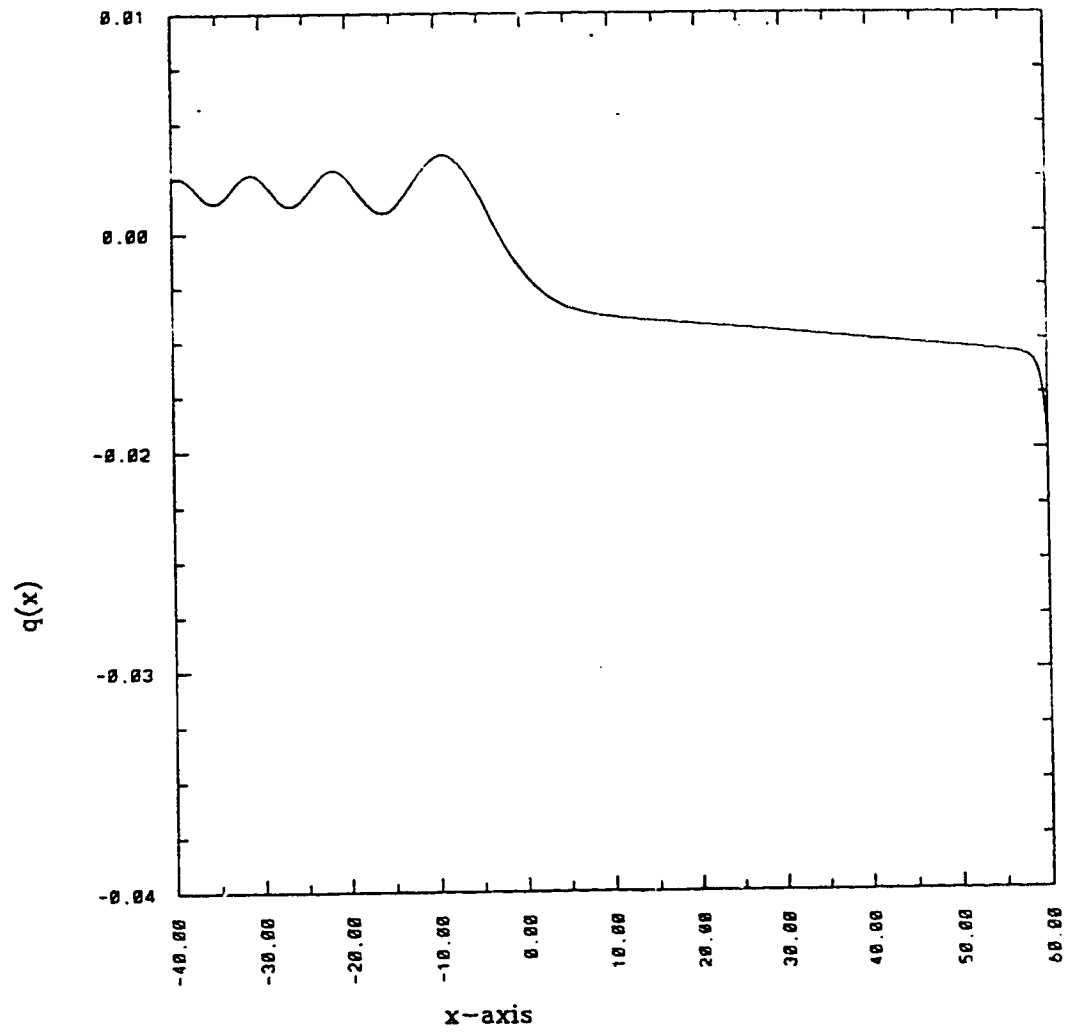


Figure 7i

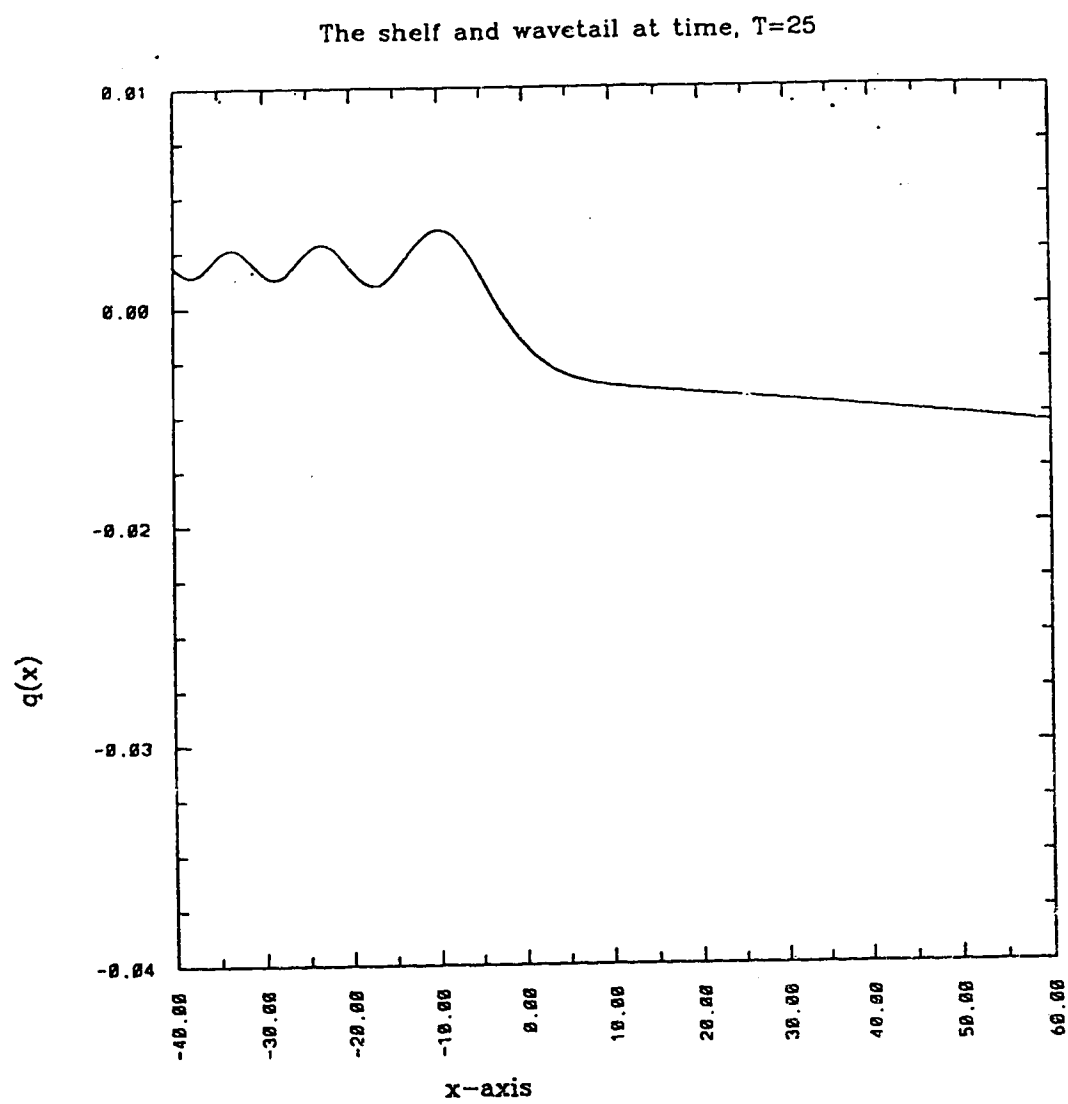


Figure 7j

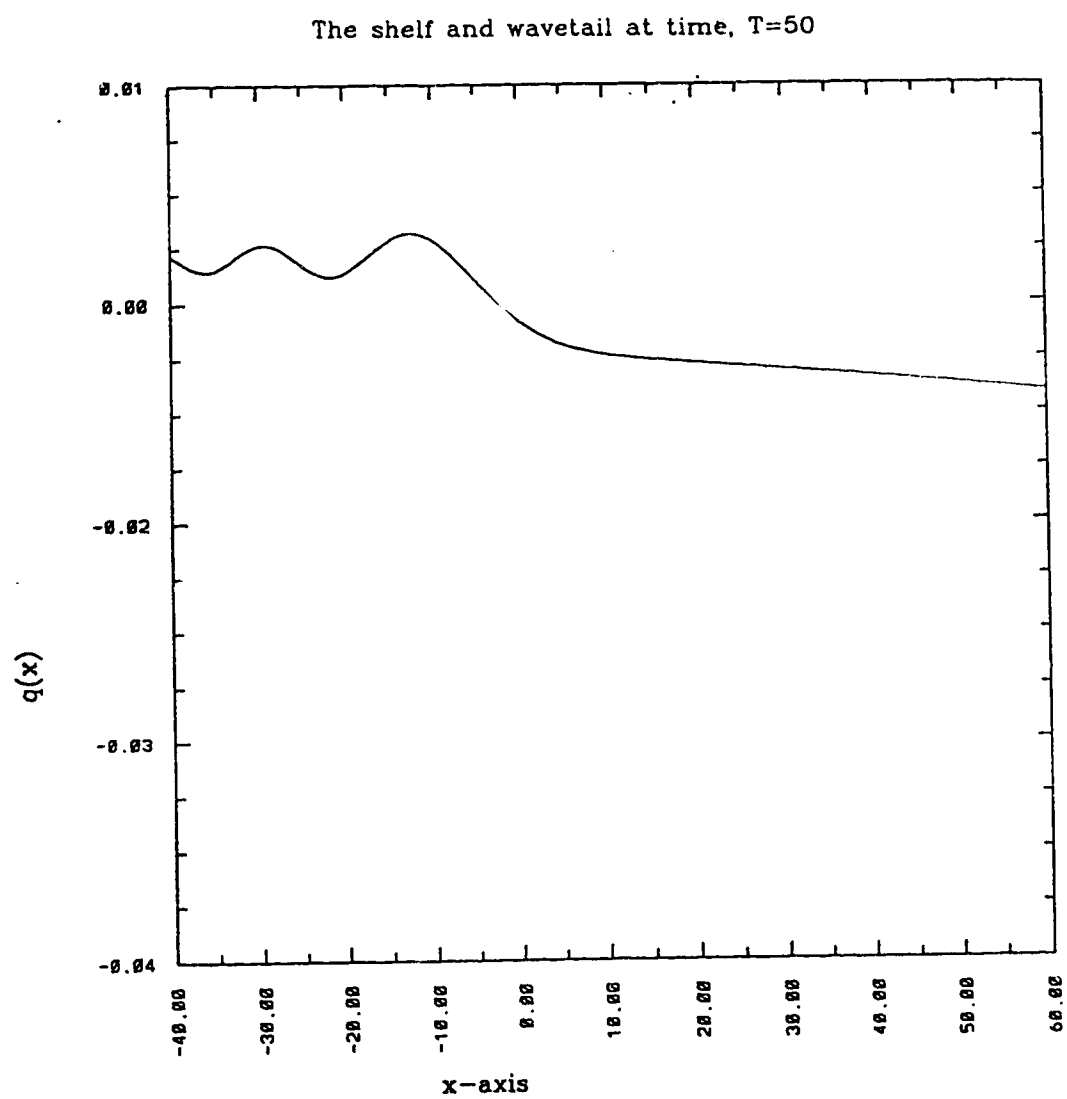


Figure 7k

We begin by introducing the stretched phase variable, Z , given by

$$Z = \nu \left\{ \xi - \frac{4}{\nu} \int_0^x \eta^2(\chi') d\chi' - \theta_0(\chi) \right\}. \quad (3.2.53a)$$

In the region where the phase variable satisfies $0 \ll (\theta - \theta_0) \sim O(\nu^{-1})$, it is possible to obtain an asymptotic solution to (3.2.2) of the form

$$q \simeq q^\dagger(Z, \chi). \quad (3.2.53b)$$

Substitution of (3.2.53) into (3.2.2) yields

$$q^\dagger_\chi - (4\eta^2(\chi) + \nu\theta_{0\chi})q^\dagger_Z - 6q^\dagger q^\dagger_Z + \nu^2 q^\dagger_{ZZZ} = \mu q^\dagger + \nu^2 q^\dagger_{ZZ}. \quad (3.2.54)$$

In solving (3.2.54), we require that the solution match the leading order behaviour of the soliton plus perturbation field in the limit as $\theta \gg 1$ because in the region of interest the solution is small, i.e. $O(\nu)$. Thus ahead of the solitary wave the solution must match $q^{(0)} + \nu q^{(1)}$ as given by (3.2.9) and (3.2.39). In view of (3.2.9) and (3.2.39), we find that the leading-order behaviour is exponentially decaying ahead of the main pulse, therefore we may neglect the nonlinear term in (3.2.54) as it will be exponentially small when compared to other terms. Thus $q^\dagger(Z, \chi)$ is governed by (approximately)

$$q^\dagger_\chi - (4\eta^2(\chi) + \nu\theta_{0\chi}(\chi))q^\dagger_Z - \mu q^\dagger = \nu^2 q^\dagger_{ZZ} - \nu^2 q^\dagger_{ZZZ}, \quad (3.2.55a)$$

subject to the matching condition

$$q^\dagger(Z, \chi) \rightarrow 8\eta^2(\chi) \left[-1 + \frac{\eta(\chi)}{15} \frac{Z^2}{\nu} - \frac{\mu}{12\eta(\chi)} \frac{Z^2}{\nu} \right] \exp\left(\frac{-2\eta(\chi)Z}{\nu}\right), \quad (3.2.55b)$$

as $Z \rightarrow 0$

and boundary condition

$$q^\dagger(Z, \chi) \xrightarrow{\text{exponentially}} 0, \quad \text{as } Z \rightarrow +\infty. \quad (3.2.55c)$$

The algebraic non-uniformities in the solution are removed by constructing a WKB solution (Bender and Orszag (1978)) to (3.2.55) in the form

$$q^\dagger \sim h(Z, \chi) \exp \left[\frac{1}{\nu} f(Z, \chi) \right] + O(\nu), \quad (3.2.56)$$

where $h(Z, \chi)$ represents the amplitude of the wave and $f(Z, \chi)$ represents the slowly varying but nonconstant phase.

Substituting (3.2.56) into (3.2.55a) we find that f and h may be determined from the pair of equations

$$f_\chi - 4\eta^2(\chi)f_Z + f_Z^3 = 0, \quad (3.2.57a)$$

$$h_\chi - 4\eta^2(\chi)h_Z + 3\{h_Z f_Z^2 + h f_Z f_{ZZ}\} = \{f_Z^2 + \theta_{0\chi}(\chi)f_Z + \mu\} h. \quad (3.2.57b)$$

3.2.5.1 The near-field WKB power-series solution

In the near field region ahead of the main pulse (i.e. Z small), the matching condition (3.2.55b) suggests a power-series solution of the form

$$f(Z, \chi) = \alpha_1(\chi)Z + \alpha_2(\chi)Z^2 + \dots, \quad (3.2.58a)$$

$$h(Z, \chi) = \beta_0(\chi) + \beta_1(\chi)Z + \dots. \quad (3.2.58b)$$

Substituting (3.2.58a) into (3.2.57a), we have

$$\begin{aligned} & (\alpha_1 Z + \alpha_2 Z^2)_\chi - 4\eta^2(\alpha_1 + 2\alpha_2 Z + 3\alpha_3 Z^2) \\ & + \alpha_1^3 + 6\alpha_1^2 \alpha_2 Z + (9\alpha_1^2 \alpha_3 + 12\alpha_1 \alpha_2^2) Z^2 \\ & + \text{higher order terms} = 0. \end{aligned} \quad (3.2.59)$$

Collecting like powers of Z we find that α_1 and α_2 must satisfy

$$Z^0 : -4\eta^2\alpha_1 + \alpha_1^3 = 0, \quad (3.2.60a)$$

$$Z^1 : \alpha_1\chi - 9\eta^2\alpha_2 + 6\alpha_1^2\alpha_2 = 0. \quad (3.2.60b)$$

From (3.2.60a) we have

$$\alpha_1 = \pm 2\eta.$$

Since the matching condition requires the solution to be exponentially decaying, we choose

$$\alpha_1 = -2\eta. \quad (3.2.61)$$

Substitution of (3.2.61) into (3.2.60b) yields

$$-2\eta\chi - 8\eta^2\alpha_2 + 24\eta^2\alpha_2 = 0. \quad (3.2.62)$$

From (3.2.18) we have $\eta\chi = -\frac{2}{3}\mu\eta - \frac{8}{15}\eta^3$ so that equation (3.2.62) may be simplified to

$$\frac{4}{3}\mu\eta + \frac{16}{15}\eta^3 + 16\eta^2\alpha_2 = 0. \quad (3.2.63)$$

Solving for α_2 we have

$$\alpha_2 = \frac{-\mu}{12\eta(\chi)} - \frac{\eta(\chi)}{15}. \quad (3.2.64)$$

Thus, to leading order we have

$$f(Z, \chi) \sim -2\eta Z - \left(-\frac{\mu}{12\eta} + \frac{\eta}{15} \right) Z^2.$$

Having determined the phase function $f(Z, \chi)$ to leading order, we now determine the amplitude function $h(Z, \chi)$ to leading order. Substitution of (3.2.58) into

(3.2.57b) yields

$$\begin{aligned}
& (\beta_0 + \beta_1 Z)_x - 4\eta^2(\beta_1 + 2\beta_2 Z) \\
& + 3(\beta_1 + 2\beta_2 Z)(\alpha_1^2 + 4\alpha_1\alpha_2 Z) \\
& + (\beta_0 + \beta_1 Z)(\alpha_1 + 2\alpha_2 Z)(2\alpha_2 + 6\alpha_3 Z) + \text{higher order terms} \\
& = [(\alpha_1^2 + 4\alpha_1\alpha_2 Z) + \theta_{0\chi}(\alpha_1 + 2\alpha_2 Z) + \mu](\beta_0 + \beta_1 Z) \\
& + \text{higher order terms.}
\end{aligned} \tag{3.2.65}$$

From (3.2.65) we see that upon collecting terms of order Z^0 we have

$$\beta_{0\chi} - 4\eta^2\beta_1 + 3\beta_1\alpha_1^2 + 6\beta_0\alpha_1\alpha_2 = \beta_0\alpha_1^2 + \theta_{0\chi}\beta_0\alpha_1 + \mu\beta_0. \tag{3.2.66}$$

From equation (3.2.66) we find that $\beta_0(\chi)$ is undetermined while

$$\beta_1(\chi) = \frac{[\beta_{0\chi} + 6\beta_0\alpha_1\alpha_2 - \beta_0\alpha_1^2 - \beta_0\theta_{0\chi}\alpha_1 - \mu\beta_0]}{[4\eta^2 - 3\alpha_1^2]}. \tag{3.2.67}$$

The matching condition (3.2.55b), however, demands that

$$\beta_0(\chi) = -8\eta^2(\chi). \tag{3.2.68a}$$

Appropriate substitutions for terms on the right-hand side of (3.2.67) yields

$$\beta_1(\chi) = -2\mu - \frac{16\eta^2}{5}. \tag{3.2.68b}$$

It follows that the amplitude function, $h(Z, \chi)$, is given by (to leading order)

$$h(Z, \chi) \sim -8\eta^2(\chi) - \left(2\mu + \frac{16\eta^2}{5}\right) Z.$$

Consequently, the leading-order near-field representation for $q^\dagger(Z, \chi)$ may be written as

$$q^\dagger(Z, \chi) \sim \left[-8\eta^2(\chi) - \left(2\mu + \frac{16}{5}\eta^2(\chi) \right) Z \right] \times \exp \left[-2\eta(\chi) \left(1 + \frac{Z}{30} + \frac{\mu Z}{24\eta^2(\chi)} \right) \frac{Z}{\nu} \right]. \quad (3.2.69)$$

3.2.5.2 The far-field WKB similarity solution

In the far-field ($Z \rightarrow +\infty$) ahead of the main pulse, the power-series solution developed above is no longer valid since the WKB series diverges for large Z and we require a similarity solution to (3.2.45). It is convenient to introduce the new stretched phase variable

$$\Theta = Z + 4 \int_0^X \eta^2(\chi') d\chi' = Z + \nu\theta_c(\chi). \quad (3.2.70)$$

Under this transformation, equations (3.2.57) become

$$f_\chi + (f_\Theta)^3 = 0, \quad (3.2.71a)$$

$$h_\chi + 3 \{ h_\Theta f_\Theta^2 + h f_\Theta f_{\Theta\Theta} \} = h \{ f_\Theta^2 + \theta_{0\chi}(\chi) f_\Theta + \mu \}. \quad (3.2.71b)$$

Equation (3.2.71a) has solution

$$f(\chi, \Theta) = -2 \left(\frac{\Theta}{3} \right)^{\frac{3}{2}} \chi^{-\frac{1}{2}}. \quad (3.2.72)$$

Substitution of (3.2.72) into (3.2.71b) yields

$$\chi h_\chi + \Theta h_\Theta = \left[\frac{\Theta}{3} - \frac{1}{2} - \frac{8\eta}{15} \left(\frac{\Theta\chi}{3} \right)^{\frac{1}{2}} - \left(\frac{\Theta\chi}{3} \right)^{\frac{1}{2}} \frac{\mu}{3\eta} + \mu\chi \right] h, \quad (3.2.73a)$$

which we solve subject to the matching condition

$$h(\chi, \Theta) \rightarrow -8\eta^2(\chi) \quad \text{as} \quad \Theta \rightarrow \nu\theta_c(\chi). \quad (3.2.73b)$$

Equation (3.2.73a) is solved using the method of characteristics. Letting s parameterize the characteristic curve we have

$$\frac{d\chi}{ds} = \chi, \quad \chi|_{s=0} = \bar{\chi}, \quad (3.2.74a)$$

$$\frac{d\Theta}{ds} = \Theta, \quad \Theta|_{s=0} = \nu\theta_c(\bar{\chi}), \quad (3.2.74b)$$

$$\begin{aligned} \frac{dh}{ds} &= \left[\frac{\Theta}{3} - \frac{1}{2} - \frac{8\eta}{15} \left(\frac{\Theta\chi}{3} \right)^{\frac{1}{2}} + \left(\frac{\Theta\chi}{3} \right)^{\frac{1}{2}} \frac{\mu}{3\eta} + \mu\chi \right] h, \\ h|_{s=0} &= -8\eta^2(\bar{\chi}). \end{aligned} \quad (3.2.74c)$$

From equation (3.2.74a) and (3.2.74b), it follows that

$$\chi = \bar{\chi}e^s, \quad (3.2.75a)$$

$$\Theta = \nu\theta_c(\bar{\chi})e^s, \quad (3.2.75b)$$

and consequently,

$$s = \frac{1}{2} \ln \left(\frac{\Theta\chi}{\nu\theta_c(\bar{\chi})\bar{\chi}} \right). \quad (3.2.76)$$

Using (3.2.76) and integrating (3.2.74c) subject to the matching condition (3.2.73b), it is found that $h(\chi, \Theta)$ is given by

$$\begin{aligned} h(\chi, \Theta) &= -8\eta^2(\chi) \left[\frac{\nu\theta_c(\bar{\chi})}{\Theta} \right]^{\frac{1}{2}} \\ &\times \exp \left[\frac{\Theta}{3} - \frac{\mu\bar{\chi}\Theta}{\nu\theta_c(\bar{\chi})} - \left(\frac{\nu\theta_c(\bar{\chi})}{3\bar{\chi}} \right)^{\frac{1}{2}} \theta_3 \left(\frac{\bar{\chi}\Theta}{\nu\theta_c(\bar{\chi})} \right) \right. \\ &\quad \left. - \frac{\nu\theta_c(\bar{\chi})}{3} + \mu\bar{\chi} + \left(\frac{\nu\theta_c(\bar{\chi})}{3\bar{\chi}} \right)^{\frac{1}{2}} \theta_2(\bar{\chi}) \right], \end{aligned} \quad (3.2.77a)$$

where $\bar{\chi}$ is determined by

$$\Theta \bar{\chi} = \nu \theta_c(\bar{\chi}) \chi. \quad (3.2.77b)$$

It follows, given (3.2.56), the far-field WKB similarity solution is

$$\begin{aligned} & -8\eta^2(\chi) \left[\frac{\nu \theta_c(\bar{\chi})}{\Theta} \right]^{\frac{1}{2}} \exp \left[\frac{\Theta}{3} - \frac{\mu \bar{\chi} \Theta}{\nu \theta_c(\bar{\chi})} - \left(\frac{\nu \theta_c(\bar{\chi})}{3} \right)^{\frac{1}{2}} \theta_0 \left(\frac{\bar{\chi} \Theta}{\nu \theta_c(\bar{\chi})} \right) \right. \\ & \quad \left. - \frac{\nu \theta_c(\bar{\chi})}{3} + \mu \bar{\chi} + \left(\frac{\nu \theta_c(\bar{\chi})}{3 \bar{\chi}} \right)^{\frac{1}{2}} \theta_0(\bar{\chi}) \right], \\ & \quad \times \exp \left[-\frac{2}{\nu} \left(\frac{\Theta}{3} \right)^{\frac{3}{2}} \chi^{-\frac{1}{2}} \right] \end{aligned}$$

where $\bar{\chi}$ satisfies $\Theta \bar{\chi} = \nu \theta_c(\bar{\chi}) \chi$. This completes the leading-order solution to the perturbation field.

The final uniform solution of the perturbed soliton is obtained by asymptotically matching the solutions from each region, which is done by adding together the solution to each region and subtracting the contributions in the overlap zones (Bender and Orszag, 1978). The time evolution of the decaying solution is shown in Figure 8.

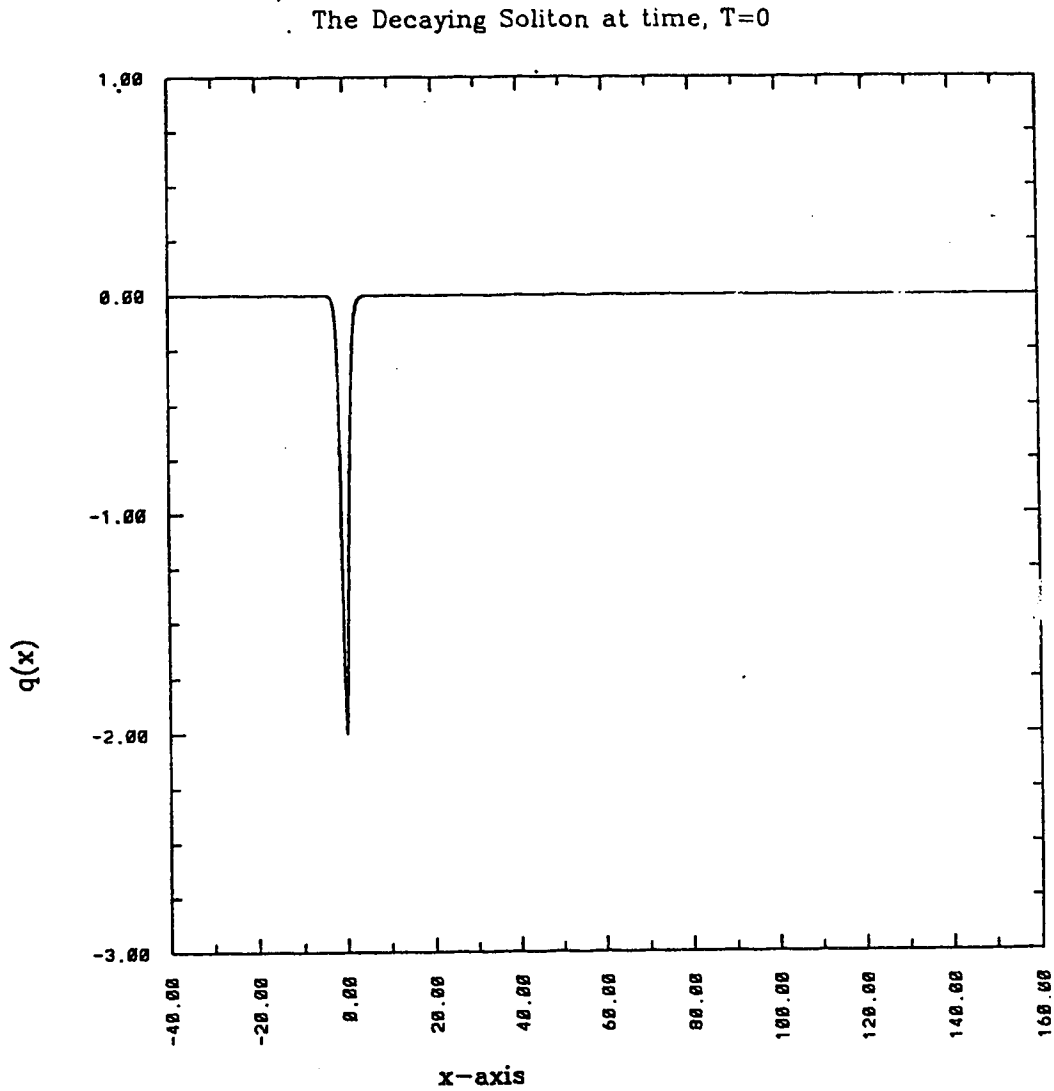


Figure 8: Evolution of the Decaying Soliton

Figures 8a-k depict the evolution of the decaying soliton at time $T = 0, 1, 2, 3, 4, 5, 10, 15, 20, 25$ and 30 , respectively for parameter value $\nu = \frac{1}{40}$.

The Decaying Soliton at time, $T=1$

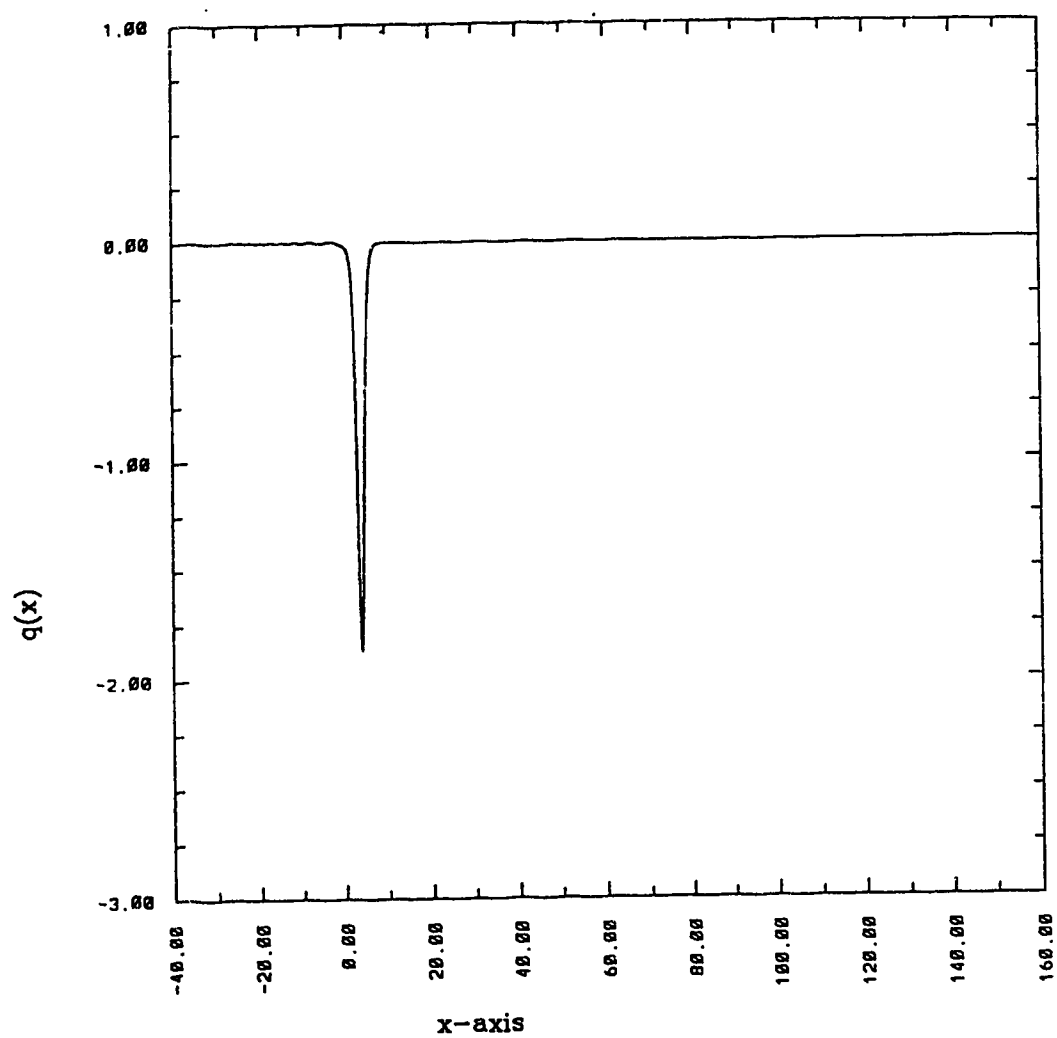


Figure 8b

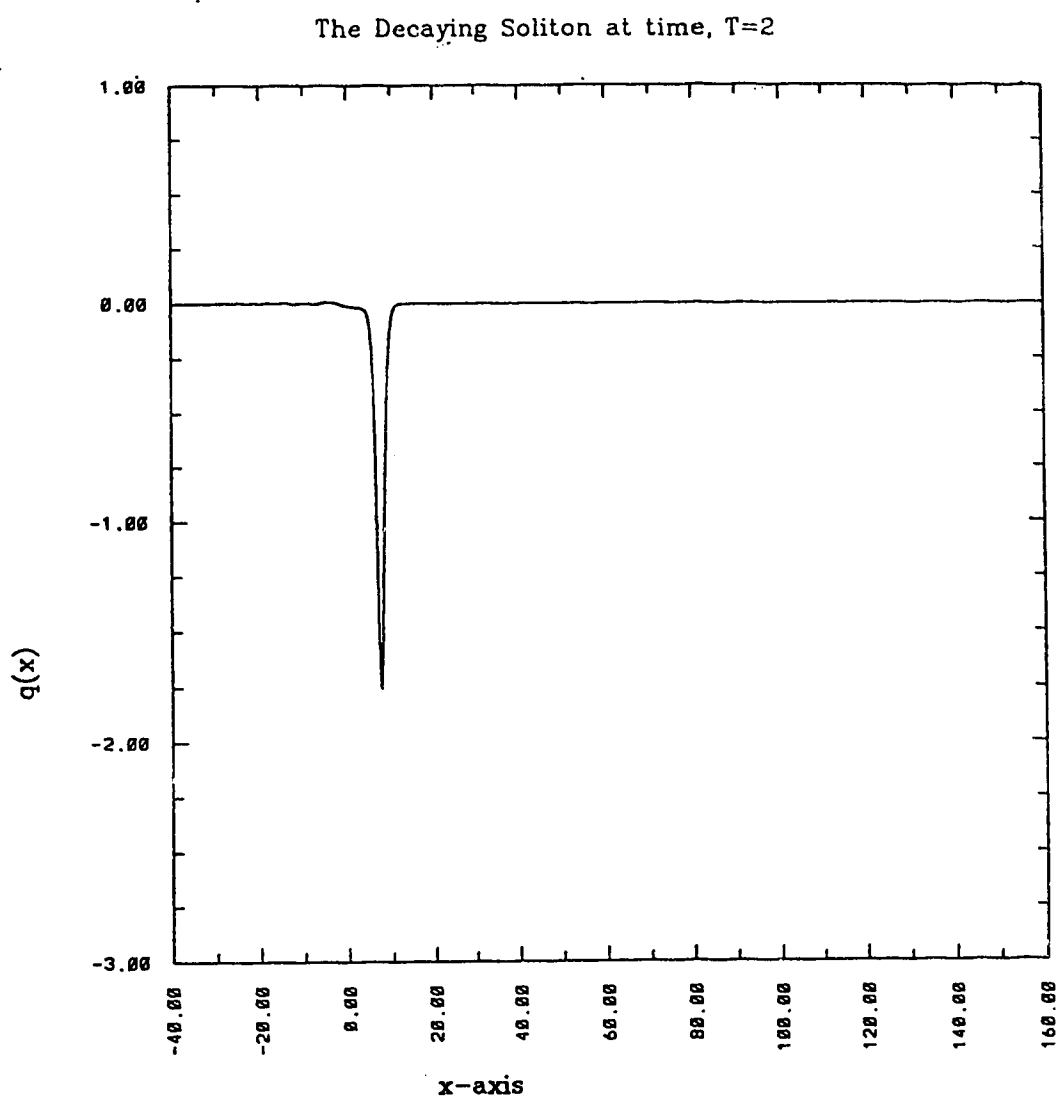


Figure 8c

The Decaying Soliton at time, $T=3$

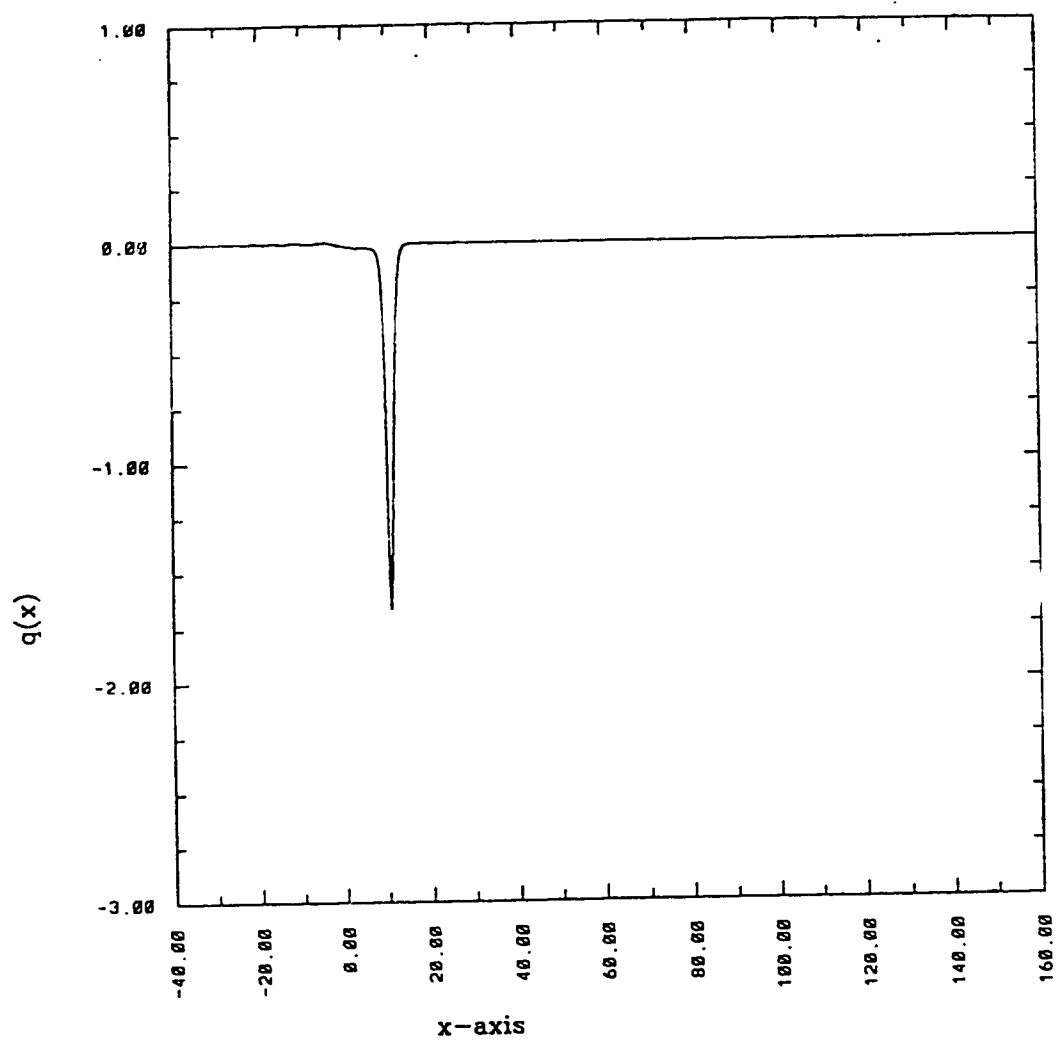


Figure 8d

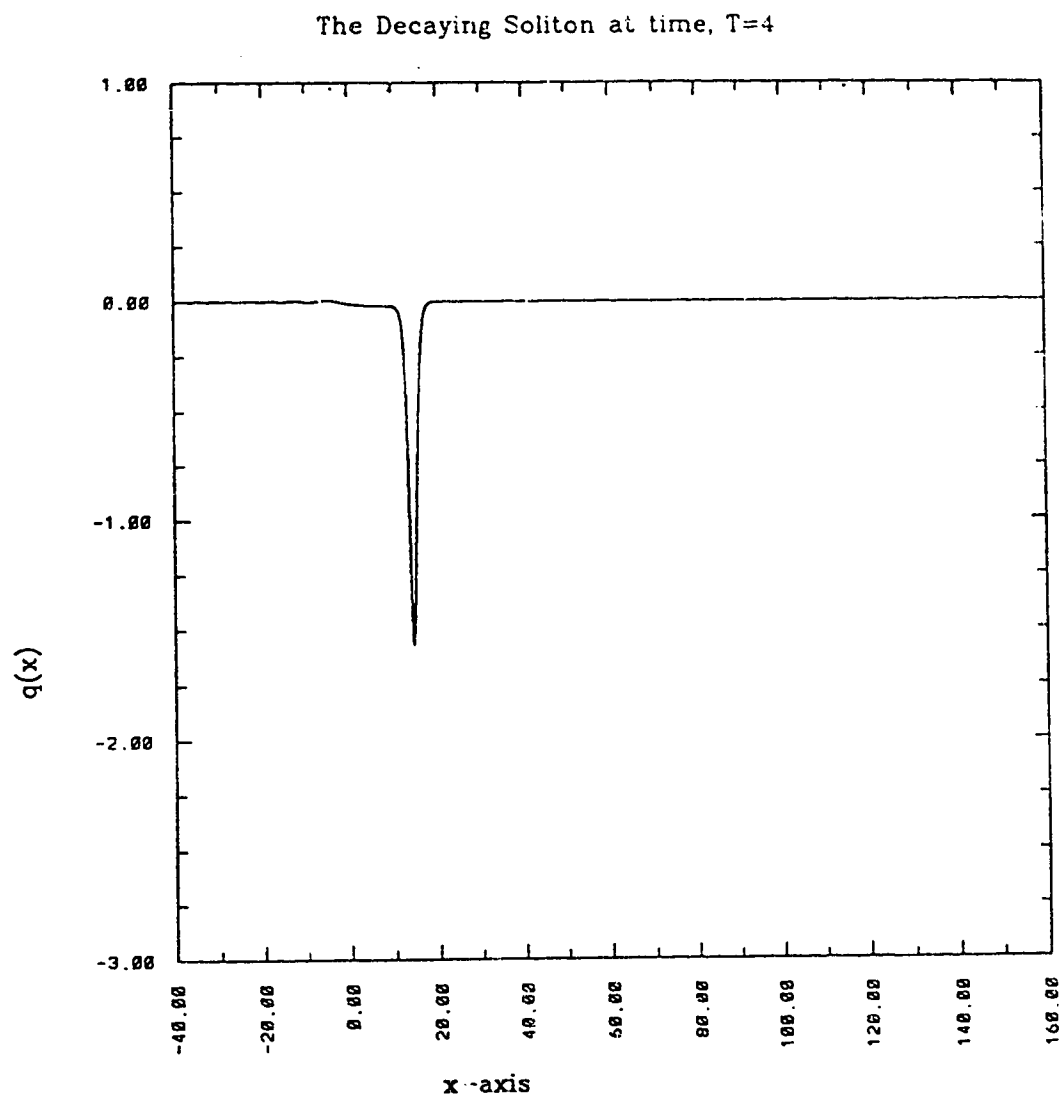


Figure 8e

The Decaying Soliton at time, $T=5$

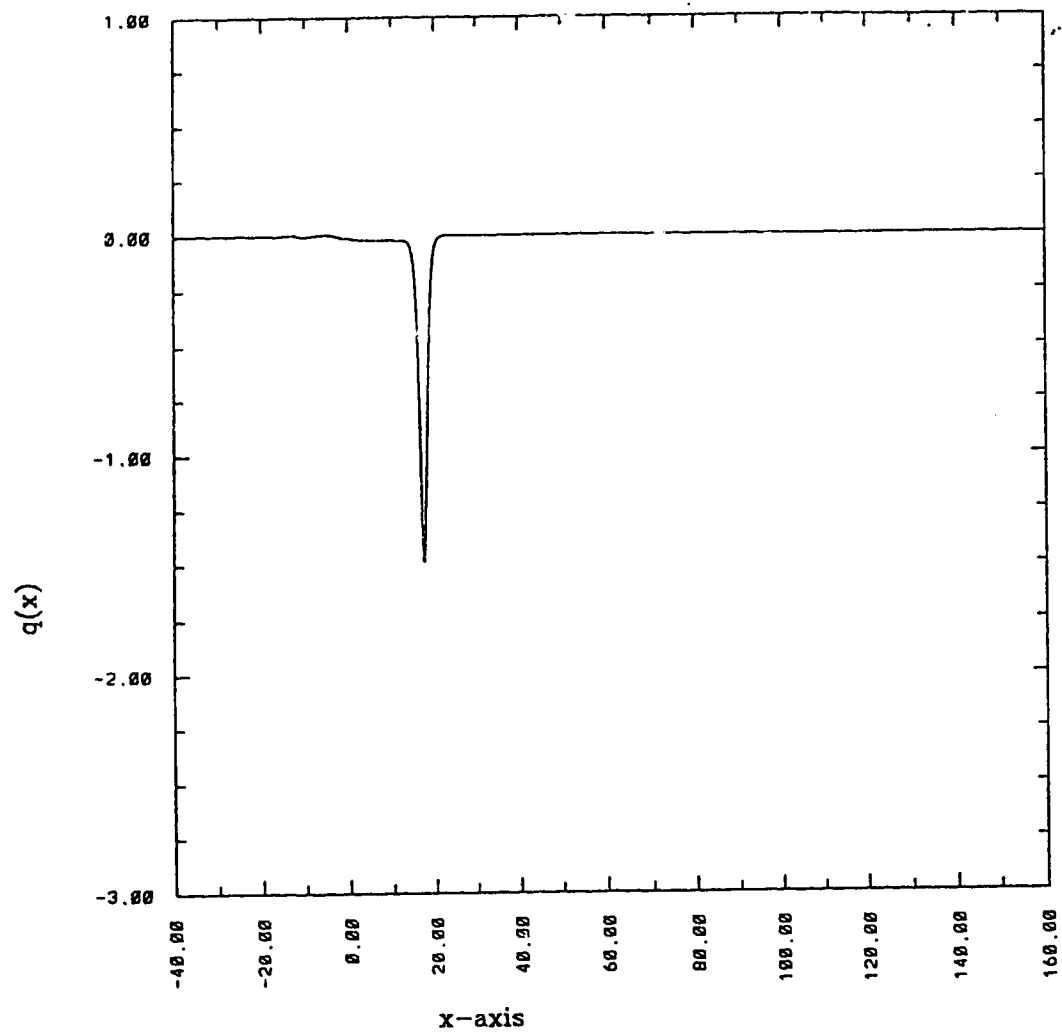


Figure 8f

The Decaying Soliton at time, $T=10$

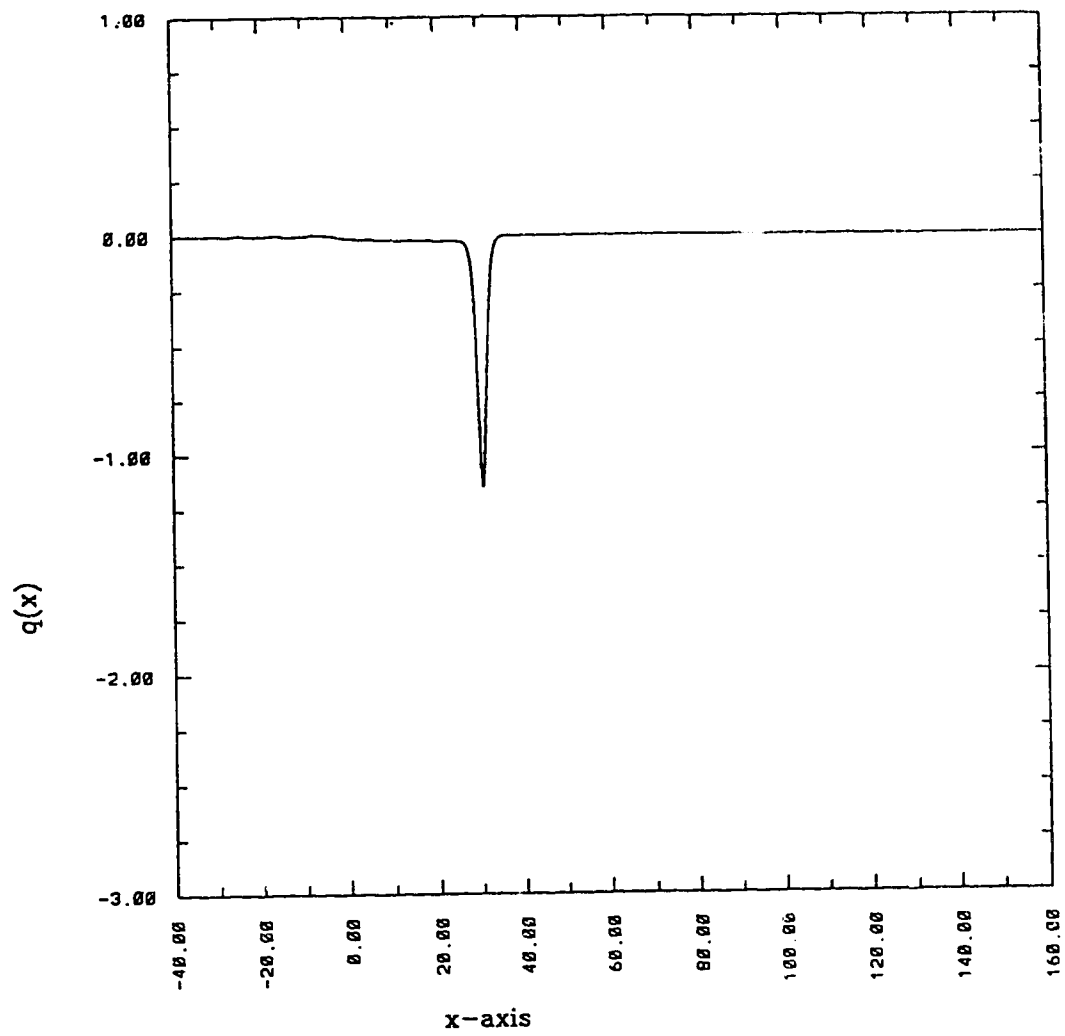


Figure 8g

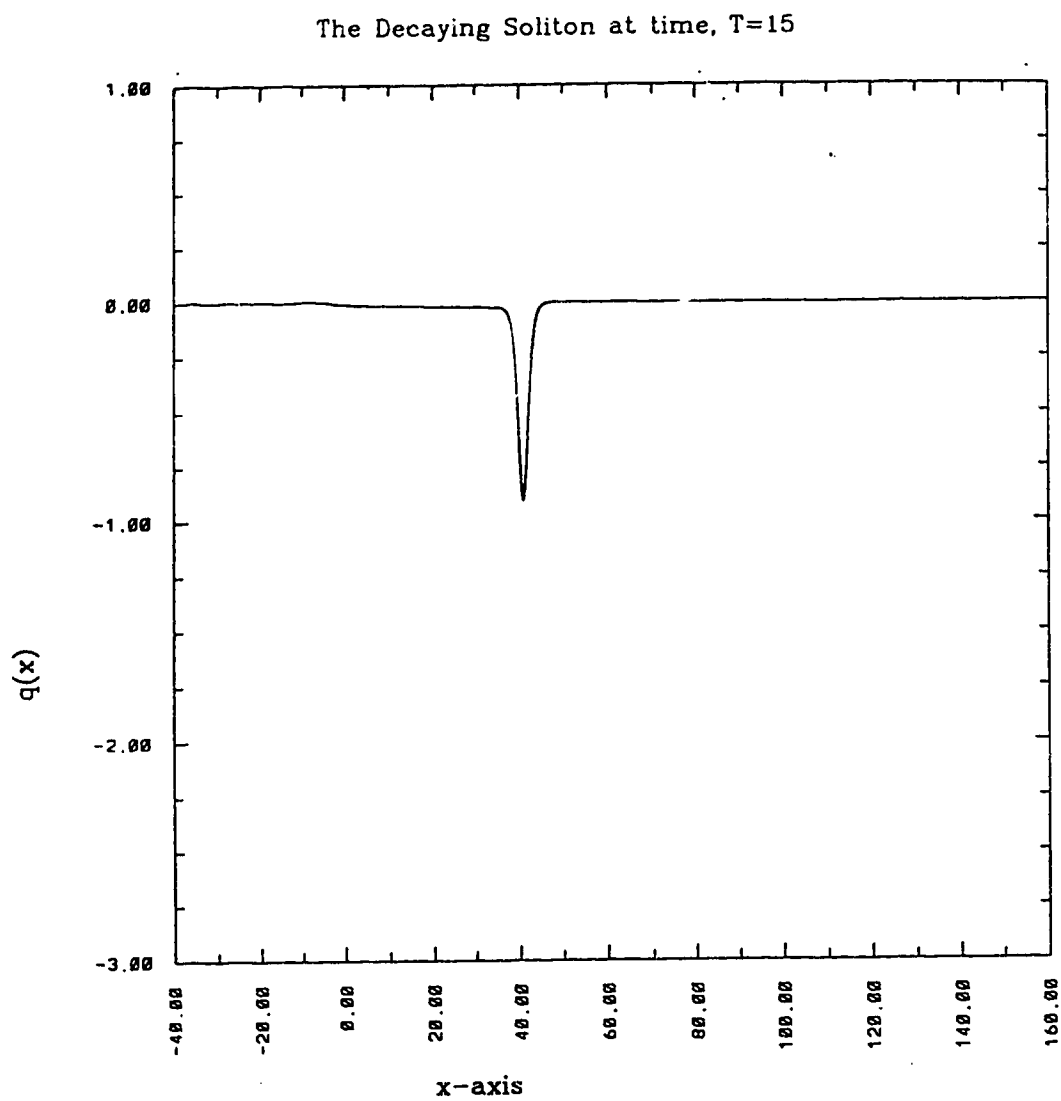


Figure 8h

The Decaying Soliton at time, $T=20$

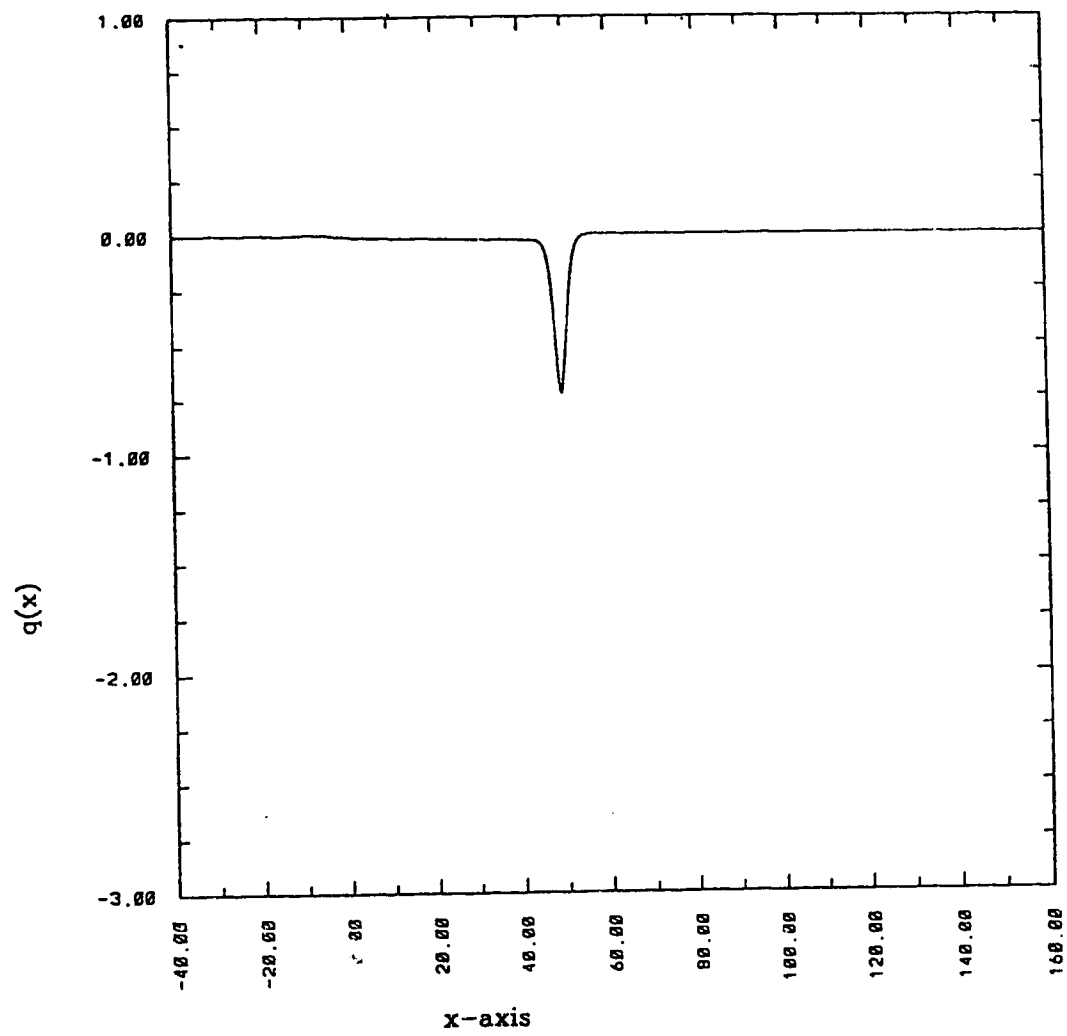


Figure 8i

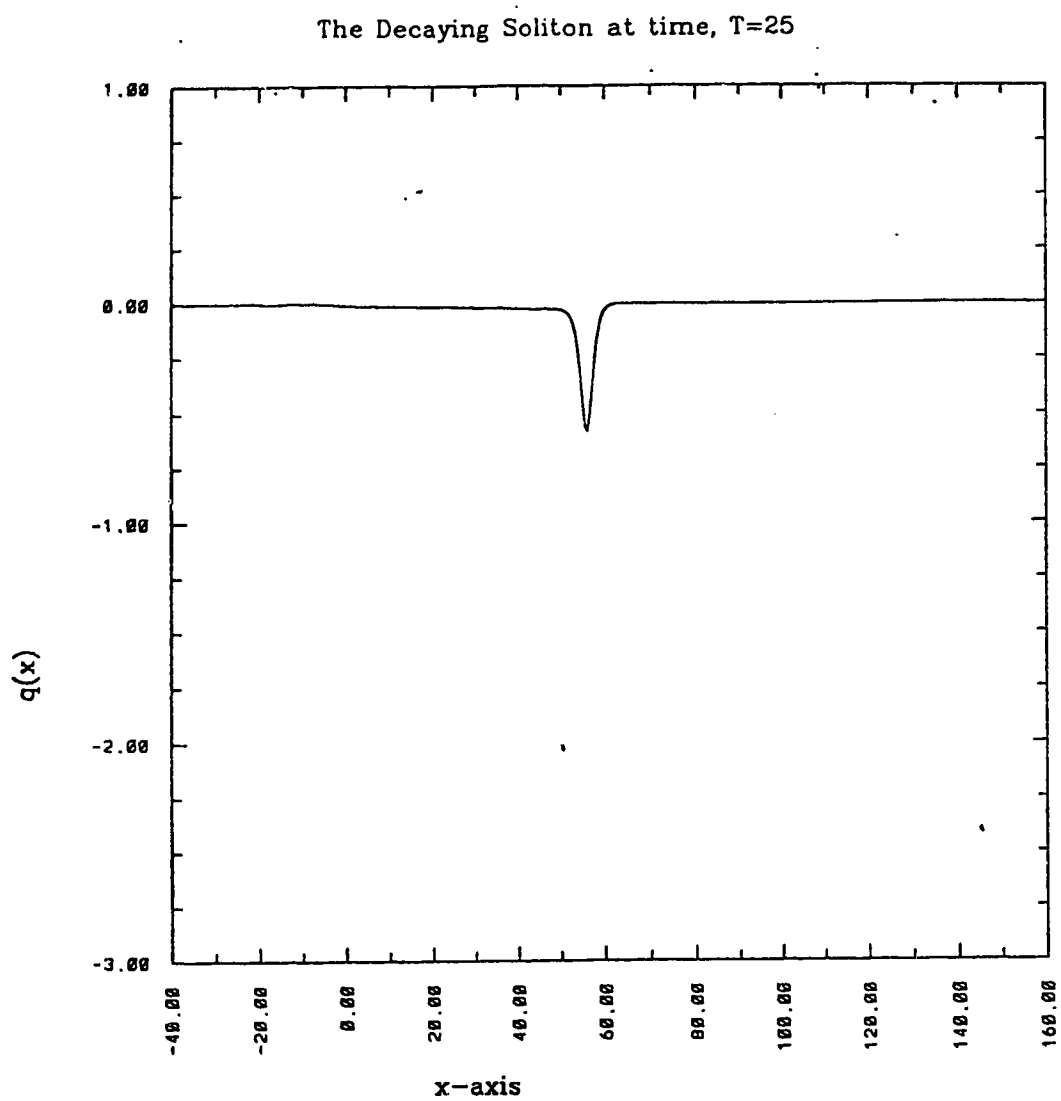


Figure 8j

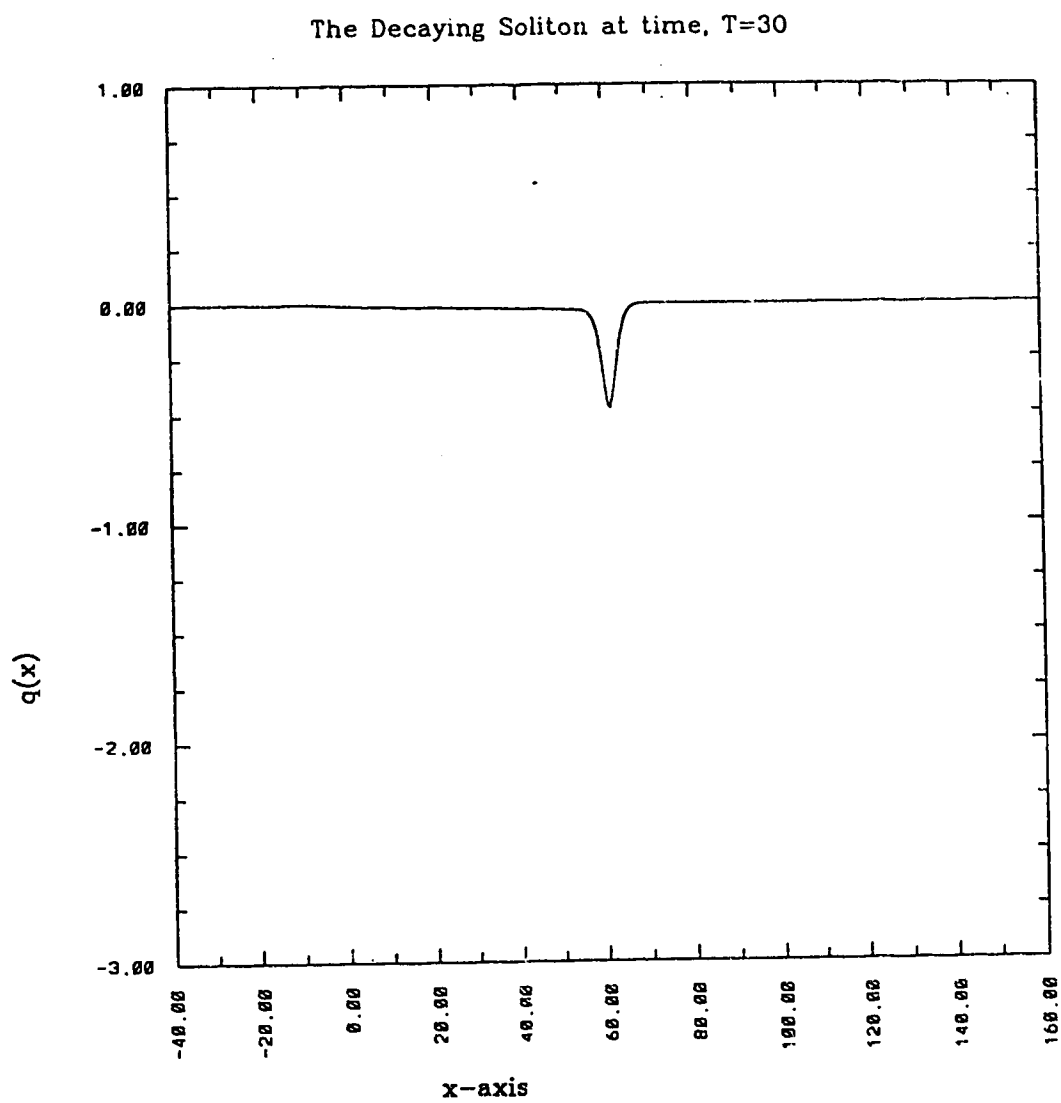


Figure 8k

Chapter 4

Numerical Solution

Zabusky and Kruskal (1965) originally solved the unforced KdV equation

$$u_t + uu_x + u_{xxx} = 0,$$

using a leap-frog scheme. Their scheme used centred differences to represent the derivatives. Hence, the terms u_t , u_x , and u_{xxx} were given by

$$\begin{aligned} u_t &= \frac{u_j^{n+1} - u_j^{n-1}}{2\Delta t} + O((\Delta t)^2), \\ u_x &= \frac{u_{j+1}^n - u_{j-1}^n}{2\Delta x} + O((\Delta x)^2), \\ u_{xxx} &= \frac{u_{j+2}^n - 2u_{j+1}^n + 2u_{j-1}^n - u_{j-2}^n}{2(\Delta x)^3} + O((\Delta x)^2). \end{aligned}$$

In order to maintain the second order accuracy of the difference scheme, they chose to approximate u by the spatial average

$$u = \frac{1}{3}(u_{j+1}^n + u_j^n + u_{j-1}^n) + O((\Delta x)^2).$$

This choice for u resulted in a scheme which not only conserved mass but also conserved energy to second order. Linear stability analysis of this scheme showed it to be stable (Vliegenthart, 1971), provided

$$\Delta t \leq \frac{(\Delta x)^3}{(4 + (\Delta x)^2|U|)},$$

where $|U|$ is taken as the maximum amplitude of u . Following this approach, Knickerbocker and Newell (1980) used this scheme to simulate the differential equation

$$u_t + 6uu_x + u_{xxx} = -\mu u,$$

where $0 < \mu \ll 1$. Their simulation, using this scheme, provided results which were in very close agreement to their asymptotic solutions.

4.1 The Numerical Scheme

Following the lead of Knickerbocker and Newell (1980), it was decided to employ the numerical scheme of Zabusky and Kruskal (1965) to simulate the equation

$$q_t - 6qq_x + q_{xxx} = \nu(-q + q_{xx}). \quad (4.1.1)$$

(Note that this is identical to equation (3.2.2) with $\mu \equiv 1$.) Under this scheme the terms in equation (4.1.1) are discretized by

$$q = \frac{1}{3} (q_{j+1}^n + q_j^n + q_{j-1}^n) + O((\Delta x)^2), \quad (4.1.2a)$$

$$q_t = \frac{q_j^{n+1} - q_j^{n-1}}{2\Delta t} + O((\Delta t)^2), \quad (4.1.2b)$$

$$q_x = \frac{q_{j+1}^n - q_{j-1}^n}{2\Delta x} + O((\Delta x)^2), \quad (4.1.2c)$$

$$q_{xx} = \frac{q_{j+1}^n - 2q_j^n + q_{j-1}^n}{(\Delta x)^2} + O((\Delta x)^2), \quad (4.1.2d)$$

$$q_{xxx} = \frac{q_{j+2}^n - 2q_{j+1}^n + 2q_{j-1}^n - q_{j-2}^n}{2(\Delta x)^3} + O((\Delta x)^2), \quad (4.1.2e)$$

where $t = n\Delta t$ and $x = j\Delta x$.

When employing this scheme to solve (4.1.1), it is necessary to calculate the terms on the right-hand side (the forcing terms) at the $(n-1)^{\text{st}}$ time step as the scheme is unconditionally unstable if these terms are calculated at the n^{th} time step. In consideration of this stability requirement, substitution of (4.1.2) into (4.1.1) leads to

$$\begin{aligned} q_j^{n+1} = q_j^{n-1} &+ \frac{2\Delta t}{\Delta x} [q_{j+1}^n + q_j^n + q_{j-1}^n] [q_{j+1}^n - q_{j-1}^n] \\ &- \frac{\Delta t}{(\Delta x)^3} [q_{j+2}^n - 2q_{j+1}^n + 2q_{j-1}^n - q_{j-2}^n] \end{aligned}$$

$$\begin{aligned}
& -\frac{2\nu\Delta t}{3} [q_{j+1}^{n-1} + q_j^{n-1} + q_{j-1}^{n-1}] \\
& + \frac{2\nu\Delta t}{(\Delta x)^2} [q_{j+1}^{n-1} - 2q_j^{n-1} + q_{j-1}^{n-1}].
\end{aligned} \tag{4.1.3}$$

To determine the linear stability condition for (4.1.3), we follow the approach of Vliegthart (1971) (assuming q to be slowly varying) and study a localized version of (4.1.3). Under this assumption, the nonlinear term in (4.1.3) is replaced by

$$\frac{6\Delta t}{\Delta x} q [q_{j+1}^n - q_{j-1}^n], \tag{4.1.4}$$

so that (4.1.3) becomes

$$\begin{aligned}
q_j^{n+1} = & q_j^{n-1} + \frac{6\Delta t}{\Delta x} q [q_{j+1}^n - q_{j-1}^n] \\
& - \frac{\Delta t}{(\Delta x)^3} [q_{j+2}^n - 2q_{j+1}^n + 2q_{j-1}^n - q_{j-2}^n] \\
& - \frac{2\nu\Delta t}{3} [q_{j+1}^{n-1} + q_j^{n-1} + q_{j-1}^{n-1}] \\
& + \frac{2\nu\Delta t}{(\Delta x)^2} [q_{j+1}^{n-1} - 2q_j^{n-1} + q_{j-1}^{n-1}],
\end{aligned} \tag{4.1.5}$$

where q in the nonlinear term represents some local value of the solution.

The exact solution of (4.1.5) may be represented by the Fourier series

$$q_j^n = \sum_{k=-\infty}^{\infty} C_k \xi^k \exp(ikj\Delta x). \tag{4.1.6}$$

To determine the amplification factor, ξ , we substitute the k^{th} term of (4.1.6) for q_j^n (i.e. let $q_j^n = \xi^n \exp(ikj\Delta x)$ in (4.1.5). This yields the equation

$$\begin{aligned}
& \xi^2 + \left\{ 4i \sin \theta \frac{\Delta t}{\Delta x} \left[\frac{1}{(\Delta x)^2} (\cos \theta - 1) - 3q \right] \right\} \xi \\
& + 2\nu\Delta t \left[\frac{1}{3} (2 \cos \theta + 1) - \frac{2}{(\Delta x)^2} (\cos \theta - 1) \right] - 1 = 0,
\end{aligned} \tag{4.1.7}$$

where $\theta = k\Delta x$, which is quadratic in ξ . It follows that ξ is given by

$$\begin{aligned} \xi = & -2i \sin \theta \frac{\Delta t}{\Delta x} \left[\frac{1}{(\Delta x)^2} (\cos \theta - 1) - 3q \right] \\ & \pm \left\{ -4 \sin^2 \theta \frac{(\Delta t)^2}{(\Delta x)^2} \left[\frac{1}{(\Delta x)^2} (\cos \theta - 1) - 3q \right]^2 \right. \\ & \left. - 2\nu \Delta t \left[\frac{1}{3} (2 \cos \theta + 1) - \frac{2}{(\Delta x)^2} (\cos \theta - 1) \right] + 1 \right\}^{1/2}. \end{aligned} \quad (4.1.8)$$

A necessary condition for stability is $|\xi| \leq 1$. If the discriminant of (4.1.8) is negative so that ξ is purely imaginary, it is readily shown that $|\xi| > 1$. It follows that a sufficient condition for stability is that the discriminant be non-negative, i.e.

$$\begin{aligned} & -4 \sin^2 \theta \frac{(\Delta t)^2}{(\Delta x)^2} \left[\frac{1}{(\Delta x)^2} (\cos \theta - 1) - 3q \right]^2 \\ & - 2\nu \Delta t \left[\frac{1}{3} (2 \cos \theta + 1) - \frac{2}{(\Delta x)^2} (\cos \theta - 1) \right] + 1 \geq 0, \end{aligned} \quad (4.1.9)$$

for all θ .

In the case of equality in (4.1.9), equation (4.1.8) yields the linear stability condition

$$\Delta t \leq \frac{(\Delta x)^3}{(4 + 6(\Delta x)^2 |q|)}. \quad (4.1.10)$$

For the discriminant strictly positive (4.1.8) yields

$$\Delta t \leq \frac{(\Delta x)^2}{\nu(4 + (\Delta x)^2)}, \quad (4.1.11)$$

as the linear stability condition. Therefore for a stable solution it is necessary that

$$\Delta t \leq \min \left\{ \frac{(\Delta x)^3}{(4 + 6(\Delta x)^2 |q|)}, \frac{(\Delta x)^2}{\nu(4 + (\Delta x)^2)} \right\}. \quad (4.1.12)$$

To show consistency of the numerical scheme, we introduce a Taylor expansion

for each term of (4.1.3) as follows.

$$u_j^{n\pm 1} = u_j^n \pm (\Delta t) \left(\frac{\partial u}{\partial t} \right)_j^n + \frac{1}{2}(\Delta t)^2 \left(\frac{\partial^2 u}{\partial t^2} \right)_j^n \pm \frac{1}{6}(\Delta t)^3 \left(\frac{\partial^3 u}{\partial t^3} \right)_j^n + \dots \quad (4.1.13a)$$

$$u_{j\pm 2}^n = u_j^n \pm 2(\Delta x) \left(\frac{\partial u}{\partial x} \right)_j^n + 2(\Delta x)^2 \left(\frac{\partial^2 u}{\partial x^2} \right)_j^n \pm \frac{4}{3}(\Delta x)^3 \left(\frac{\partial^3 u}{\partial x^3} \right)_j^n + \dots \quad (4.1.13b)$$

$$u_{j\pm 1}^n = u_j^n \pm (\Delta x) \left(\frac{\partial u}{\partial x} \right)_j^n + \frac{1}{2}(\Delta x)^2 \left(\frac{\partial^2 u}{\partial x^2} \right)_j^n \pm \frac{1}{6}(\Delta x)^3 \left(\frac{\partial^3 u}{\partial x^3} \right)_j^n + \dots \quad (4.1.13c)$$

$$\begin{aligned} u_{j\pm 1}^{n-1} = & u_j^n \pm (\Delta x) \left(\frac{\partial u}{\partial x} \right)_j^n - (\Delta t) \left(\frac{\partial u}{\partial t} \right)_j^n \\ & + \frac{1}{2}(\Delta x)^2 \left(\frac{\partial^2 u}{\partial x^2} \right)_j^n \mp (\Delta x)(\Delta t) \left(\frac{\partial^2 u}{\partial x \partial t} \right)_j^n \\ & + \frac{1}{2}(\Delta t)^2 \left(\frac{\partial^2 u}{\partial t^2} \right)_j^n + \dots \end{aligned} \quad (4.1.13d)$$

Substituting (4.1.13) into (4.1.3) we find that the truncation error is given by

$$\begin{aligned} & (\Delta t)^2 \left[-2\mu \frac{\partial u}{\partial t} + 2\mu \frac{\partial^3 u}{\partial^2 x \partial t} \right]_j^n \\ & + (\Delta t)(\Delta x)^2 \left[\frac{1}{2} \left(\frac{\partial^5 u}{\partial x^5} \right) - 2u \left(\frac{\partial^3 u}{\partial x^3} \right) - 4 \left(\frac{\partial u}{\partial x} \right) \left(\frac{\partial^2 u}{\partial x^2} \right) - \frac{1}{6} \left(\frac{\partial^4 u}{\partial x^4} \right) \right]_j^n \\ & + O((\Delta t)^3 + (\Delta t)(\Delta x)^4). \end{aligned} \quad (4.1.14)$$

Clearly,

$$\frac{\text{truncation error}}{(\Delta t)} \longrightarrow 0, \quad \text{as } (\Delta t), (\Delta x) \rightarrow 0.$$

Hence, the numerical scheme is consistent.

Having shown that the numerical scheme (4.1.2) is linearly stable and consistent, we implemented this scheme on a convex C210 vector processor using the values $\Delta x = 1/10$ and $\Delta t = 1/5010$. The phase position of the travelling soliton at time, t_0 , was determined using parabolic interpolation under the following algorithm.

Let $Y_m = \max_n |y_n|$, where y_n , $\{n = 0, 1, 2, \dots, N\}$ are the discrete values of the numerical solution at time, $t = t_0$. Then denoting the neighbouring values of Y_m as Y_{m-1} , Y_{m+1} , the discrete pairs (X_{m-1}, Y_{m-1}) , (X_m, Y_m) and (X_{m+1}, Y_{m+1}) are substituted into the parabolic equation

$$y = ax^2 + bx + c, \quad (4.1.15)$$

to determine the coefficients a , b , and c . The coefficients a , b , and c are given by

$$a = \Delta^{-1} [x_n y_{n+1} - x_{n+1} y_n - (x_{n-1} y_{n+1} - x_{n+1} y_{n-1}) + x_{n-1} y_n - x_n y_{n-1}], \quad (4.1.16a)$$

$$b = \Delta^{-1} [y_n x_{n+1}^2 - y_{n+1} x_n^2 - (y_{n-1} x_{n+1}^2 - y_{n+1} x_{n-1}^2) + y_{n-1} x_n^2 - y_n x_{n-1}^2], \quad (4.1.16b)$$

$$c = \Delta^{-1} [y_{n-1} (x_n x_{n+1}^2 - x_{n+1} x_n^2) - y_n (x_{n-1} x_{n+1}^2 - x_{n+1} x_{n-1}^2) + y_{n+1} (x_{n-1} x_n^2 - x_n x_{n-1}^2)], \quad (4.1.16c)$$

where

$$\Delta = x_n x_{n+1}^2 - x_{n+1} x_n^2 - (x_{n-1} x_{n+1}^2 - x_{n+1} x_{n-1}^2) + x_{n-1} x_n^2 - x_n x_{n-1}^2. \quad (4.1.16d)$$

Having determined a , b , and c , the phase position of the soliton at time t_0 is given by

$$x_0 = -b/2a, \quad (4.1.17)$$

from which is calculated the current amplitude, y_0 , given by

$$y_0 = ax_0^2 + bx_0 + c. \quad (4.1.18)$$

4.2 Comparison of Numerical Results to Perturbation Solution

To compare the numerical and perturbation solutions, it was decided to calculate the relative error of the phase position and the amplitude, the relative error being defined by

$$\delta_A = \frac{|A_p - A_n|}{A_n} \times 100\%, \quad (4.2.1)$$

where subscript p denotes the result from the perturbation theory of chapter 3 and subscript n denotes the numerical result from chapter 4, section 1.

Both the phase position and the amplitudes compare favourably with maximum error, over times $0 < t < 50$, given in the table below for the cases where the perturbation parameter $\nu = 1/40$ and $\nu = 1/100$ (μ is taken to have the value $\mu = 1.0$ for both cases) (see Figures 9 and 10).

	Maximum Error	
	$\nu = 1/40$	$\nu = 1/100$
Amplitude	0.612%	0.191%
Phase Position	1.53%	0.223%

Although the phase position and amplitude of the two solutions (numerical and perturbation) agree quite well, there are noticeable differences in the behaviour of the two solutions in the region of the shelf and the oscillatory wavetail (Figure 11). In the region of the wavetail, while the period of oscillation between the numerical and perturbation solutions is in close agreement, the amplitude of the oscillation differs significantly, with the amplitude of the wave in the perturbation solution being at least one order of magnitude larger than that of the numerical solution. Similarly, the shelf height, as determined by the perturbation solution, is also significantly greater than the shelf height determined numerically.

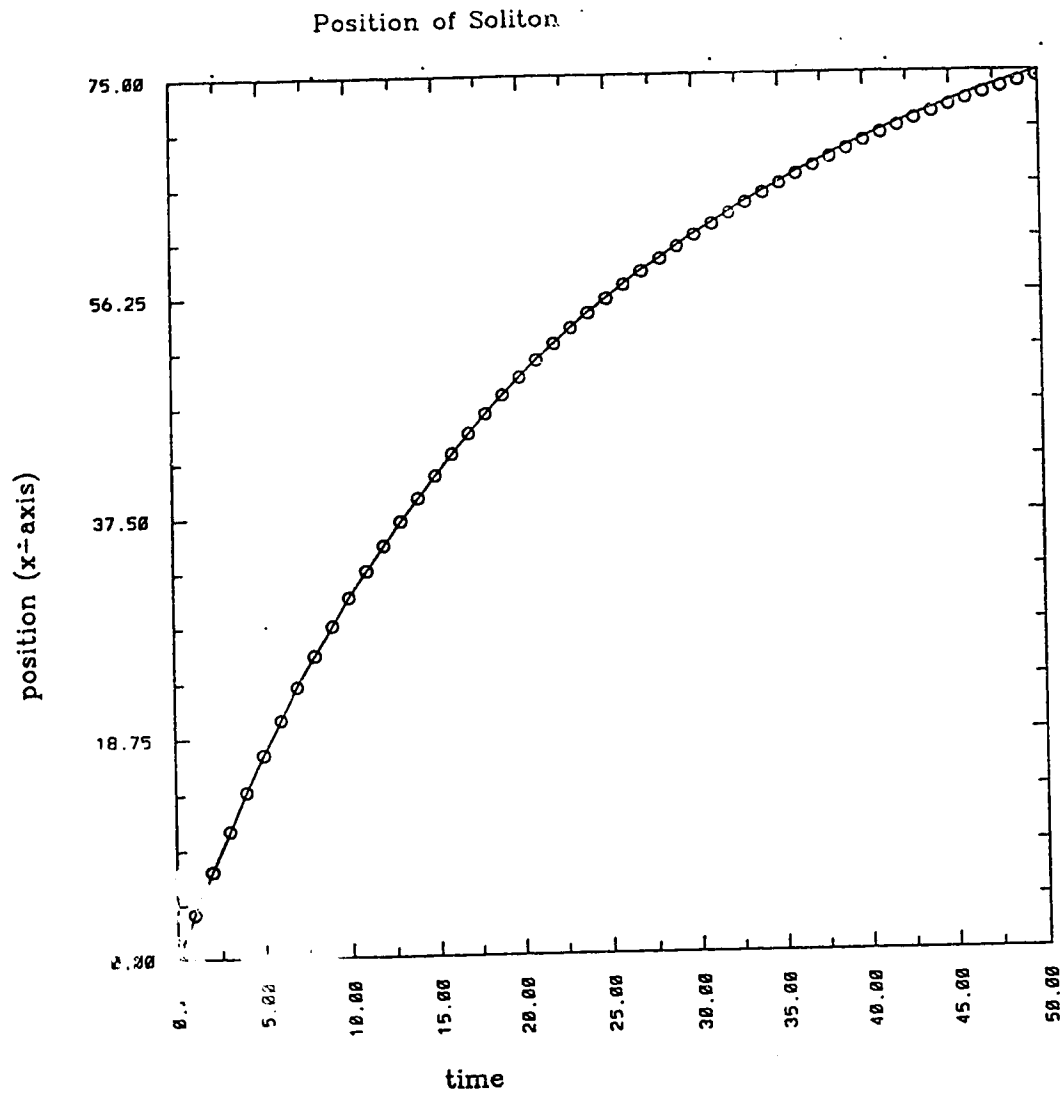


Figure 9: Comparison of Phase Position

Figures 9a and 9b show a comparison of the phase position vs time of the decaying soliton for parameter values $\nu = \frac{1}{40}$ and $\frac{1}{100}$ respectively. The solid line represents the perturbation solution while the numerical solution is represented by circles.

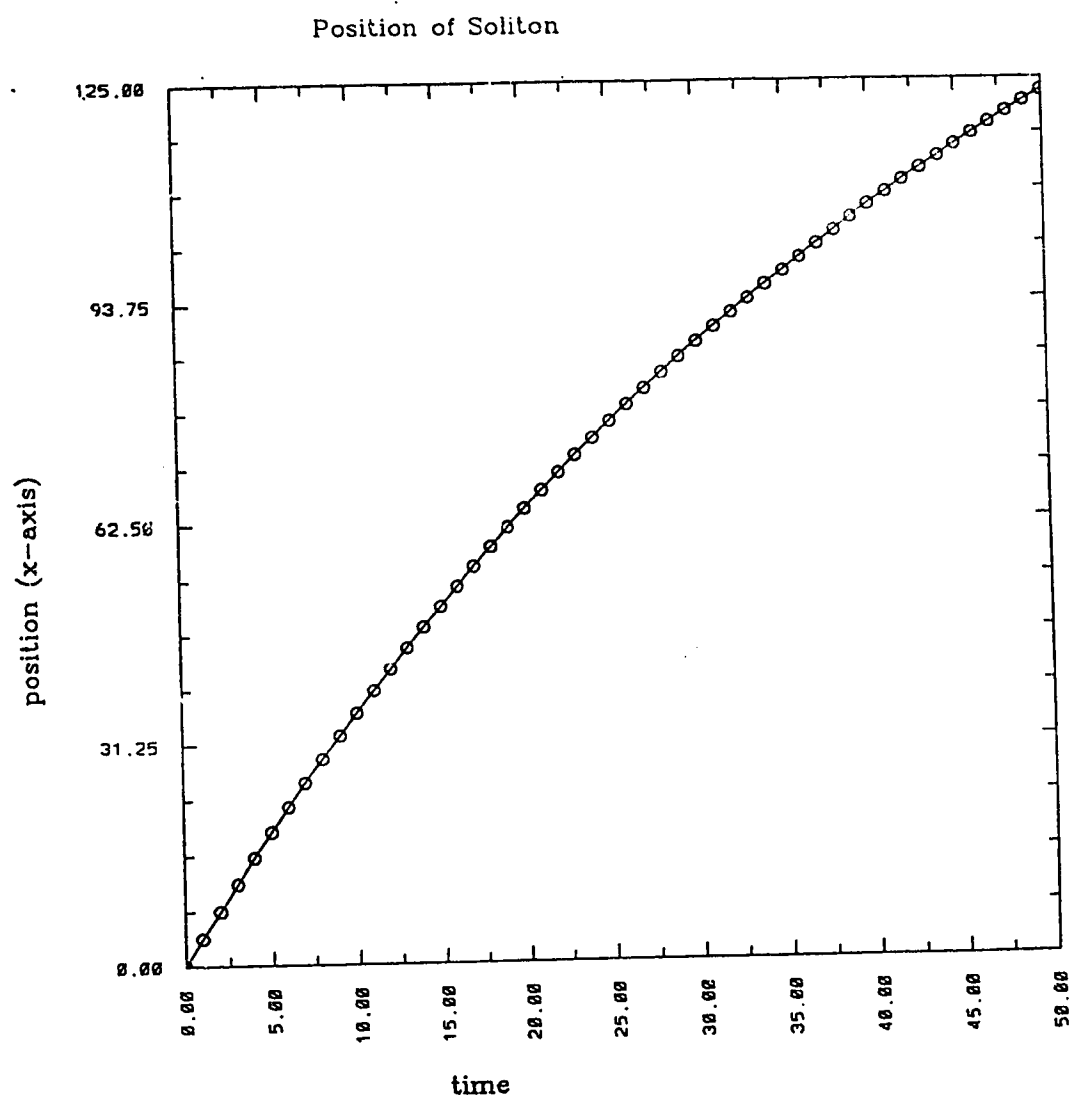


Figure 9b

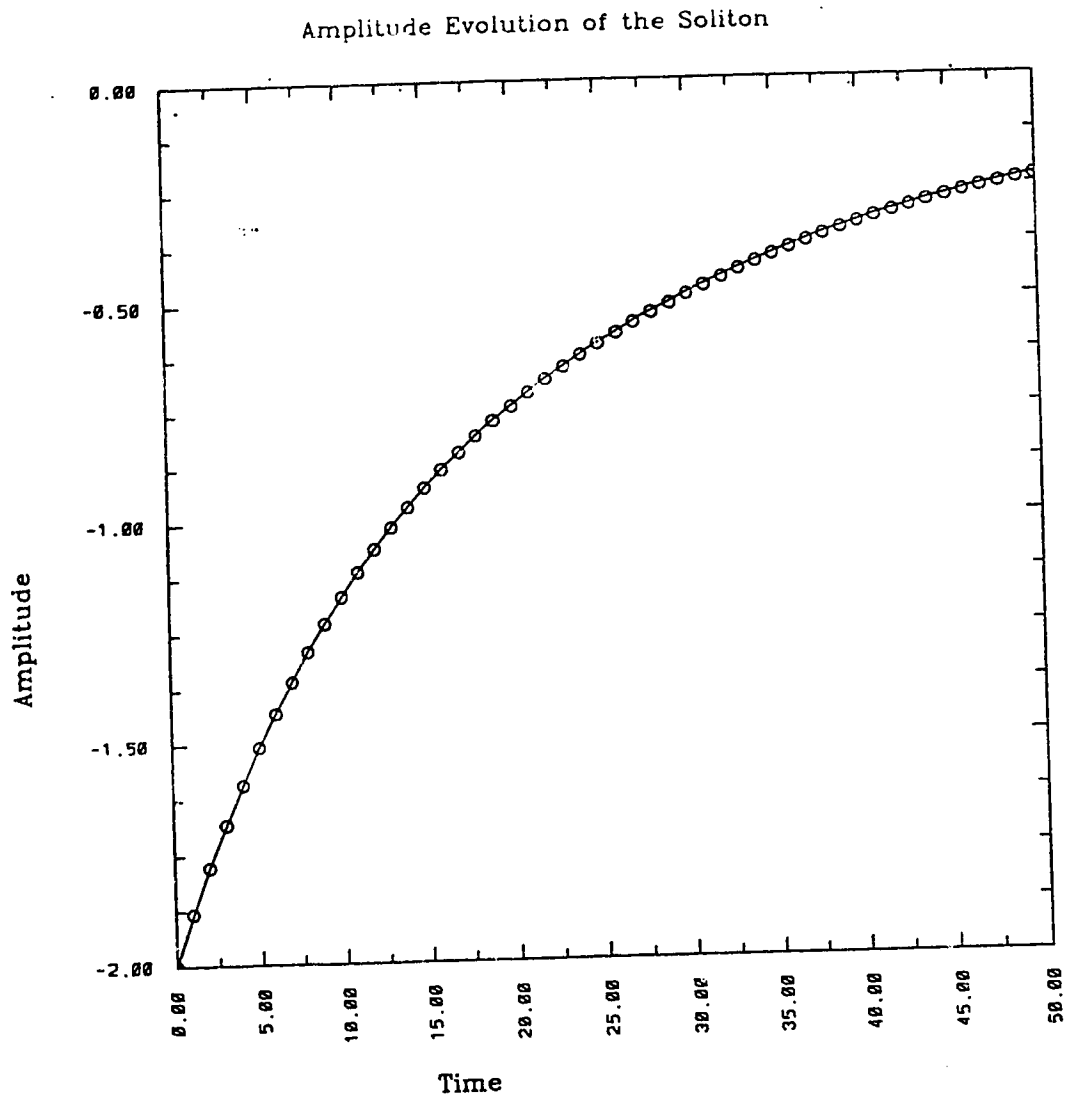


Figure 10: Comparison of the Amplitude Evolution

Figures 10a and 10b show a comparison of the amplitude vs time of the decaying soliton for parameter values $\nu = \frac{1}{40}$ and $\frac{1}{100}$ respectively. The solid line represents the perturbation solution while the numerical solution is represented by circles.

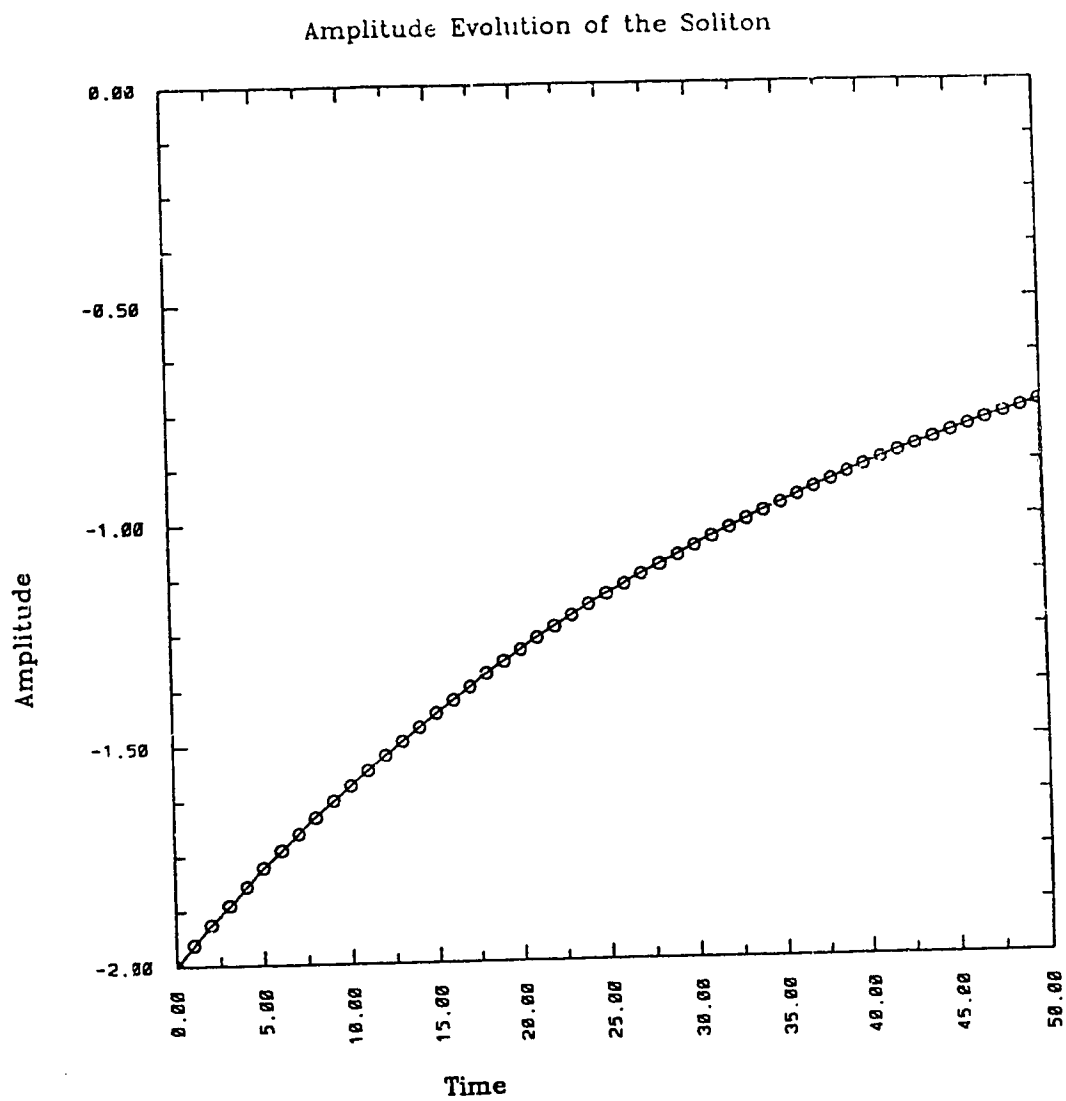


Figure 10b

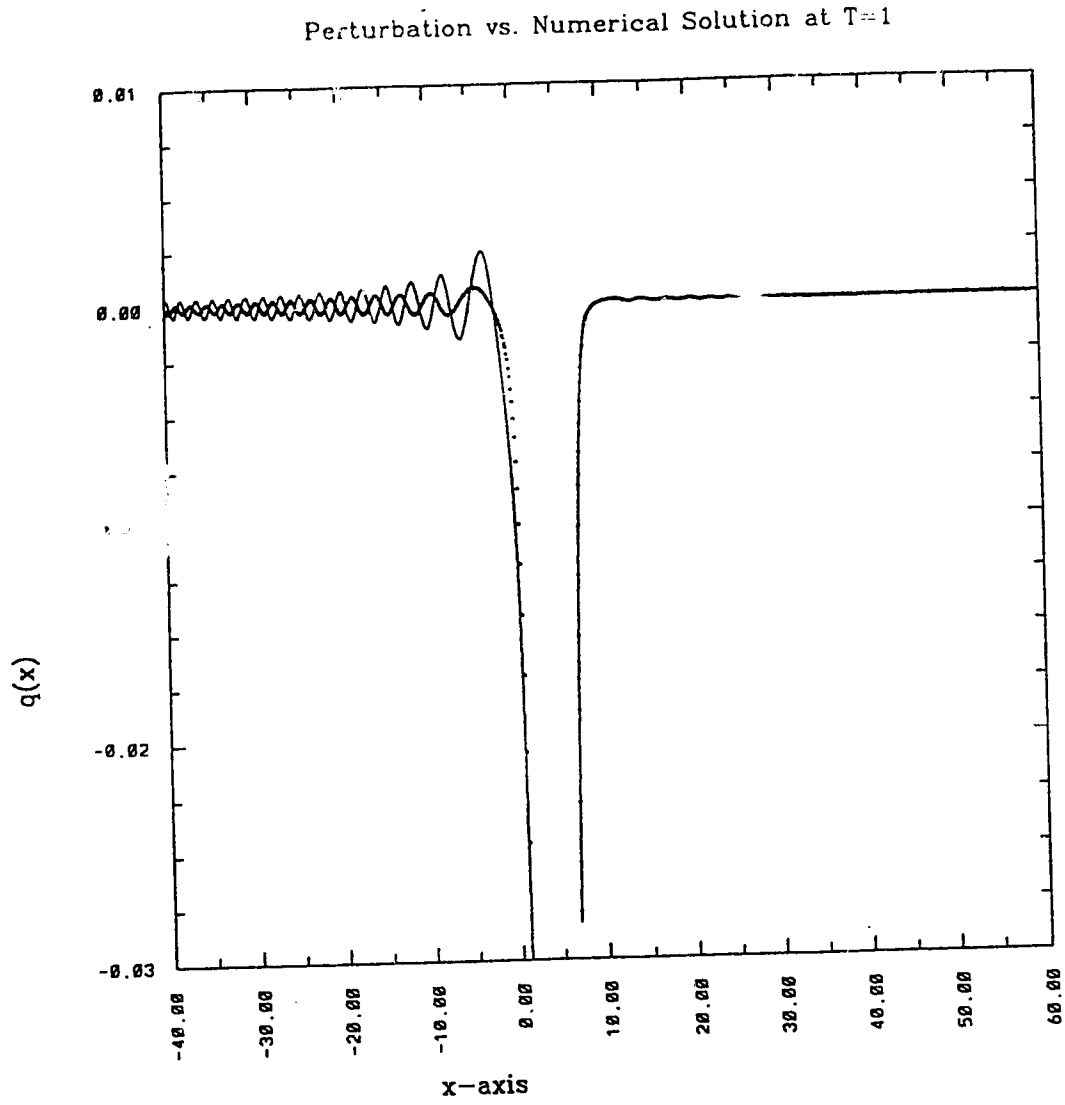


Figure 11: Comparison of Shelf and Wavetail Regions

Figures 11a-j show a comparison of the perturbation solution (thin line) to the numerical solution (dark line) in the region of the shelf and wavetail for times $T = 1, 2, 3, 4, 5, 10, 15, 20, 25$, and 50 with parameter $\nu = \frac{1}{100}$.

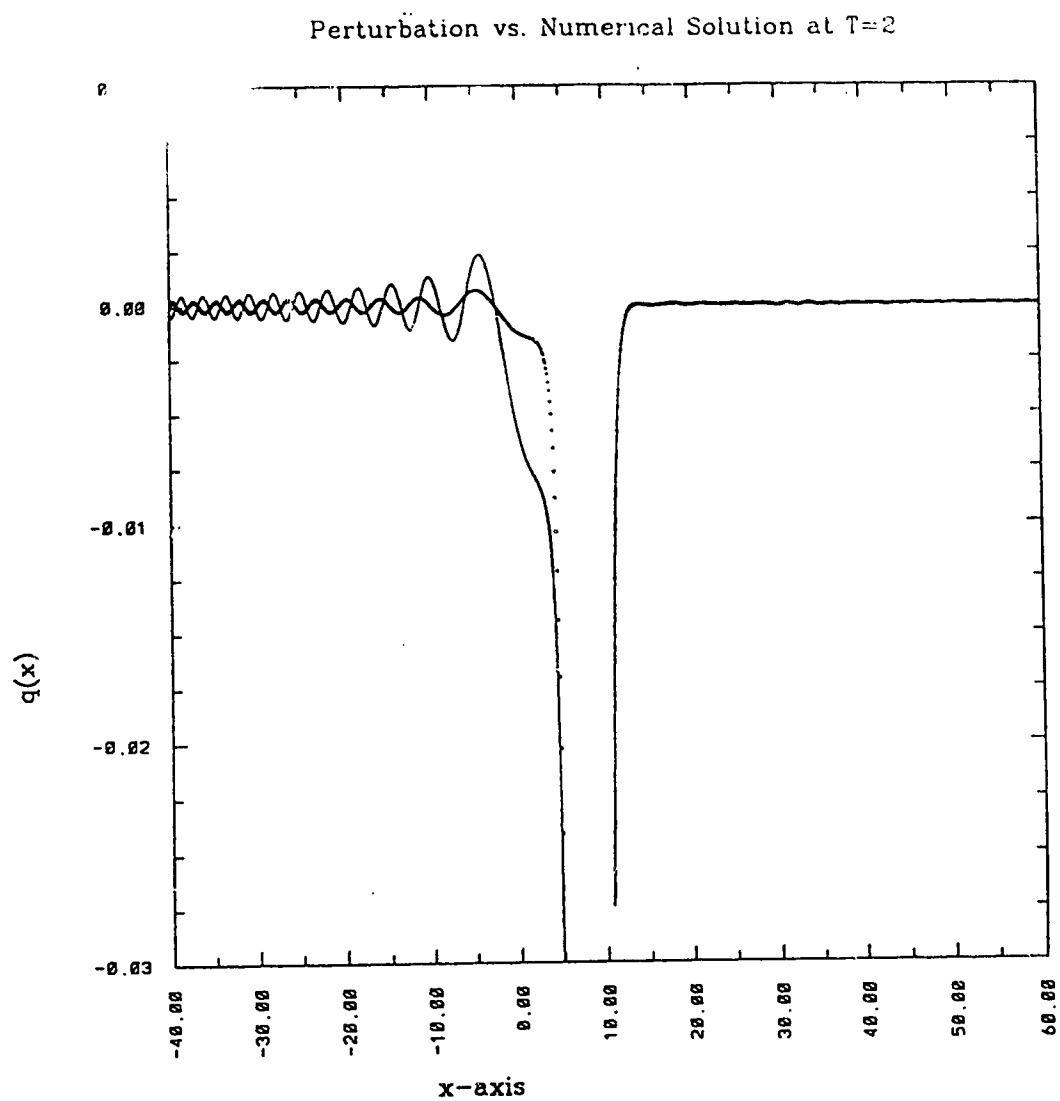


Figure 11b

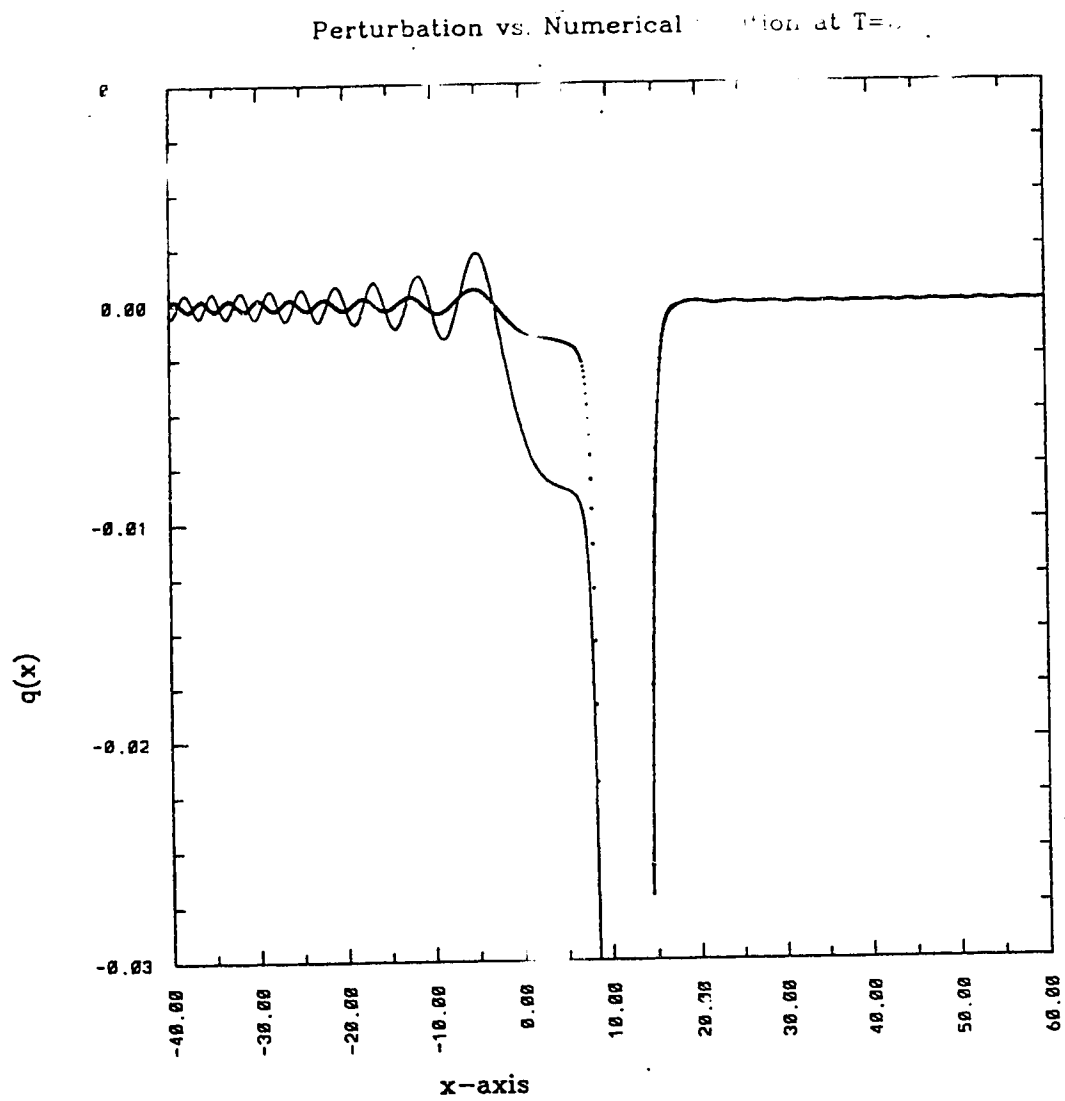


Figure 11c

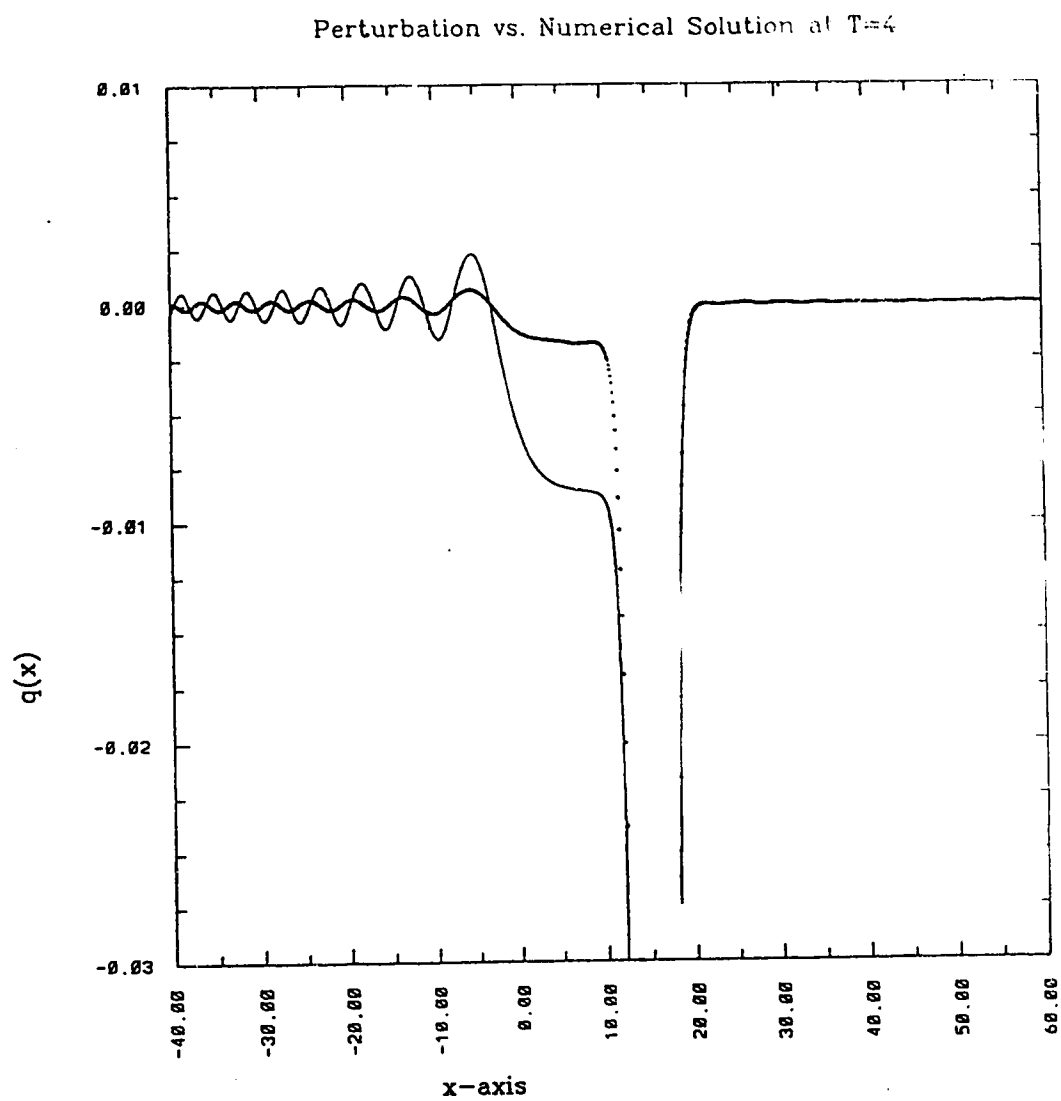


Figure 11d

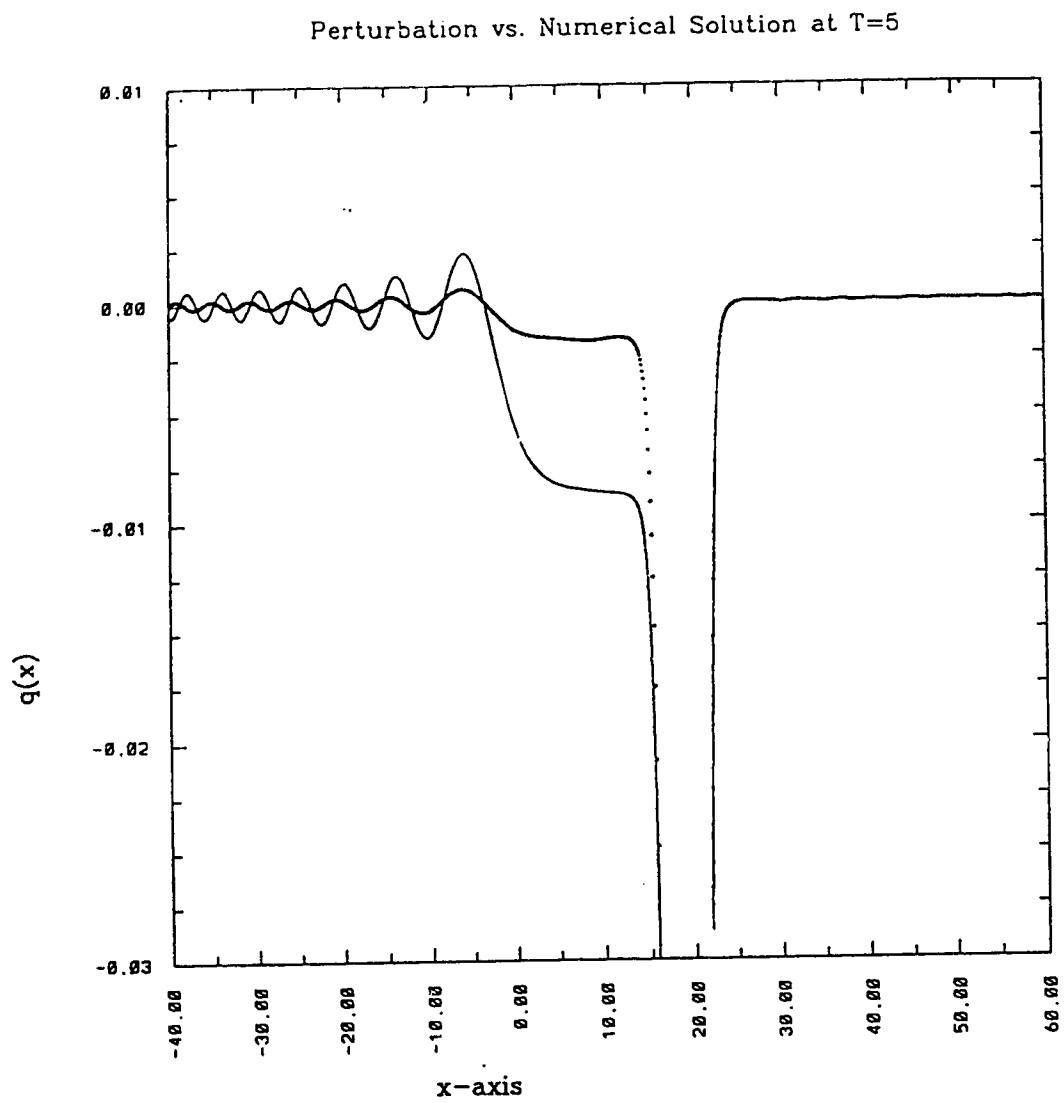


Figure 11e

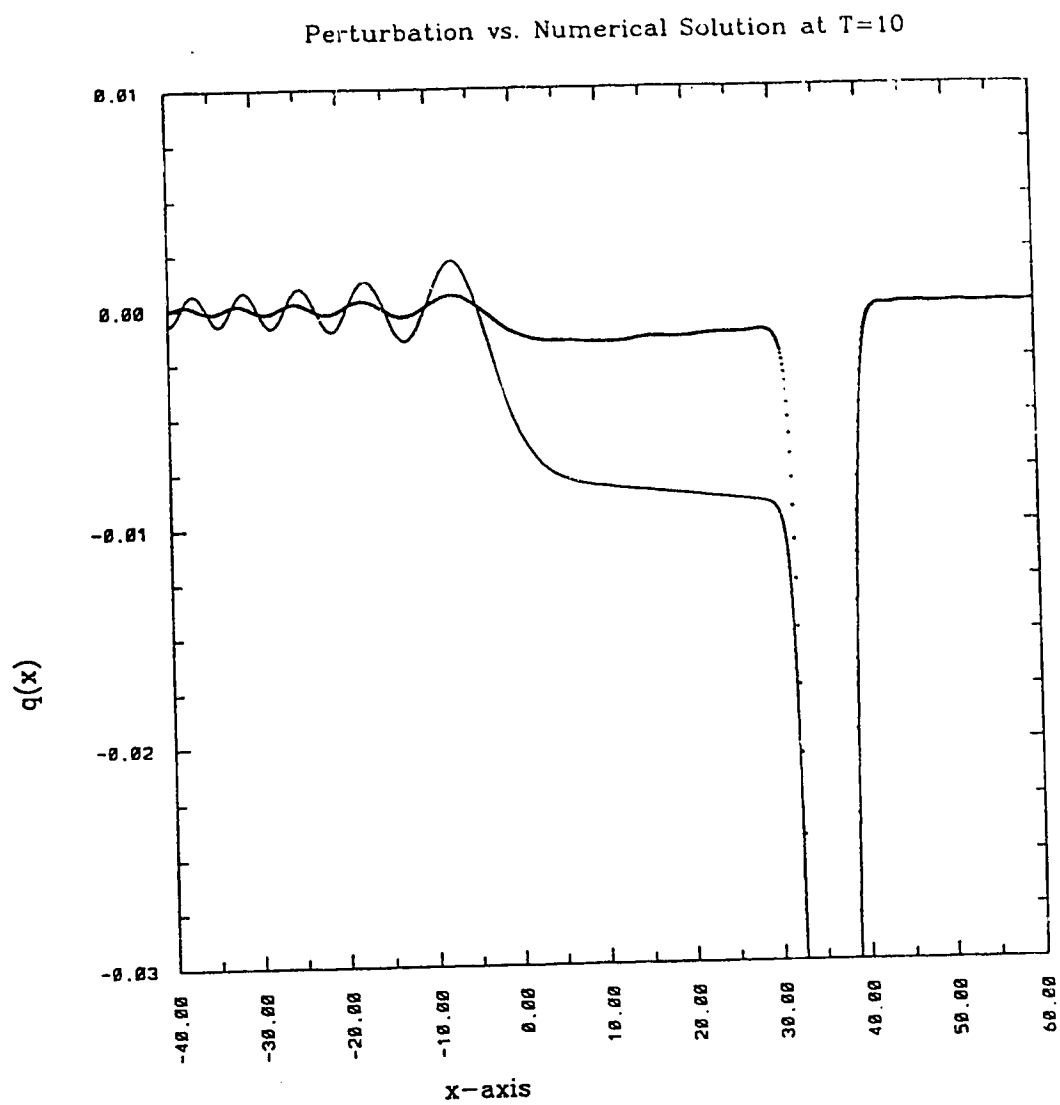


Figure 11f

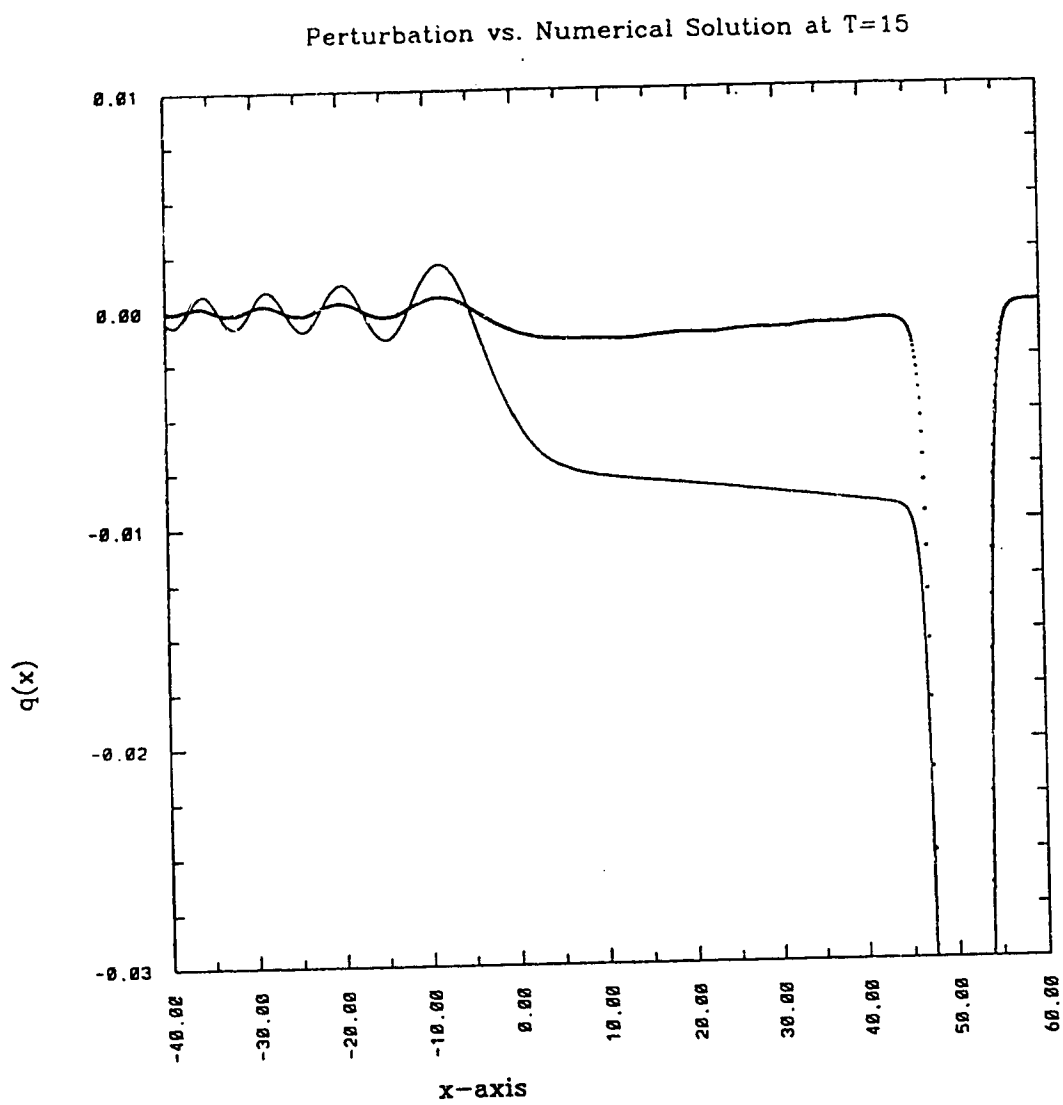


Figure 11g

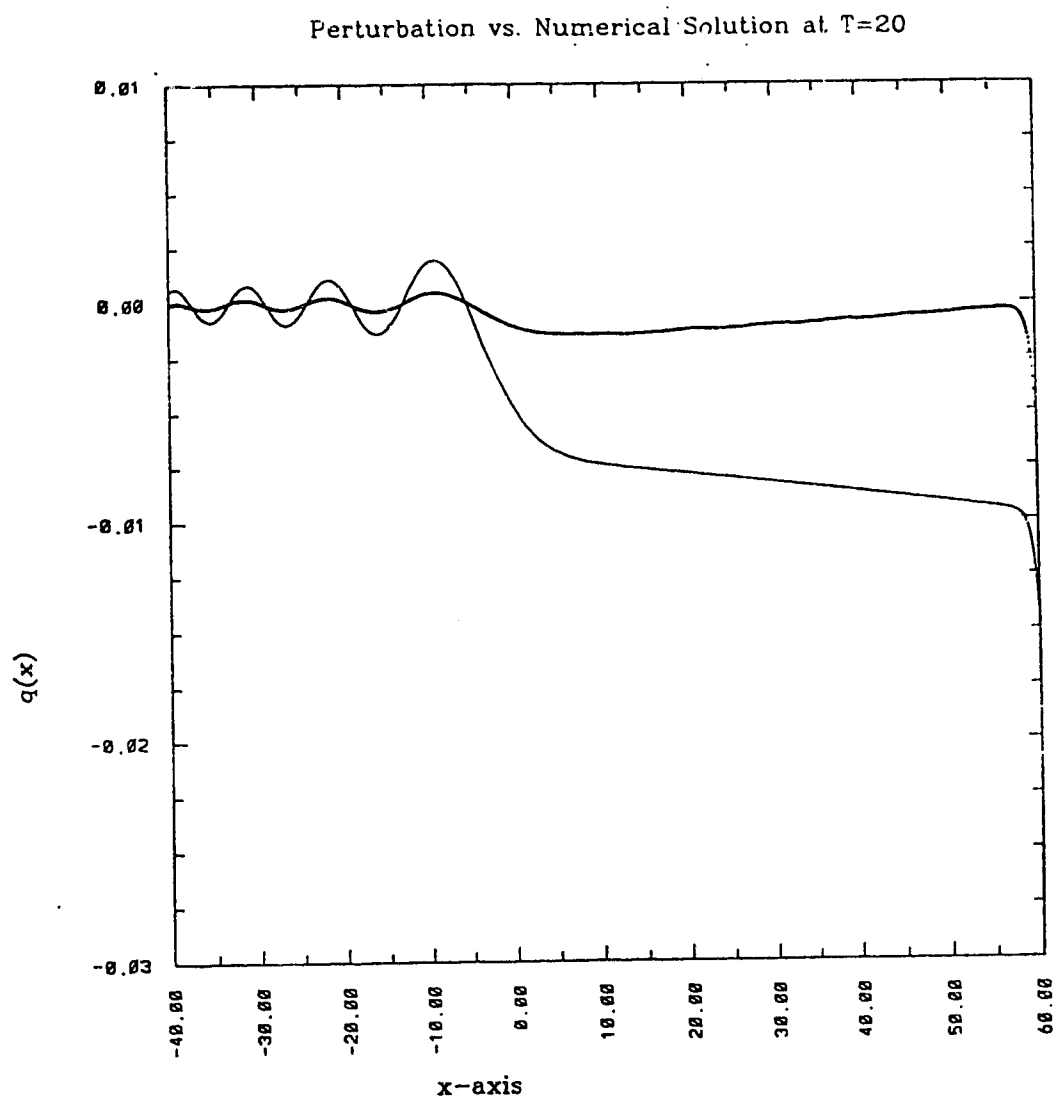


Figure 11h

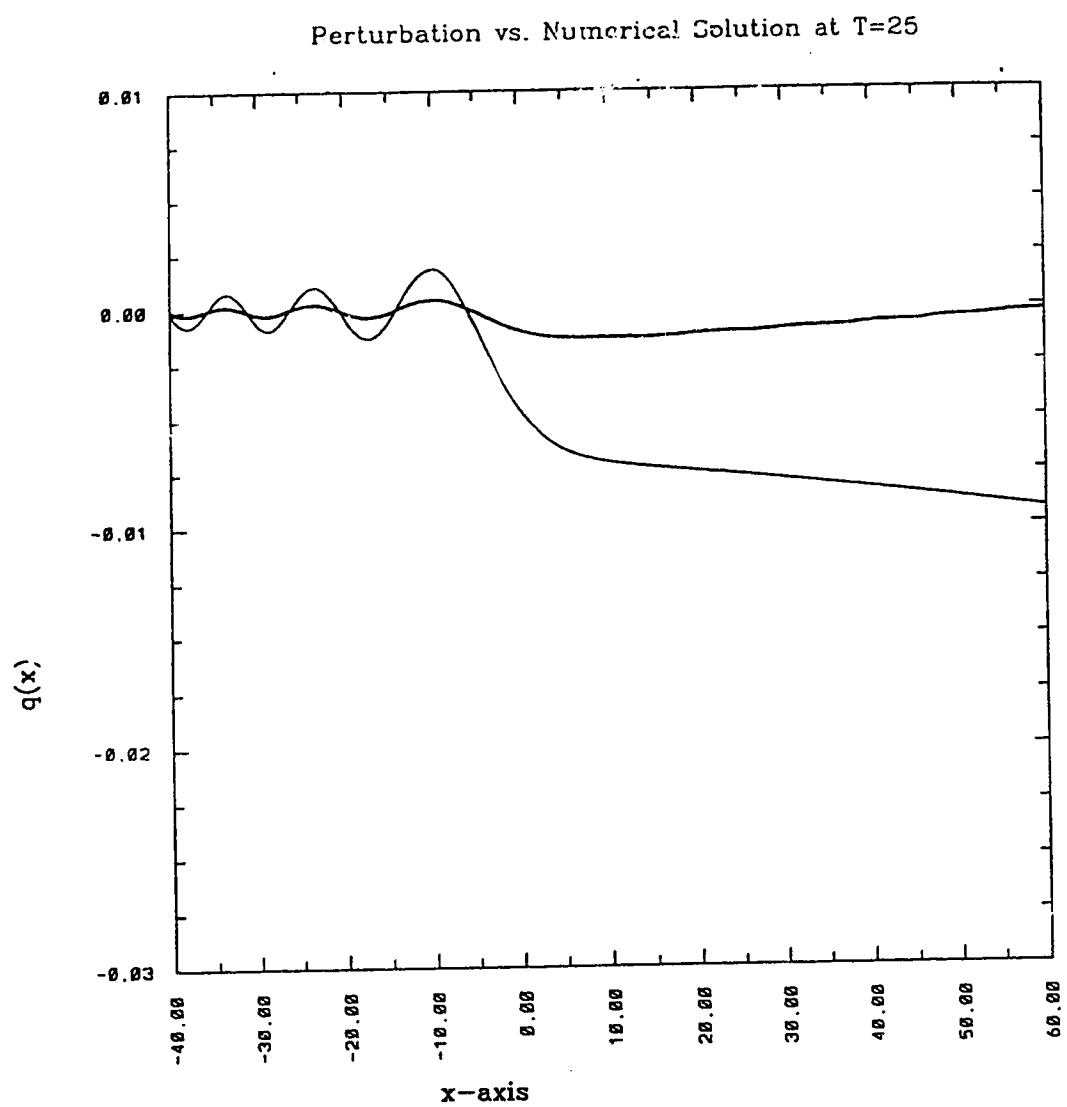


Figure 11i

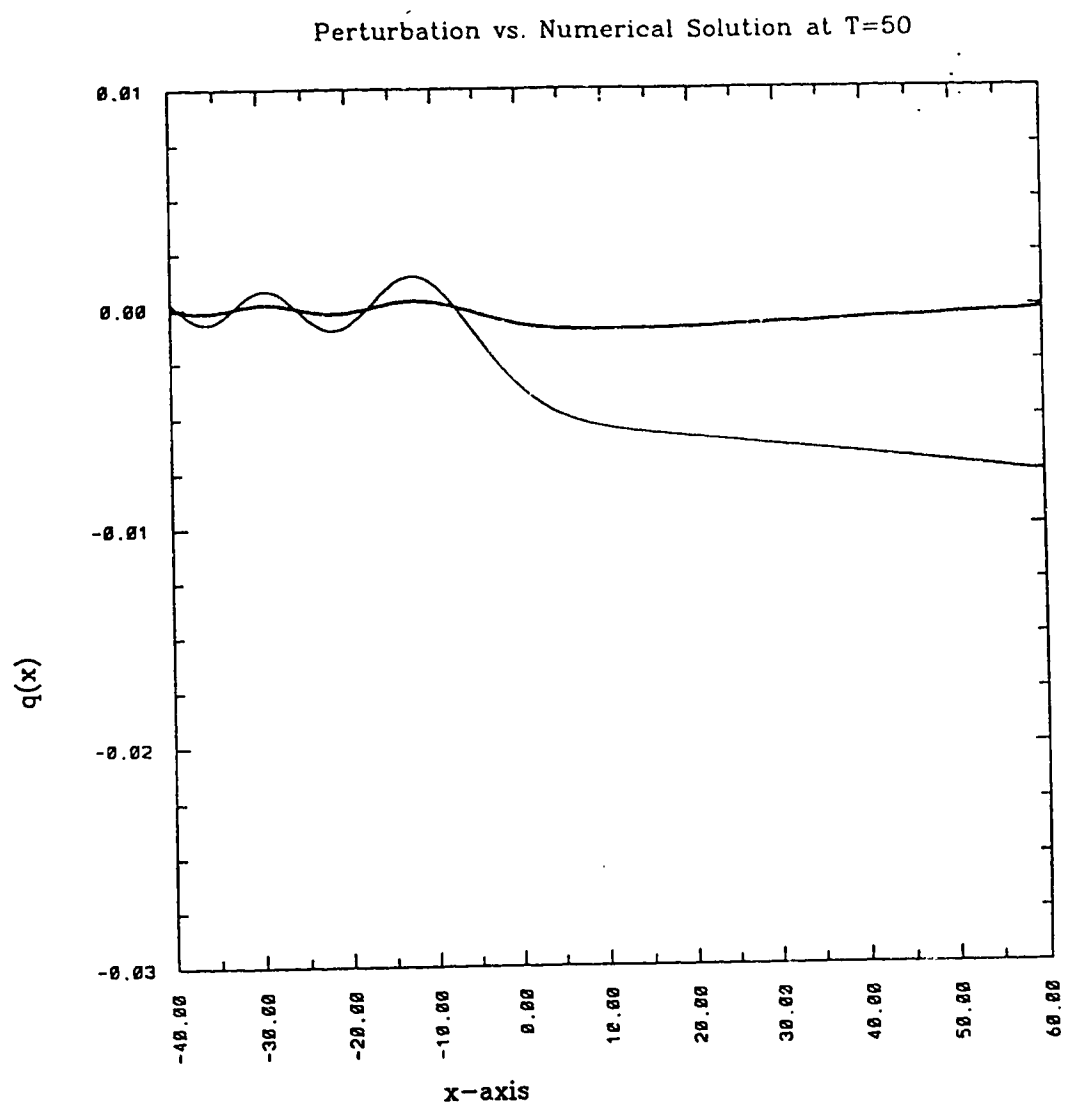


Figure 11j

Defining the mass of the wave, M , at time, T , by

$$M(T) = \int_{-\infty}^{\infty} q dx = \sum_{i=1}^N q(x_i) \Delta x_i, \quad (4.2.2)$$

where q is the calculated solution values (either numerical or perturbation), we find that, while the region of the wavetail ($-\infty < x < 0$) makes little contribution to the total mass, the shelf region ($0 < x < x_c$, where $x_c \equiv$ the phase position) contributes significantly. It is worthwhile to note that the total mass of the perturbation solution is significantly greater than the total mass of the numerical solution (Figure 12). Although the error in the numerical scheme is of order $\frac{1}{100}((\Delta x)^2)$, it is possible to verify the accuracy of the mass of the numerical scheme using a conservation law approach. This approach is necessary since for the choice $\Delta x = \frac{1}{10}$ the magnitude of the error for the numerical scheme is larger than the solution in the region of the shelf.

Following a conservation law approach, the mass balance law for the travelling soliton is

$$\frac{\partial}{\partial T} \int_{-\infty}^{\infty} q dx = -\nu \int_{-\infty}^{\infty} q dx. \quad (4.2.3)$$

With mass defined by (4.2.2), the integro-differential equation (4.2.3) may be rewritten as the differential equation

$$M_T = -\nu M \quad (4.2.4)$$

which has solution

$$M(T) = M_0 e^{-\nu T} \quad (4.2.5)$$

where M_0 is the mass of the soliton at time $T = 0$. A comparison of the mass of the numerical solution to that predicted by the conservation law approach was found to be favorable for both $\nu = \frac{1}{40}$ and $\nu = \frac{1}{100}$ and is shown in Figure 13.

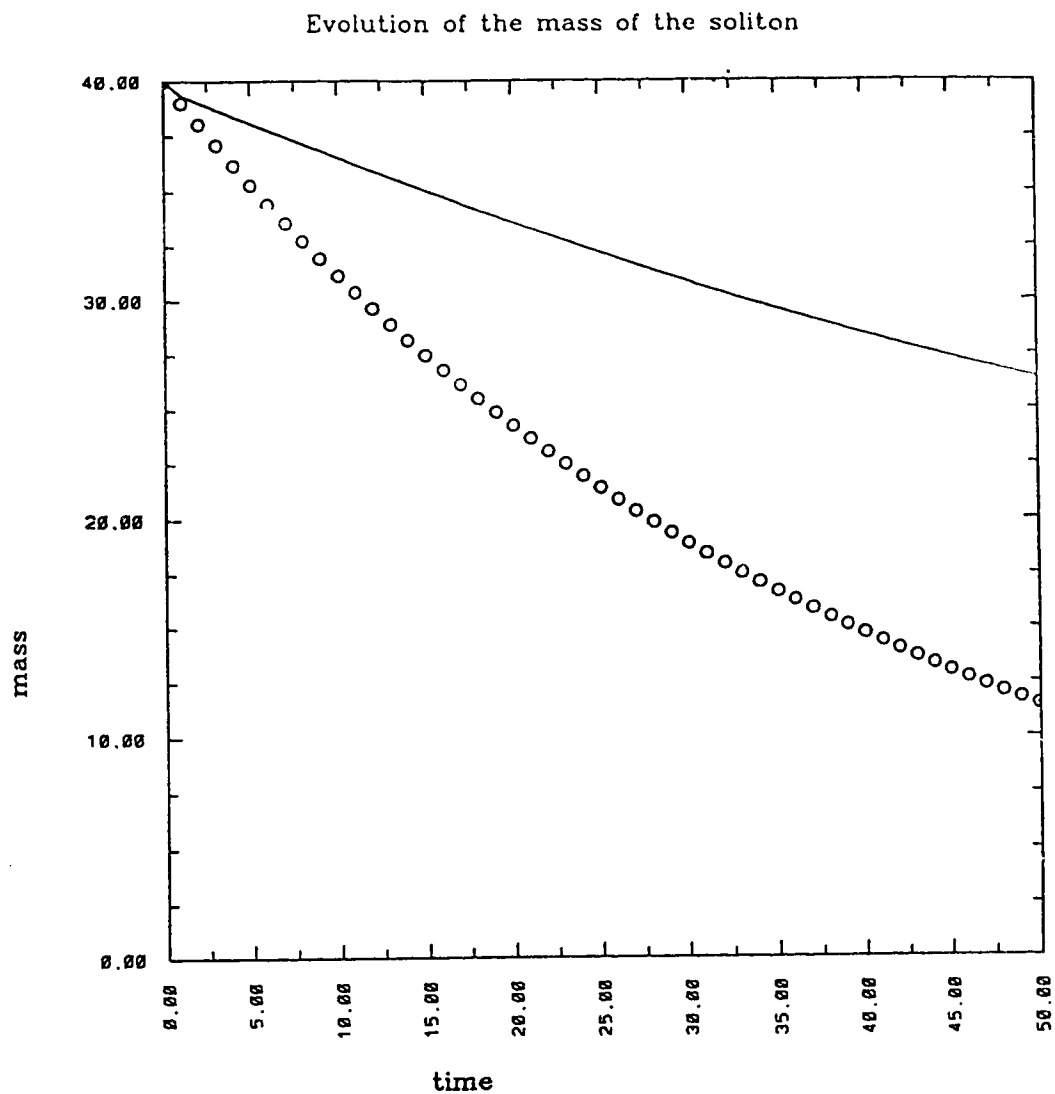


Figure 12: Comparison of Mass

Figures 12a and 12b show a comparison, with parameter values $\nu = \frac{1}{40}$ and $\frac{1}{100}$ respectively, of the “mass” of the perturbation solution (solid line) with that of the numerical solution (circles) for times $0 \leq T \leq 50$.

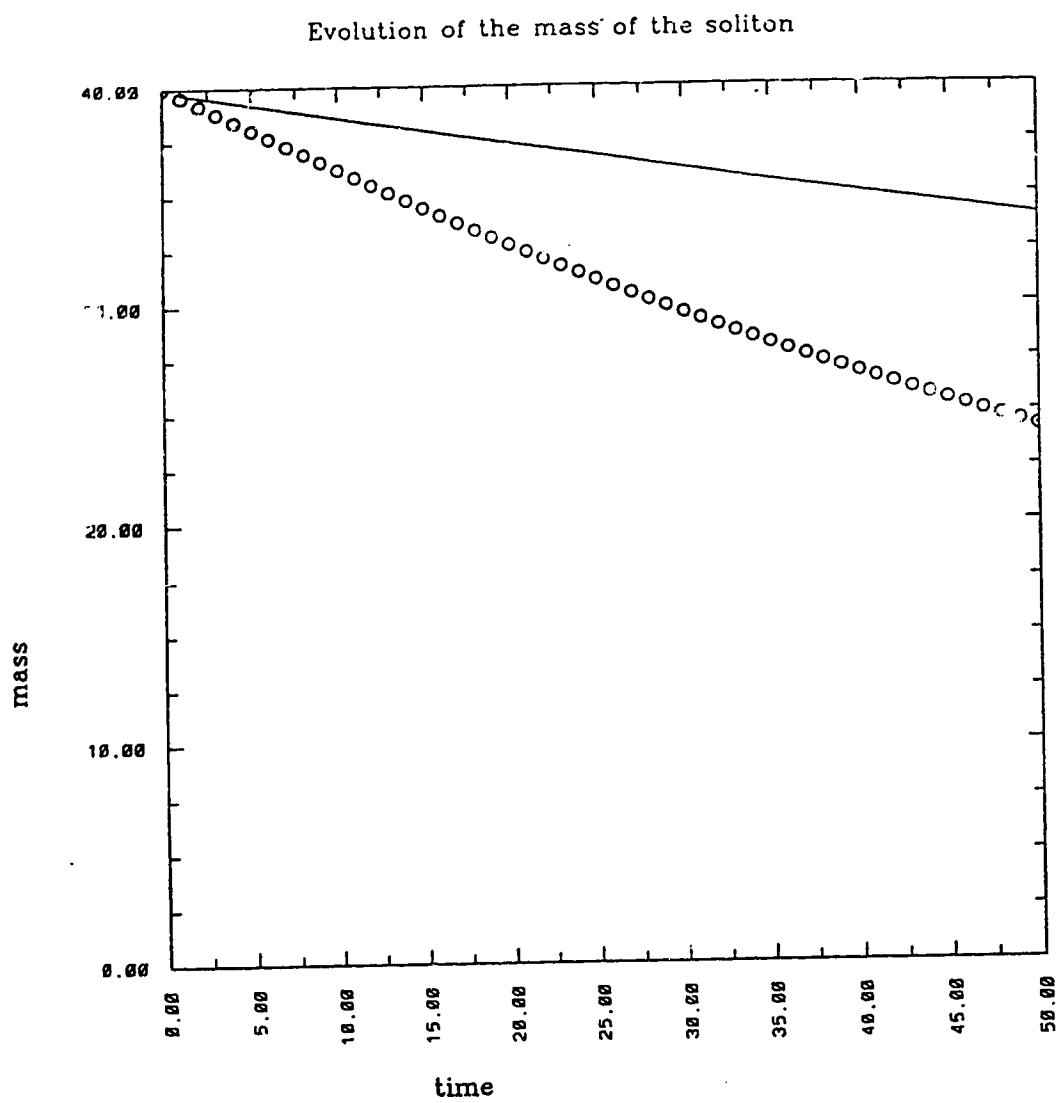


Figure 12b

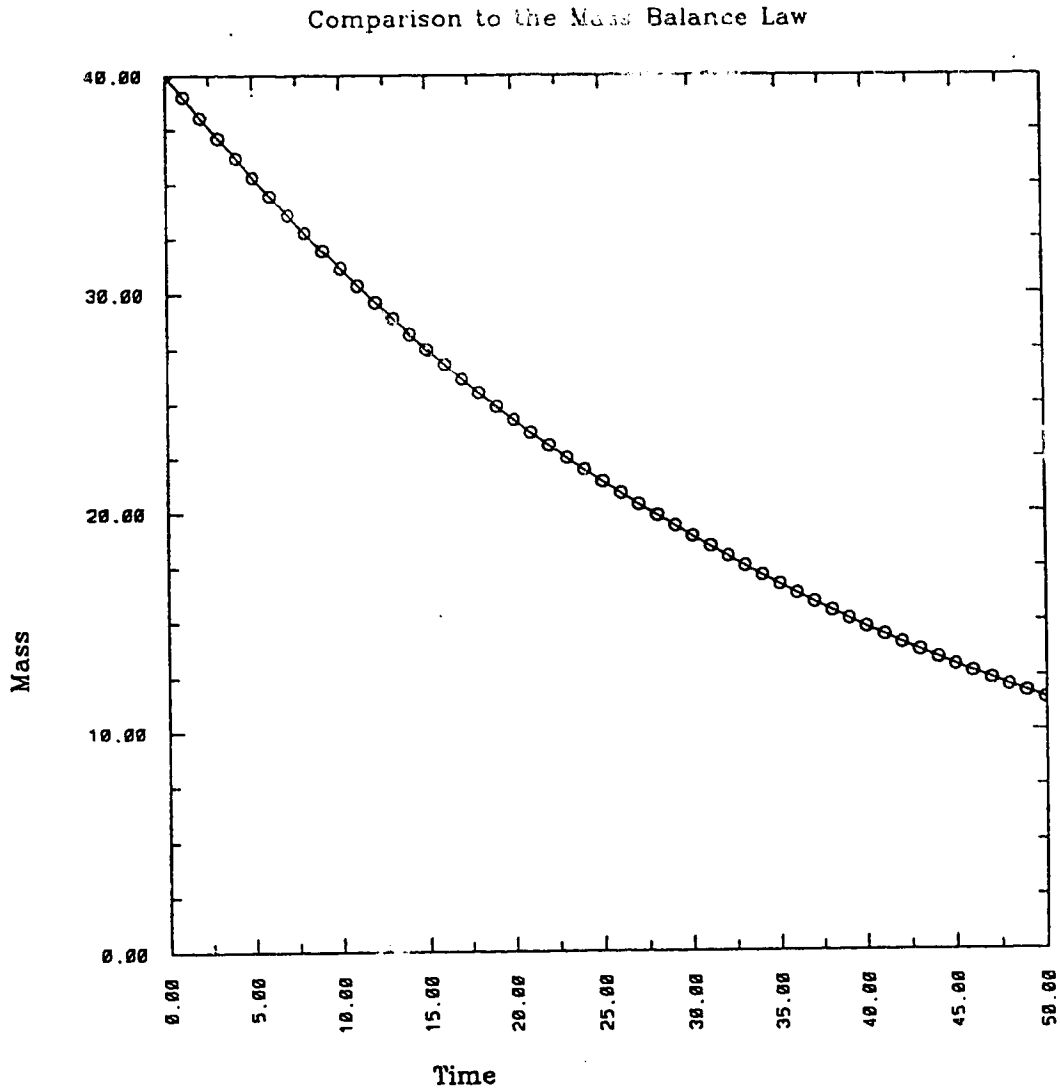


Figure 13: Comparison of Mass

Figures 13a and 13b show a comparison, with parameter values $\nu = \frac{1}{40}$ and $\frac{1}{100}$ respectively, of the “mass” as predicted by the conservation law (solid line) with that of the numerical solution (circles) for times $0 \leq T \leq 50$.

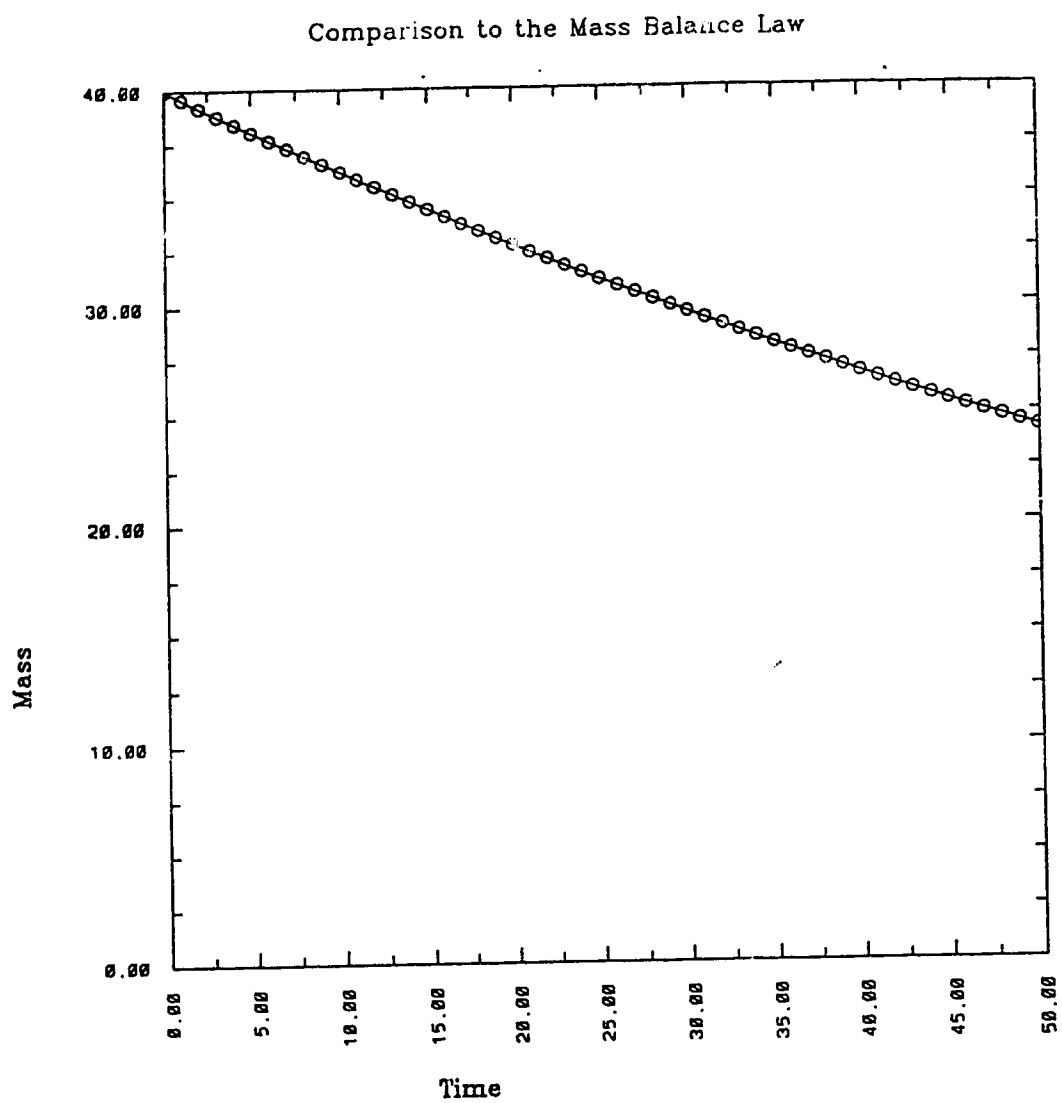


Figure 13b

While it may be expected that the extra mass in the perturbation solution may be accounted for by the mass of the shelf, this was only found to be true for times $T \sim O(\nu^{-1/2})$. The difference in mass of the two solutions is not unexpected, however, since the asymptotic solution developed in Chapter 3 did not require a mass balance, but was developed using energy balance laws as was the solution of Swaters and Sawatzky (1989).

The perturbation theory developed in Chapter 3 predicts a shelf with initial amplitude given by (3.2.27). It is interesting to note that predicted shelf is not monotonic (as was the case in both Knickerbocker and Newell (1980) and Swaters and Sawatzky (1989)) and that the time at which the derivative changes sign is approximately $T \sim \nu^{-\frac{1}{2}}$. It is possible that there may be some relationship between this non-monotonic behaviour and the observation that the shelf region does not fully account for the additional mass in the perturbation solution as was the case in Knickerbocker and Newell (1980). (Swaters and Sawatzky (1989) presented no numerical work for comparison.)

Although the mass of the numerical and perturbation solutions was found not to be in good agreement, a plot of the energy, E , defined by

$$E = \int_{-\infty}^{\infty} \frac{1}{2} q^2 dx = \sum_{i=1}^N \frac{1}{2} q(x_i) q(x_i) \Delta x_i,$$

shows that the perturbation and numerical solutions agree favorably over times $0 < T < 50$ (see Figure 14). (N.B. Recall that the numerical scheme was chosen to conserve both mass and energy.)

Evolution of the energy of the soliton

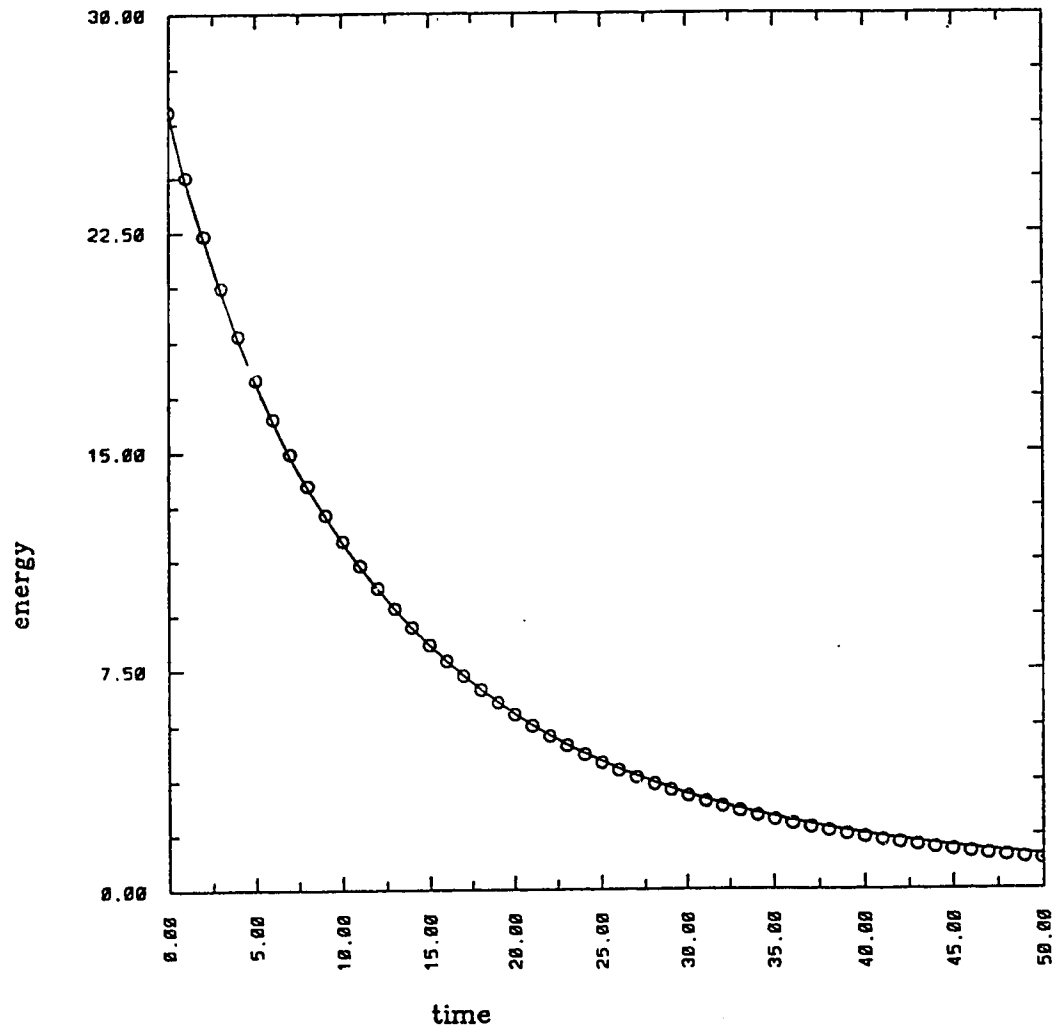


Figure 14: Comparison of Energy

Figures 14a and 14b show a comparison, with parameter values $\nu = \frac{1}{40}$ and $\frac{1}{100}$ respectively, of the “energy” of the perturbation solution (solid line) with that of the numerical solution (circles) for times $0 \leq T \leq 50$.

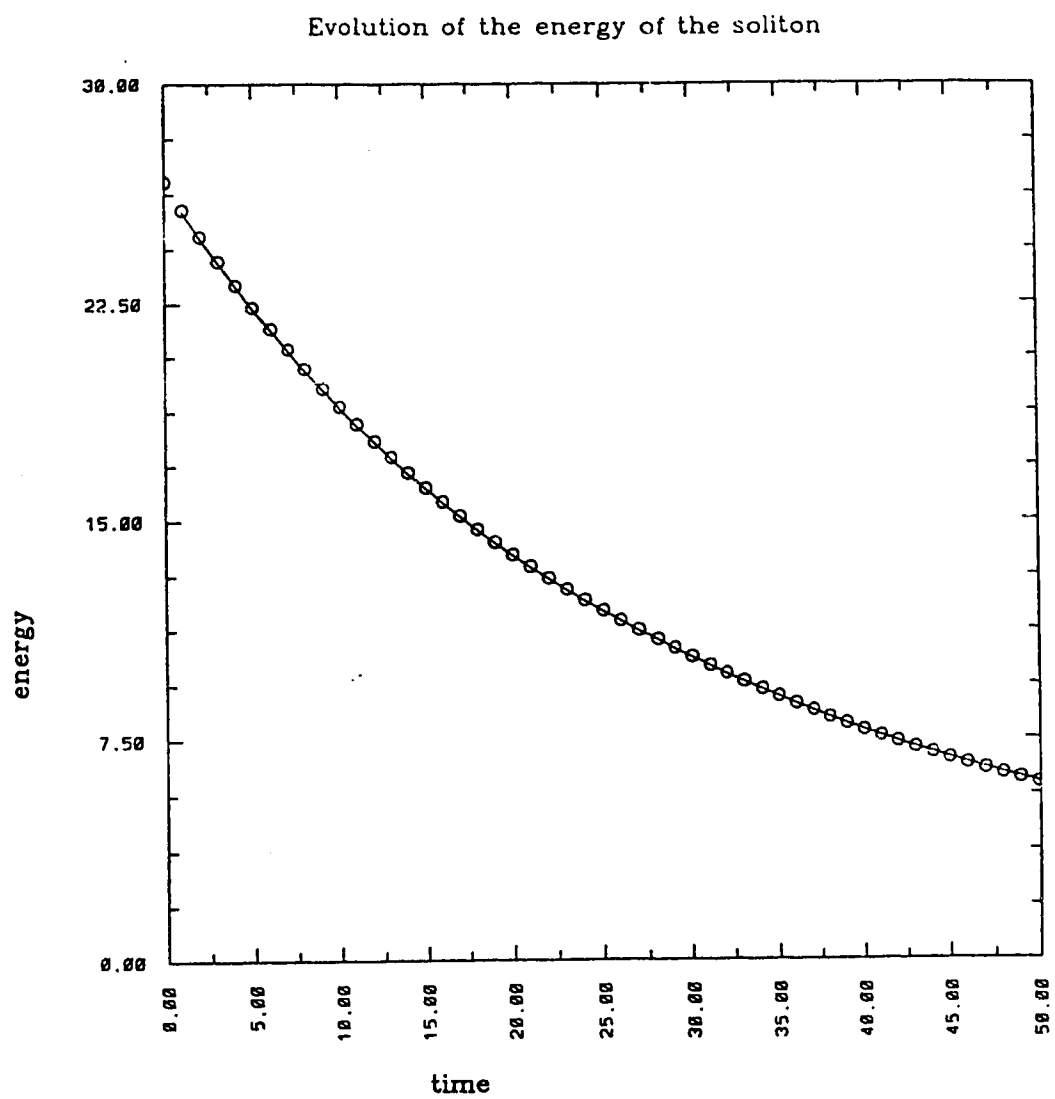


Figure 14b

Chapter 5

Calculation of the Vertical Momentum Flux and Conclusion

As indicated at the end of chapter 3, a uniformly valid solution for the vorticity field may be obtained via asymptotic matching. In what follows, the uniform solution is calculated in terms of the original (non-dimensional) variables.

Ahead of the solitary wave, the near-field and far-field solutions are, respectively,

$$q_{\text{near}}^{\dagger}(Z, \chi) \sim \left[-8\eta^2(\chi) - \left(2\mu + \frac{16}{5}\eta^2(\chi) \right) Z \right] \times \exp \left[-2\eta(\chi) \left(1 + \frac{Z}{30} + \frac{\mu Z}{24\eta^2(\chi)} \right) \frac{Z}{\nu} \right], \quad (5.0.1)$$

$$q_{\text{far}}^{\dagger}(\chi, \Theta) \sim -8\eta^2(\chi) \left[\frac{\nu\theta_c(\bar{\chi})}{\Theta} \right] \exp \left[\frac{\Theta}{3} - \frac{\mu\bar{\chi}\Theta}{\nu\theta_c(\bar{\chi})} - \left(\frac{\nu\theta_c(\bar{\chi})}{3\bar{\chi}} \right)^{\frac{1}{2}} \theta_0 \left(\frac{\bar{\chi}\Theta}{\nu\theta_c(\bar{\chi})} \right) - \frac{\nu\theta_c(\bar{\chi})}{3} + \mu\bar{\chi} + \left(\frac{\nu\theta_c(\bar{\chi})}{3\bar{\chi}} \right)^{\frac{1}{2}} \theta_0(\bar{\chi}) \right] \times \exp \left[\frac{-2}{\nu} \left(\frac{\Theta}{3} \right)^{\frac{3}{2}} \chi^{-\frac{1}{2}} \right]. \quad (5.0.2)$$

Substituting $\Theta = Z + \nu\theta_c(\chi)$ into (5.0.2), we have

$$q_{\text{far}}^{\dagger}(\chi, Z) \sim -8\eta^2(\chi) \left[\frac{\nu\theta_c(\bar{\chi})}{Z + \nu\theta_c(\chi)} \right] \times \exp \left[\frac{Z + \nu\theta_c(\chi)}{3} - \frac{\mu\bar{\chi}(Z + \nu\theta_c(\chi))}{\nu\theta_c(\bar{\chi})} - \left(\frac{\nu\theta_c(\bar{\chi})}{3\bar{\chi}} \right)^{\frac{1}{2}} \theta_0 \left(\frac{\bar{\chi}(Z + \nu\theta_c(\chi))}{\nu\theta_c(\bar{\chi})} \right) - \frac{\nu\theta_c(\bar{\chi})}{3} + \mu\bar{\chi} + \left(\frac{\nu\theta_c(\bar{\chi})}{3\bar{\chi}} \right)^{\frac{1}{2}} \theta_0(\bar{\chi}) \right]$$

$$\times \exp \left[\frac{-2}{\nu} \left(\frac{Z + \nu \theta_c(\chi)}{3} \right)^{\frac{2}{3}} \chi^{-\frac{1}{2}} \right]. \quad (5.0.3)$$

Adding (5.0.1) and (5.0.3), then subtracting (3.2.73b), the contribution of the overlap between the two solutions yields

$$\begin{aligned} q^\dagger(Z, \chi) \sim & \left[-8\eta^2(\chi) - \left(2\mu + \frac{16}{5}\eta^2(\chi) \right) Z \right] \\ & \times \exp \left[-2\eta(\chi) \left(1 + \frac{Z}{30} + \frac{\mu Z}{24\eta^2(\chi)} \right) \frac{Z}{\nu} \right] \\ & - 8\eta^2(\chi) \left[\frac{\nu \theta_c(\bar{\chi})}{Z + \nu \theta_c(\chi)} \right] \\ & \times \exp \left[\frac{Z + \nu \theta_c(\chi)}{3} - \frac{\mu \bar{\chi}(Z + \nu \theta_c(\chi))}{\nu \theta_c(\bar{\chi})} \right. \\ & - \left(\frac{\nu \theta_c(\bar{\chi})}{3\bar{\chi}} \right)^{\frac{1}{2}} \theta_0 \left(\frac{\bar{\chi}(Z + \nu \theta_c(\chi))}{\nu \theta_c(\bar{\chi})} \right) \\ & \left. - \frac{\nu \theta_c(\bar{\chi})}{3} + \mu \bar{\chi} + \left(\frac{\nu \theta_c(\bar{\chi})}{3\bar{\chi}} \right)^{\frac{1}{2}} \theta_c(\bar{\chi}) \right] \\ & \times \exp \left[\frac{-2}{\nu} \left(\frac{Z + \nu \theta_c(\chi)}{3} \right)^{\frac{2}{3}} \chi^{-\frac{1}{2}} \right] \\ & + 8\eta^2(\chi). \end{aligned} \quad (5.0.4)$$

The near field ahead of the soliton is matched to first order to the solution for the main pulse. The solution of the main pulse to first order given by (3.2.9) and (3.2.33) is

$$\begin{aligned} q(\theta, \chi) \sim & -2\eta^2(\chi) \text{sech}^2[\eta(\theta - \theta_0)] \\ & + \nu \left\{ \frac{\mu}{6\eta(\chi)} [3\text{sech}^2\phi(1 - \phi \tanh \phi) + \tanh \phi - 1 \right. \\ & \quad \left. - \phi \text{sech}^2\phi(\phi \tanh \phi - 2)] \right. \\ & + \frac{\eta(\chi)}{15} [12\text{sech}^2\phi(1 - \phi \tanh \phi) + 4(\tanh \phi - 1) \\ & \quad \left. + 2\phi \text{sech}^2\phi(\phi \tanh \phi - 2)] \right\} \end{aligned}$$

$$+\frac{1}{2}\theta_{0x} [\text{sech}^2 \phi (\phi \tanh \phi - 1)] \Big\}. \quad (5.0.5)$$

With $Z = \nu(\theta - \theta_0)$, the solution of the near field ahead of the soliton, (5.0.1), may be rewritten as

$$\begin{aligned} q_{\text{near}}^\dagger(\theta, \chi) \sim & \left[-8\eta^2(\chi) - \nu \left(2\mu + \frac{16\eta^2(\chi)}{5} \right) (\theta - \theta_0) \right] \\ & \times \exp[-2\eta(\chi)(\theta - \theta_0)] \\ & \times \left(1 + \frac{\nu(\theta - \theta_0)}{30} + \frac{\mu\nu(\theta - \theta_0)}{24\eta^2(\chi)} \right) \Big]. \end{aligned} \quad (5.0.6)$$

The matching condition, (3.2.55b), with the same substitution for Z , becomes

$$\begin{aligned} q_{\text{match}}^\dagger = & 8\eta^2(\chi) \left[-1 + \frac{\nu\eta(\chi)}{15}(\theta - \theta_0)^2 - \frac{\mu\nu}{12\eta(\chi)}(\theta - \theta_0)^2 \right] \\ & \times \exp[-2\eta(\chi)(\theta - \theta_0)]. \end{aligned} \quad (5.0.7)$$

Thus, by adding (5.0.5) and (5.0.6), then subtracting (5.0.7), we have a uniform solution for the main pulse and near-field given by

$$\begin{aligned} q(\theta, \chi) \sim & -2\eta^2(\chi)\text{sech}^2[\eta(\theta - \theta_0)] \\ & + \nu \left\{ \frac{\mu}{6\eta(\chi)} [3\text{sech}^2 \phi (1 - \phi \tanh \phi) \right. \\ & \quad \left. + \tanh \phi - 1 \right. \\ & \quad \left. - \phi \text{sech}^2 \phi (\phi \tanh \phi - 2)] \right. \\ & + \frac{\eta(\chi)}{15} [12\text{sech}^2 \phi (1 - \phi \tanh \phi) \\ & \quad \left. + 4(\tanh \phi - 1) \right. \\ & \quad \left. + 2\phi \text{sech}^2 \phi (\phi \tanh \phi - 2)] \right. \\ & \left. + \frac{1}{2}\theta_{0x} [\text{sech}^2 \phi (\phi \tanh \phi - 1)] \right\} \\ & + \nu \left[-8\eta^2(\chi) + \nu \left(2\mu - \frac{16\eta^2(\chi)}{5} \right) (\theta - \theta_0) \right] \\ & \times \exp[-2\eta(\chi)(\theta - \theta_0)] \end{aligned}$$

$$\begin{aligned}
& \times \left(1 + \frac{\nu(\theta - \theta_0)}{30} - \frac{\mu\nu(\theta - \theta_0)}{24\eta^2(\chi)} \right) \\
& - \nu 8\eta^2(\chi) \left[-1 + \frac{\nu\eta(\chi)}{15}(\theta - \theta_0)^2 - \frac{\mu\nu}{12\eta(\chi)}(\theta - \theta_0)^2 \right] \\
& \times \exp[-2\eta(\chi)(\theta - \theta_0)].
\end{aligned} \tag{5.0.8}$$

Similarly, the solution for the shelf region may be matched to the trailing edge ($\theta \rightarrow -\infty$) of the main pulse; given (3.2.45), the solution of the shelf region along with matching condition (3.2.44b), we have (in terms of the variables θ and χ)

$$\begin{aligned}
q_{\text{shelf}}(\theta, \chi) \sim & \nu \left(\frac{-\mu}{3\eta(\hat{\chi}(\theta, \chi))} - \frac{8\eta(\hat{\chi}(\theta, \chi))}{15} \right) \\
& \times \exp[-\mu(\hat{\chi}(\theta, \chi) - \chi)],
\end{aligned} \tag{5.0.9a}$$

where

$$\hat{\chi}(\theta, \chi) = \frac{-3}{4\mu} \ln \left[\frac{\{10\mu(\exp[8\nu(\theta + \theta_c(\chi))/30] - 1)\}}{-8\eta^2(0)} + 1 \right], \tag{5.0.9b}$$

and overlap

$$q_{\text{shelf, pulse}}(\theta, \chi) \sim \frac{-\mu}{3\eta(\chi)} - \frac{8\eta(\chi)}{15}. \tag{5.0.10}$$

Thus the uniformly valid solution for the shelf and main pulse is given by (5.0.5) plus (5.0.9a) minus (5.0.10), is

$$\begin{aligned}
q(\theta, \chi) \sim & -2\eta^2(\chi)\text{sech}^2[\eta(\theta - \theta_0)] \\
& + \nu \left\{ \frac{\mu}{6\eta(\chi)} [3\text{sech}^2\phi(1 - \phi \tanh \phi) \right. \\
& \quad \left. + \tanh \phi - 1 \right. \\
& \quad \left. - \phi \text{sech}^2\phi(\phi \tanh \phi - 2)] \right. \\
& + \frac{\eta(\chi)}{15} [12\text{sech}^2\phi(1 - \phi \tanh \phi) \\
& \quad + 4(\tanh \phi - 1) \\
& \quad \left. + 2\phi \text{sech}^2\phi(\phi \tanh \phi - 2)] \right\}
\end{aligned}$$

$$\begin{aligned}
& + \frac{1}{2} \theta_{0\chi} [\text{sech}^2 \phi (\phi \tanh \phi - 1)] \Big\} \\
& + \nu \left(\frac{-\mu}{3\eta(\hat{\chi})} - \frac{8\eta(\hat{\chi})}{15} \right) \exp[-\mu(\hat{\chi} - \chi)] \\
& + \nu \left(\frac{\mu}{3\eta(\chi)} + \frac{8\eta(\chi)}{15} \right). \tag{5.0.11}
\end{aligned}$$

Finally, we match the solution for the dispersive wavetail to that of the shelf given by (3.2.52)

$$\tilde{q}_{\text{tail}} \sim \left(\frac{-\mu}{3\eta(\hat{\chi})} - \frac{8\eta(\hat{\chi})}{15} \right) \exp[-\mu(\hat{\chi} - \chi)] \int_{-\infty}^{\frac{\ell}{(3r)^{\frac{1}{3}}}} \text{Ai}(s) ds. \tag{5.0.12}$$

With boundary condition (3.2.48c), the uniform solution may be written as

$$\begin{aligned}
\tilde{q}_{\text{tail shelf}} & \sim -\nu \left(\frac{\mu}{3\eta(\hat{\chi})} + \frac{8\eta(\hat{\chi})}{15} \right) \exp[-\mu(\hat{\chi} - \chi)] \\
& \times \left[1 + \int_{-\infty}^{\frac{\ell}{(3r)^{\frac{1}{3}}}} \text{Ai}(s) ds \right] \\
& + \nu \left(\frac{\mu}{3\eta(0)} + \frac{8\eta(0)}{15} \right). \tag{5.0.13}
\end{aligned}$$

Combining solutions (5.0.4), (5.0.8), (5.0.11), and (5.0.13) yields a uniform solution valid for the entire interval $(-\infty, \infty)$.

5.1 Velocity Field Calculations

The uniformly valid approximation for the interval $(-\infty, \infty)$ is given by

$$\begin{aligned}
q(\theta, \chi) & = -2\eta^2 \text{sech}^2[\eta(\theta - \theta_0)] \\
& + \nu \left\{ \frac{\mu}{6\eta} [3\text{sech}^2 \phi (1 - \phi \tanh \phi) + \tanh \phi - 1 \right. \\
& \quad \left. - \phi \text{sech}^2 \phi (\phi \tanh \phi - 2)] \right. \\
& + \frac{\eta}{15} [12\text{sech}^2 \phi (1 - \phi \tanh \phi) + 4(\tanh \phi - 1) \\
& \quad \left. + 2\phi \text{sech}^2 \phi (\phi \tanh \phi - 2)] \right\}
\end{aligned}$$

$$\begin{aligned}
& + \frac{1}{2} \theta_{0\chi} \left[\text{sech}^2 \phi (\phi \tanh \psi - 1) \right] \Big\} \\
& + \nu \left\{ -8\eta^2 - \nu \left(2\mu + \frac{16\eta^2}{5} \right) (\theta - \theta_0) \right\} \\
& \quad \times \exp \left[-2\eta(\theta - \theta_0) \left(1 + \frac{\nu(\theta - \theta_0)}{30} + \frac{\mu\nu(\theta - \theta_0)}{24\eta^2} \right) \right] \\
& - \nu 8\eta^2 \left\{ -1 + \frac{\nu\eta}{15} (\theta - \theta_0)^2 - \frac{\mu\nu}{12\eta} (\theta - \theta_0)^2 \right\} \\
& \quad \times \exp[-2\eta(\theta - \theta_0)] \\
& + \nu \left\{ -8\eta^2 \left[\frac{\theta_c(\bar{\chi})}{\theta - \theta_0 + \theta_c(\chi)} \right] \right. \\
& \quad \times \exp \left[\frac{\nu(\theta - \theta_0 + \theta_c(\chi))}{3} - \frac{\mu\bar{\chi}(\theta - \theta_0 + \theta_c(\chi))}{\theta_c(\bar{\chi})} \right. \\
& \quad \left. - \left(\frac{\nu\theta_c(\bar{\chi})}{3\bar{\chi}} \right)^{\frac{1}{2}} \theta_0 \left(\frac{\bar{\chi}(\theta - \theta_0 + \theta_c(\chi))}{\theta_c(\bar{\chi})} \right) \right. \\
& \quad \left. \left. - \frac{\nu\theta_c(\bar{\chi})}{3} + \mu\bar{\chi} + \left(\frac{\nu\theta_c(\bar{\chi})}{3\bar{\chi}} \right)^{\frac{1}{2}} \theta_0(\bar{\chi}) \right] \right. \\
& \quad \left. \times \exp \left[-2 \left(\frac{\theta - \theta_0 + \theta_c(\chi)}{3} \right)^{\frac{3}{2}} \chi^{-\frac{1}{2}} \right] \right. \\
& \quad \left. + 8\eta^2 \right\} \\
& + \nu \left\{ \left(\frac{-\mu}{3\eta(\bar{\chi})} - \frac{8\eta(\bar{\chi})}{15} \right) \exp[-\mu(\bar{\chi} - \chi)] \right. \\
& \quad \left. + \frac{\mu}{3\eta} + \frac{8\eta}{15} \right\} \\
& - \nu \left\{ \left(\frac{\mu}{3\eta(\bar{\chi})} + \frac{8\eta(\bar{\chi})}{15} \right) \exp[-\mu(\bar{\chi} - \chi)] \right. \\
& \quad \left. \times \int_{-\infty}^{\frac{\chi}{(3\tau)^{\frac{1}{3}}}} Ai(s) ds \right\} \\
& + \nu \left(\frac{\mu}{3\eta(0)} + \frac{8\eta(0)}{15} \right). \tag{5.1.1}
\end{aligned}$$

The streamfunction is given by multiplying equation (5.1.1) by the vertical struc-

ture solution (equations (3.1.3), (3.1.14a-e)), restated here for completeness:

$$\phi_n(t) = A_n J_0(t) + B_n Y_0(t), \quad (5.1.2a)$$

where

$$A_n = K_n B_n, \quad (5.1.2b)$$

$$B_n = \frac{2}{c_n \gamma^{1/2}} \left[\{ K_n^2 t^2 [J_0^2(t) + J_1^2(t)] \right. \\ \left. + 2K_n t^2 [J_0(t)Y_0(t) + J_1(t)Y_1(t)] \right. \\ \left. + t^2 [Y_0^2(t) + Y_1^2(t)] \right] \Bigg|_{\Lambda_n}^{\Lambda_n e^{\gamma/2}}^{-1/2}, \quad (5.1.2c)$$

in which

$$K_n = \frac{-[Y_0(\Lambda_n) + Y_0(\Lambda_n e^{\gamma/2})]}{[J_0(\Lambda_n) + J_0(\Lambda_n e^{\gamma/2})]},$$

and

$$c_n = \frac{2S_0 e^{-\gamma/2}}{\gamma \Lambda_n}, \quad (5.1.2d)$$

where Λ_n satisfies

$$J_0(\Lambda_n)Y_0(\Lambda_n e^{\gamma/2}) - J_0(\Lambda_n e^{\gamma/2})Y_0(\Lambda_n) = 0. \quad (5.1.2e)$$

With the streamfunction, $\psi(z, \xi, T)$, as given in (2.2.13), we have

$$\psi(z, \xi, T) = q(\theta, \chi) \phi(z), \quad (5.1.3a)$$

with

$$\theta = \xi - \frac{4}{\nu} \int_0^{\nu T} \eta^2(\tau) d\tau, \quad (5.1.3b)$$

and

$$\chi = \nu T. \quad (5.1.3c)$$

It follows that the velocity field is given by

$$u = -\psi_z = -q\phi_z, \quad (5.1.4a)$$

$$w = \psi_x = q_x\phi \equiv q_\theta\phi, \quad (5.1.4b)$$

since $\xi = x - ct$. Thus the horizontal velocity, u , is given by

$$\begin{aligned} u &= -q(\theta, \chi)\phi_z, \\ &= -q(\theta, \chi)(\phi_0)_z, \end{aligned} \quad (5.1.5)$$

where

$$\begin{aligned} (\phi_0)_z &= (\phi_0)_t \\ &= -(A_n J_1(t) + B_n Y_1(t)) \frac{\lambda_0}{\gamma} [S(z)]^{-\frac{1}{2}} \gamma S(z) \\ &= -(A_n J_1(t) + B_n Y_1(t)) \lambda_0 [S(z)]^{\frac{1}{2}} \\ &= -\lambda_0 S(z) \left[A_n J_1 \left(\frac{2\lambda_0}{\gamma} S^{\frac{1}{2}}(z) \right) + B_n Y_1 \left(\frac{2\lambda_0}{\gamma} S^{\frac{1}{2}}(z) \right) \right]. \end{aligned} \quad (5.1.6)$$

Similarly, the vertical velocity, w , is given by

$$w = q_x\phi, \quad (5.1.7)$$

where

$$\begin{aligned} q_x &= 4\eta^3 \text{sech}^2[\eta(\theta - \theta_0)] \tanh[\eta(\theta - \theta_0)] \\ &\quad + \nu \left\{ \frac{\mu}{6\eta} [-6\text{sech}^2\phi \tanh\phi \phi_\theta (1 - \phi \tanh\phi) \right. \end{aligned}$$

$$\begin{aligned}
& + 3\text{sech}^2 \phi (-\phi_\theta \tanh \phi - \phi \text{sech}^2 \phi(\phi_\theta)) + \text{sech}^2 \phi(\phi_\theta) \\
& - \phi_\theta \text{sech}^2 \phi(\phi \tanh \phi - 2) + 2\phi \text{sech}^2 \phi \tanh \phi(\phi_\theta)(\phi \tanh \phi - 2) \\
& - \phi \text{sech}^2 \phi(\phi_\theta \tanh \phi + \phi \text{sech}^2 \phi(\phi_\theta))] \\
& + \frac{\eta}{15} [-24\text{sech}^2 \phi \tanh \phi(\phi_\theta)(1 - \phi \tanh \phi) \\
& + 12\text{sech}^2 \phi(-\phi_\theta \tanh \phi - \phi \text{sech}^2 \phi(\phi_\theta)) + 4\text{sech}^2 \phi(\phi_\theta) \\
& + 2\phi_\theta \text{sech}^2 \phi(\phi \tanh \phi - 2) - 4\phi \text{sech}^2 \phi \tanh \phi(\phi_\theta)(\phi \tanh \phi - 2) \\
& + 2\phi \text{sech}^2 \phi(\phi_\theta \tanh \phi + \phi \text{sech}^2 \phi(\phi_\theta))] \\
& + \frac{1}{2} \theta_{0x} [-2\text{sech}^2 \phi \tanh \phi(\phi_\theta)(\phi \tanh \phi - 1) \\
& + \text{sech}^2 \phi(\phi_\theta \tanh \phi + \phi \text{sech}^2 \phi(\phi_\theta))] \Big\} \\
& + \nu \left\{ \nu \left(2\mu - \frac{16\eta^2}{5} \right) \right\} \exp \left[-2\eta(\theta - \theta_0) \right. \\
& \quad \times \left(1 + \frac{\nu(\theta - \theta_0)}{30} - \frac{\mu\nu(\theta - \theta_0)}{24\eta^2} \right) \Big] \\
& + \nu \left\{ -8\eta^2 + \nu \left(2\mu - \frac{16\eta^2}{5} \right) (\theta - \theta_0) \right\} \\
& \quad \times \left[-2\eta \left(1 + \frac{\nu(\theta - \theta_0)}{30} - \frac{\mu\nu(\theta - \theta_0)}{24\eta^2} \right) - 2\eta(\theta - \theta_0) \left(\frac{\nu}{30} - \frac{\mu\nu}{24\eta^2} \right) \right] \\
& \quad \times \exp \left[-2\eta(\theta - \theta_0) \left(1 + \frac{\nu(\theta - \theta_0)}{30} - \frac{\mu\nu(\theta - \theta_0)}{24\eta^2} \right) \right] \\
& - \nu 8\eta^2 \left\{ \frac{2\nu\eta}{15}(\theta - \theta_0) - \frac{2\mu\nu}{12\eta}(\theta - \theta_0) \right\} \exp[-2\eta(\theta - \theta_0)] \\
& - \nu 8\eta^2 \left\{ -1 + \frac{\nu\eta}{15}(\theta - \theta_0)^2 - \frac{\mu\nu}{12\eta}(\theta - \theta_0)^2 \right\} \\
& \quad \times (-2\eta) \exp[-2\eta(\theta - \theta_0)] \\
& + \nu \left\{ -8\eta^2 \left[\frac{\theta'_c(\bar{\chi})\bar{\chi}_\theta(\theta - \theta_0 + \theta_c(\chi)) + \theta_c(\bar{\chi})}{(\theta - \theta_0 + \theta_c(\chi))^2} \right] \right. \\
& \quad \times \exp \left[\frac{\nu(\theta - \theta_0 + \theta_c(\chi))}{3} - \frac{\mu\bar{\chi}(\theta - \theta_0 + \theta_c(\chi))}{\theta_c(\bar{\chi})} \right. \\
& \quad \left. \left. - \left(\frac{\nu\theta_c(\bar{\chi})}{3\bar{\chi}} \right)^{\frac{1}{2}} \theta_0 \left(\frac{\bar{\chi}(\theta - \theta_0 + \theta_c(\chi))}{\theta_c(\bar{\chi})} \right) \right] \right\}
\end{aligned}$$

$$\begin{aligned}
& -\frac{\nu\theta_c(\bar{\chi})}{3} + \mu\bar{\chi} + \left(\frac{\nu\theta_c(\bar{\chi})}{3\bar{\chi}}\right)^{\frac{1}{2}} \theta_0(\bar{\chi}) \Big] \\
& \times \exp \left[-2 \left(\frac{(\theta - \theta_0 + \theta_c(\chi))}{3} \right)^{\frac{3}{2}} \chi^{-\frac{1}{2}} \right] \\
& - 8\eta^2 \left[\frac{\theta_c(\bar{\chi})}{(\theta - \theta_0 + \theta_c(\chi))} \right] \\
& \times \left\{ \frac{\nu}{3} - \left(\frac{[\mu\bar{\chi}\theta(\theta - \theta_0 + \theta_c(\chi)) + \mu\bar{\chi}]\theta_c(\bar{\chi}) - \mu\bar{\chi}[\theta - \theta_0 + \theta_c(\chi)]\theta'_c(\bar{\chi})\bar{\chi}\theta}{\theta_c^2(\bar{\chi})} \right) \right. \\
& \quad - \frac{1}{2} \left(\frac{\nu\theta_c(\bar{\chi})}{3\bar{\chi}} \right)^{-\frac{1}{2}} \left(\frac{\nu\theta'_c(\bar{\chi})\bar{\chi}\theta 3\bar{\chi} - \nu\theta_c(\bar{\chi})3\bar{\chi}\theta}{9\bar{\chi}^2} \right) \\
& \quad \times \theta_0 \left(\frac{\bar{\chi}(\theta - \theta_0 + \theta_c(\chi))}{\theta_c(\bar{\chi})} \right) \\
& \quad - \left(\frac{\nu\theta_c(\bar{\chi})}{3\bar{\chi}} \right)^{\frac{1}{2}} \theta'_0 \left(\frac{\bar{\chi}(\theta - \theta_0 + \theta_c(\chi))}{\theta_c(\bar{\chi})} \right) \\
& \quad \times \left(\frac{[\bar{\chi}\theta(\theta - \theta_0 + \theta_c(\chi)) + \bar{\chi}]\theta_c(\bar{\chi}) - \bar{\chi}(\theta - \theta_0 + \theta_c(\chi))\theta'_c(\bar{\chi})\bar{\chi}\theta}{\theta_c^2(\bar{\chi})} \right) \\
& \quad - \frac{\nu\theta'_c(\bar{\chi})}{3} \bar{\chi}\theta + \mu\bar{\chi}\theta + \frac{1}{2} \left(\frac{\nu\theta_c(\bar{\chi})}{3\bar{\chi}} \right)^{-\frac{1}{2}} \\
& \quad \times \left[\frac{\nu\theta'_c(\bar{\chi})\bar{\chi}\theta 3\bar{\chi} - \nu\theta_c(\bar{\chi})3\bar{\chi}\theta}{9\bar{\chi}^2} \right] \theta_0(\bar{\chi}) \\
& \quad \left. + \left(\frac{\nu\theta_c(\bar{\chi})}{3\bar{\chi}} \right)^{\frac{1}{2}} \theta'_0(\bar{\chi})\chi\theta \right\} \\
& \times \exp \left[\frac{\nu(\theta - \theta_0 + \theta_c(\chi))}{3} - \frac{\mu\bar{\chi}(\theta - \theta_0 + \theta_c(\chi))}{\theta_c(\bar{\chi})} \right. \\
& \quad - \left(\frac{\nu\theta_c(\bar{\chi})}{3\bar{\chi}} \right)^{\frac{1}{2}} \theta_0 \left(\frac{\bar{\chi}(\theta - \theta_0 + \theta_c(\chi))}{\theta_c(\bar{\chi})} \right) \\
& \quad \left. - \frac{\nu\theta_c(\bar{\chi})}{3} + \mu\bar{\chi} + \left(\frac{\nu\theta_c(\bar{\chi})}{3\bar{\chi}} \right)^{\frac{1}{2}} \theta_0(\bar{\chi}) \right] \\
& \times \exp \left[-2 \left(\frac{(\theta - \theta_0 + \theta_c(\chi))}{3} \right)^{\frac{3}{2}} \chi^{-\frac{1}{2}} \right] \\
& - 8\eta^2 \left[\frac{\theta_c(\bar{\chi})}{\theta - \theta_0 + \theta_c(\chi)} \right]
\end{aligned}$$

$$\begin{aligned}
& \times \exp \left[\frac{\nu(\theta - \theta_0 + \theta_c(\chi))}{3} - \frac{\mu\bar{\chi}(\theta - \theta_0 + \theta_c(\chi))}{\theta_c(\bar{\chi})} \right. \\
& \quad - \left(\frac{\nu\theta_c(\bar{\chi})}{3\bar{\chi}} \right)^{\frac{1}{2}} \theta_0 \left(\frac{\bar{\chi}(\theta - \theta_0 + \theta_c(\chi))}{\theta_c(\bar{\chi})} \right) \\
& \quad \left. - \frac{\nu\theta_c(\bar{\chi})}{3} + \mu\bar{\chi} + \left(\frac{\nu\theta_c(\bar{\chi})}{3\bar{\chi}} \right)^{\frac{1}{2}} \theta_0(\bar{\chi}) \right] \\
& \times \left(\left(\frac{\theta - \theta_0 + \theta_c(\chi)}{3} \right)^{\frac{1}{2}} \chi^{-\frac{1}{2}} \right) \\
& \times \exp \left[-2 \left(\frac{\theta - \theta_0 + \theta_c(\chi)}{3} \right)^{\frac{3}{2}} \chi^{-\frac{1}{2}} \right] \Big\} \\
& + \nu \left\{ - \left(\frac{\mu}{3\eta^2(\bar{\chi})} + \frac{8}{15} \right) \eta'(\bar{\chi}) \bar{\chi}_\theta \exp[-\mu(\bar{\chi} - \chi)] \right. \\
& \quad \left. - \left(\frac{\mu}{3\eta(\bar{\chi})} + \frac{8\eta(\bar{\chi})}{15} \right) (-\mu\bar{\chi}_\theta) \exp[-\mu(\bar{\chi} - \chi)] \right\} \\
& - \nu \left\{ \left(\frac{\mu}{3\eta^2(\bar{\chi})} + \frac{8}{15} \right) \eta'(\bar{\chi}) \bar{\chi}_\theta \exp[-\mu(\bar{\chi} - \chi)] \right. \\
& \quad \times \int_{-\infty}^{\frac{\xi}{(3T)^{\frac{1}{3}}}} Ai(s) ds \\
& \quad + \left(\frac{\mu}{3\eta(\bar{\chi})} + \frac{8\eta(\bar{\chi})}{15} \right) (-\mu\bar{\chi}_\theta) \exp[-\mu(\bar{\chi} - \chi)] \\
& \quad \times \int_{-\infty}^{\frac{\xi}{(3T)^{\frac{1}{3}}}} Ai(s) ds \\
& \quad \left. + \left(\frac{\mu}{3\eta(\bar{\chi})} + \frac{8\eta(\bar{\chi})}{15} \right) \exp[-\mu(\bar{\chi} - \chi)] Ai \left(\frac{\xi}{(3T)^{\frac{1}{3}}} \right) \frac{1}{(3T)^{\frac{1}{3}}} \right\}. \tag{5.1.8}
\end{aligned}$$

Defining the fluid speed $v = (u^2 + w^2)^{\frac{1}{2}}$, a gray level scale plot (Figure 15) of the region from $-40 \leq x \leq 60$ and $0 \leq Z \leq 1$ reveals that the highest speeds occur in the region of the pycnocline with a cell-like behaviour in the region of the wavetail. Since a contour plot of the vertical velocity field (Figure 16) reveals that in the lee of the solitary wave the vertical velocity is entirely positive, the cell-like behaviour must occur due to changes in the horizontal velocity (which is shown as a contour plot in Figure 17). The vertical velocity indicates complete upwelling. Hence, there

is, indeed, enhanced vertical mixing occurring due to the passage of the soliton. The complete flow field is depicted as a contour plot of the streamfunction in Figure 18.

5.2 Vertical Flux Calculations

The vertical kinematic momentum flux (i.e. the z -momentum flux across surfaces of $z = \text{constant}$) is proportional to the rate of change of the vertical velocity w in the z -direction, i.e. $\frac{\partial w}{\partial z}$. This simplified approach was discussed in Section 2.1 when a first order closure scheme was invoked to incorporate turbulent effects into the solution. It follows that

$$\frac{\tau_{zz}}{\rho} \propto \frac{\partial w}{\partial z} = q_z(x, t) \phi_z(z). \quad (5.2.1)$$

The solutions for $q_z(x, t)$ and $\phi_z(z)$ are given by equations (5.1.9) and (5.1.7) respectively.

Figure 19 shows a contour plot of the vertical kinematic momentum flux. The plot indicates that the greatest flux occurs in the region of the wavetail. The momentum decreases as one travels upward. Since the vertical velocities decrease only slightly over time (see Figure 16), this suggests that there is a continual upwards forcing occurring in the region of the shelf and the wavetail.

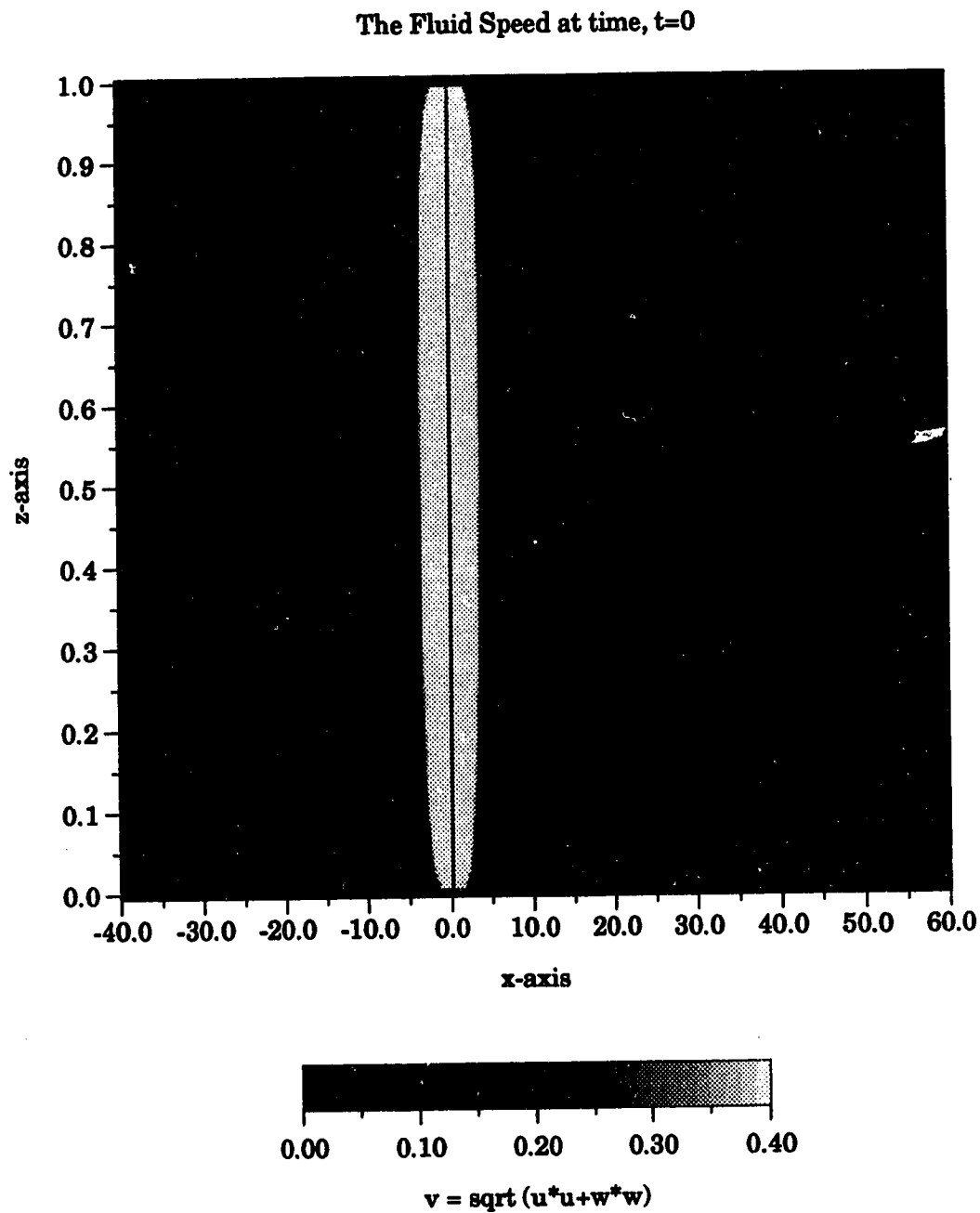


Figure 15: The Fluid Speed

The fluid speed, $v = (u^2 + w^2)^{\frac{1}{2}}$, is shown as a gray level scale plot with parameters $\mu = 1.0$ and $\nu = \frac{1}{100}$. Figures 15a-j show the evolution of the fluid speed for times $T = 0, 1, 5, 10, 15, 20, 25, 30, 40$, and 50 , respectively. Plots are shown with $0 \leq z \leq 1$ and $-40 \leq x \leq 60$.

The Fluid Speed at time, $t=1$

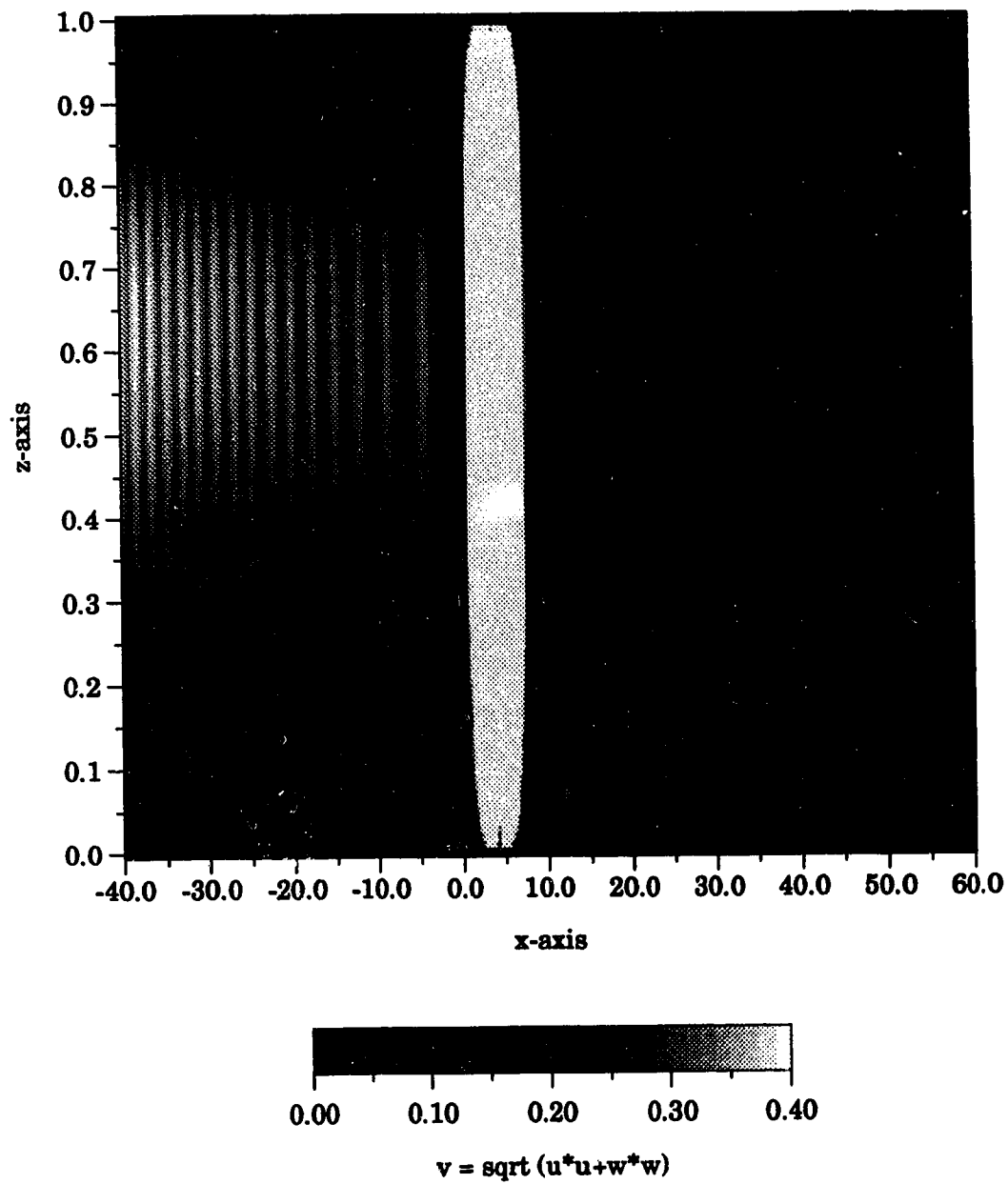


Figure 15b

The Fluid Speed at time, $t=5$

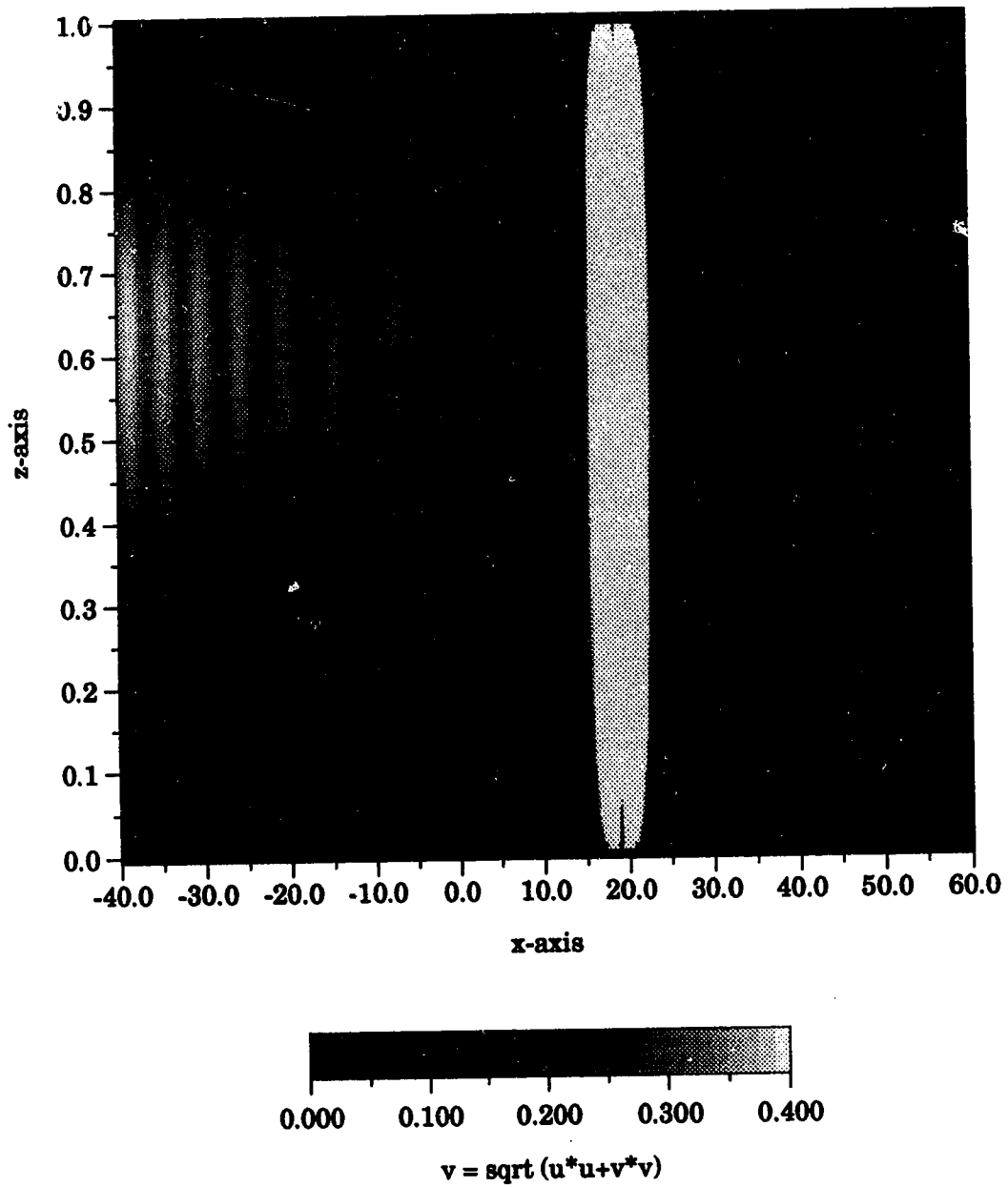


Figure 15c

The Fluid Speed at time, $t=10$

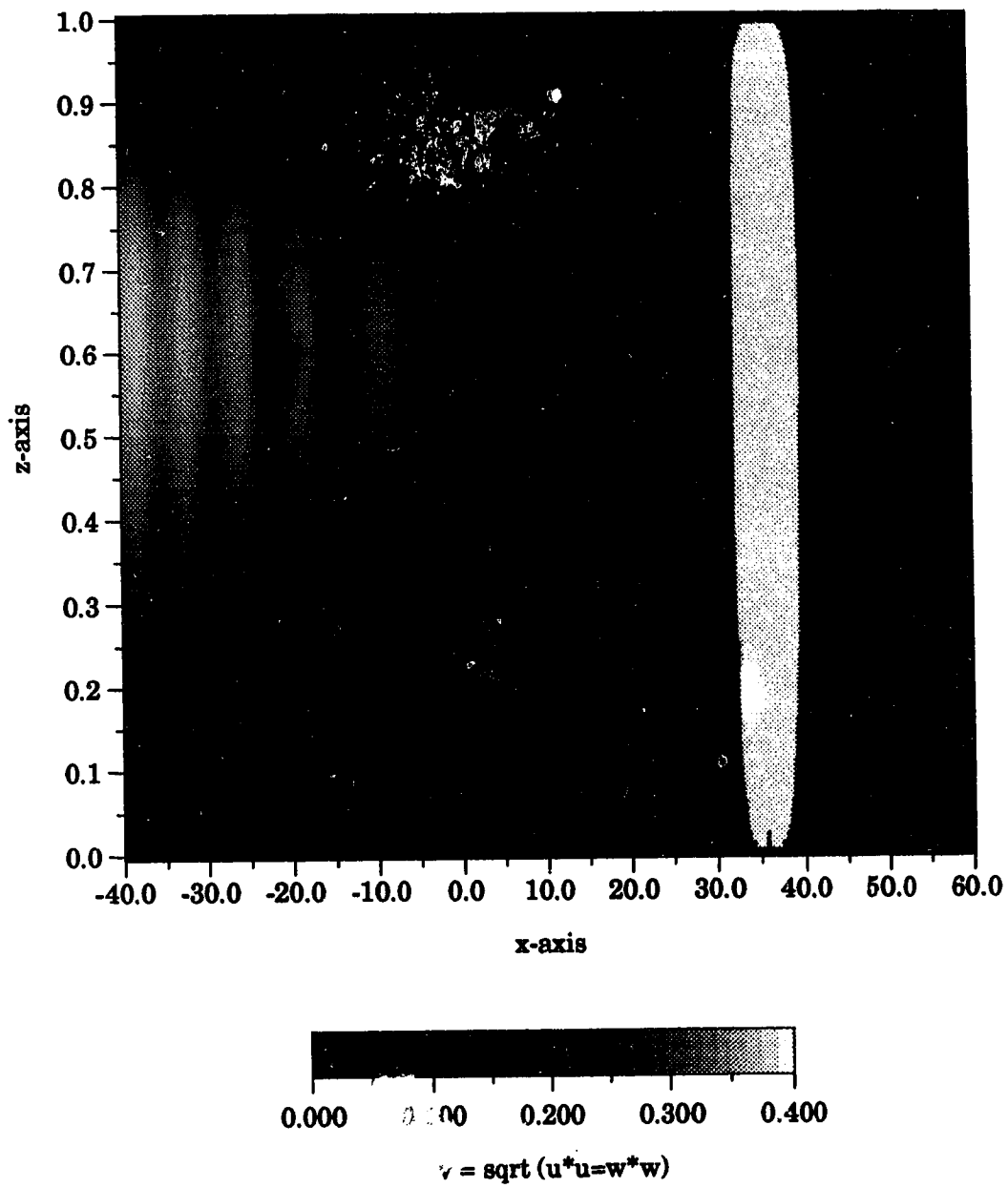


Figure 15d

The Fluid Speed at time, $t=15$

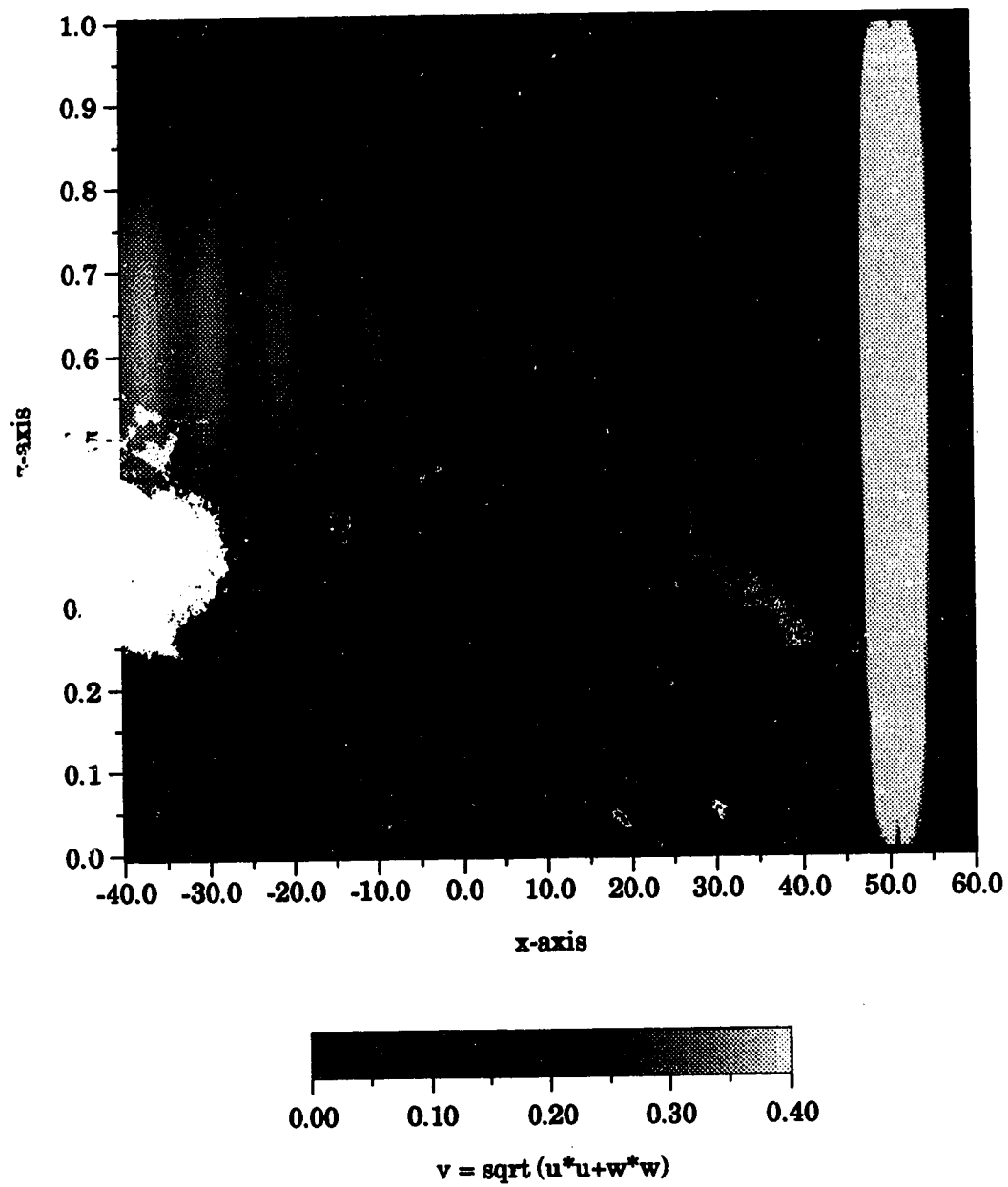


Figure 15e

The Fluid Speed at time, $t=20$

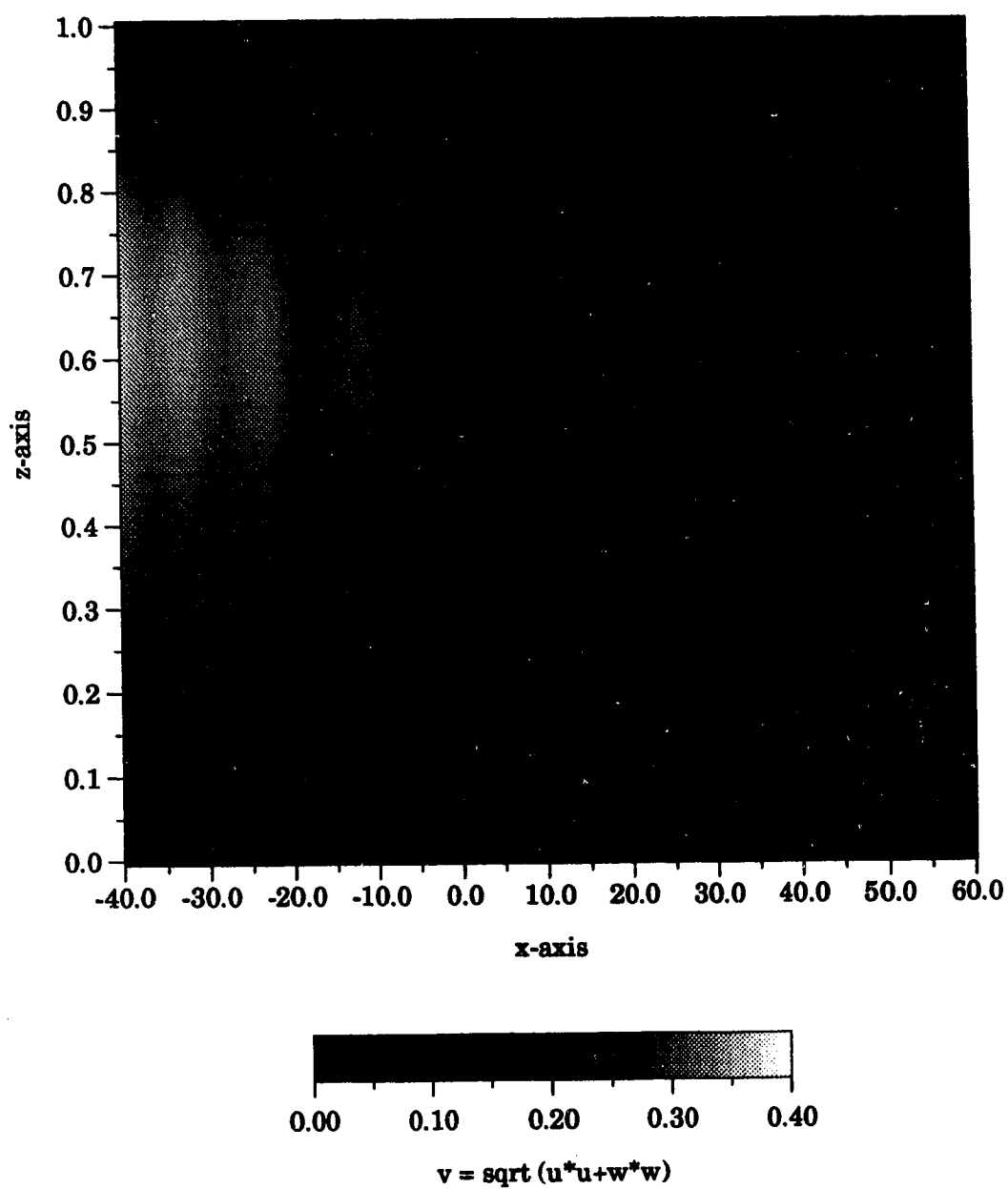


Figure 15f

The Fluid Speed at time, $t=25$

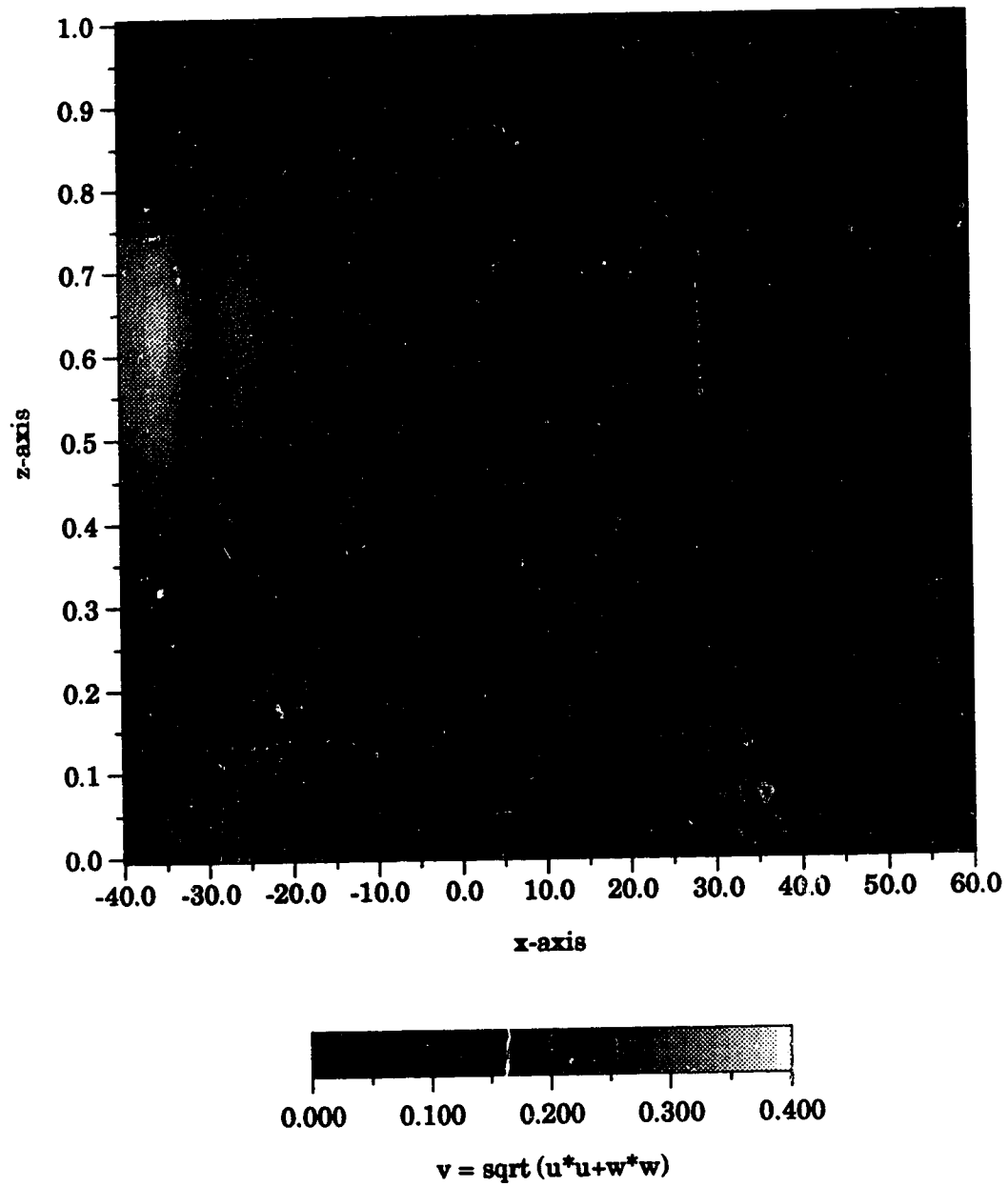


Figure 15g

The Fluid Speed at time, $t=30$

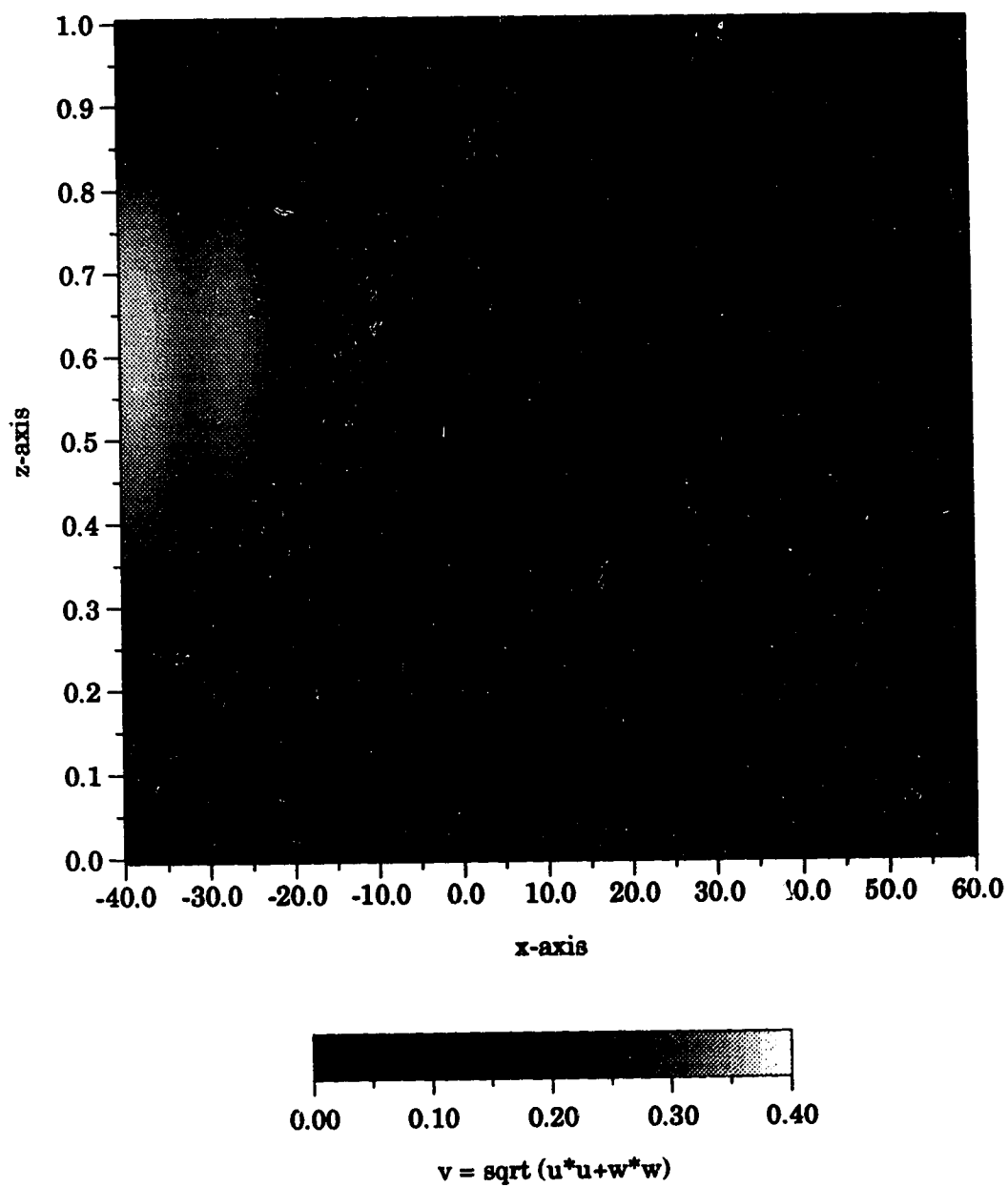


Figure 15h

The Fluid Speed at time, $t=40$

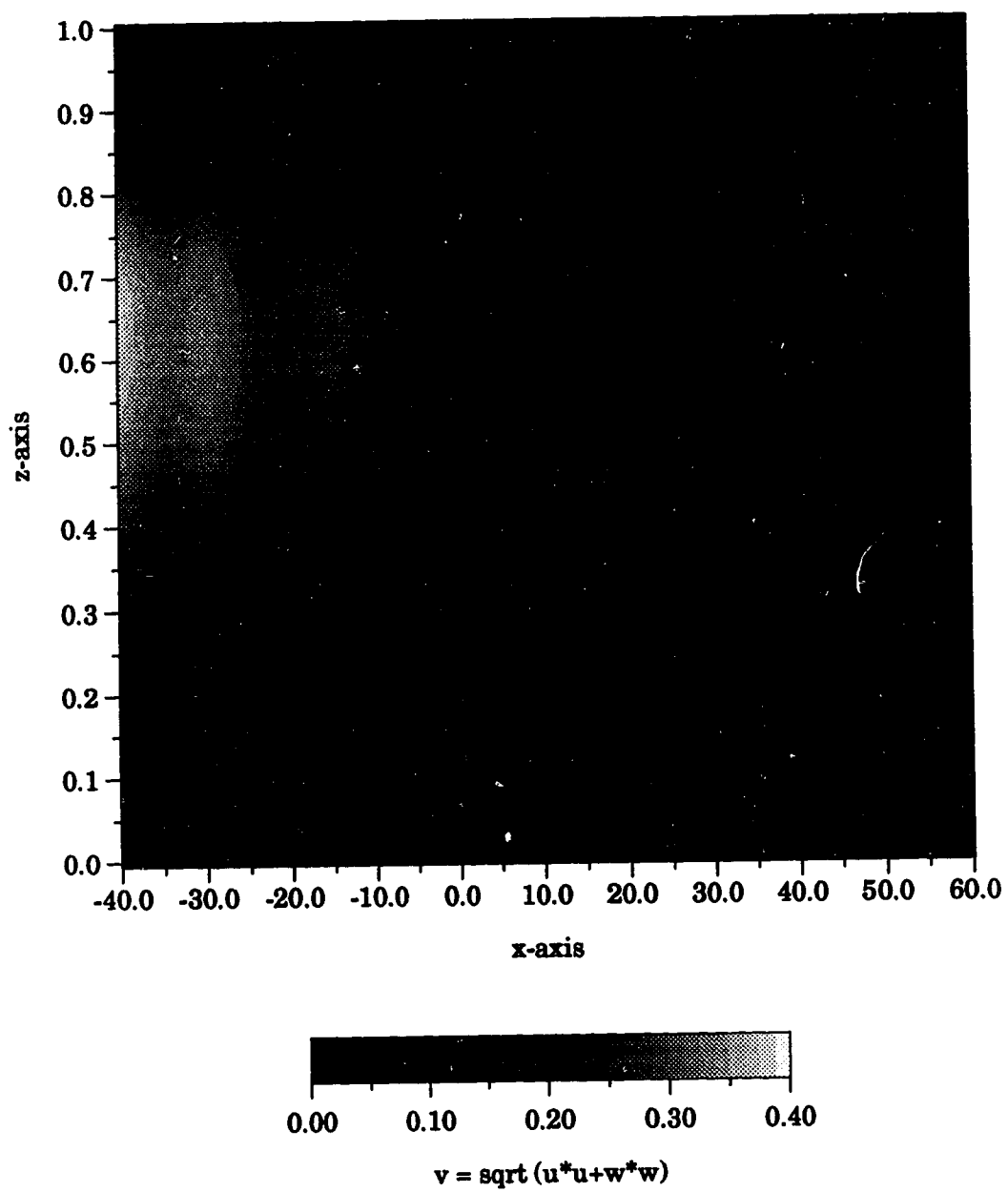


Figure 15i

The Fluid Speed at time, $t=50$

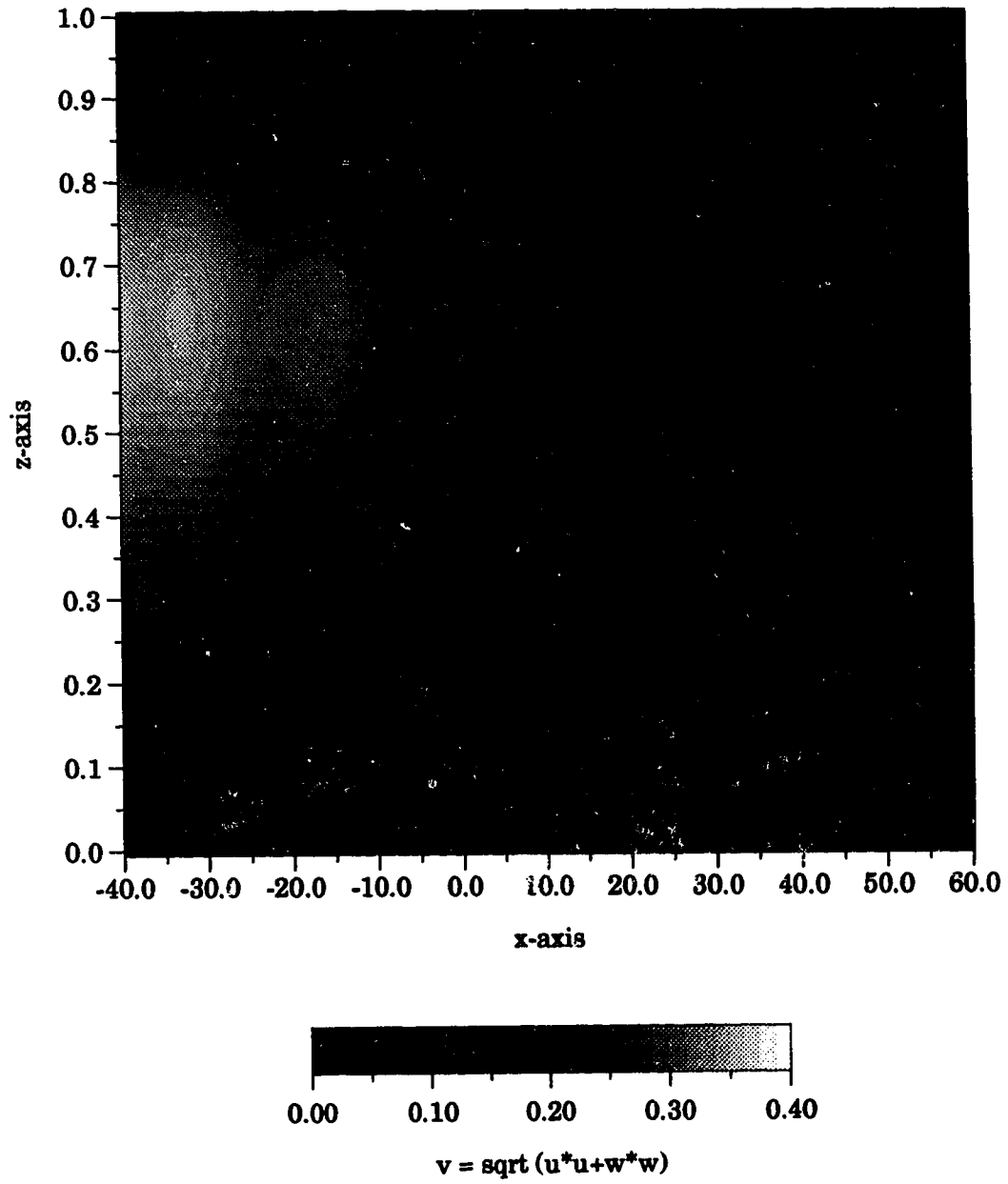


Figure 15j

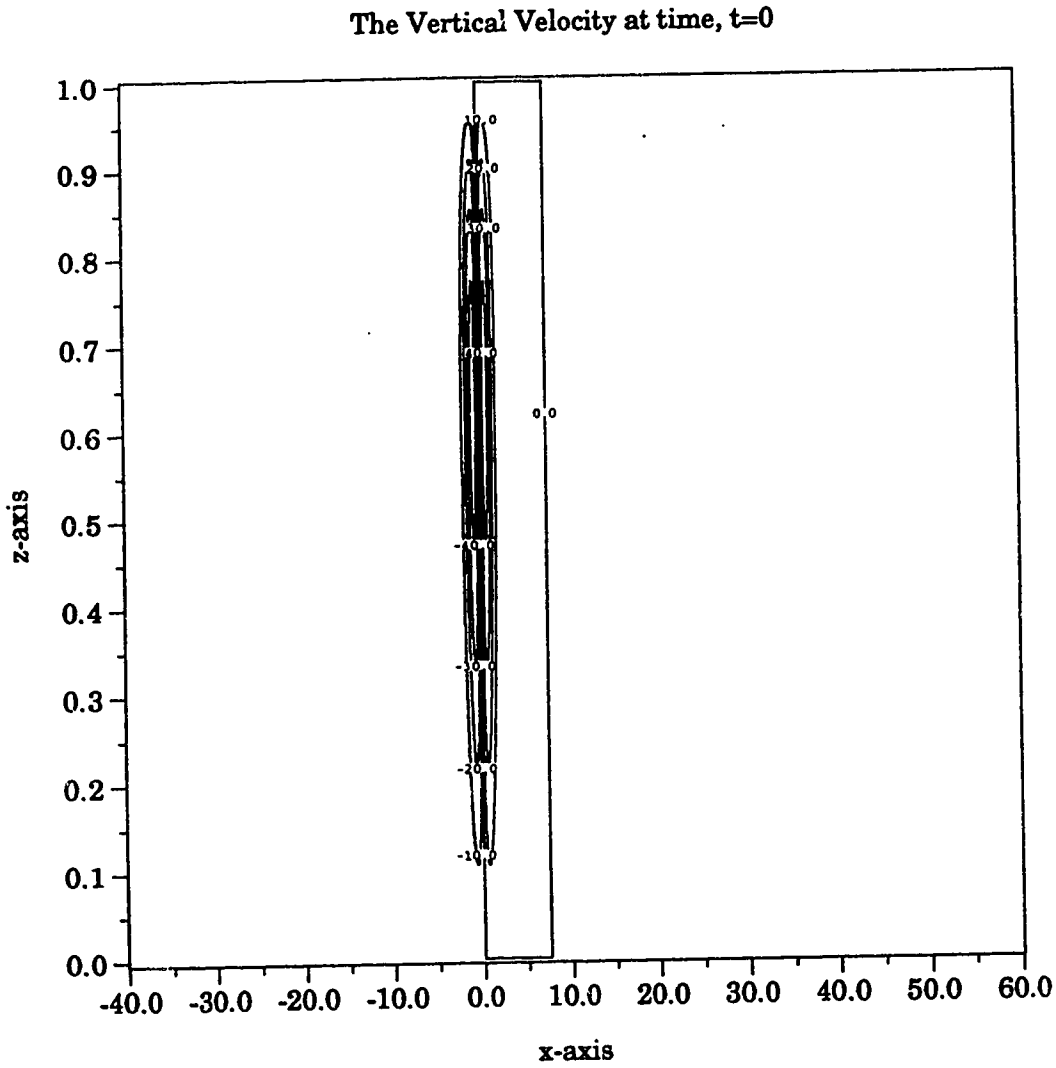


Figure 16: The Vertical Velocity

The vertical velocity, w , as determined by the streamfunction with parameters $\mu = 1.0$ and $\nu = \frac{1}{100}$. Figures 16a-j show the evolution of the vertical velocity for times, $T = 0, 1, 5, 10, 15, 20, 25, 30, 40$, and 50 , respectively. Plots are shown with $0 \leq z \leq 1$ and $-40 \leq x \leq 60$.

The Vertical Velocity at time, $t=1$

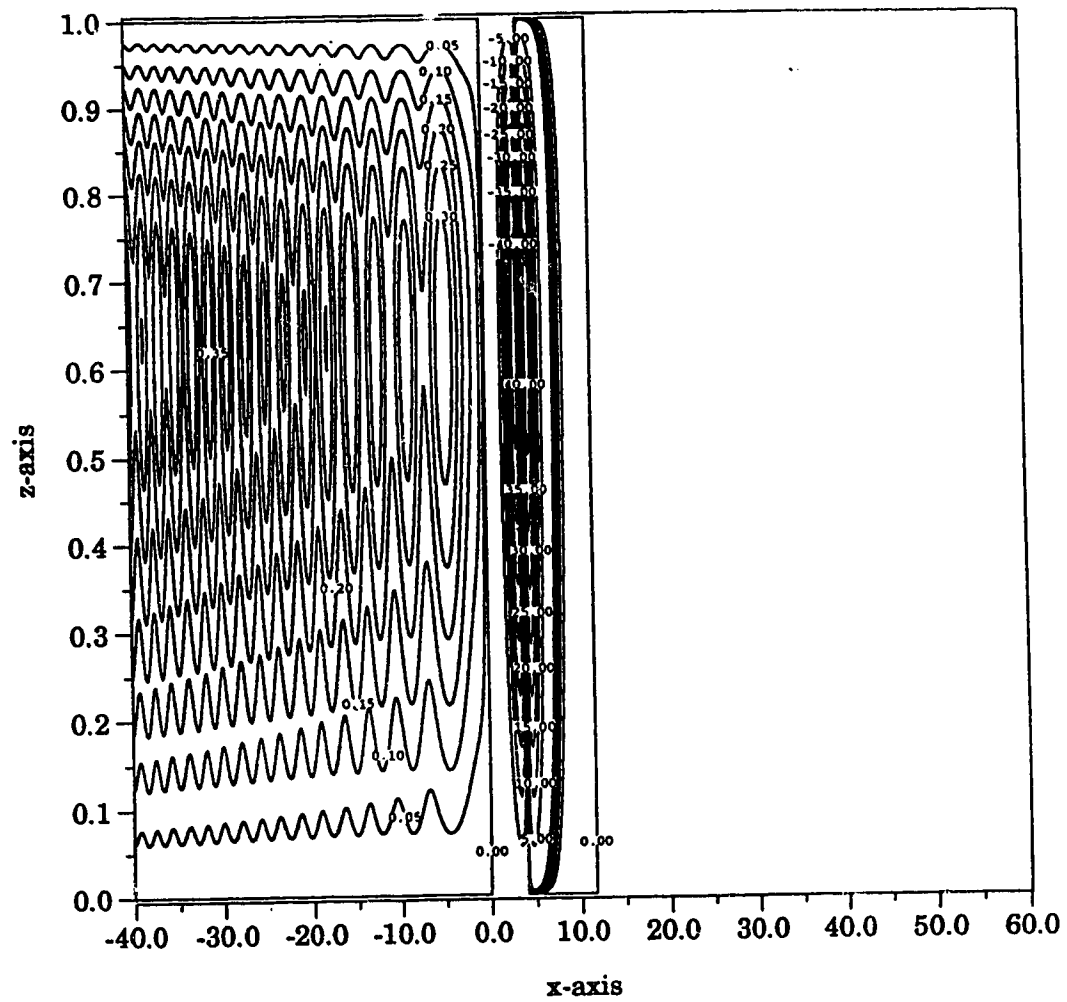


Figure 16b

The Vertical Velocity at time, $t=5$

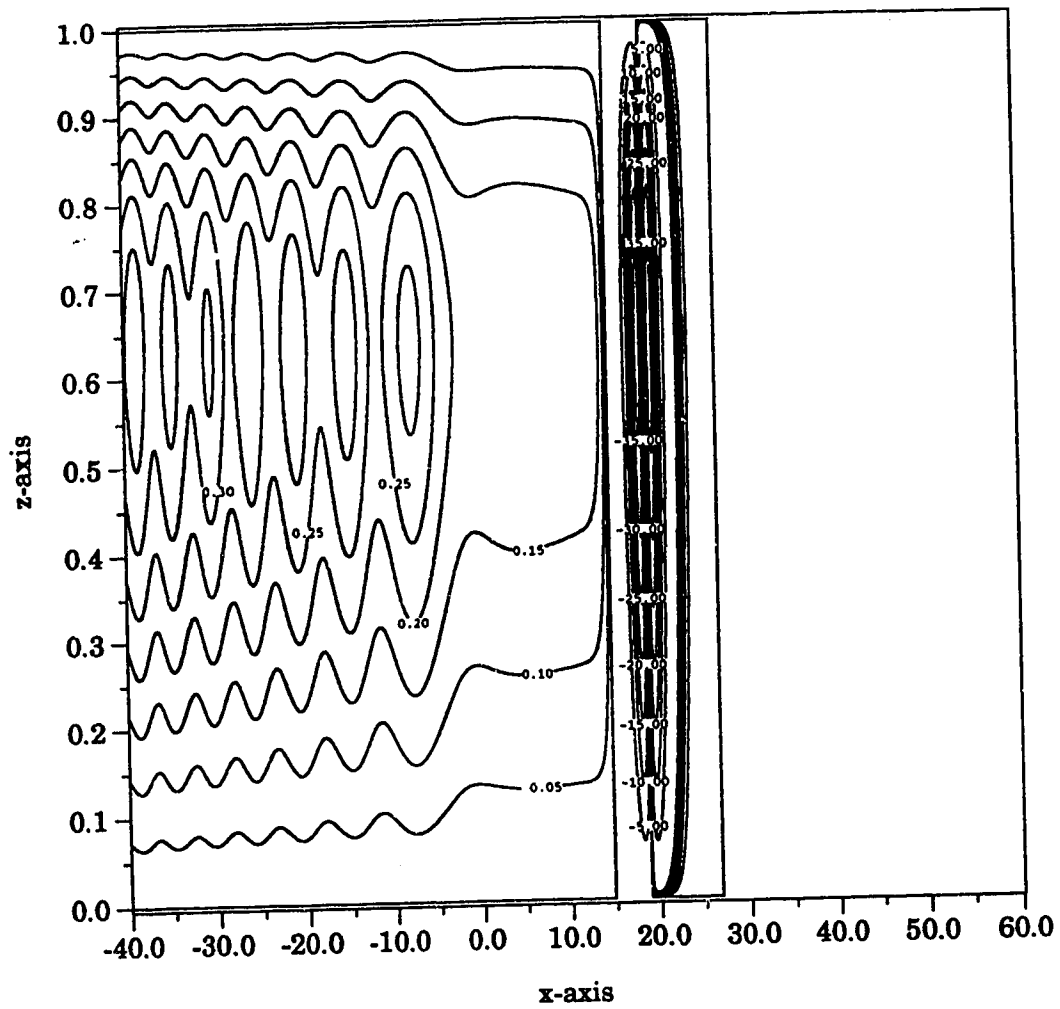


Figure 16c

The Vertical Velocity at time, $t=10$

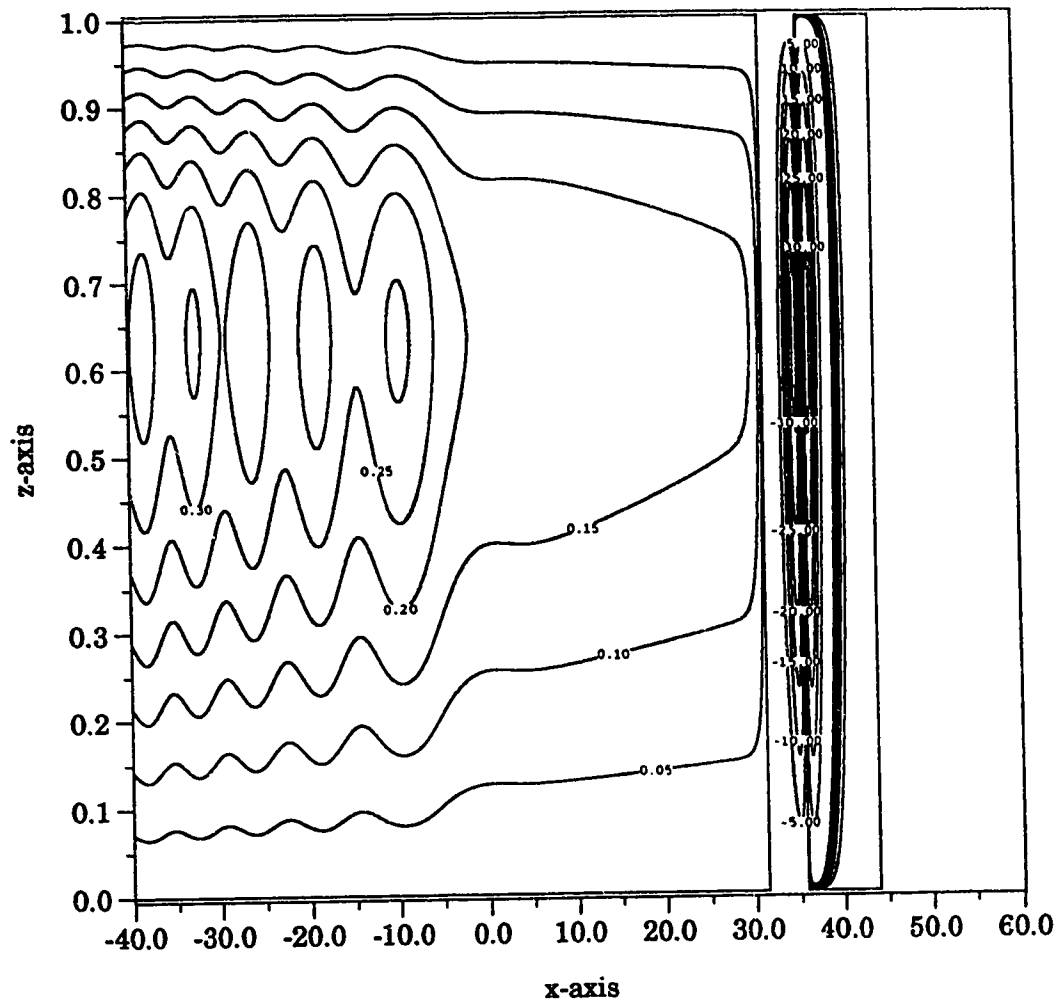


Figure 16d

The Vertical Velocity at time, $t=15$

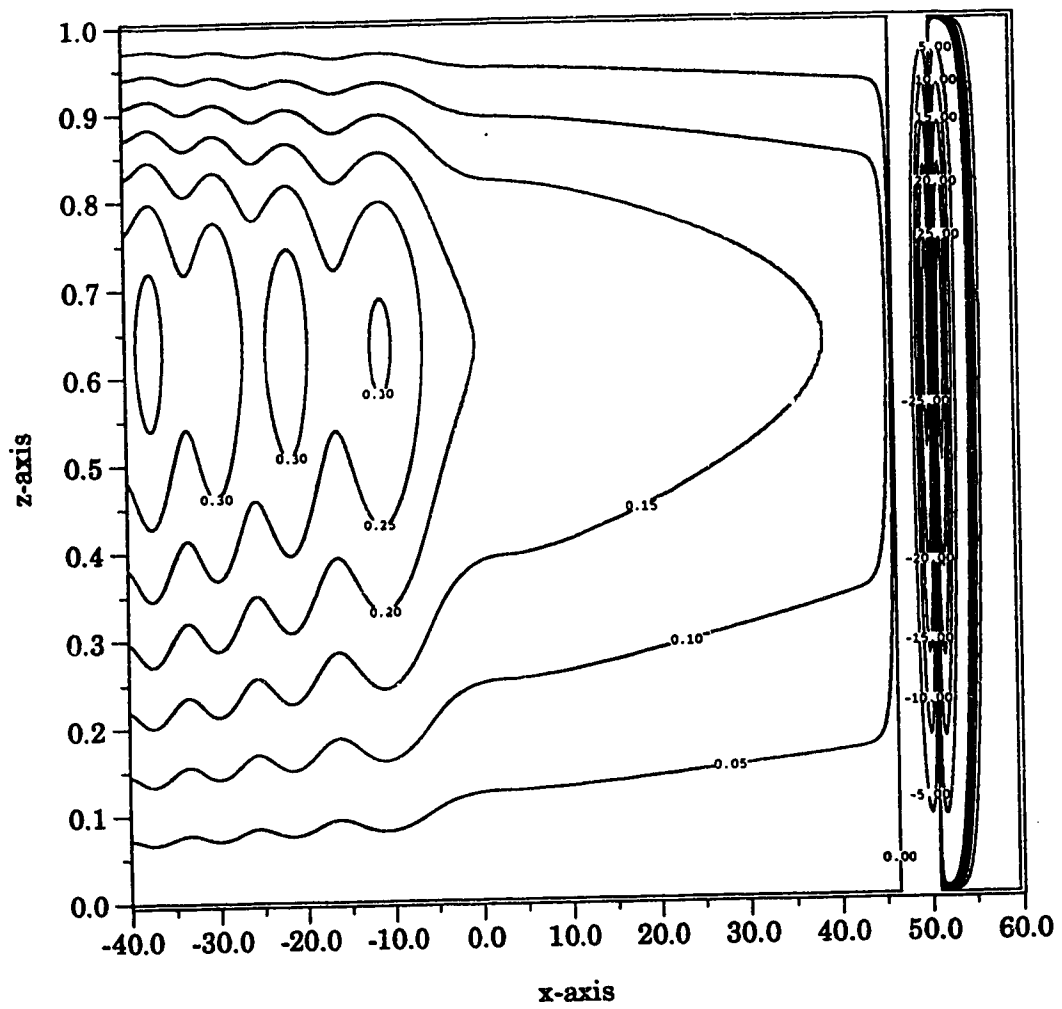


Figure 16e

The Vertical Velocity at time, $t=20$

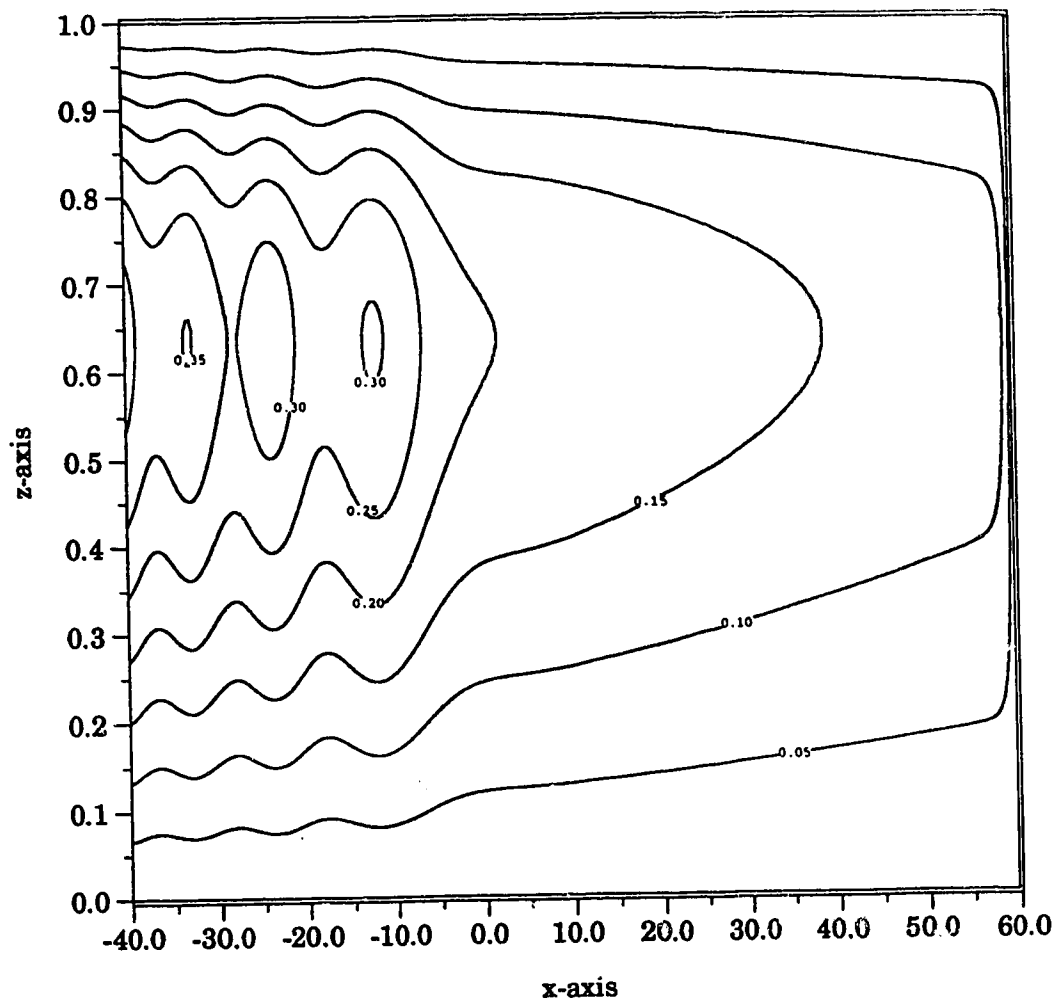


Figure 16f

The Vertical Velocity at time, $t=25$

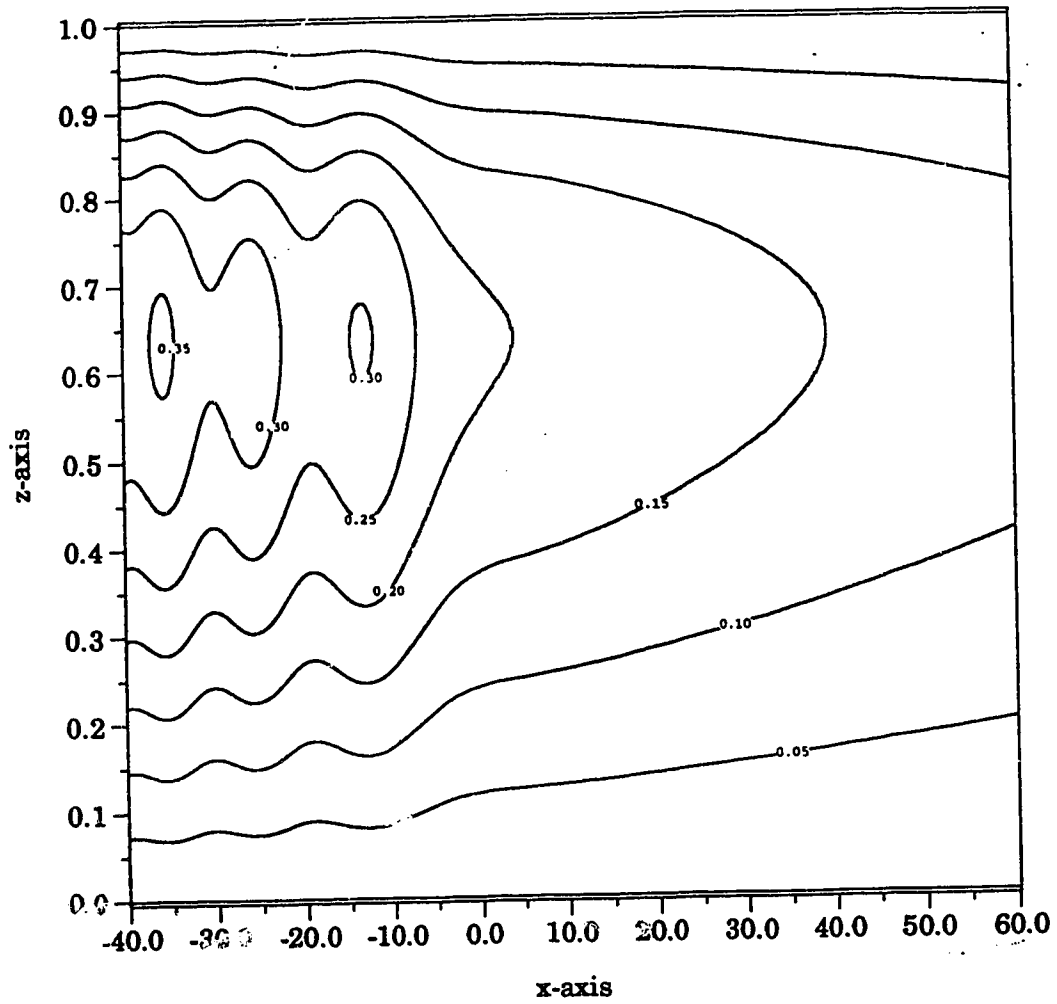


Figure 16g

The Vertical Velocity at time, $t=30$

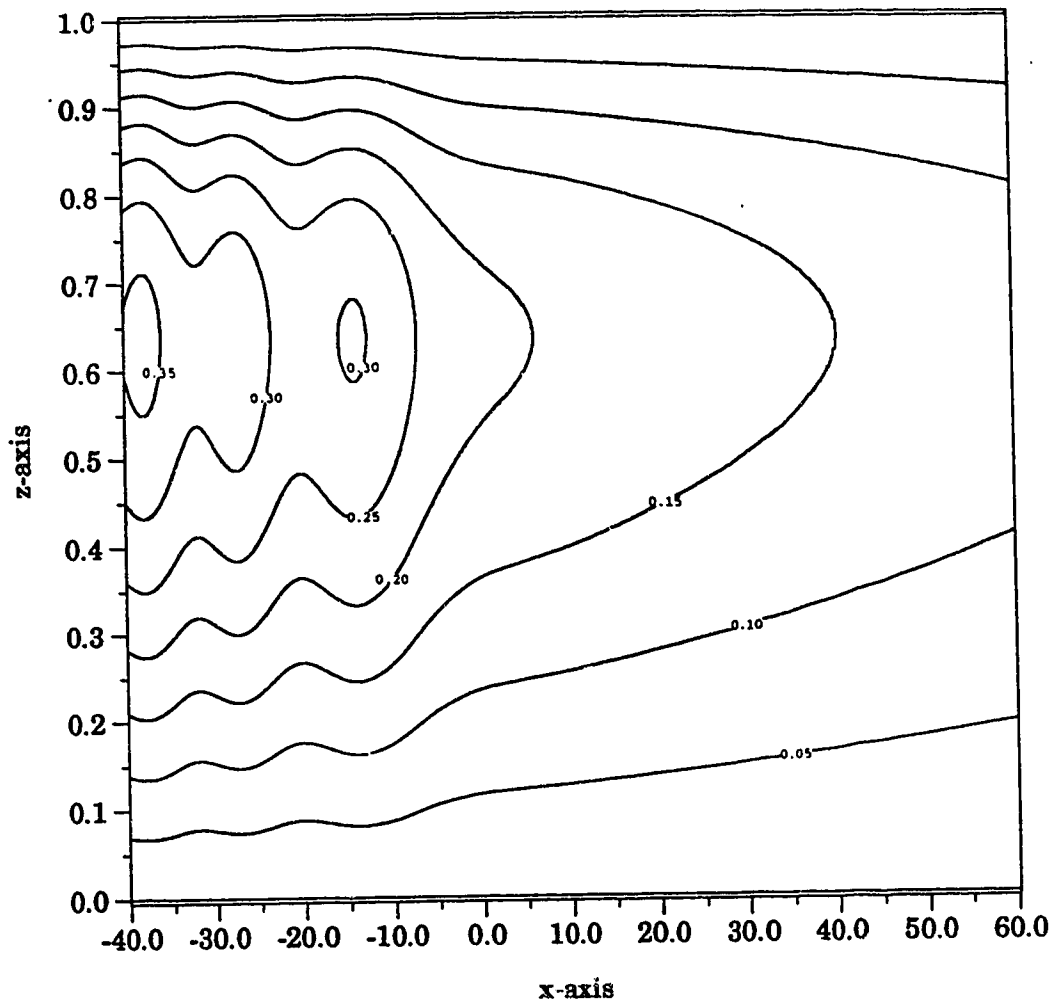


Figure 16h

The Vertical Velocity at time, $t=40$

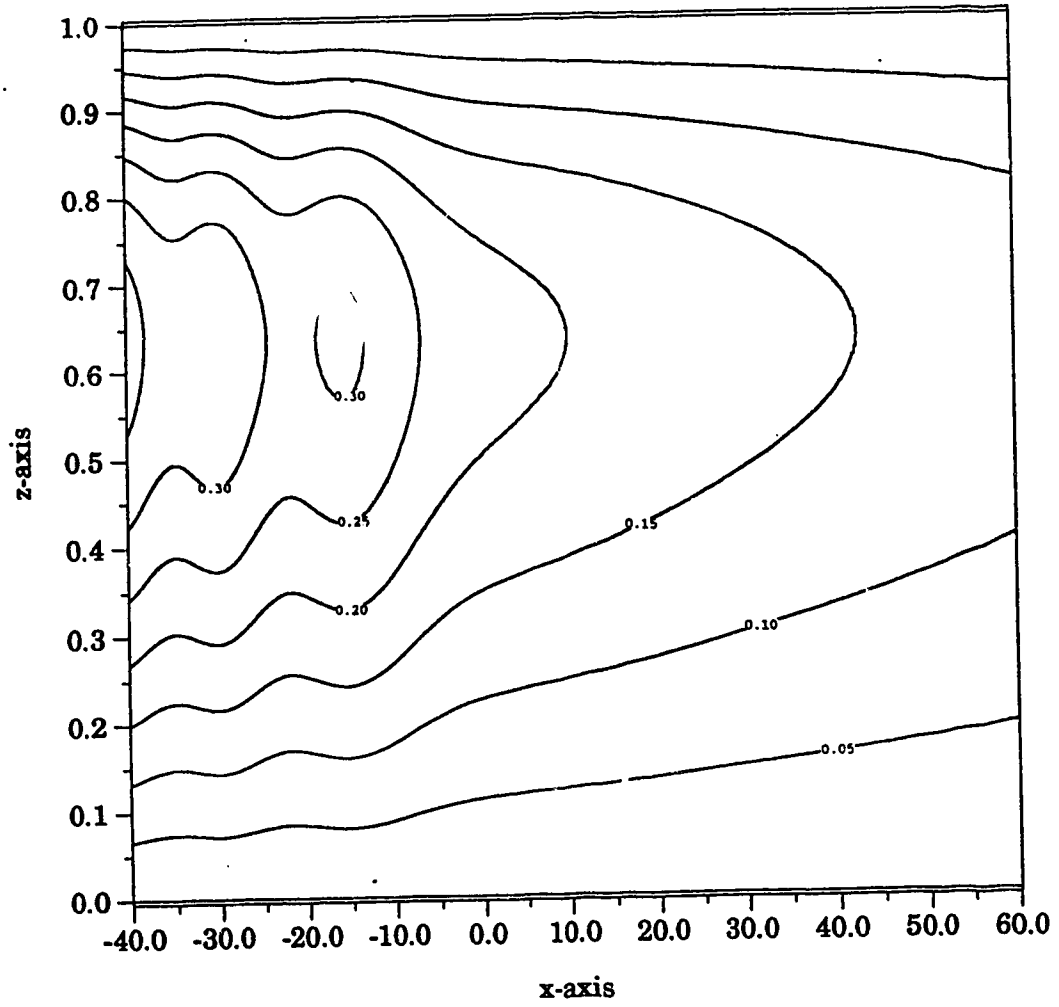


Figure 16i

The Vertical Velocity at time, $t=50$

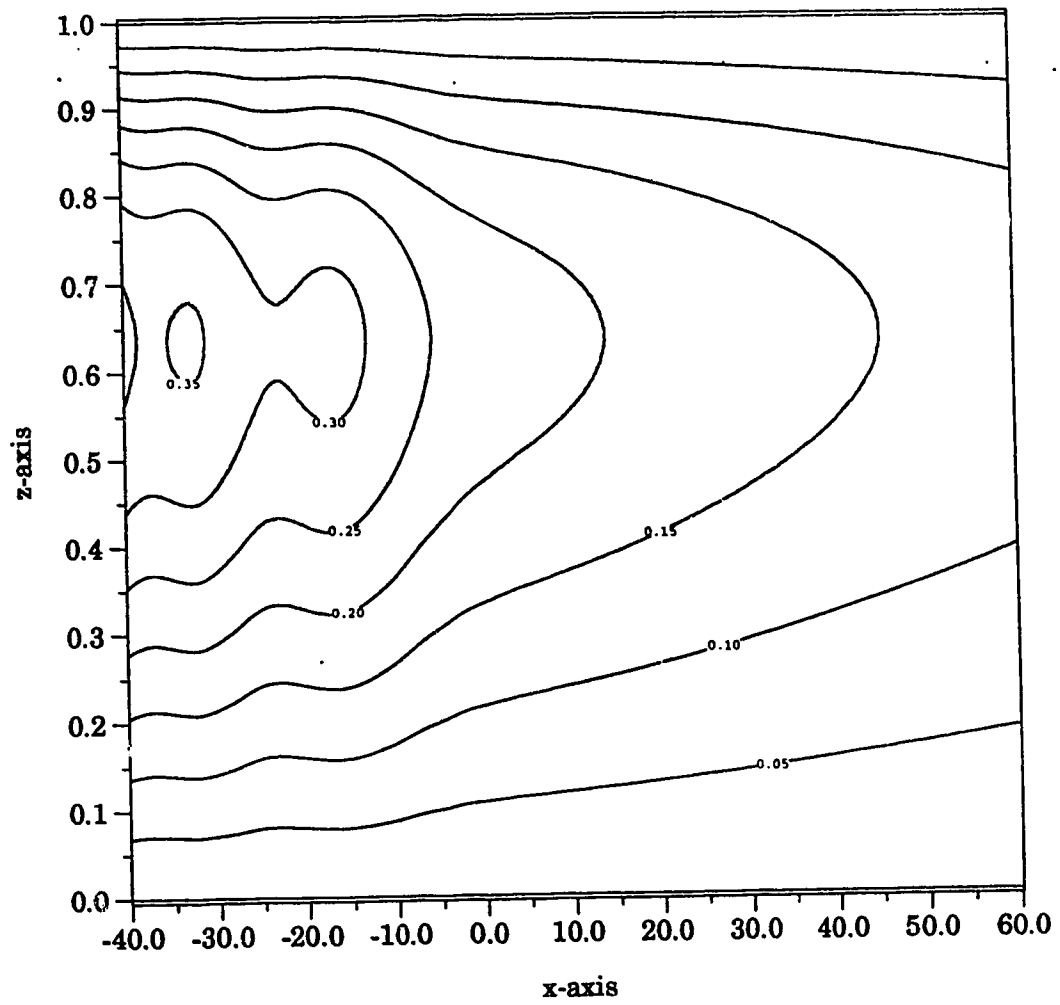


Figure 16j

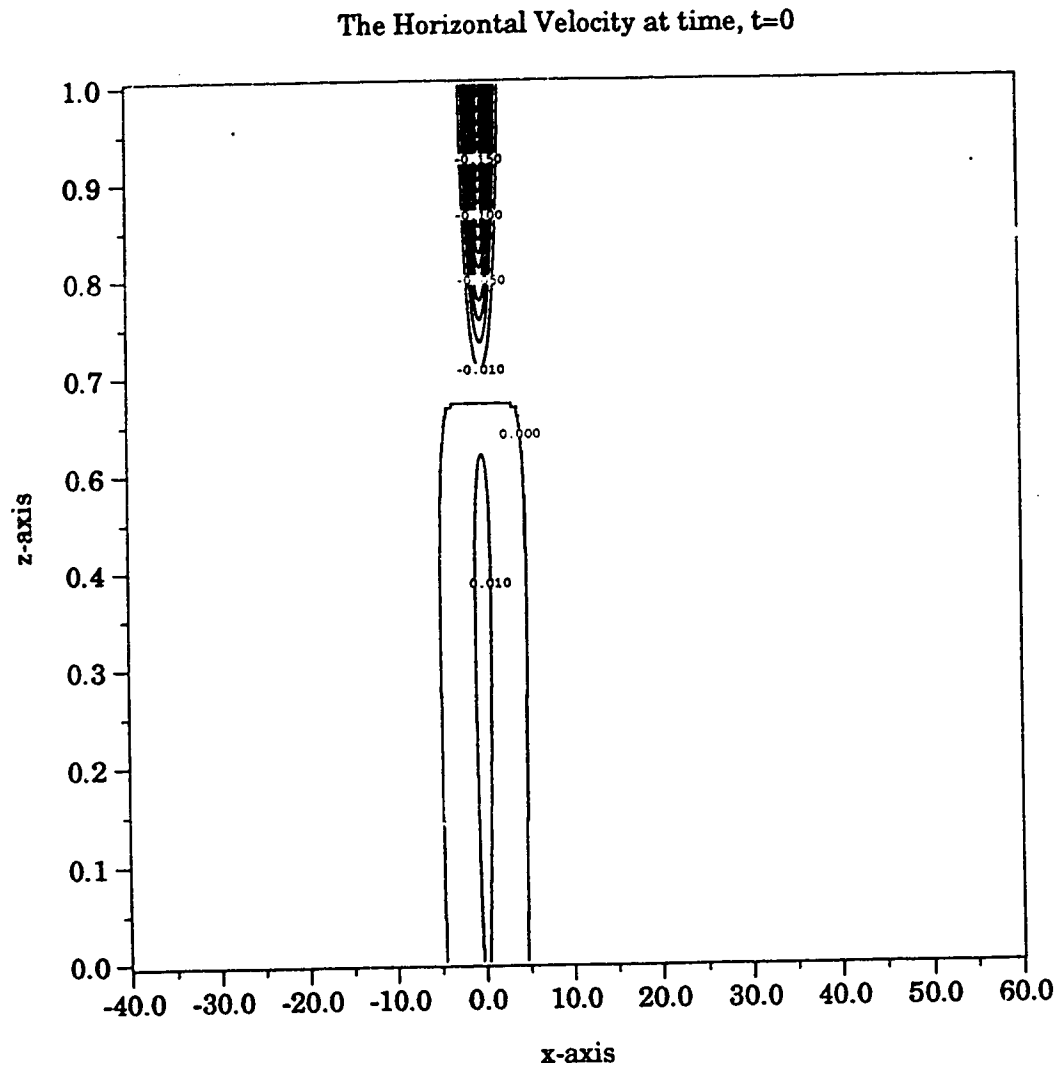


Figure 17: The Horizontal Velocity

The horizontal velocity, u , as determined by the streamfunction with parameters $\mu = 1.0$ and $\nu = \frac{1}{100}$. Figures 17a-j show the evolution of the horizontal velocity for times, $T = 0, 1, 5, 10, 15, 20, 25, 30, 40$, and 50, respectively. Plots are shown with $0 \leq z \leq 1$ and $-40 \leq x \leq 60$.

The Horizontal Velocity at time, $t=1$

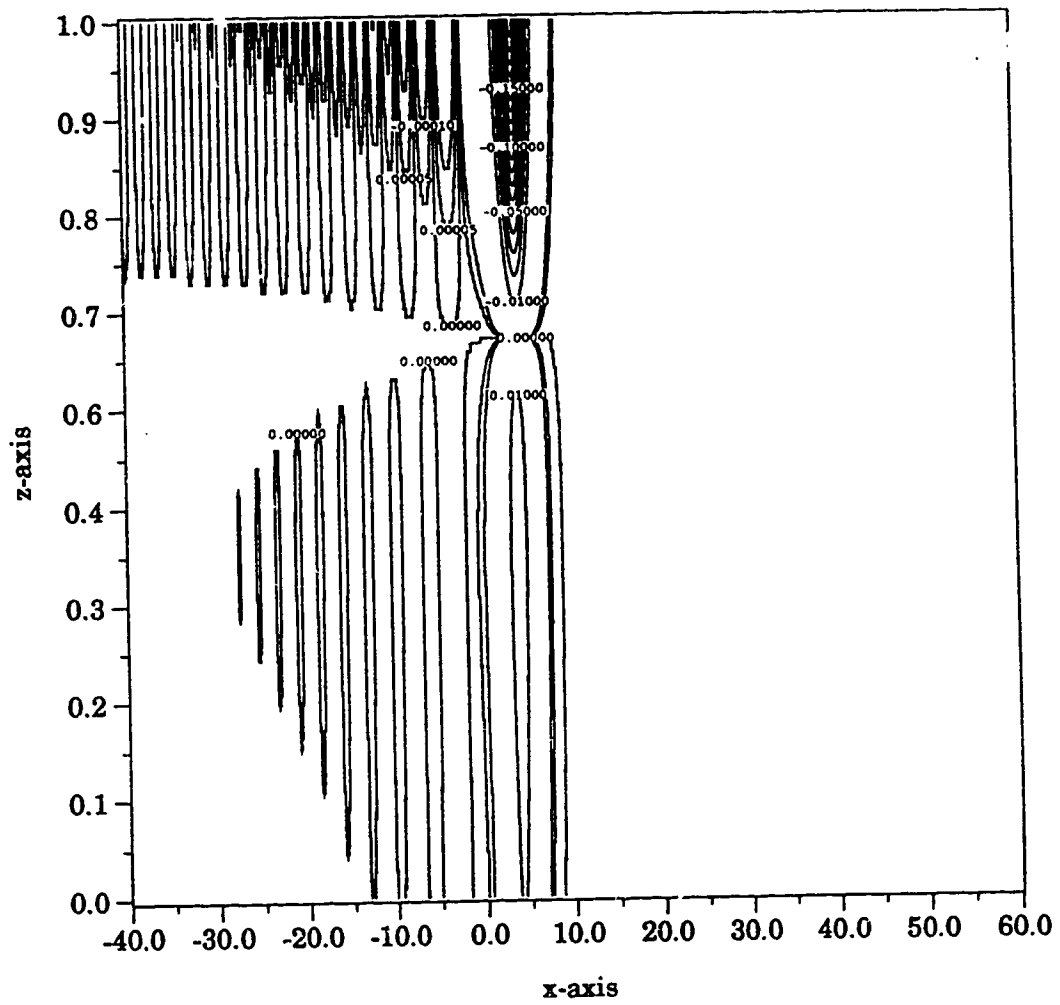


Figure 17b

The Horizontal Velocity at time, $t=5$

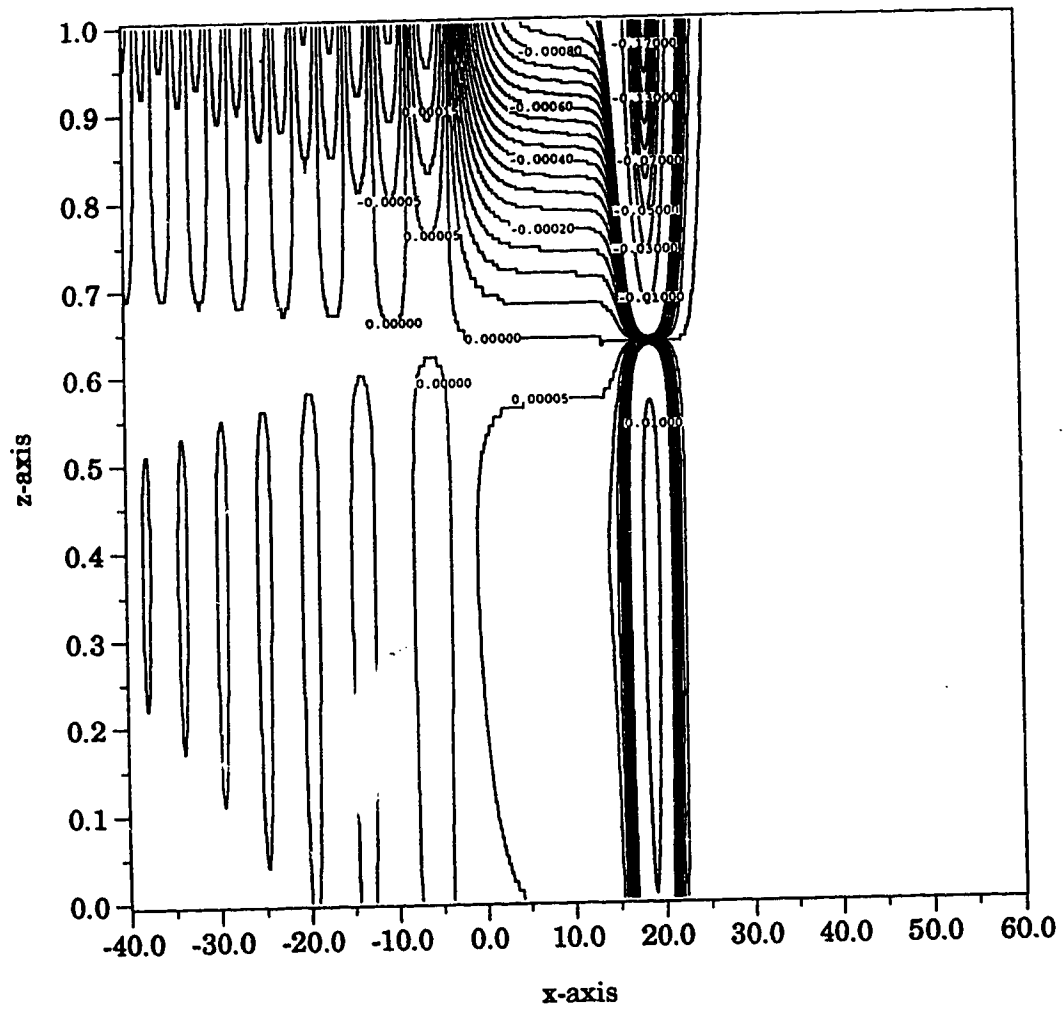


Figure 17c

The Horizontal Velocity at time, $t=10$

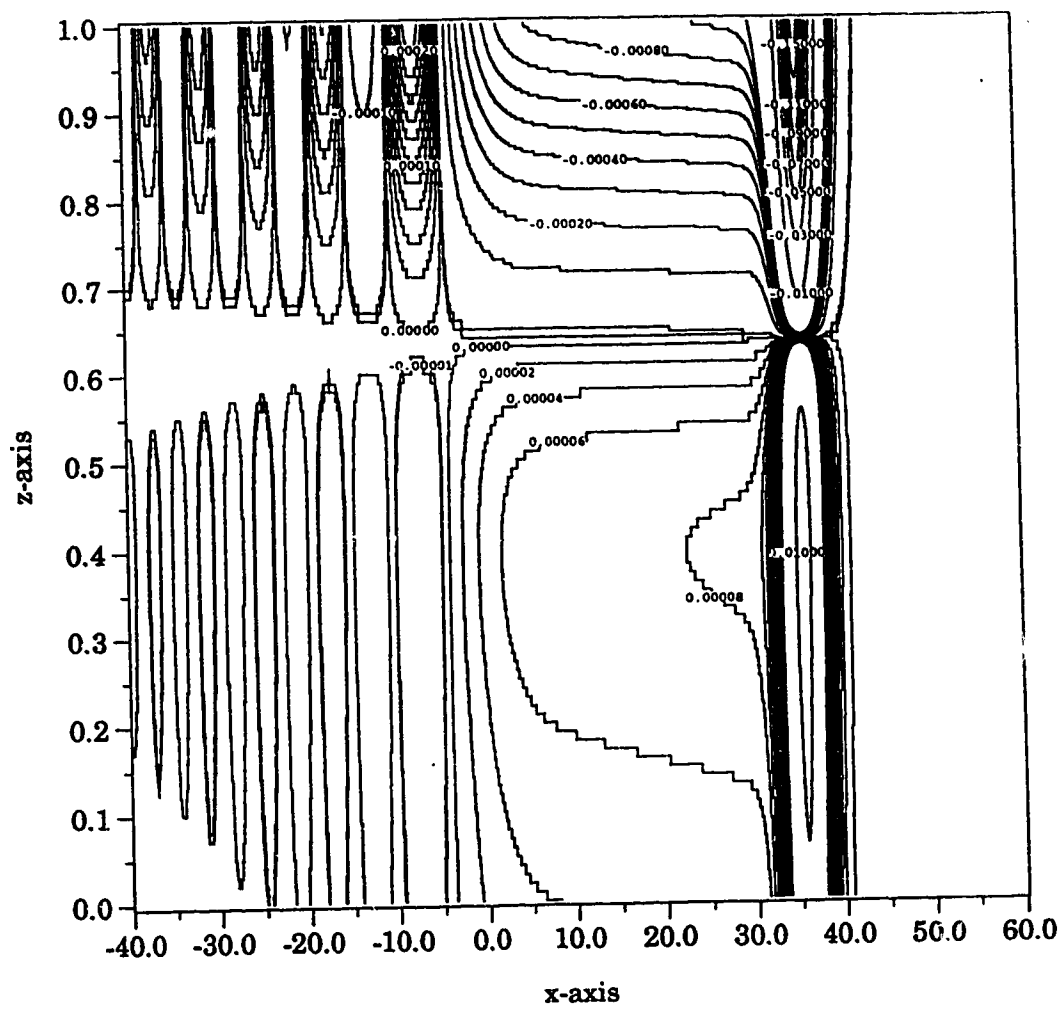


Figure 17d

The Horizontal Velocity at time, $t=15$

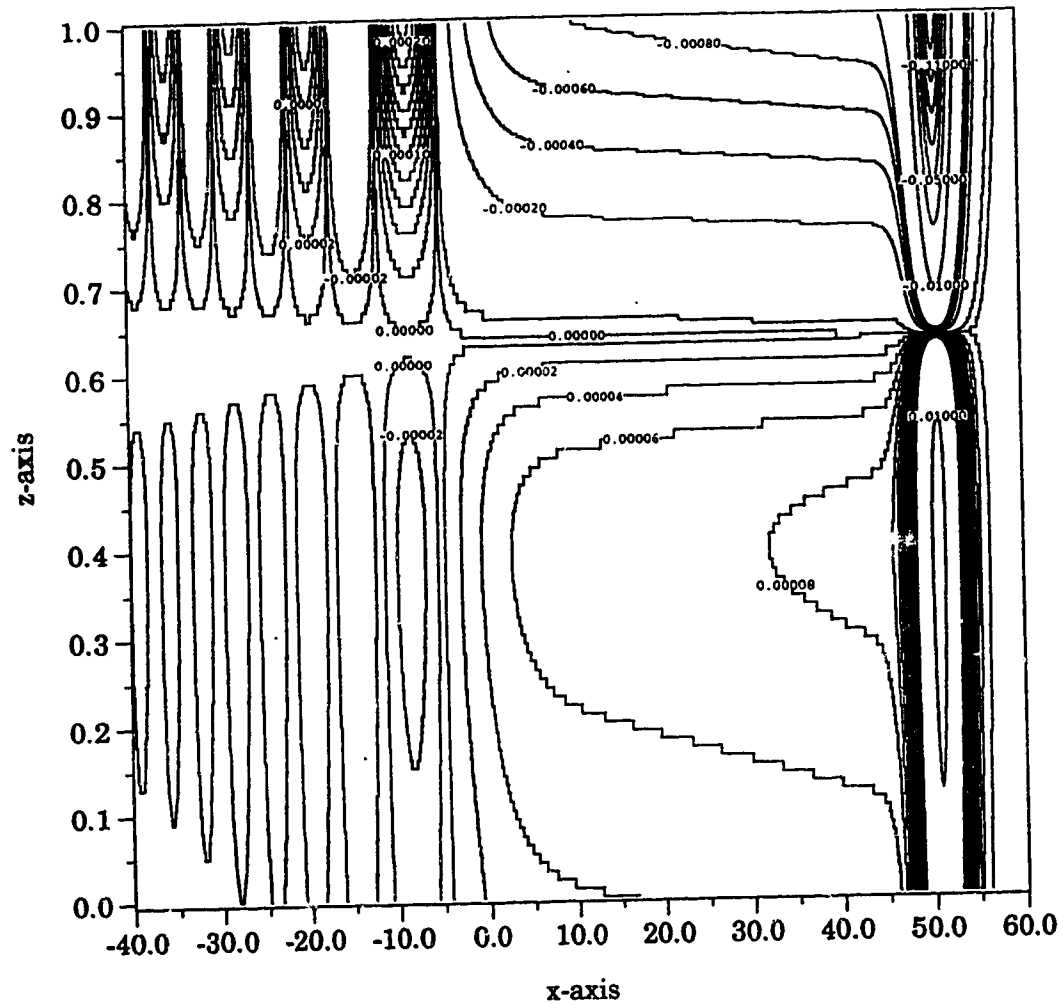


Figure 17e

The Horizontal Velocity at time, $t=20$

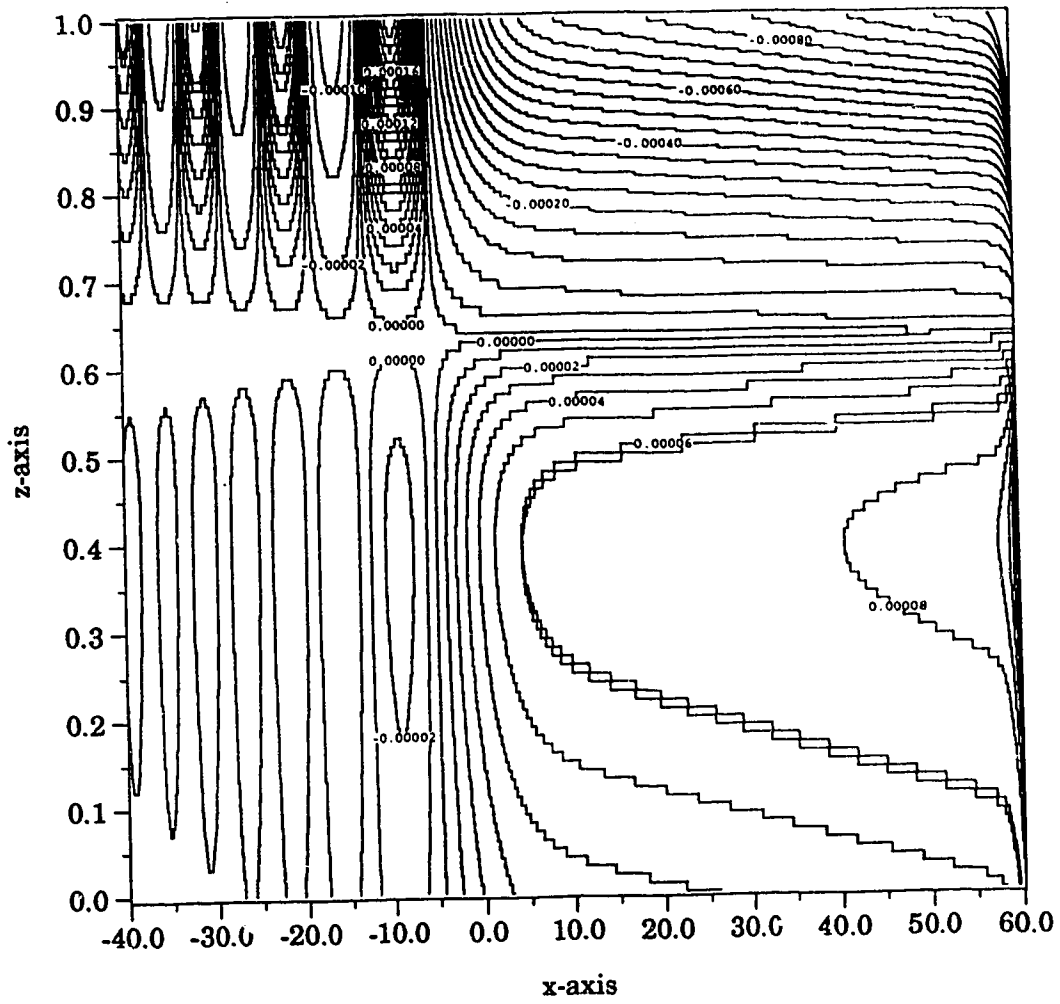


Figure 17f

The Horizontal Velocity at time, $t=25$

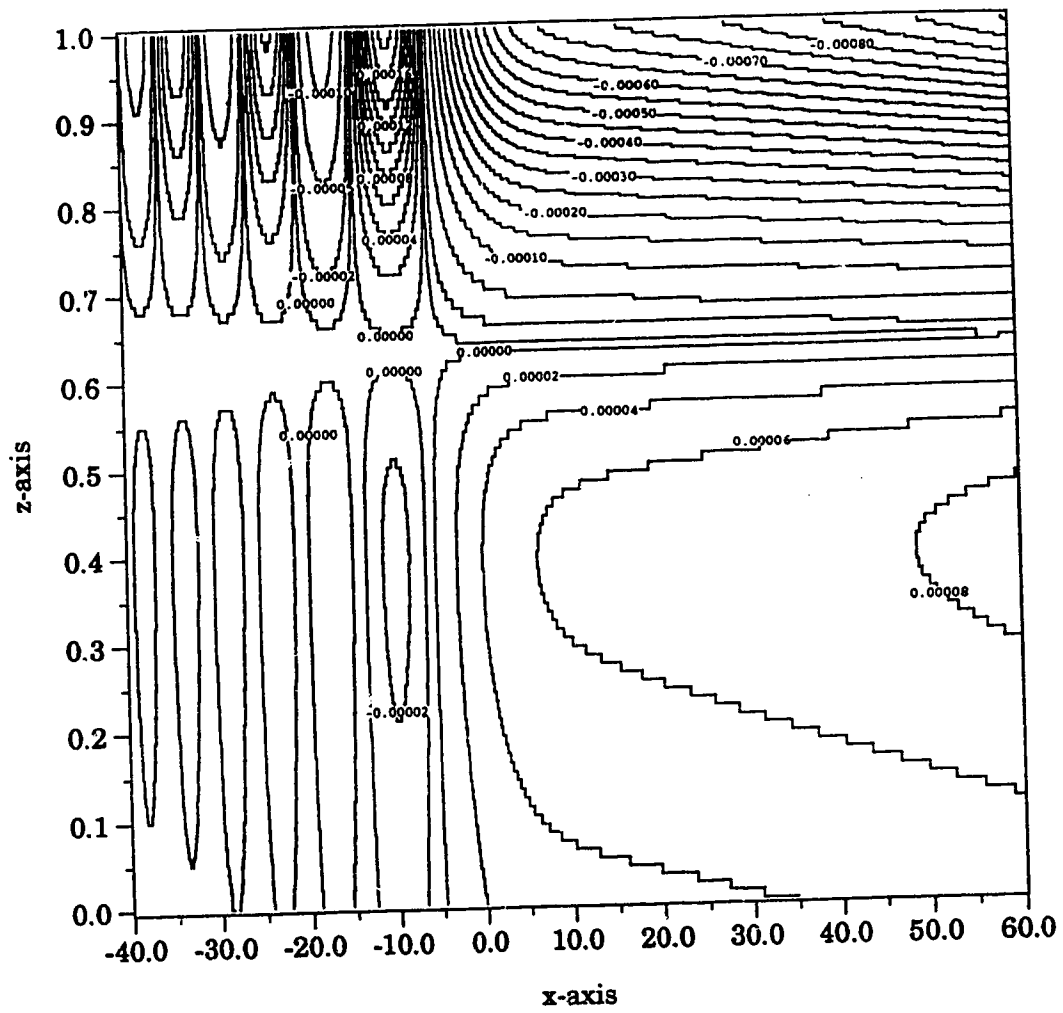


Figure 17g

The Horizontal Velocity at time, $t=30$

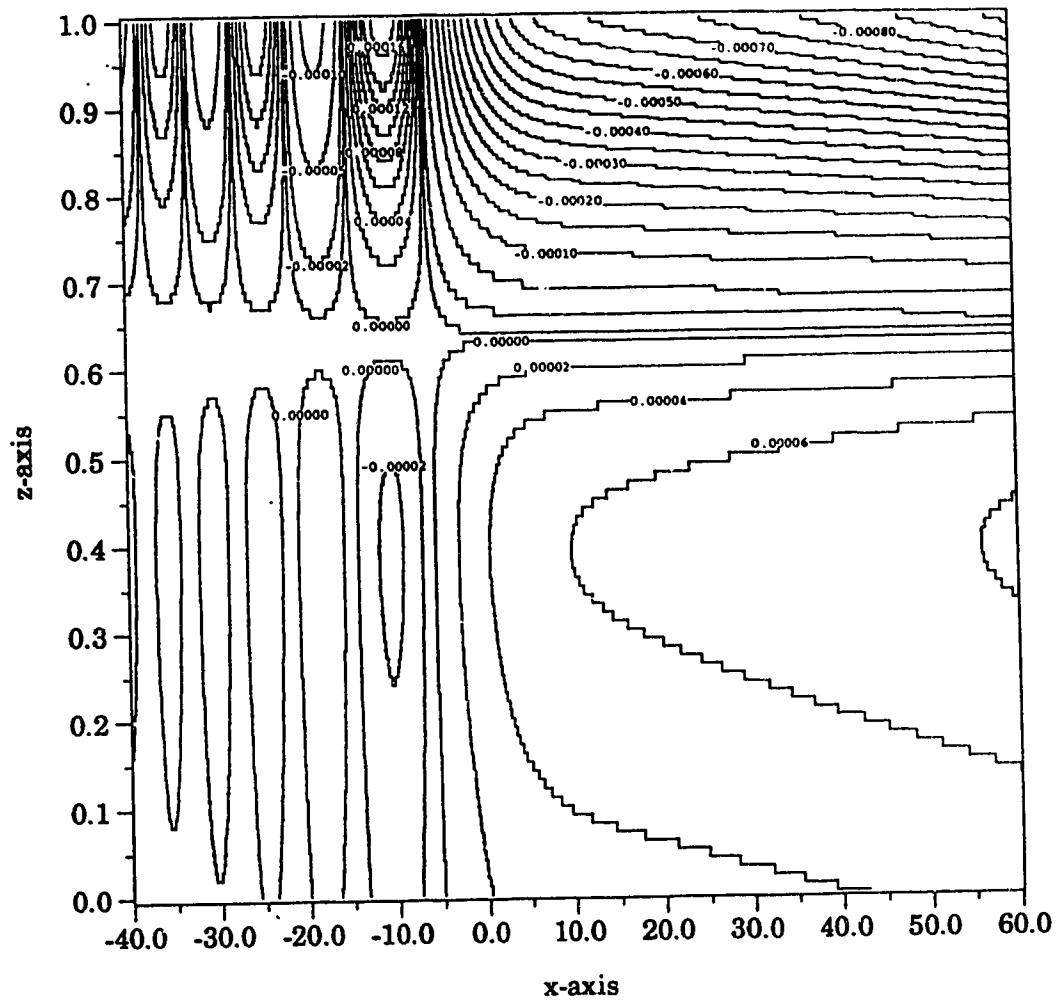


Figure 17h

The Horizontal Velocity at time, $t=40$

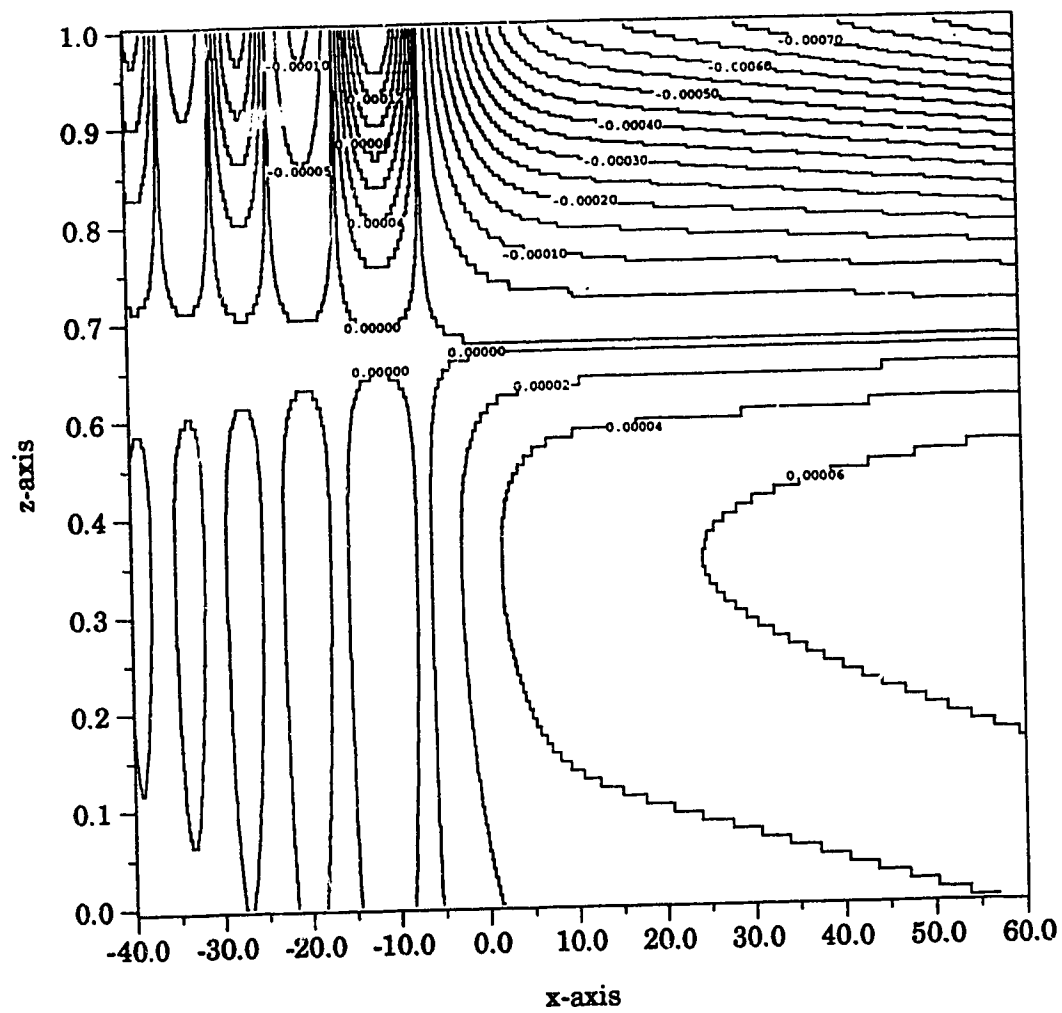


Figure 17i

The Horizontal Velocity at time, $t=50$

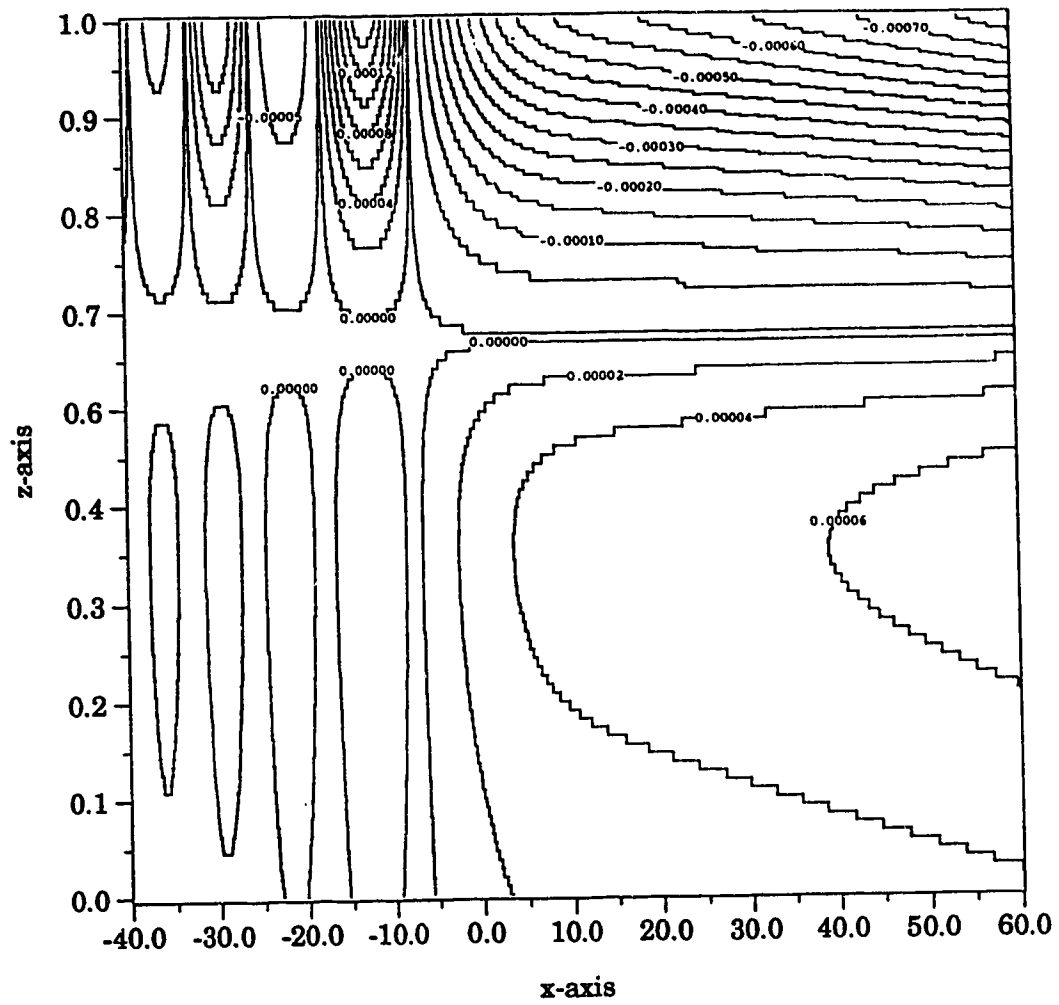


Figure 17j

The Streamfunction at time, $t=0$

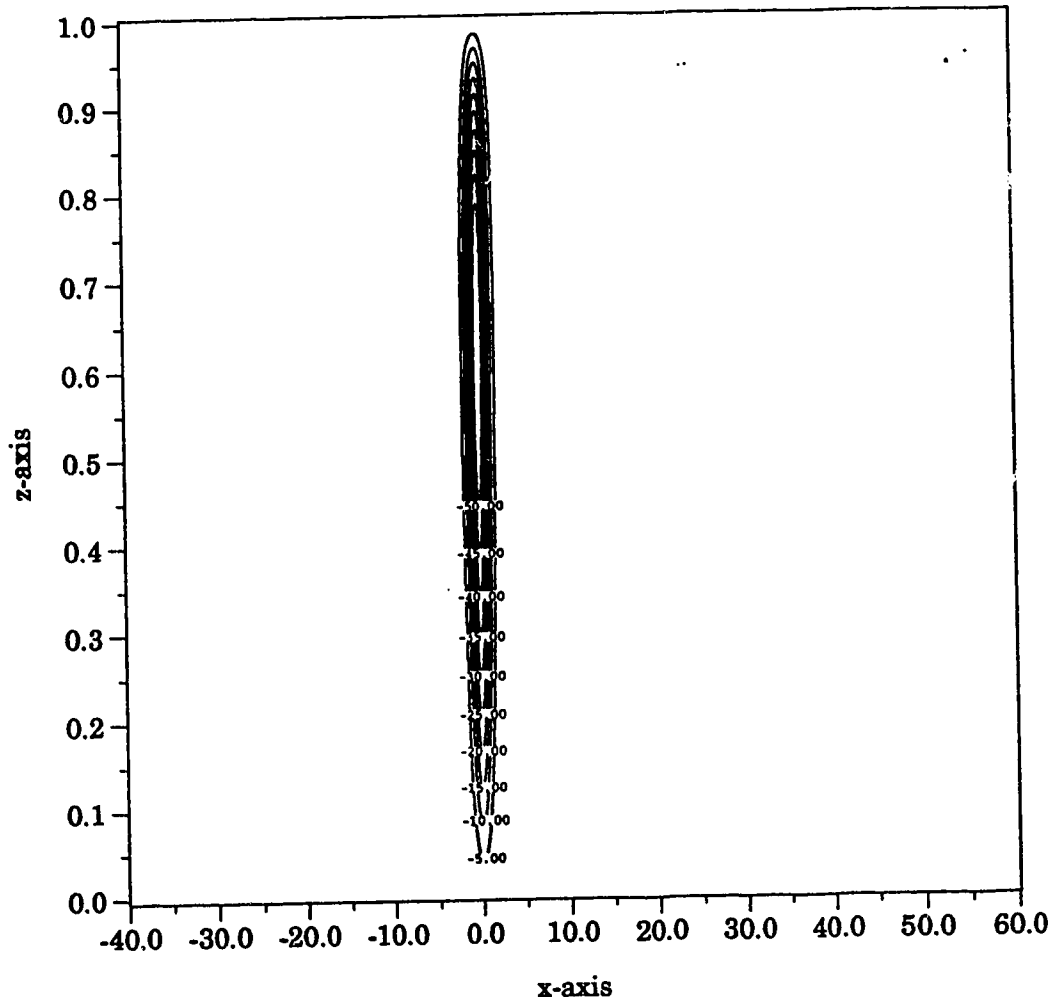


Figure 18: Contour Plot of Streamfunction

The flow field as a contour plot of the streamfunction with parameters $\mu = 1.0$, $\nu = \frac{1}{100}$. Figures 18a-j show the development of the streamfunction for times $T = 0, 1, 5, 10, 15, 20, 25, 30, 40$, and 50 , respectively. Plots are shown with $0 \leq z \leq 1$ and $-40 \leq x \leq 60$.

The Streamfunction at time, $t=1$

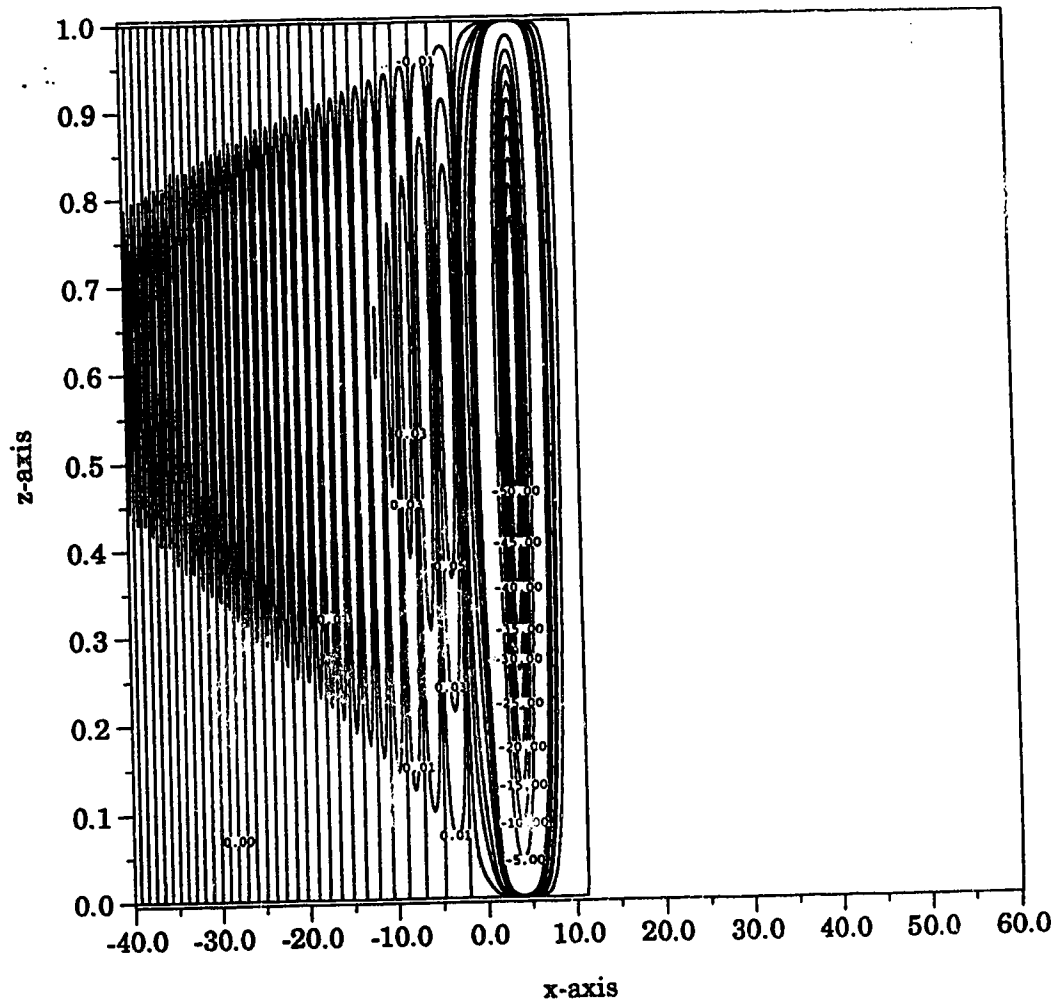


Figure 18b

The Streamfunction at time, $t=5$

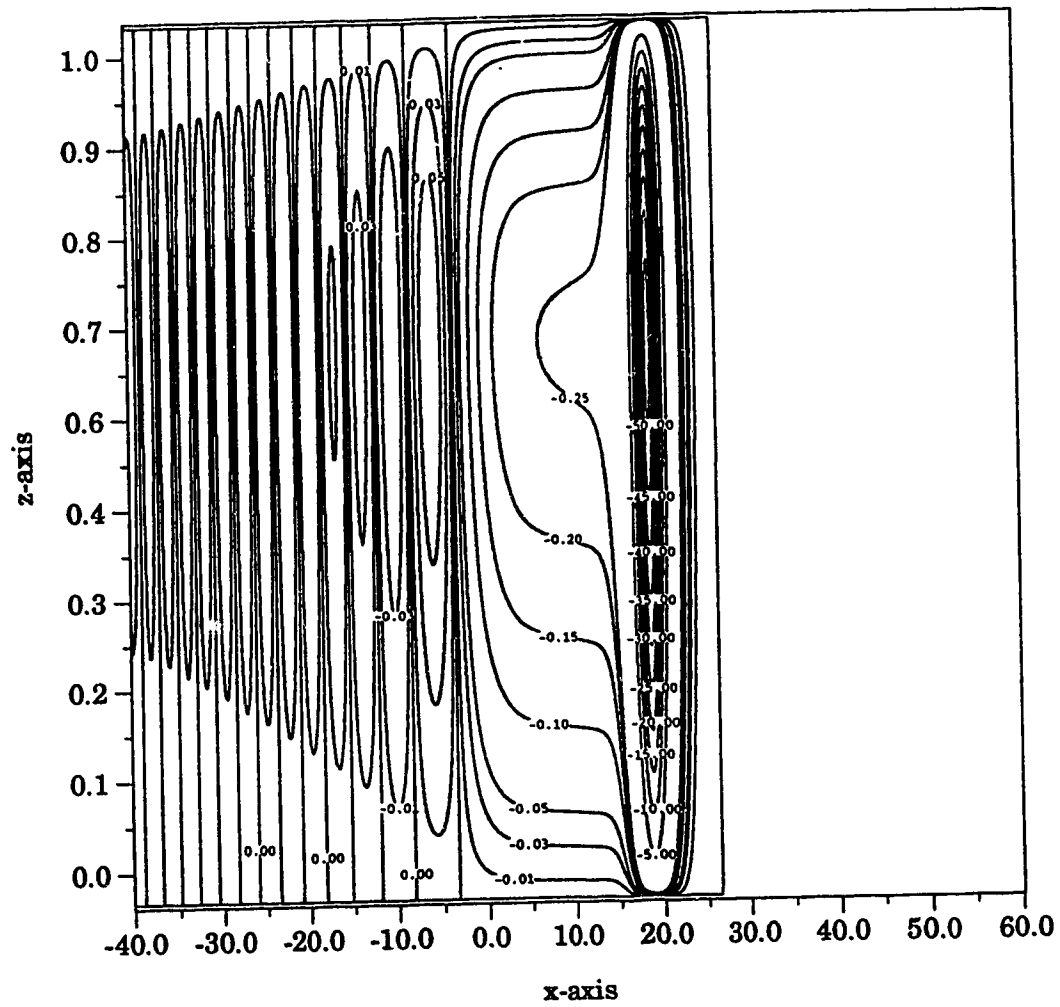


Figure 18c

The Streamfunction at time, $t=10$

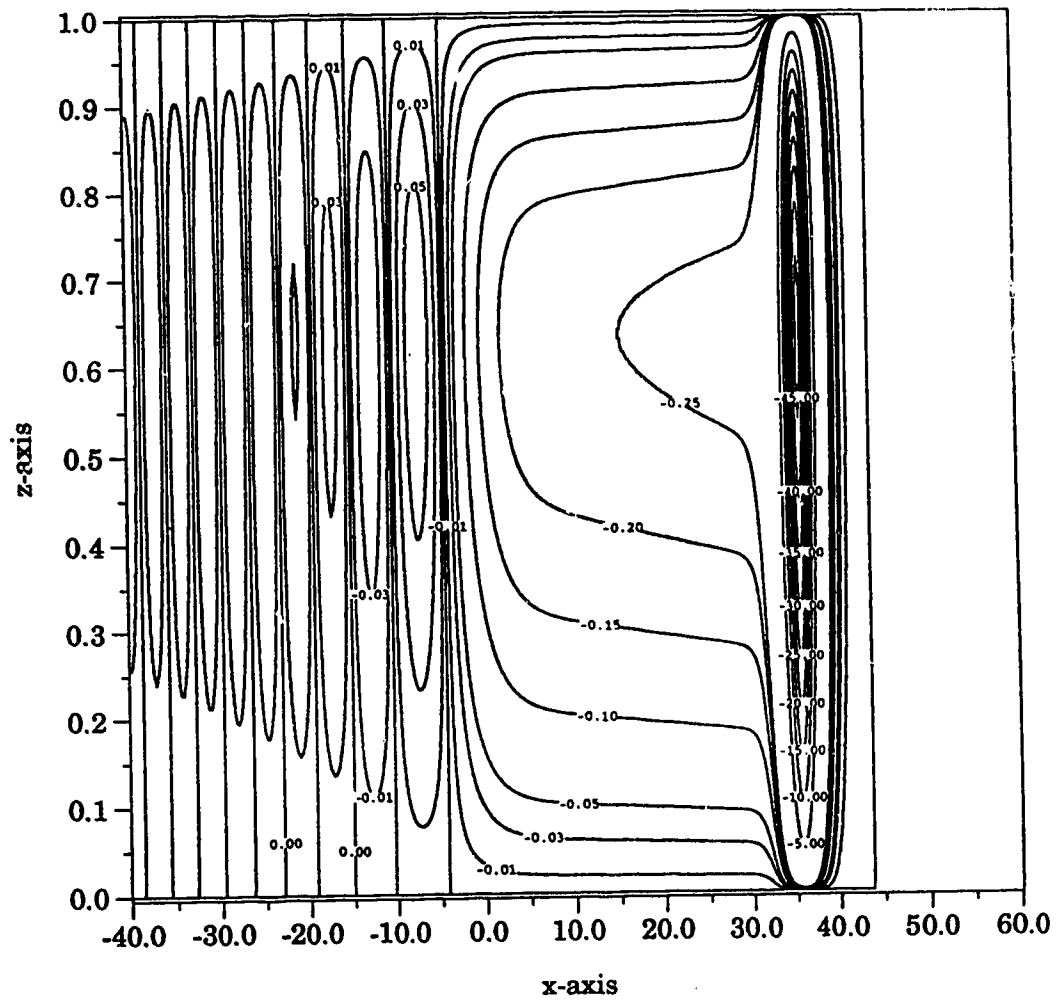


Figure 18d

158

The Streamfunction at time, $t=20$

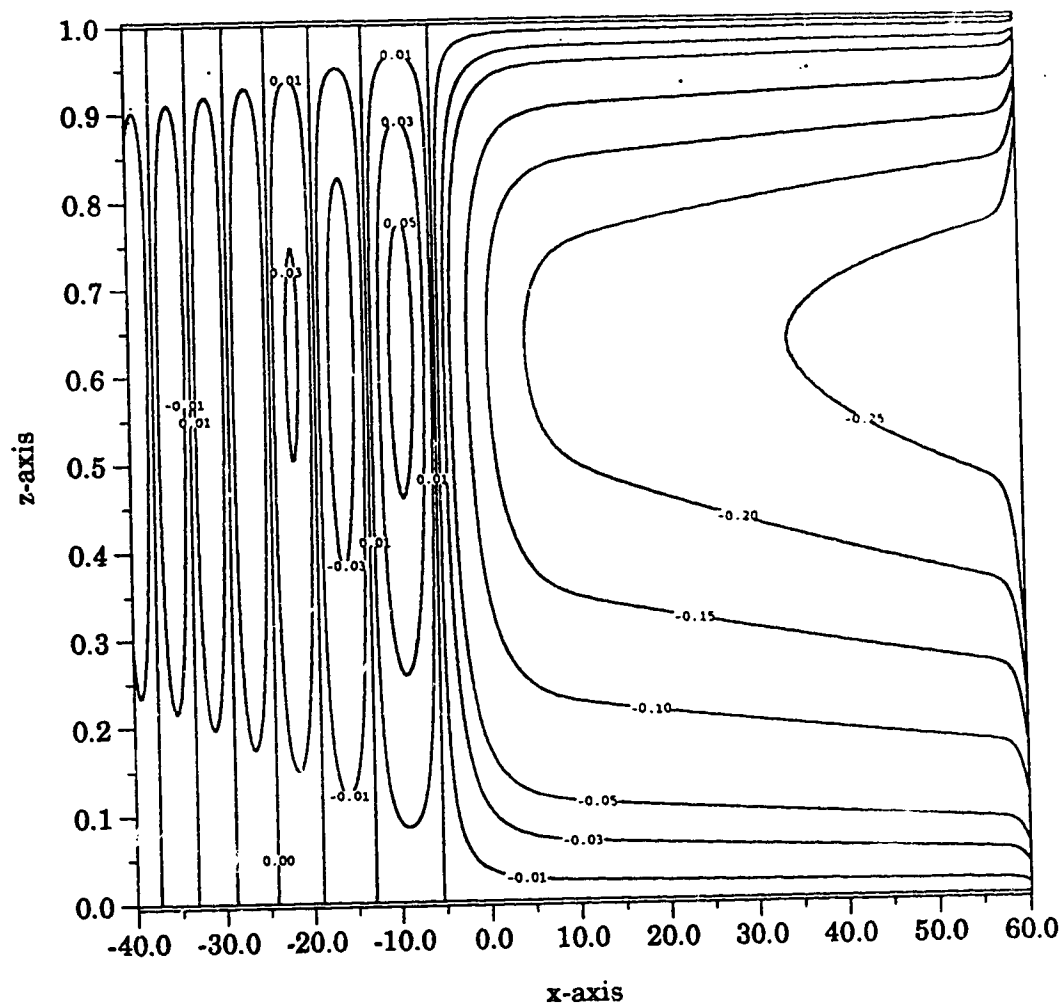


Figure 18f

The Streamfunction at time, $t=25$

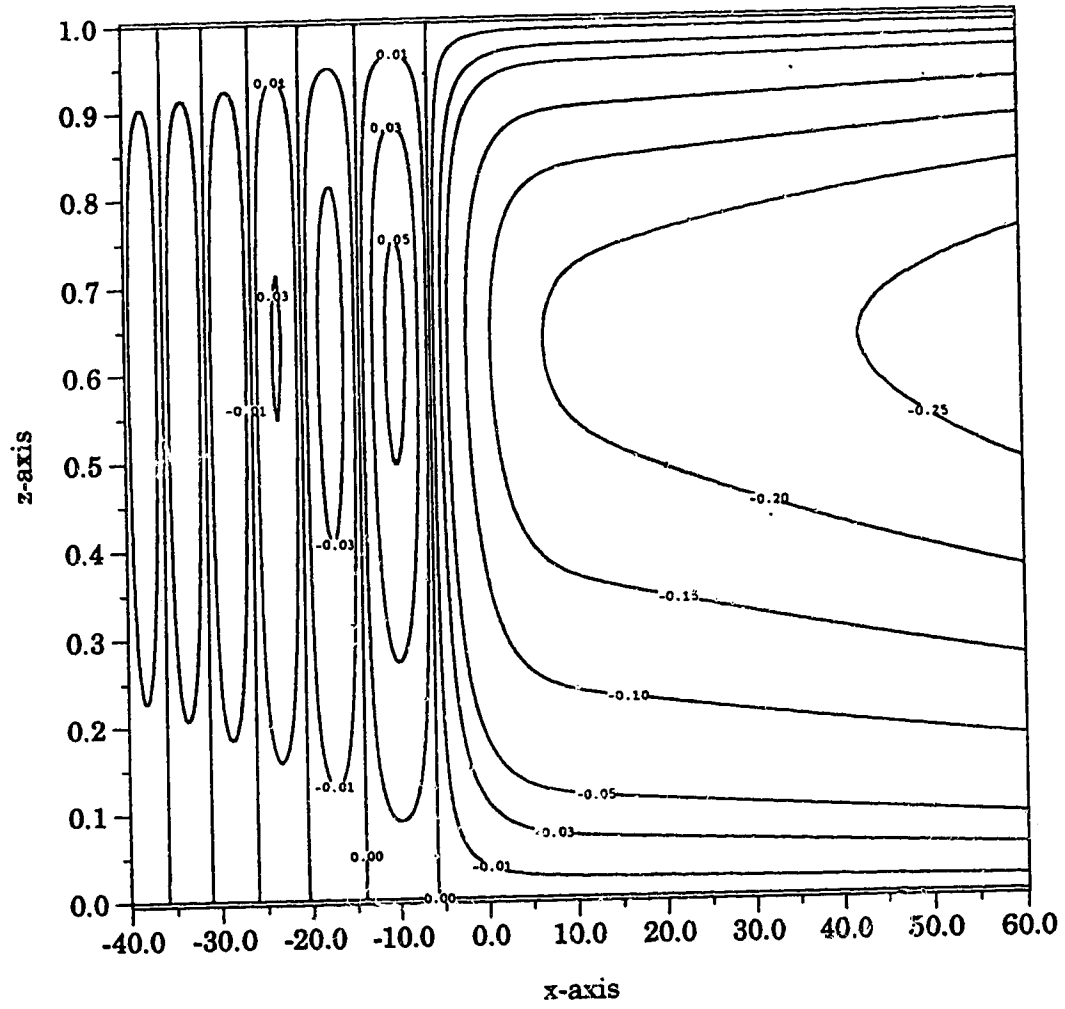


Figure 18g

The Streamfunction at time, $t=30$

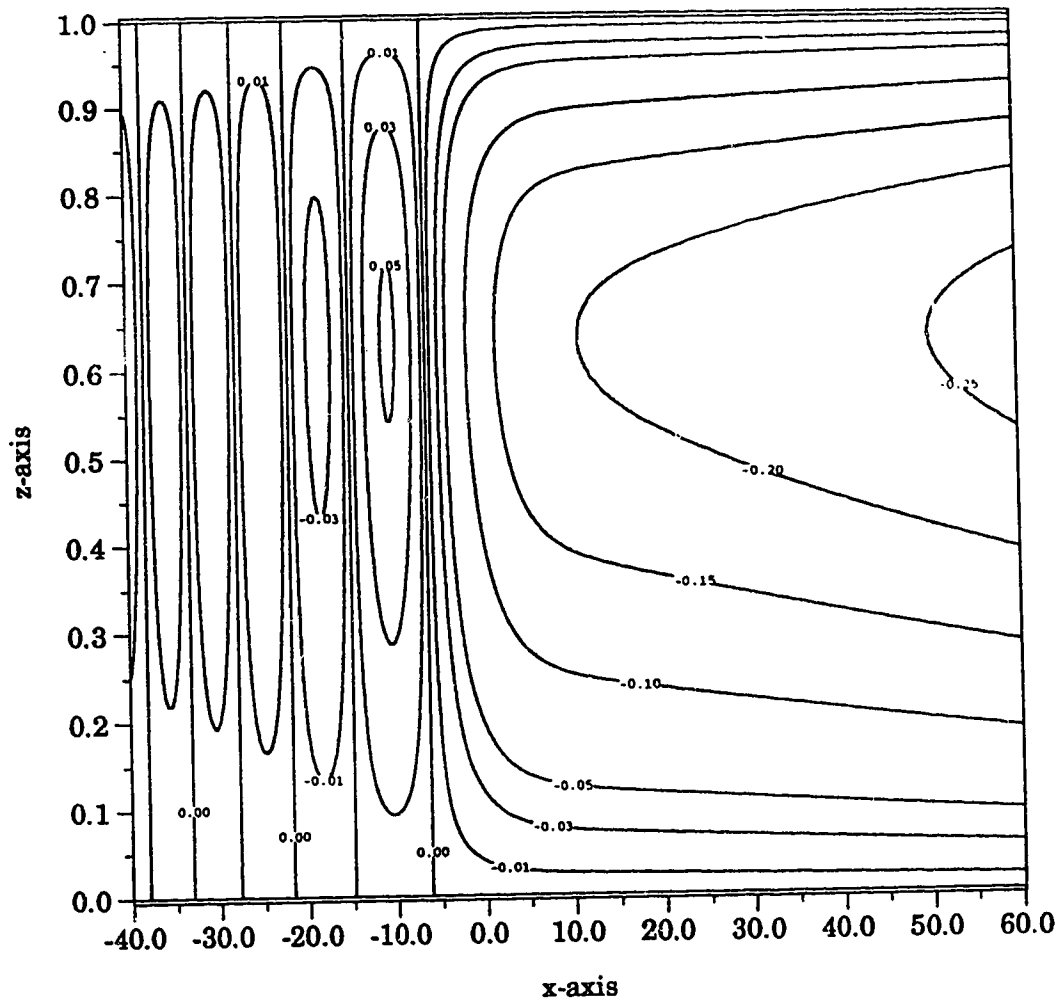


Figure 18h

The Streamfunction at time, $t=40$

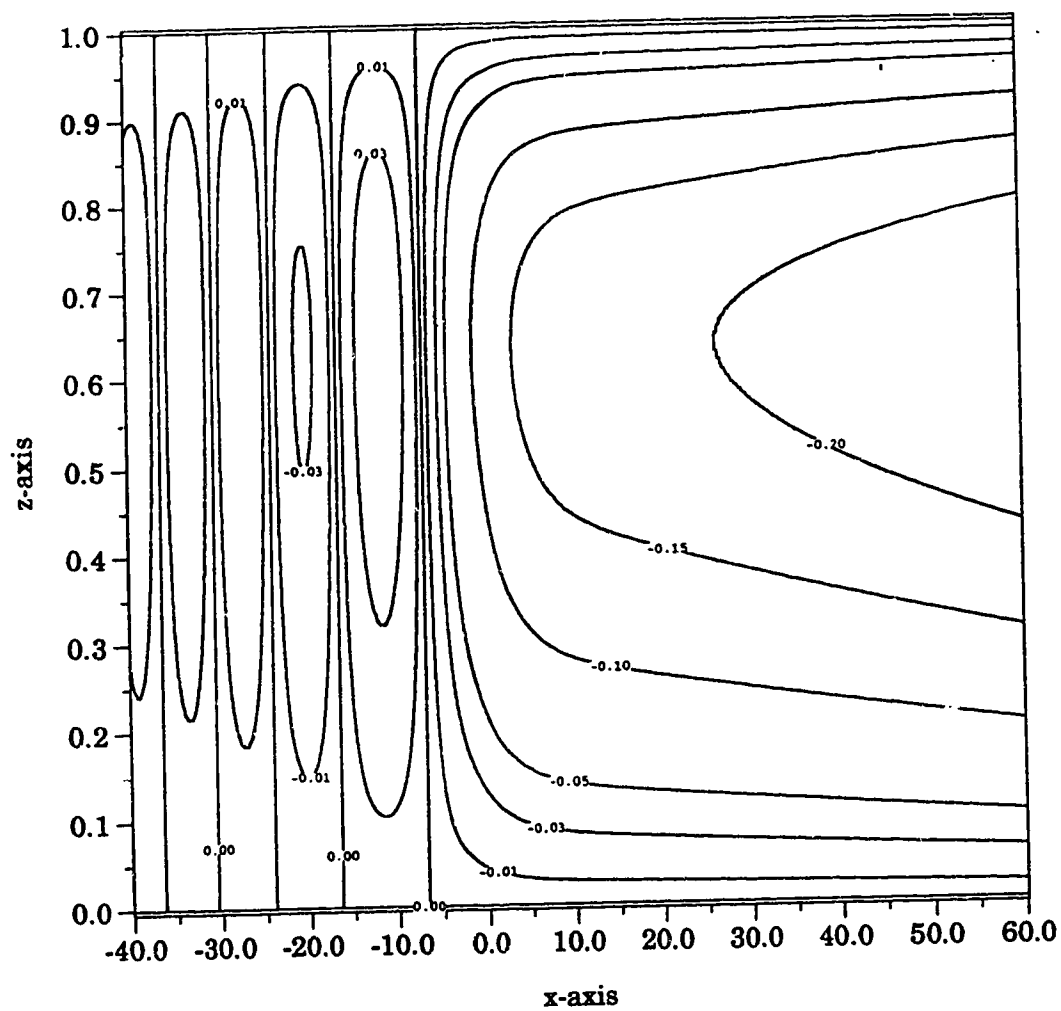


Figure 18i

The Streamfunction at time, $t=50$

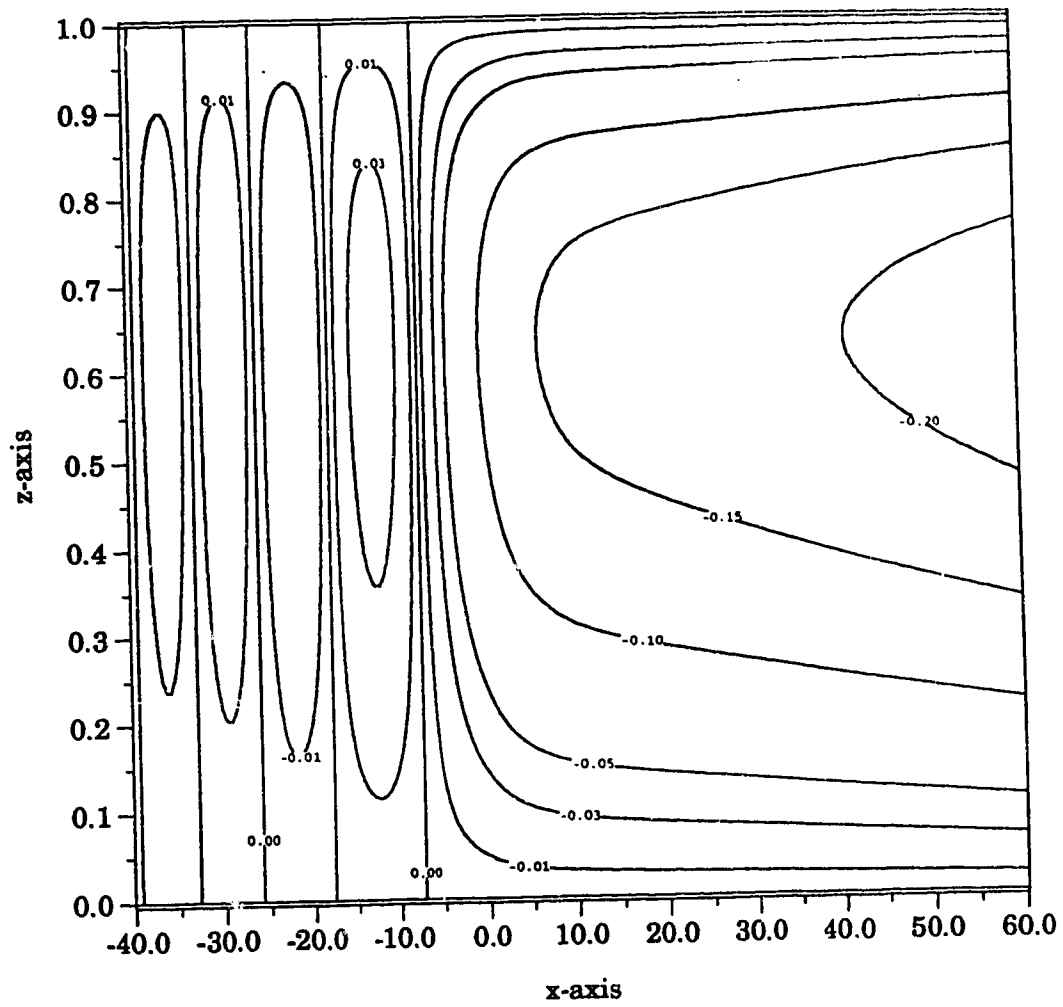


Figure 18j

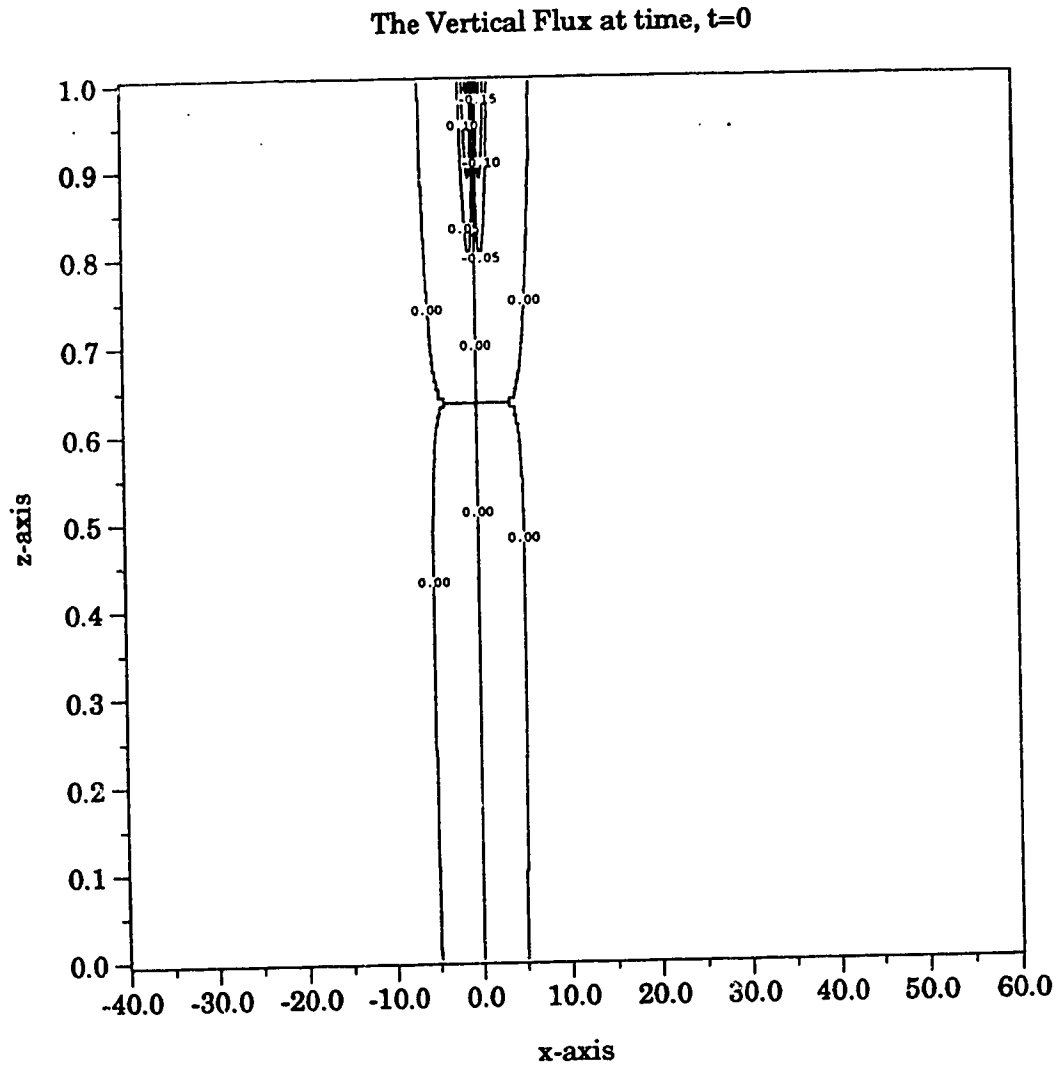


Figure 19: Contour Plot of Vertical Kinematic Momentum Flux

Figures 19a-j show lines of constant vertical momentum flux, with parameters $\mu = 1.0$, $\nu = \frac{1}{100}$, for times $T = 0, 1, 5, 10, 15, 20, 25, 30, 40$, and 50 . Plots shown with $0 \leq z \leq 1$ and $-40 \leq x \leq 60$.

The Vertical Flux at time, $t=1$

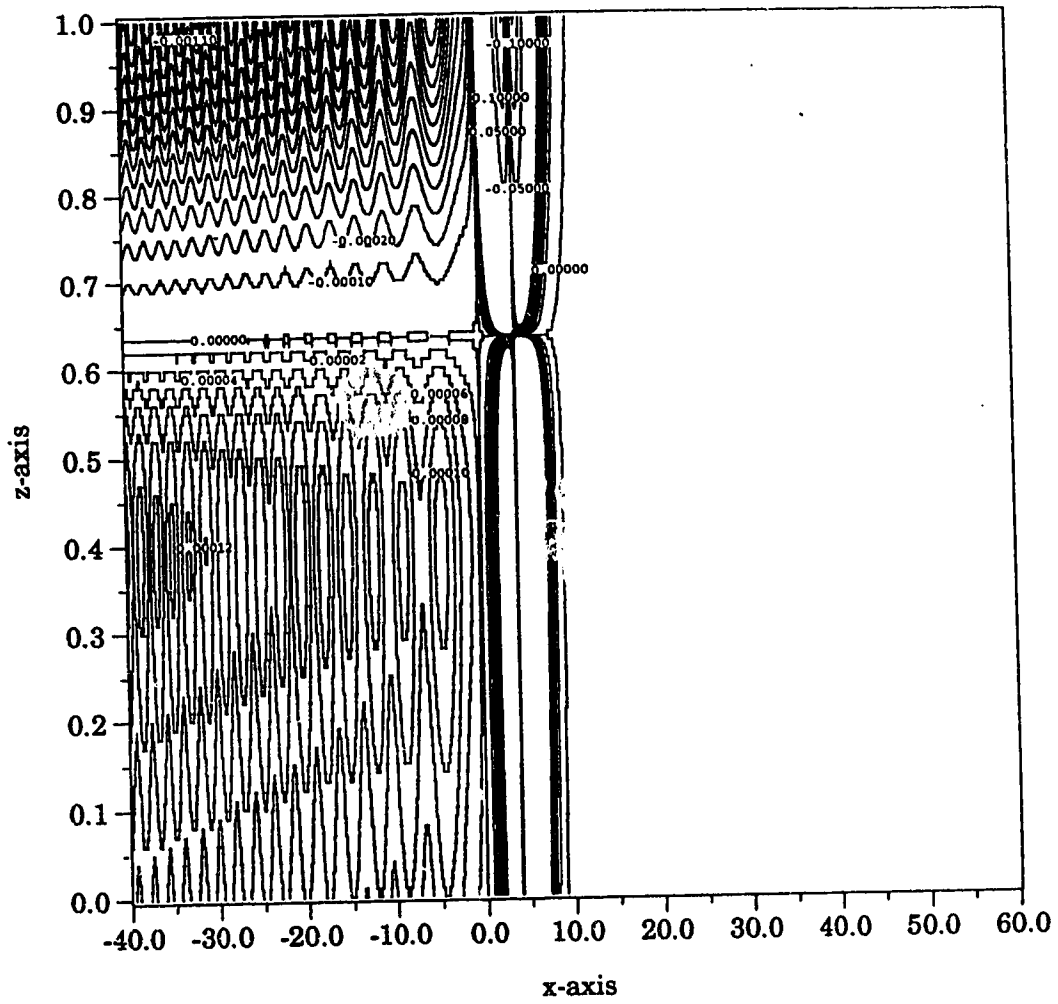


Figure 19b

The Vertical Flux at time, $t=5$

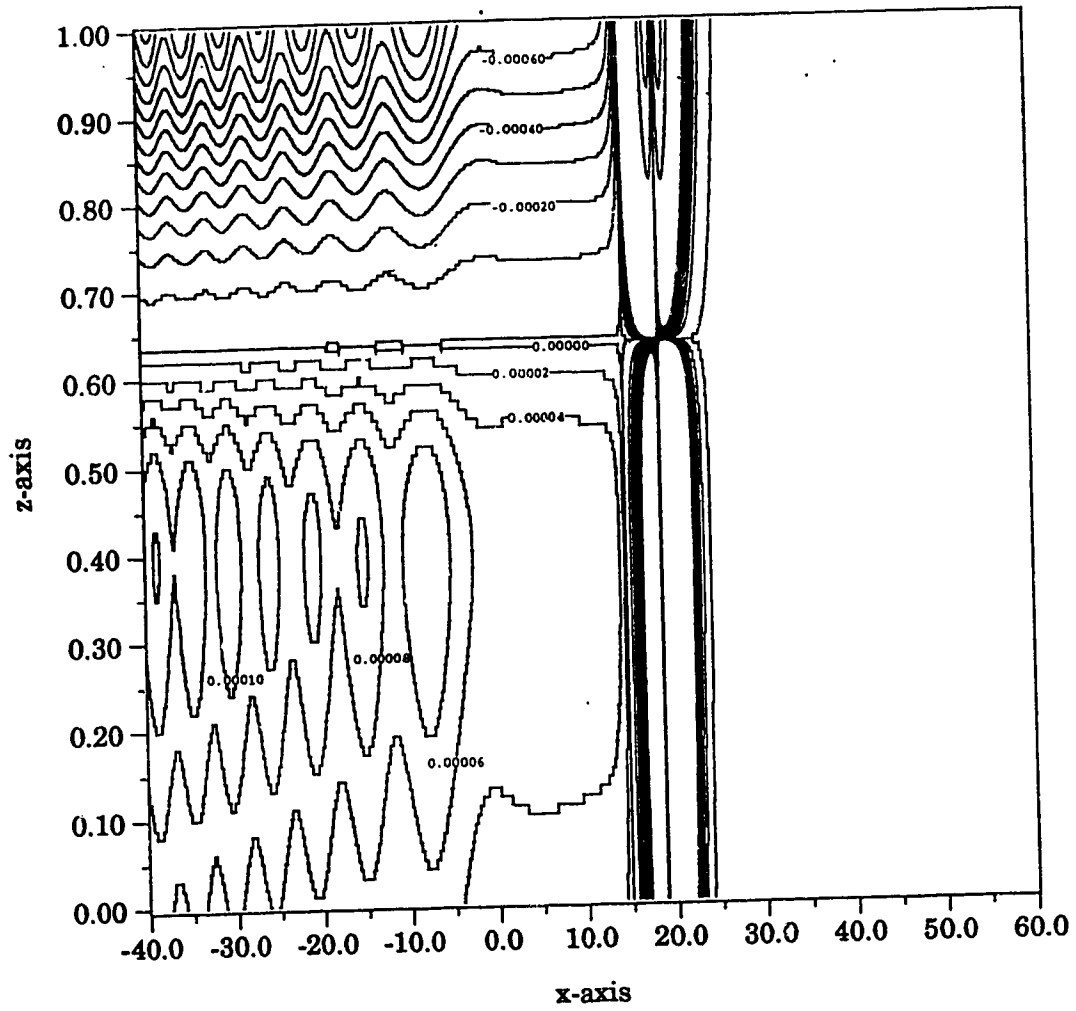


Figure 19c

The Vertical Flux at time, $t=10$

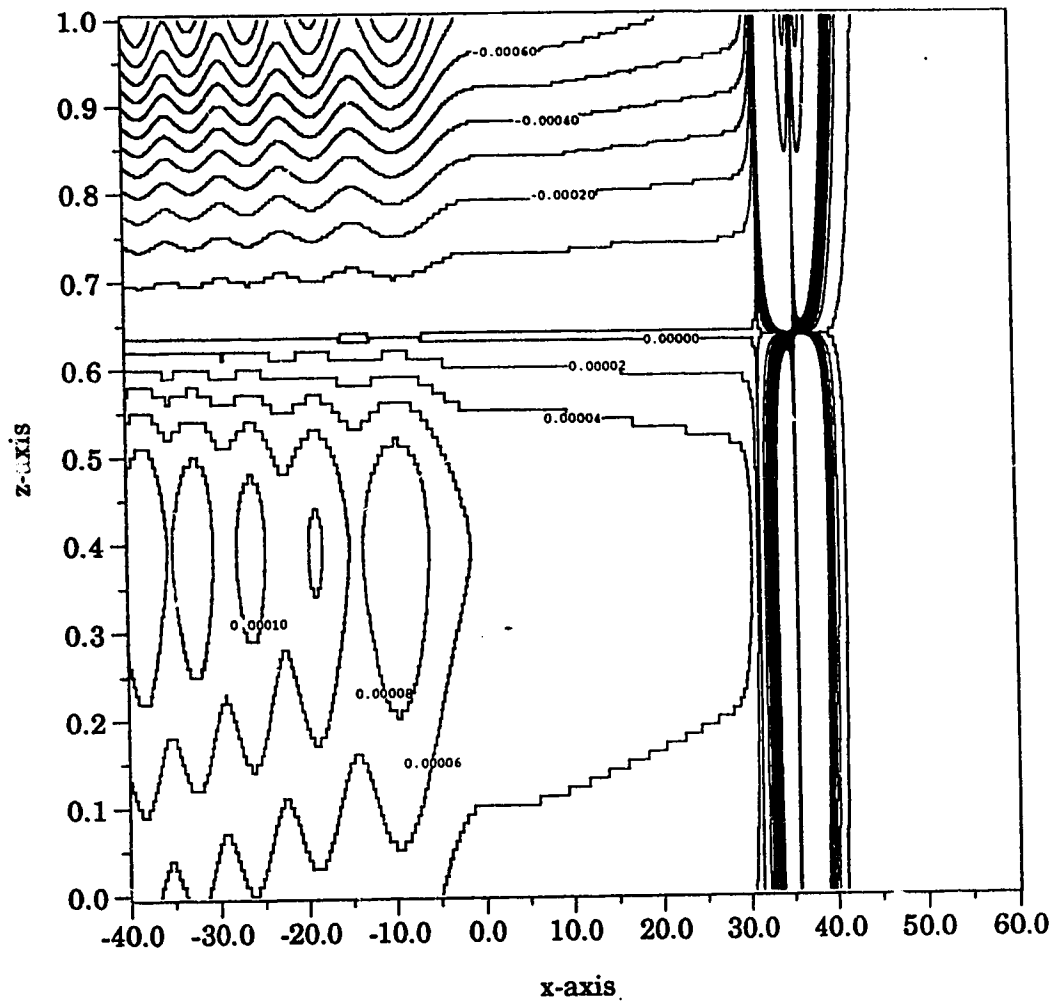


Figure 19d

The Vertical Flux at time, $t=15$

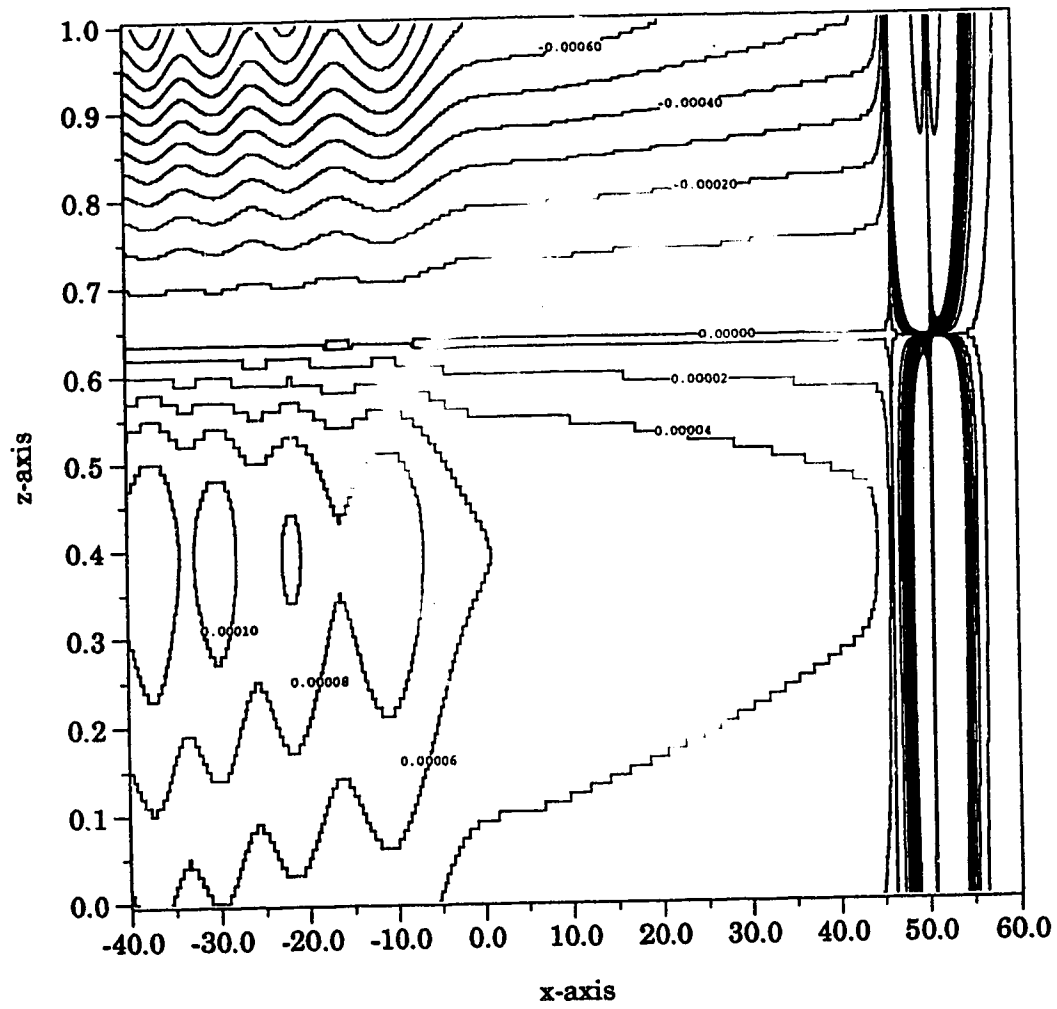


Figure 19e

The Vertical Flux at time, $t=20$

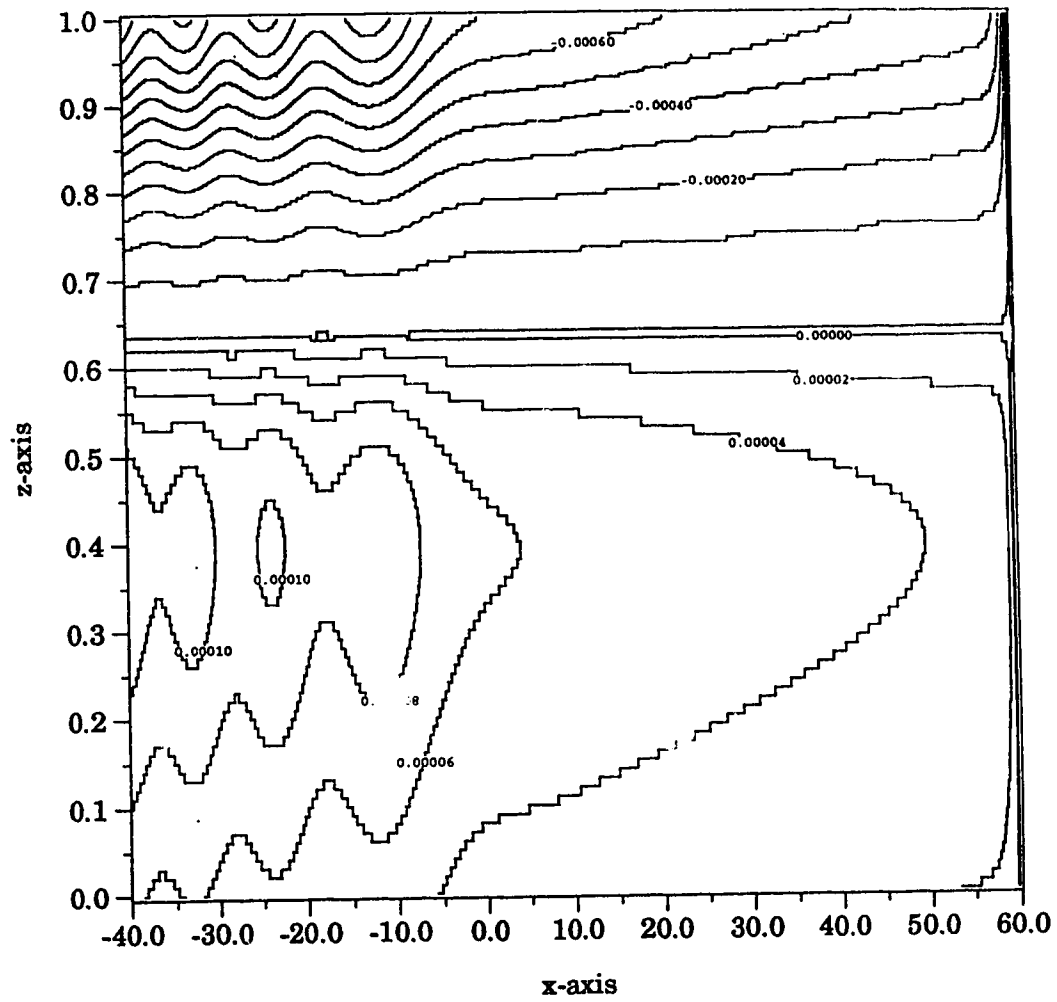


Figure 19f

The Vertical Flux at time, $t=25$

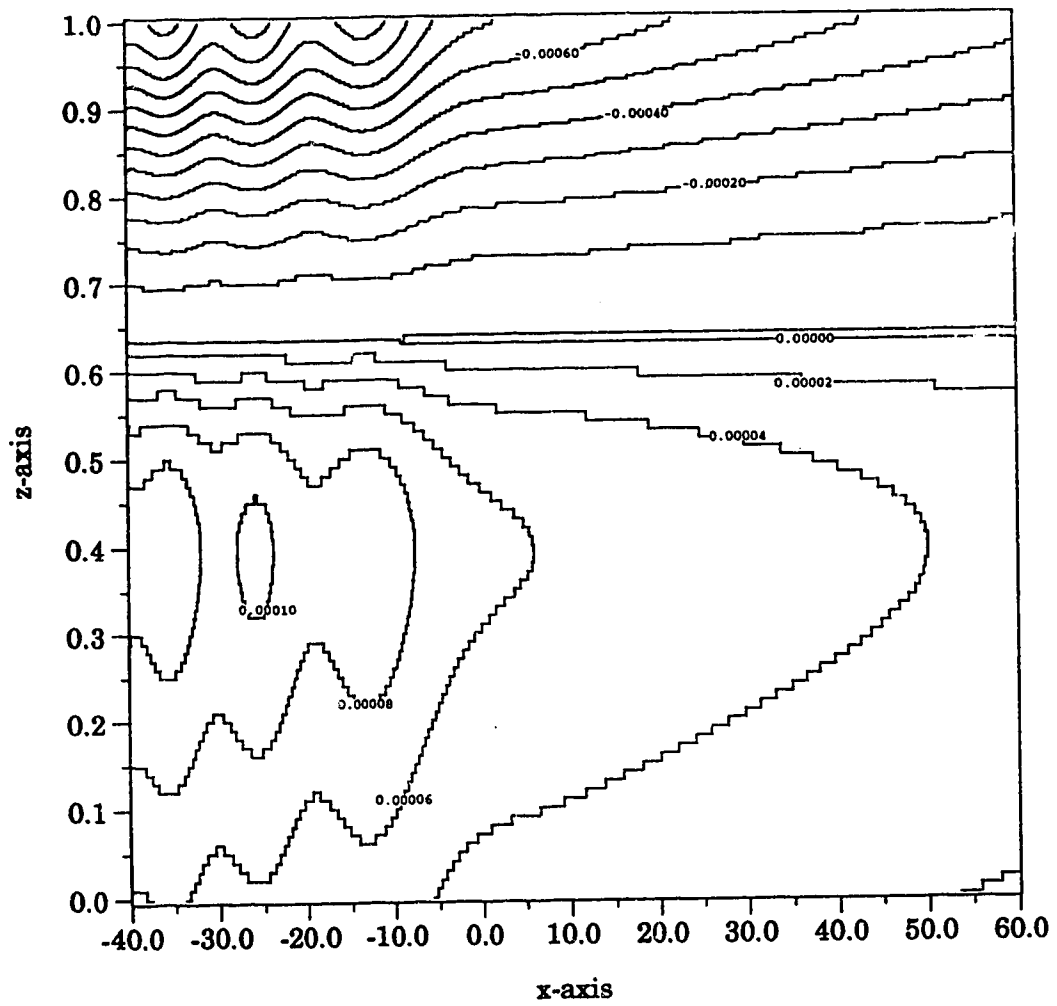


Figure 19g

The Vertical Flux at time, $t=30$

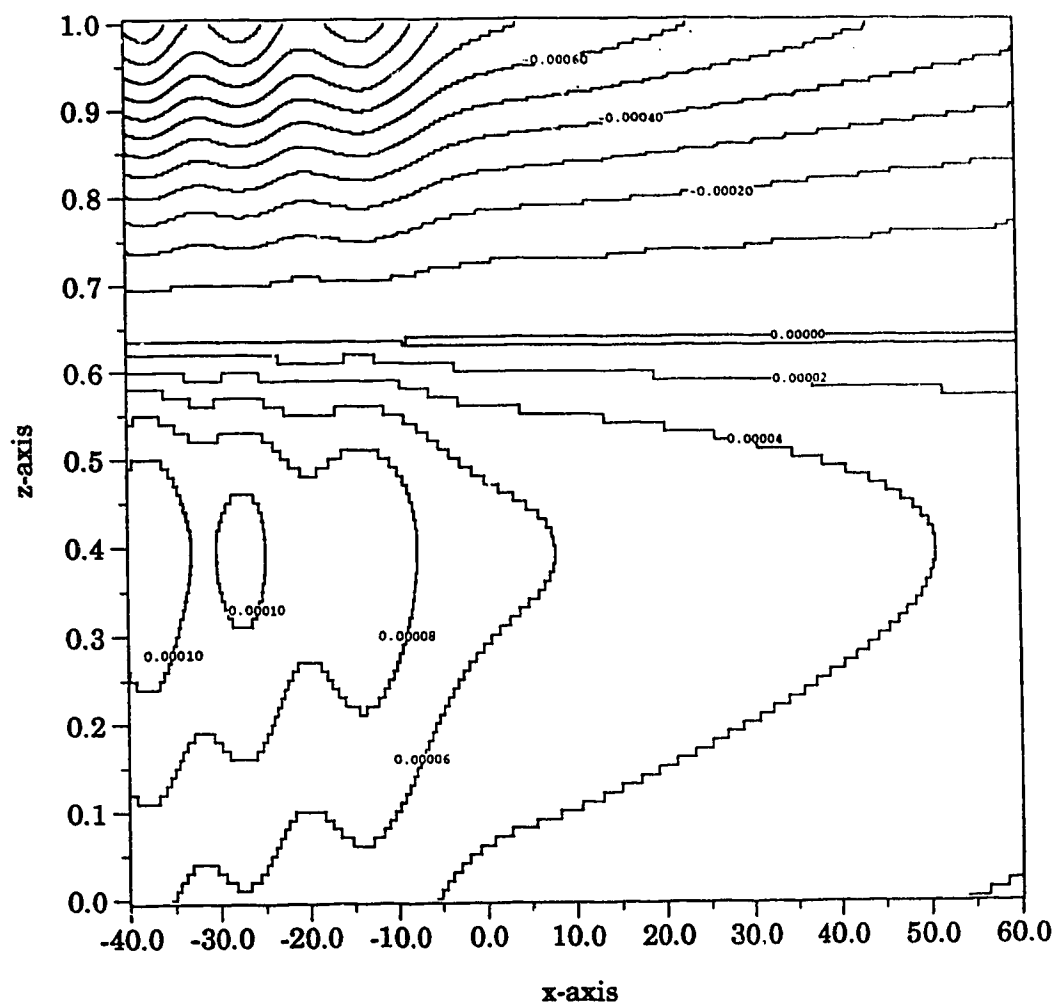


Figure 19h

The Vertical Flux at time, $t=40$

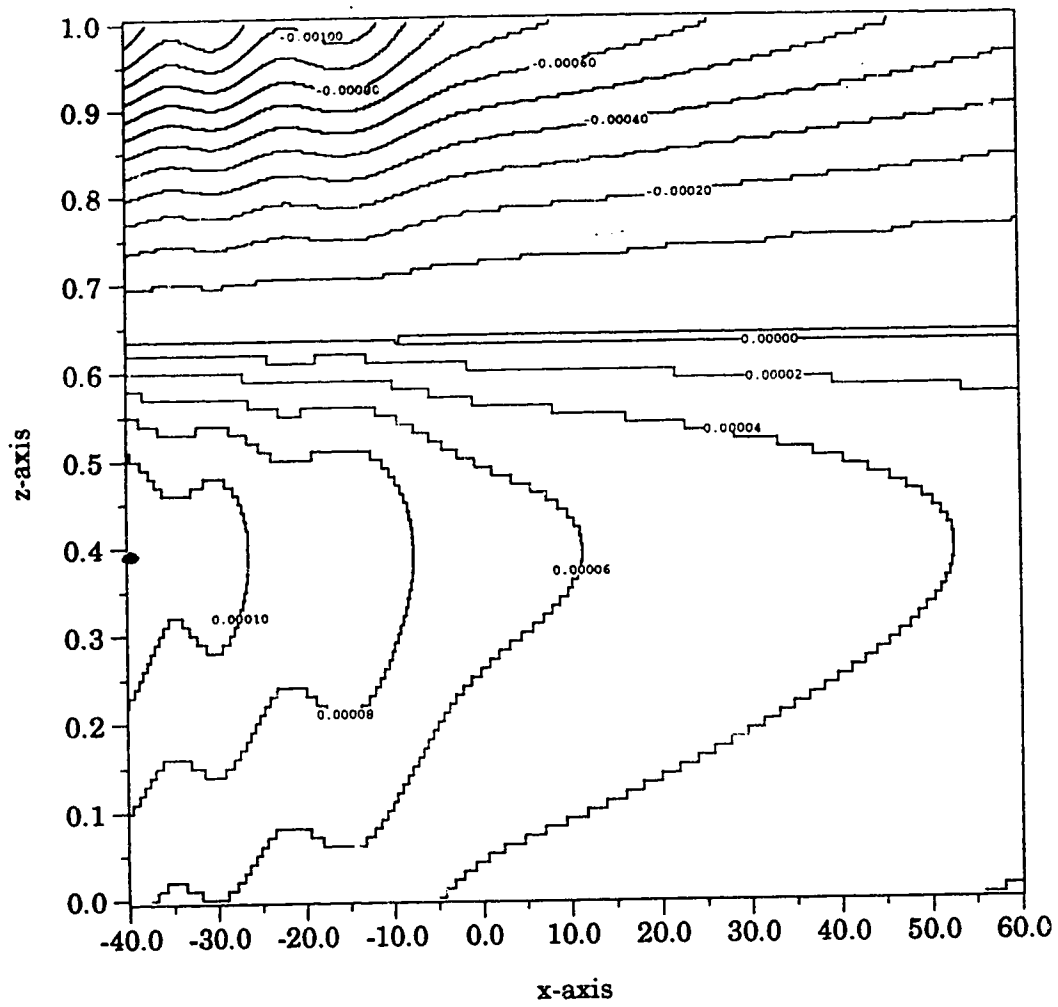


Figure 19i

The Vertical Flux at time, $t=50$

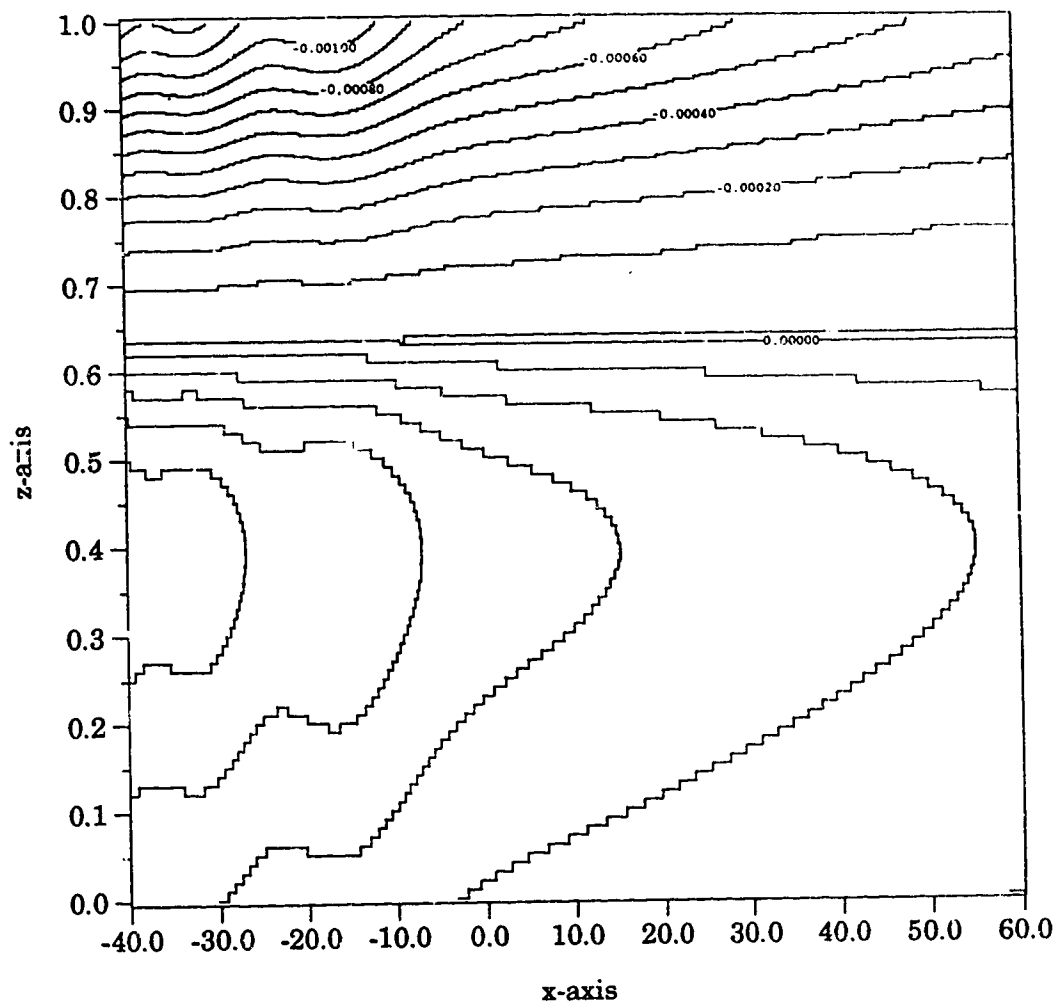


Figure 19j

5.3 Conclusion

Sandstrom et al (1989) concluded from their observations that enhanced mixing occurred due to the passage of internal solitary waves. By using a simple first-order closure scheme to represent the turbulent dissipation of a single soliton, we have developed a model which demonstrates that in the lee of the wave there is, indeed, enhanced vertical mixing in the region of the pycnocline. In addition to the upwelling, our model also demonstrates vertical shear in the horizontal velocity field.

The model presented in this thesis satisfies energy balance laws but fails to satisfy mass balance laws (in fact, the solution creates mass, primarily in the shelf region of the dissipating soliton). Despite the model's failure to satisfy the mass balance law, the author suggests that the model presented here does demonstrate that a turbulent dissipation mechanism is partially responsible for the enhanced mixing found to occur after the passage of internal solitary waves. However, while the vertical velocity field indicates that continual upwelling occurs in the lee of the soliton, the vertical kinematic momentum flux seems to indicate that this upwelling may not act as a nutrient pump but may merely be the restoration of the pycnocline to its undisturbed state (i.e. the buoyancy forces may be acting to restore the fluid to its hydrostatic state with very little, if any, entrainment occurring).

Bibliography

- [1] Ablowitz, M.J. and Ladik, J.F., 1976: "A nonlinear difference scheme and inverse scattering," *Stud. Appl. Math.* **55**, 213-229.
- [2] Abramowitz, M. and Stegun, I.A., 1967: *Handbook of Mathematical Functions*, Dover Press.
- [3] Bender, M.L. and Orszag, S.A., 1978: *Advanced Mathematical Methods for Scientists and Engineers*, McGraw-Hill.
- [4] Benjamin, T.B., 1966: "Internal waves of finite amplitude and permanent form," *J. Fluid Mech.* **25**(2), 241-270.
- [5] Bogucki, D. and Garrett, C., 1993: "A simple model for the shear-induced decay of an internal solitary wave," *J. Phys. Ocean.* **23**, 1767-1776.
- [6] Djorđjevic, V.D. and Redekopp, L.G., 1978: "The fission and disintegration of internal solitary waves moving over two-dimensional topography," *J. Phys. Ocean.* **8**, 1016-1024.
- [7] Drazin, P.G. and Johnson, R.S., 1989: *Solitons: An Introduction*, Cambridge University Press, 226 pp.
- [8] Drazin, P.G. and Reid, W.H., 1981: *Hydrodynamic Stability*, Cambridge University Press.
- [9] Fournier, R.O., Marra, J., Bohrer, R., and Van Det, M., 1977: "Plankton dynamics and nutrient enrichment of the Scotian shelf," *J. Fish. Res. Board Can.* **34**, 1004-1018.
- [10] Frisch, U. and Orszag, S.A., 1990: "Turbulence: Challenges for theory and experiment," *Physics Today*, January, 24-32.
- [11] Gear, J.A. and Grimshaw R., 1983: "A second order theory for solitary waves in shallow fluids," *Phys. Fluids* **26**, 1, 14-29.
- [12] Gill, A.E., 1982: *Atmosphere-Ocean Dynamics*, Academic Press, 662 pp.
- [13] Greig, I.S. and Morris, J.L., 1976: "A hopscotch method for the Korteweg-de Vries equation," *J. Comp. Phys.* **20**, 64-80.

- [14] Grimshaw, R., 1979: "Slowly varying solitary waves. I. Korteweg-de Vries equation," *Proc. R. Soc. Lond. A* **368**, 359-375.
- [15] —, 1983: "Solitary waves in density stratified fluids," *Nonlinear Deformation Waves*, IUTAM Symp. Tallinn 1982, ed. U. Nigul, J. Engelbrecht, Springer, Berlin Heidelberg.
- [16] —, 1984: "Theory of solitary waves in shallow fluids," *Math. Res. Rep.* No. 14, University of Melbourne.
- [17] Haberman, R., 1987: *Elementary Applied Partial Differential Equations*, 2nd Edition, Prentice Hall, 547 pp.
- [18] Holloway, G., 1984: "Effects of velocity fluctuations on vertical distributions of phytoplankton," *J. Mar. Res.* **42**, 559-571.
- [19] Johnson, R.S., 1970: "A non-linear equation incorporating damping and dispersion," *J. Fluid Mech.* **42**, part 1, 49-60.
- [20] —, 1973: "On an asymptotic solution of the Korteweg-de Vries equation with slowly varying coefficients," *J. Fluid Mech.* **60**, part 4, 813-824.
- [21] Karpman, V.I. and Maslov, E.M., 1978: "Structure of tails produced under the action of perturbations on solitons," *Soviet Phys. JETP* **48**, 252-259.
- [22] Kaup, D.J. and Newell, A.C., 1978: "Solitons as particles, oscillators, and in slowly changing media: a singular perturbation theory," *Proc. R. Soc. London A* **361**, 413-446.
- [23] Knickerbocker, C.J. and Newell, A.C., 1980: "Shelves and the Korteweg-de Vries equation," *J. Fluid Mech.* **98**, part 4, 803-818.
- [24] Kodama, Y. and Ablowitz, M.J., 1981: "Perturbations of solitons and solitary waves," *Stud. Appl. Math.* **64**, 225-245.
- [25] Koop, C.G. and Butler, G., 1981: "An investigation of internal solitary waves in a two-fluid system," *J. Fluid Mech.* **112**, 225-251.
- [26] Leblond, P.H. and Mysak, L.A., 1978: *Waves in the Ocean*, Elsevier, 602 pp.
- [27] Lee, C.-Y. and Beardsley, R.C., 1974: "The generation of a long nonlinear internal wave in a weakly stratified shear flow," *J. Geophys. Res.* **79**(3), 453-462.

- [28] Lighthill, J., 1986: *An Informal Introduction to Theoretical Fluid Mechanics*, Oxford University Press, 260 pp.
- [29] Maslowe, S.A. and Redekopp, L.G., 1980: "Long nonlinear waves in stratified shear flows," *J. Fluid Mech.* 101, part 2, 321–348.
- [30] Mysak, L.A., 1984: "Nonlinear internal waves," *Hydrodynamics of Lakes*, Springer-Verlag Wien-New York, Hutter, K. (ed.).
- [31] —, 1986: "El Niño, interannual variability and fisheries in the northeast Pacific Ocean," *Can. J. Fish Aqua. Sci.* 43(2), 464–497.
- [32] Mysak, L.A., Hsieh, W.W. and Parsons, T.R., 1982: "On the relationship between interannual baroclinic waves and fish populations in the northeast Pacific," *Bio. Ocean.* 2(1), 63–103.
- [33] Newell, A.C., 1977: "Finite amplitude instabilities of partial difference equations," *SIAM J. Appl. Math.* 33(1), 133–160.
- [34] Osborn, T.R., 1980: "Estimates of the local rate of vertical diffusion from dissipation measurements," *J. Phys. Ocean.* 10, 83–89.
- [35] Ostrovsky, L.A. and Stepanyants, Yu.A., 1990: "Do internal solitons exist in the ocean?," *Rev. Geophys.* 27(3), 293–310.
- [36] Pedlosky, J., 1987: *Geophysical Fluid Dynamics*, 2nd Edition, Springer.
- [37] Quon, C. and Sandstrom, H., 1990: "A numerical algorithm to study internal solitary waves," *J. Comp. Phys.* 86, 168–186.
- [38] Sandstrom, H. and Elliot, J.A., 1984: "Internal tide and solitons on the Scotian shelf: A nutrient pump at work," *J. Geophys. Res.* 89(C4), 6415–6426.
- [39] Sandstrom, H., Elliott, J.A. and Cochrane, N.A., 1989: "Observing groups of solitary internal waves and turbulence with BATFISH and Echo-Sounder," *J. Phys. Ocean.* 19, 987–997.
- [40] Satsuma, J., Ablowitz, M.J., and Kodama, Y., 1979: "On an internal wave equation describing a stratified fluid with finite depth," *Phys. Let.* 73A(4), 283–286.

- [41] Stull, R.B., 1988: *An Introduction to Boundary Layer Meteorology*, Kluwer Academic Publishers, 666 pp.
- [42] Swaters, G.E., 1988: "Critical-layer absorption of neutral ageostrophic vorticity wave perturbations of baroclinic jets," *Geophys. Astrophys. Fluid Dynamics* 43, 1-41.
- [43] —, 1989: "A perturbation theory for the solitary-drift-vortex solutions of the Hasegawa-Mima equation," *J. Plasma Phys.* 41, part 3, 523-539.
- [44] —, 1991: "On the baroclinic instability of cold-core coupled density fronts on a sloping continental shelf," *J. Fluid Mech.* 224, 361-382.
- [45] Swaters, G.E. and Mysak, L.A., 1985: "Topographically-induced baroclinic eddies near a coastline with application to the northeast Pacific," *J. Phys. Ocean.* 15(11), 1470-1485.
- [46] Swaters, G.E. and Sawatzky, R.P., 1989: "Viscoelastic modulation of solitary pressure pulses in nonlinear fluid-filled distensible tubes," *Q.J. Mech. Appl. Math.* 42, part 2, 213-237.
- [47] Vliementhart, A.C., 1971: "On finite-difference methods for the Kortweg-de Vries equation," *J. Eng. Math.* 5(2), 137-155.
- [48] Warn, T. and Brasnett, B., 1983: "The amplification and capture of atmospheric solitons by topography: A theory of the onset of regional blocking," *J. Atmos. Sci.* 40, 28-38.
- [49] Witham, G.B., 1974: *Linear and Nonlinear Waves*, Academic Press, New York.
- [50] Zabusky, N.J. and Kruskal, M.D., 1965: "Interaction of "solitons" in a collisionless plasma and the recurrence of initial states," *Phys. Rev. Lett.* 15(6), 240-243.
- [51] Zauderer, E., 1983: *Partial Differential Equations of Applied Mathematics*, John Wiley & Sons, 779 pp.

Appendix A

The following is the FORTRAN source code used to generate the data for the asymptotic solution developed in Chapter 3.

```
PROGRAM TDIS
REAL*8 X,XC,ETA,ETA0,PHI,TH,TH0DT,MU,NU,U0,U1,ST,
1    TH0,UT,SCH2,FT,UTAIL,S1,UTL,OVRLP,NORM,
2    U0N,U1N,UTAILN,OVRLPN,UTS,UTSN,SHELF,ET,
3    T0,FTA,XBGN,XEND,UPLT(11,1001),EPSN,
4    STALOC,STLC(11,1001),MASS,ENERGY,
5    THETAC,THETA0
CHARACTER BLNK
BLNK=' '
OPEN(UNIT=6,FILE='tdis.out')
OPEN(UNIT=7,FILE='tdis.dat')
OPEN(UNIT=8,FILE='tdis.mas')
OPEN(UNIT=9,FILE='tdis.nrg')
OPEN(UNIT=10,FILE='tdis.sol')
C
C    INITIAL AMPLITUDE
C
ETA0=-2.D0
C
C    DISSIPATION PARAMETER
C
NU=1.0D0/100.0D0
MU=1.D0
C
C    FAST TIME LOOP
C
DO 100 I=2,100
    FT = DFLOAT(I-1)
    ST = NU*FT
C
C    PHASE POSITION
C
XC=THETAC(ST)
C
C    PHASE SHIFT
C
TH0=THETA0(ST)
```

```

C
C   AMPLITUDE PARAMETER
C
      ETA=ET(ST)
C
C   DERIVATIVE OF PHASE SHIFT W.R.T. ST
C
      TH0DT=-MU/(3.D0*ETA)+8.D0*ETA/15.D0
      WRITE(6,20) NU
      WRITE(6,21) MU
      WRITE(6,22) FT
      WRITE(6,23) XC
      WRITE(6,24) ETA
      WRITE(6,25) TH0
      WRITE(6,26) TH0DT
      WRITE(6,*) ' '
20      FORMAT(' The dissipation parameter nu = ',F10.5)
21      FORMAT(' The dissipation parameter mu = ',F10.5)
22      FORMAT(' The fast time t = ',F10.5)
23      FORMAT(' The phase position = ',F10.5)
24      FORMAT(' The amplitude = ',F10.5)
25      FORMAT(' The phase shift = ',F10.5)
26      FORMAT(' The phase shift derivative = ',F10.5)
C
C   PHASE DO LOOP
C
      XBGN=-40.D0
      XEND=160.D0
      DO 200 J=1,2001
        X=XBGN+(XEND-XBGN)*DFLOAT(J-1)/2000.D0
C
C   ARRIVAL TIME
C
      IF (X.GE.0.D0) T0=-((3.D0/(4.D0*MU))
1          *DLOG(((10.D0*MU*(DEXP(8.D0*NU*X/30.D0)
2          -1.D0))/(-8.D0))+1.D0)
      IF (X.LE.0.D0) T0=0.D0
      FTA=T0/NU
C
C   AIRY INTEGRAL ARGUMENT
C
      IF (FT .NE. 0.D0) S1= X/((3.D0*FT)**(1.D0/3.D0))

```

```

C
  TH=X-XC
  PHI=ETA*(TH-TH0)
  SCH2=1.D0/(DCOSH(PHI)**2)
  NORM = -2.D0*ETA0**2
  IF (FT .EQ. 0.D0) OVRLP=0.D0
  IF (FT .EQ.0.D0) GOTO 1000
  IF (X.LE.XC) OVRLP=-NU*(8.D0*ETA/15.D0 + MU / (3.D0 * ETA))
1    *DEXP(-MU*T0)
  IF (X.GT.XC) OVRLP=0.D0
1000 CONTINUE
C
C   MAIN PULSE
C
  U0=-2.D0*ETA**2*SCH2
  U0N=U0/NORM
  IF (FT .NE. 0.D0)U1=NU*((MU/(6.D0*ETA))
1    *((3.D0*(1.D0-PHI*DTANH(PHI))*SCH2)
1      +DTANH(PHI)-1
2      -(PHI*SCH2)*(PHI*DTANH(PHI)-2.D0))
3    +(ETA/15.D0)*((12.D0*SCH2*(1.D0-PHI*DTANH(PHI)))
4      +4.D0*(DTANH(PHI)-1.D0)
5      +(2.D0*PHI*SCH2*(PHI*DTANH(PHI)-2.D0)))
6    +(TH0DT/2.D0)*(SCH2*(PHI*DTANH(PHI)-1.D0)))
  IF (FT .EQ. 0.D0) U1=0.D0
C
C   WAVE TAIL
C
  IF (X.LE.XC) SHELF=-NU*(MU/(3.D0*ET(T0))+(8.D0*ET(T0)/15.D0))
1    *DEXP(-MU*(ST-T0))
  IF (X.GT.XC) SHELF=0.D0
  IF (FT .NE.0.D0) UTAIL=UTL(S1)*SHELF
  IF (FT.EQ.0.D0) UTAIL=0.D0
C
C   SHELF AND TAIL SOLN
C
  UTS = U1+UTAIL-OVRLP
  UTSN =UTS/NORM
C
C   COMPLETE SOLUTION
C
  UT=U0+UTAIL+U1-OVRLP

```

```

C      WRITE(7,30) X,UT
30     FORMAT(2F15.5)
      MASS = MASS + UT
      ENERGY = ENERGY + 0.5D0*UT**2
200    CONTINUE
      WRITE(6,22) FT
      WRITE(6,*) 'MASS = ',MASS
      WRITE(6,*) 'ENERGY = ',ENERGY
      WRITE(6,*) '      '
      WRITE(7,900) BLNK
900    FORMAT(A1)
      WRITE(8,902) FT,MASS
      WRITE(9,902) FT,ENERGY
      WRITE(10,903) FT,XC,-2.D0*ETA**2
902    FORMAT(2F15.5)
903    FORMAT(3F15.5)
      MASS = 0.D0
      ENERGY = 0.D0
100    CONTINUE
      CLOSE(UNIT=6)
      CLOSE(UNIT=7)
      CLOSE(UNIT=8)
      CLOSE(UNIT=9)
      CLOSE(UNIT=10)
      STOP
      END

C
C      DISPERSIVE WAVE TAIL SOLUTION
C
      DOUBLE PRECISION FUNCTION UTL(S)
      REAL*8 S,EBS,ERR,ANS,ERT,UL,LL,DAI,DQDAG
      EXTERNAL DAI,DQDAG
      INTEGER INT
      EBS=3.D0
      ERR=1.D-6
      IF(S.EQ.0.D0) UTL=2.D0/3.D0
      IF(S.EQ.0.D0) RETURN
      IF(S.LT.0.D0) UL=0.D0
      IF(S.LT.0.D0) LL=S
      IF(S.LT.0.D0) INT=6
      IF(S.GT.0.D0) UL=S

```

```

IF(S.GT.0.D0) LL=0.D0
IF(S.GT.0.D0) INT=2
CALL DQDAG(DAI,LL,UL,EBS,ERR,INT,ANS,ERT)
IF(S.LT.0.D0) UTL=2.D0/3.D0-ANS
IF(S.GT.0.D0) UTL=2.D0/3.D0+ANS
RETURN
END
C   DOUBLE PRECISION FUNCTION INTGRD(SP)
C   REAL*8 AI,AIP,SP
C   CALL AIRY(SP,AI,AIP)
C   INTGRD=AI
C   RETURN
C   END
DOUBLE PRECISION FUNCTION ET(X)
REAL*8 U,N0,ET2,X
U=1.0D0
N0=1.0D0
ET2 = ((10.D0 * U * N0**2 * DEXP(-4.D0 * U * X / 3.D0))
1      /(10.D0 * U - 8 * N0**2 * (DEXP(-4.D0 * U * X / 3.D0)
2      -1.D0)))
ET = DSQRT(ET2)
RETURN
END
DOUBLE PRECISION FUNCTION THETAC(X)
REAL*8 V,U,N0,X
U=1.0D0
V=1.0D0/100.0D0
N0=1.0D0
THETAC = (30.D0 / (8.D0 * V))*DLOG(((10.D0* U - 8.D0 * N0**2
1      *(DEXP(-4.D0* U * X / 3.D0) -1.D0))
2      /(10.D0 * U)))
RETURN
END
DOUBLE PRECISION FUNCTION THETA0(X)
REAL*8 N0,U,BETA1,BETA2,X
U=1.0D0
N0=1.0D0
BETA1=DSQRT((8.D0 * N0**2 * DEXP(-4.D0 * U * X / 3.D0))
1      /(10.D0 * U + 8.D0 * N0**2))
BETA2=DSQRT((10.D0 * U - 8.D0 * N0**2
1      * (DEXP(-4.D0 * U * X / 3.D0) - 1.D0))
2      / (8.D0 * N0**2

```



```

3          * DEXP(-4.D0 * U * X / 3.D0)))
THETA0 = 0.5D0 * DSQRT(4.D0 / (5.D0 * U))
1          * (-3.D0 * DASIN(BETA1)
2          +3.D0 * DASIN(DSQRT((8.D0*N0**2)
3 /(10.D0*U+8.D0*N0**2)))-BETA2+DSQRT((10.D0*U)/(8.D0*N0**2)))
RETURN
END

```

Appendix B

The following is the FORTRAN source code used to generate the numerical solution developed in Chapter 4.

```
PROGRAM FKDV
REAL*8 Q1(-1:2200),Q2(-1:2200),Q3(-1:2200),DT,DX,X(0:2200)
REAL*8 M1,M2,M3,E1,E3,DELTA E,MU,XLOC,YVAL,X1M(3),Q1M(3)
INTEGER N,J,K,L
CHARACTER BLNK
OPEN(UNIT=6,FILE='fkdv.out')
OPEN(UNIT=7,FILE='fkdv.dat')
OPEN(UNIT=8,FILE='mass.out')
OPEN(UNIT=9,FILE='ener.out')
OPEN(UNIT=10,FILE='amp.out')
BETA=0.0050D0
BLNK=' '
MU=1.0D0/100.0D0
M1=0.0D0
M2=0.0D0
M3=0.0D0
E1=0.0D0
E3=0.0D0
DELTA E=0.0D0
TIME=0.0D0
DX=0.1D0
DT=1.0D0/5010.0D0
DO 10 J=0,2200
    Q1(J)=0.0D0
    Q2(J)=0.0D0
    Q3(J)=0.0D0
    X(J)=0.0D0
10 CONTINUE
    Q1(-1)=0.0D0
    Q2(-1)=0.0D0
    Q3(-1)=0.0D0
    X(0)=-40.0D0
    DO 20 J=1,2200
        X(J)=X(0)+J*DX
20 CONTINUE
```

```

C      X(J)=X(0)+J*DX
      DO 100 J=0,800
        Q1(J)=-2.0D0/COSH(X(J))**2
C      WRITE(7,901) X(J),Q1(J)
C 901   FORMAT(2F15.5)
      100 CONTINUE
C      WRITE(7,903) BLNK
C 903   FORMAT(A1)
C
      DO 401 J=0,800
        M1=M1+Q1(J)
        M2=M2+Q2(J)
        M3=M3+Q3(J)
        E3=E3+0.50D0*Q3(J)**2
        E1=E1+0.50D0*Q1(J)**2
401    CONTINUE
      DELTAE=E3-E1
      WRITE(6,*) 'TIME = ',TIME
      WRITE(6,*) 'MASS = ',M1,' ',M2,' ',M3
      WRITE(6,*) 'ENERGY = ',E3,' ',E1,' ',DELTAE
      WRITE(6,*) '
      WRITE(8,901) TIME,M1
      WRITE(9,901) TIME,E1
      CALL FMAX(X,Q1,X1M,Q1M)
      CALL PARA(X1M,Q1M,XLOC,YVAL)
      WRITE(10,902) TIME,XLOC,YVAL
902    FORMAT(3F15.5)
      DO 210 J=1,802
        Q2(J)=-2.0D0/COSH(X(J)-4.0D0*DT)**2
&      -(DT/DX**3)*(Q1(J+2)-2.0D0*Q1(J+1)+2.0D0*Q1(J-1)
&      -Q1(J-2))
&      +(2.0D0*DT/DX)*(Q1(J+1)+Q1(J)+Q1(J-1))*(Q1(J+1)-Q1(J-1))
&      + 2.0D0*MU * ((-DT*(-2.0D0/COSH(X(J)-4.0D0*DT)**2))
&      + (DT/DX**2)*((-2.0D0/COSH(X(J+1)-4.0D0*DT)**2)
&      -2.0D0*(-2.0D0/COSH(X(J)-4.0D0*DT)**2)
&      +(-2.0D0/COSH(X(J-1)-4.0D0*DT)**2)))
210    CONTINUE
      TIME=TIME+DT
C
C
C
      DO 310 J=1,804

```

```

      Q3(J)=Q1(J)
&      -(DT/DX**3)*(Q2(J+2)-2.0D0*Q2(J+1)+2.0D0*Q2(J-1)
&      -Q2(J-2))
&      +(2.0D0*DT/DX)*(Q2(J+1)+Q2(J)+Q2(J-1))*(Q2(J+1)-Q2(J-1))
&      + 2.0D0*MU*(-DT*Q1(J))
&      +(DT/DX**2)*(Q1(J+1)-2.0D0*Q1(J)+Q1(J-1)))
310  CONTINUE
      TIME=TIME+DT
C
C
      DO 400 J=0,2200
          M1=M1+Q1(J)
          M2=M2+Q2(J)
          M3=M3+Q3(J)
          E3=E3+0.50D0*Q3(J)**2
          E1=E1+0.50D0*Q1(J)**2
400  CONTINUE
      DELTAE=E3-E1
C      WRITE(6,*) 'TIME = ',TIME
C      WRITE(6,*) 'MASS = ',M1,' ',M2,' ',M3
C      WRITE(6,*) 'ENERGY = ',E3,' ',E1,' ',DELTAE
C      WRITE(6,*) ' '
C      DO 2000 J=1,100999
C      WRITE(6,*) J,' ',Q1(J),' ',Q2(J),' ',Q3(J)
C2000 CONTINUE
      DO 1000 L=0,100
      DO 1100 N=1,1670
          M1=0.0D0
          M2=0.0D0
          M3=0.0D0
          E1=0.0D0
          E3=0.0D0
          DELTAE=0.0D0
          DO 1111 J=1,2198
              Q1(J)=Q2(J)
&              -(DT/DX**3)*(Q3(J+2)-2.0D0*Q3(J+1)+2.0D0*Q3(J-1)
&              -Q3(J-2))
&              +(2.0D0*DT/DX)*(Q3(J+1)+Q3(J)+Q3(J-1))*(Q3(J+1)-Q3(J-1))
&              + 2.0D0*MU * ((-DT*Q2(J))
&              +(DT/DX**2)*(Q2(J+1)-2.0D0*Q2(J)+Q2(J-1)))
1111  CONTINUE
          TIME=TIME+DT

```

```

C
C
      DO 1121 J=1,2198
        Q2(J)=Q3(J)
      &   -(DT/DX**3)*(Q1(J+2)-2.0D0*Q1(J+1)+2.0D0*Q1(J-1)
      &   -Q1(J-2))
      &   +(2.0D0*DT/DX)*(Q1(J+1)+Q1(J)+Q1(J-1))*(Q1(J+1)-Q1(J-1))
      &   + 2.0D0*MU * ((-DT*Q3(J))
      &   +(DT/DX**2)*(Q3(J+1)-2.0D0*Q3(J)+Q3(J-1)))
1121    CONTINUE
      TIME=TIME+DT
C
C
C
      DO 1131 J=1,2198
        Q3(J)=Q1(J)
      &   -(DT/DX**3)*(Q2(J+2)-2.0D0*Q2(J+1)+2.0D0*Q2(J-1)
      &   -Q2(J-2))
      &   +(2.0D0*DT/DX)*(Q2(J+1)+Q2(J)+Q2(J-1))*(Q2(J+1)-Q2(J-1))
      &   +2.0D0*MU * ((-DT*Q1(J))
      &   +(DT/DX**2)*(Q1(J+1)-2.0D0*Q1(J)+Q1(J-1)))
1131    CONTINUE
      TIME=TIME+DT
C    IF (MOD(N,167) .EQ. 0) THEN
C    ENDIF
C      DO 1141 J=1,90+6*(N-1)+1998*L
C        Q2(J)=Q2(J)+(BETA/2.0D0)*(Q3(J+1)-2.0D0*Q2(J)+Q1(J-1))
C1141    CONTINUE
C
C
C
1100    CONTINUE
C      DO 1300 J=1,10100
C        IF ((-20.D0 .LE. X(J)).AND.(X(J).LE. 20.D0))
C          1      WRITE(6,*) X(J),' ',Q3(J)
C 1300    CONTINUE
      WRITE(6,*) 'COMPUTING MASS AND ENERGY'
      DO 1400 J=0,2200
        M1=M1+Q1(J)
        M2=M2+Q2(J)
        M3=M3+Q3(J)
        E1=E1+0.50D0*Q1(J)**2

```

```

      E3=E3+0.50D0*Q3(J)**2
1400  CONTINUE
      DELTAE=E3-E1
      WRITE(6,*) 'TIME = ',TIME,' SECONDS'
      WRITE(6,*) 'MASS = ',M1,' ',M2,' ',M3
      WRITE(6,*) 'ENERGY = ',E3,' ',E1,' ',DELTAE
      WRITE(6,*) '      '
      WRITE(8,901) TIME,M3
      WRITE(9,901) TIME,E3
      CALL FMAX(X,Q3,X1M,Q1M)
      CALL PARA(X1M,Q1M,XLOC,YVAL)
      WRITE(10,902) TIME,XLOC,YVAL
      DO 1301 J=0,2000
        WRITE(7,901) X(J),Q3(J)
1301  CONTINUE
        WRITE(7,903) BLNK
1000 CONTINUE
      CLOSE(UNIT=6)
      CLOSE(UNIT=7)
      CLOSE(UNIT=8)
      CLOSE(UNIT=9)
      CLOSE(UNIT=10)
      STOP
      END
      SUBROUTINE FMAX(X,Y,XMAX,YMAX)
      REAL*8 X(0:2200),Y(-1:2200),XMAX(3),YMAX(3),MAX
      INTEGER I,J,LYMAX
      MAX=Y(0)
      DO 200 I=0,2199
        IF(ABS(Y(I+1)).GT.ABS(MAX)) THEN
          MAX=Y(I+1)
          LYMAX=I+1
        ENDIF
200  CONTINUE
      XMAX(1)=X(LYMAX-1)
      XMAX(2)=X(LYMAX)
      XMAX(3)=X(LYMAX+1)
      YMAX(1)=Y(LYMAX-1)
      YMAX(2)=Y(LYMAX)
      YMAX(3)=Y(LYMAX+1)
      RETURN
      END

```

```

SUBROUTINE PARA(X,Y,XLOC,YVAL)
REAL*8 X(3),Y(3),A1,A,B1,B,C1,C,DETA,XLOC,YVAL
INTEGER I,J
    DETA=(X(2)*X(3)**2-X(3)*X(2)**2)
1   -(X(1)*X(3)**2-X(3)*X(1)**2)
2   +(X(1)*X(2)**2-X(2)*X(1)**2)
    C1=Y(1)*(X(2)*X(3)**2-X(3)*X(2)**2)
1   -Y(2)*(X(1)*X(3)**2-X(3)*X(1)**2)
2   +Y(3)*(X(1)*X(2)**2-X(2)*X(1)**2)
    B1=(Y(2)*X(3)**2-Y(3)*X(2)**2)
1   -(Y(1)*X(3)**2-Y(3)*X(1)**2)
2   +(Y(1)*X(2)**2-Y(2)*X(1)**2)
    A1=(X(2)*Y(3)-X(3)*Y(2))
1   -(X(1)*Y(3)-X(3)*Y(1))
2   +(X(1)*Y(2)-X(2)*Y(1))
    C=C1/DETA
    B=B1/DETA
    A=A1/DETA
    XLOC=-B/(2.D0*A)
    YVAL=C+B*XLOC+A*XLOC**2
RETURN
END

```